1-1-2012

# Phytochemical studies on the medicinal plant Sutherlandia frutescens

Xiang Fu
*University of Mississippi*

PHYTOCHEMICAL STUDIES ON THE MEDICINAL PLANT *SUTHERLANDIA*

*FRUTESCENS*

A Dissertation
Presented for the degree of
Doctor of Philosophy
In the Department of Pharmacognosy, School of Pharmacy
The University of Mississippi

by

XIANG FU

October 2012

**ABSTRACT**

*Sutherlandia frutescens* (L.) R. Br (Fabaceae) is a multipurpose medicinal plant with diverse biological activities, and has been widely used for the treatment of cancer, AIDS, diabetes, and infectious diseases in southern Africa. The primary goal of this study was to investigate the chemical constituents of *S. frutescens* and develop an analytical method to analyze this plant and the dietary supplements derived from this plant.

The dissertation is composed of six chapters. Chapter 1 introduces the general background of *S. frutescens*, including traditional uses and chemical and biological studies on the plant. Chapter 2 describes the phytochemical studies that have led to the identification of eight new cycloartane-type triterpene glycosides, sutherlandiosides A–H, and four new flavonol glycosides, sutherlandins A–D. The structures of these compounds were established by a combination of chemical methods and extensive spectroscopic analyses and X-ray crystallography. Several cycloartane glycosides possess unique carbon skeletons. Chapter 3 describes an improved method for determination of the absolute configuration of monosaccharides, which is based on structure elucidation of sutherlandins. Chapter 4 summarizes the results of the biological activities of the isolated compounds from *S. frutescens*. The major compound sutherlandioside B in the plant showed some antiviral activities against EBV and Tacaribe virus. Chapter 5 presents a newly established HPLC-based analytical method for standardization of the herbal products using the isolated new compounds. Chapter 6 provides concluding remarks for the study of *S. frutescens*. A brief description of future studies is proposed.

## DEDICATION

This work is dedicated to my family, who always loves me, believes me, supports me, and encourages me to soar higher…

Special dedication is to my wife, whose love makes me strong.

# LIST OF ABBREVIATIONS AND SYMBOLS

| | |
|---|---|
| AIDS | acquired immunodeficiency syndrome |
| AP-1 | activator protein-1 |
| Api | apiosyl |
| ATCC | American type culture collection |
| BCL | bicuculline |
| BSA | bovine serum albumin |
| ca. | circa |
| CD4 | cluster of differentiation 4 |
| CE | capillary electrophoresis |
| CFU | colony forming unit |
| CHX | cycloheximide |
| CNS | central nervous system |
| COSY | correlation spectroscopy |
| COX-2 | cyclooxygenase-2 |
| CREB | cyclic AMP response element binding protein |
| CYP | cytochrome P450 |
| D- | *dexter* |
| DEPT | distortionless enhancement by polarization transfer |
| DPPH | 2,2-diphenyl-1-picrylhydrazyl |
| DQF-COSY | double quantum filtered correlation spectroscopy |
| EBV | Epstein-Barr virus |
| ELSD | evaporative light scattering detector |
| EMSA | electrophoretic mobility shift assay |
| ESI | electrospray ionization |
| FCS | fetal calf serum |
| FDA | Food and Drug Administration |
| FFAs | free fatty acids |
| FMLP | L-formyl-L-methionyl-L-leucyl-L-phenylalanine |
| FMOC-Cl | fluorenylmethyl chloroformate |
| FT-IR | Fourier transform infrared spectroscopy |
| GABA | γ-aminobutyric acid |
| GC | gas chromatography |
| Glc | glucosyl |
| GooF | goodness of fit |
| HDL | high-density lipoprotein |
| HFD | high fat diet |
| HIV | human immunodeficiency virus |

| | |
|---|---|
| HMG | 3-hydroxy-3-methylglutaroyl |
| HMQC | heteronuclear multiple quantum coherence |
| HMBC | heteronuclear multiple-bond correlation spectroscopy |
| HPLC | high performance liquid chromatography |
| HRESIMS | high-resolution electron spray ionization mass spectra |
| $IC_{50}$ | half maximal inhibitory concentration |
| I.D. | internal diameter |
| IL-1β | interleukin-1β |
| iNOS | inducible isoform of NOS |
| IR | infrared |
| *J* | coupling constant |
| L- | *laevus* |
| LC | liquid chromatography |
| LDH | lactate dehydrogenase |
| LDL | low-density lipoprotein |
| LOD | limit of detection |
| LOQ | limit of quantitation |
| LPS | lipopolysaccharide |
| MAPKs | mitogen-activated protein kinases |
| *m/z* | mass-to-charge ratio |
| MBC | minimum bactericidal concentration |
| MFC | minimum fungicidal concentration |
| MIC | minimum inhibitory concentration |
| MOPS | 3-(*N*-morpholino)propanesulfonic acid |
| mRNA | messenger RNA |
| MRSA | methicillin-resistant *Staphylococcus aureus* |
| MS | mass spectrometry |
| NBT/PES | nitro blue tetrazolium/phenazine ethosulfate |
| NCCAM | National Center for Complementary and Alternative Medicine |
| NCNPR | National Center for Natural Products Research |
| NF-κB | nuclear transcription factor-κB |
| NIAID | National Institute of Allergy and Infectious Diseases |
| NIH | National Institutes of Health |
| NMR | nuclear magnetic resonance |
| NO | nitric oxide |
| NOE | nuclear Overhauser effect |
| NOESY | nuclear Overhauser effect spectroscopy |
| NOS | nitric oxide synthase |
| OADC | oleic acid, albumin, dextrose and catalase medium |
| OD | optical density |
| ODS | octadecyl silane |

| | |
|---|---|
| PBMCs | peripheral blood mononuclear cells |
| PCT | picrotoxin |
| PDA | photodiode array |
| PIAS1 | protein inhibitor of activated STAT1 |
| PKC | protein kinase C |
| PMT | photomultiplier tube |
| PPARγ | peroxisome proliferator-activated receptor γ |
| psig | pound-force per square inch gauge |
| PTZ | pentylenetetrazole |
| *R-* | *rectus* |
| $r^2$ | correlation coefficient |
| $R_f$ | retardation factor |
| RNA | ribonucleic acid |
| ROESY | rotating frame nuclear Overhauser effect spectroscopy |
| ROS | reactive oxygen species |
| RP | reversed-phase |
| rpm | revolutions per minute |
| RSD | relative standard deviation |
| *S-* | *sinister* |
| SADC | South African Development Community |
| SIC | selected ion chromatogram |
| SIM | selected ion monitoring |
| SIR | selected ion recording |
| SMPD3 | sphingomyelin phosphodiesterase 3, sphingomyelinase-2 |
| SQD | single quadrupole detector |
| STZ | streptozotocin |
| T2DM | type 2 diabetes mellitus |
| TEAC | Trolox equivalent anti-oxidant capacity |
| TFAA | total free amino acids |
| TLC | thin-layer chromatography |
| TNF-α | tumor necrosis factor-α |
| TPA | 12-*O*-tetradecanoylphorbol-13-acetate |
| $t_R$ | retention time |
| tRNA | transfer ribonucleic acid |
| tRNA$^{Arg}$ | arginyl-tRNA synthetase |
| Trolox | 6-hydroxy-2,5,7,8-tetramethylchroman-2-carboxylic acid |
| UPLC | ultra performance liquid chromatography |
| USDA | United States Department of Agriculture |
| UV | ultraviolet |
| XIC | extracted ion chromatogram |
| Xyl | xylosyl |

| | |
|---|---|
| Å | angstrom |
| $\delta$ | chemical shift value |
| $\Delta t_R$ | retention time difference |
| $\nu_{max}$ | maximum frequency |
| $\lambda_{max}$ | maximum wavelength |

# ACKNOWLEDGMENTS

**TABLE OF CONTENTS**

# LIST OF TABLES

# LIST OF FIGURES

# CHAPTER 1

## LITERATURE REVIEW OF BIOLOGICAL AND CHEMICAL STUDIES ON

## *SUTHERLANDIA FRUTESCENS*

### 1.1. Taxonomy and geographical distribution

*Sutherlandia frutescens* (L.) R. Br (Fabaceae) is a medicinal plant native to the southern part of Africa, including South Africa, Lesotho, the southern part of Namibia, Botswana, and Zimbabwe, with major distribution in the Western Cape and Karoo regions of South Africa. It is a legume shrub with small leaves and flowers and characterized by balloon-like pods as fruits. The leaves taste slightly bitter and have an aromatic smell. The flowers have a "tubular-like" shape and a bright red orange color (Soumyanath, 2006; Van Wyk and Albrecht, 2008).

Previous research was unable to clearly define the taxa that are closely related to *S. frutescens*. The South African *Sutherlandia* genus could be regarded as "one variable taxon, *S. frutescens*". (Moshe, 1998). For instance, *S. humilis* was considered as a dwarf form of *S. frutescens* (Olivier, 2009). Being morphologically similar to *Lessertia*, *Sutherlandia* is occasionally regarded as the genus *Lessertia*, and therefore "*Lessertia frutescens*" is actually referred to the plant "*Sutherlandia frutescens*" in several papers (Johnson, Syce *et al.*, 2007; Van Wyk and Albrecht, 2008; Shaik, Singh *et al.*, 2011).

## 1.2. Medicinal use

*S. frutescens* is well known for its multiple medicinal usages in South Africa. Its leaves, stems, flowers, pods, and roots are generally medicinal parts of the plant, while seeds are less used due to a high content of a toxic component L-canavanine (Shaik, Singh *et al.*, 2011).

*S. frutescens* is also called "cancer bush" because the local healers use it to treat cancer patients. With a long history of use, especially by the Khoi and Nama people for centuries in South Africa, its medicinal uses are not limited to cancer. Dietary supplements containing this plant material have been claimed to have analgesic, antidiabetic, anti-inflammatory, antipyretic, and anti-infective effects. (Van Wyk and Albrecht, 2008). Significant medicinal use is described below.

The herbal preparations of *S. frutescens* have been used as a tonic for weakness and poor appetite. The widespread cultivation in South Africa has also made it an inexpensive herbal remedy for local consumers. This is important in southern Africa where Western pharmaceutical products are either unaffordable or inaccessible. Various commercial products containing powdered plant material or extracts are available in the local markets as dietary supplements (Van Wyk, 2008).

Pain and stress relieving effects are another important medical properties of *S. frutescens* by local people. It has been served as a medication for a variety of ailments, including stomachache, intestinal ailment, liver pain, kidney ailment, backache, and wound healing. It has also been applied to relieve stress, depression, and anxiety, and to treat seizure, epilepsy, and convulsions (Ojewole, 2008).

The plant is notable for its use for viral and bacterial infections. The treatment of

chickenpox, a known viral infection, with *S. frutescens* has long been documented (Moshe, 1998). It is common that local people drink it as an herbal tea to treat diarrhea or dysentery, urinary tract infections, cough, and influenza. The infusion of this plant has also been used for washing wounds and eyes. Particularly, the products are gaining popularity in South Africa as an herbal treatment of human immunodeficiency virus (HIV) infection in acquired immunodeficiency syndrome (AIDS) patients (Mills, Cooper *et al.*, 2005; Mills, Singh *et al.*, 2006).

The anti-inflammatory and antipyretic effects of *S. frutescens* have been shown in the treatment of peptic ulcers, gastritis, esophagitis, bronchitis with leaf extracts, and the topical use for pustules and wound inflammation. Leaf decoctions are used to cure fevers, and relieve different types of rheumatic symptoms, such as rheumatoid arthritis.

Recently, the herbal products of *S. frutescens* have been increasingly used for the treatment of type 2 diabetes mellitus (T2DM) (Sia, 2004). With the swiftly increasing incidence of diabetes worldwide since the mid-1990s, the use of this plant for T2DM is expected to be growing in southern Africa.

## 1.3.  Biological activities

The growing interest in diverse biological activities of *S. frutescens* has provided tremendous impetus for the studies of the mechanism of actions of this plant. Recent investigations on biological activities of *S. frutescens* have been focused on the traditional use and historical herbal remedies of the plant with the potential benefits of anticancer, anti-inflammatory, anti-infectious, and emotional regulation effects. These studies have shown more evidence in support of its multipurpose medicinal use.

### 1.3.1. Antiproliferative effects

The so-called "cancer bush" has been popularly used for the treatment of "internal cancer" by indigenous people. Local healers claimed anecdotal "facts" that the herbal products of *S. frutescens* benefited cancer patients and improved their quality of life. However, scientific evidence remains insufficient (Van Wyk and Albrecht, 2008).

Recent investigations have disclosed possible mechanisms of its antiproliferative effects in support of the claims by traditional healers. The purported anticancer effect was first credited to the cytotoxic effect of L-canavanine, a non-standard amino acid among a paucity of early identified chemical components in *S. frutescens*. As an L-arginine antimetabolite, L-canavanine has been proven to inhibit human pancreatic cancer cells (Cann, van Netten *et al.*, 1995). However, more evidence showed that this activity is not only due to the cytotoxic effects contributed by canavanine. (Stander, Marais *et al.*, 2009)

Tai *et al.* performed a preliminary study and observed the cytotoxic effect of the ethanol extract from the leaves of *S. frutescens* on the breast cancer cell lines (MCF7, and MDA-MB-468) and human leukemia cell lines (Jurkat, and HL60) (Tai, Cheung *et al.*, 2004). The ethanol extract showed a concentration dependent inhibitory effect against the proliferation of the breast cancer cell lines than the leukemia cell lines.

Na *et al.* noted that the methanol extract of *S. frutescens* displayed a DNA binding suppression effect on one of the most important transcription factors called nuclear factor $\kappa$B (NF-$\kappa$B) (Na, Mossanda *et al.*, 2004), which plays a key role in immune responses and is pathologically associated with cancer, inflammation and immune defective diseases. An electrophoretic mobility shift assay (EMSA) revealed that the DNA binding activity of NF-$\kappa$B

induced by a known tumor promoter phorbol ester 12-*O*-tetradecanoylphorbol-13-acetate (TPA) was attenuated by the extract in nontumorigenic human mammary epithelial cells (MCF10A). (Na, Mossanda *et al.*, 2004). Since activation of NF-κB has been frequently observed in many cancers, and suppression of NF-κB restricts the proliferation of cancer cells, this study indicated that the inhibition of binding of NF-κB to DNA may contribute to the cancer chemopreventive effect of the plant. Interestingly, a contrary result from an in vivo test on female ICR mouse skin showed that the TPA-induced activation of NF-κB was not affected by the methanol extracts of *S. frutescens* using the same EMSA analysis (Kundu, Mossanda *et al.*, 2005). Instead, inhibitions from other TPA induced transcription factors, activator protein-1 (AP-1) and cyclic AMP response element binding protein (CREB) were observed along with the diminished expression of the key component c-Fos. While NF-κB as the upstream target needs to be verified in future studies, these results have shown that other transcription factors such as AP-1 and CREB could also be involved in the regulation of the cancer related progression.

In relation to the activation of NF-κB, the overexpression of cyclooxygenase-2 (COX-2) induced by TPA was found to be inhibited by the methanol extract in in vitro studies using MCF10A cells and in vivo studies on female ICR mouse skin. Because COX-2 overexpression is correlated to the angiogenesis and cell resistance to apoptosis, inhibition of COX-2 was thought to be beneficial for prevention and treatment of cancer (Menter, Schilsky *et al.*, 2010).

The apoptotic effect of the aqueous extract of *S. frutescens* was observed on Chinese Hamster Ovary and neoplastic cells, such as cervical carcinoma cell (Caski) and T lymphoma cell (Jurkat) (Chinkwo, 2005). The observed apoptosis was shown in the morphological change, phosphatidylserine externalization, chromatin condensation, and nuclear fragmentation of Caski and Jurkat cells. The aqueous extract induced apoptosis of 84% of Jurkat cells that was comparable

to the known apoptotic inducer staurosporine.

Reid *et al.* reported the antimutagenic effects of the dichloromethane and 90% methanol extracts of *S. frutescens* (Reid, Maes *et al.*, 2006). With the hypothesis that a plant extract with indicated antimutagenicity is possibly an anticarcinogen, the authors screened 42 South African plant extracts by Ames tests using two histidine-requiring strains of *Salmonella typhimurium* (TA98, and TA100) grown on histidine-poor medium. The dichloromethane extract of *S. frutescens* was the only one of the screened extracts out of the four traditionally used herbal treatments with indicated antimutagenic activity at the concentration of 5 mg/mL in the presence of liver S9 fraction as the metabolic activator.

Stander *et al.* investigated the influences of *S. frutescens* extracts on human tumorigenic or nontumorigenic cell lines, including cell growth, morphology, gene expression, and apoptotic effect on of human breast adenocarcinoma cell line (MCF-7) and nontumorigenic epithelial mammary gland cells (MCF-12A) exposed to the 70% ethanol extract or water extract of *S. frutescens* (Stander, Marais *et al.*, 2007; Stander, Marais *et al.*, 2009). Statistically significant cell growth inhibition, decreased cell density, as well as induced increase of apoptosis and autophagy activity were observed on both cell lines after exposure to the extract. Gene expression profiles by microarray analysis with 20173 known human 60-mer oligonucleotide probes showed that a total of 345 genes were differentially expressed in the tested MCF-7 cells under the 70% ethanol extract exposure, including genes that are importantly associated with the proliferation and apoptosis regulation, cell cycle arrest and NF-$\kappa$B activation, such as tumor necrosis factor receptor superfamily member 10a and b (DR4, DR5) gene and protein inhibitor of activated STAT1 (*PIAS1*) gene. Notably, for this tumorigenic cell line, the down-regulated *PIAS1* gene was associated with the possible apoptosis induction, while the up-regulated neutral

sphingomyelinase-2 (*SMPD3*) gene was related to the increase of ceramide level that contributes to DNA fragmentation (Stander, Marais *et al.*, 2007). Compared to the nontumorigenic cell MCF-12A, the apoptotic effects were more obvious in the tumorigenic cell line MCF-7. This study revealed the selective effect of the water extract of *S. frutescens* on nontumorigenic and nontumorigenic cells, and indicated the presence of other biologically active compounds than L-canavanine in this plant to exert activities with special selectivity on tumorigenic cells. They also suggested these compounds of interest may include our newly published sutherlandiosides A–D (Stander, Marais *et al.*, 2009).

Additional evidence of apoptosis induction activities of this plant was shown in a recent report (Vorster, Stander *et al.*, 2012). Aqueous extracts of *S. frutescens* have shown different influences on the proliferation, morphology, and cell cycle dynamics of MCF-7 and MCF-12A cell lines. Mitotic index counts showed the alterations in actively cycling cells, with a 5.27% decrease for the MCF-7 cell line, while a 0.1% increase for the MCF-12A cell line, which were also reflected in a flow cytometric analysis of cell cycle dynamics, showing an increase in $G_1$-phase of both cells (12.19% for MCF-7, 4.82% for MCF-12A) and subsequent decrease in S-phase and $G_2$/M-phase of cells. Fluorescence microscopy and flow cytometric externalization of Annexin V showed the significant induction of autophagy, and revealed an early apoptosis in both cell lines (4.68% increase in MCF-7, 0.72% increase in MCF-12A) and subsequent change to necrosis. Different from the previous studies using ethanol extracts (Stander, Marais *et al.*, 2009), the aqueous extracts didn't show S-phase cell cycle arrest, but exhibited a more likely cytostatic effect rather than cytotoxic effect (Vorster, Stander *et al.*, 2012). The different effects also suggested possible synergistic activities of multiple active components in *S. frutescens* that may act through the crosstalk of distinct mechanisms.

The apoptosis-inducing effects on a human esophageal cancer cell line (SNO) by an aqueous 70% ethanol extract of *S. frutescens* leaves and stems and 70% ethanol extract of *S. tomentosa* leaves was recently reported (Skerman, Joubert *et al.*, 2011). A non-cancerous peripheral blood mononuclear cell line (PBMCs) was selected in the experiment for comparison. *S. tomentosa* is closely related to *S. frutescens* and more regionally restricted to the Cape coastal area of South Africa. Similar chemical constituents and biological activities are expected to be present. The significantly decreased SNO cell viabilities were shown in the ATP assay under the treatment of the two extracts. These treatments also noticeably changed the morphology of the SNO cells. Morphological features that could be classified as apoptotic ones, such as shrinkage, detached and condensed spherical cell shape, membrane blebbing, and apoptotic bodies were shown, to some extent, in the treatment of these extracts at the concentration as low as 2.5 mg/mL, and the changes were similar to those of SNO cells when treated with the known apoptotic inducer cycloheximide (CHX). Necrotic like cells with noticeable debris were observed at the concentrations of 5 mg/mL for the extracts of *S. frutescens* and *S. tomentosa* respectively, with swelling shape similar to those treated with the known necrosis inducer $H_2O_2$. Further apoptosis verifications indicated a concentration-dependent apoptotic stage distribution and an intrinsic apoptotic pathway activation in a caspase-independent manner (Skerman, Joubert *et al.*, 2011).

The aforementioned studies suggest that apoptosis induction seems to be the most prominent effect associated with the anticancer activities of *S. frutescens*, which may be contributed by different chemotypes synergistically (Tai, Cheung *et al.*, 2004).

### 1.3.2. Antidiabetic and hypolipidemic effects

To address the claim that *S. frutescens* can be used for the treatment of diabetes, Sia *et al.*

gave several rational explanations that relate to its antidiabetic potential (Sia, 2004). The author's rationale was based on the activities related to pancreatic β-cell protection and insulin interferences of the known constituents such as L-canavanine and pinitol. Oxidative stress was considered to be the toxic cause for the pancreatic β-cells because of their low capacity of scavenging reactive oxygen species (ROS). In this case, as an intrinsic source of nitric oxide (NO) in the human body, L-arginine was thought to be one of the possible contributors of the NO induced oxidative injury of these sensitive cells by production of pro-inflammatory cytokines and reactive oxygen radicals in autoimmune diabetes. Structurally close to L-arginine, L-canavanine may interfere with the uptake of L-arginine and delay the onset of autoimmune diabetes. The activity of pinitol in reducing pro-inflammatory cytokines such as tumor necrosis factor-α (TNF-α) and interleukin-1β (IL-1β) was also mentioned as one contributor of β-cell protection (Tai, Cheung *et al.*, 2004). On the other hand, the activity of pinitol was attributed to the capability of exerting insulin-like effect in reducing blood sugar level (Bates, Jones *et al.*, 2000). The blood glucose concentration reduction effect of *S. frutescens* was observed comparable to the first generation of sulfonylurea type hypoglycemic drug chlorpropamide when treating streptozotocin (STZ) induced rats with 800 mg/kg of the shoot aqueous extract of *S. frutescens* and 250 mg/kg of chlorpropamide, respectively, while the effect of the extract lasted longer than that of chlorpropamide (Ojewole, 2004).

Insulin resistance, characterized by the diminished response to insulin, appears in the prediabetic state. Glucose uptake is reduced at this stage, and pancreatic β-cells secrete higher levels of insulin to maintain normal blood glucose levels (normoglycemia or euglycemia). The ultimate exhaustion of secreting insulin leads to hyperglycemia and diabetes (Tiganis, 2011).

Considering the fact that high fat feeding can induce insulin resistance, Chadwick *et al.*

used a developed high fat diet (40.08% energy per 100 grams) called OB/IR which was proved to be effective in inducing obesity, insulin resistance, and a typical prediabetic state with high serum insulin level in Wistar rats (Chadwick, Roux *et al.*, 2007). Although blood glucose levels of the rats were not changed much among treatment and control groups, this high fat feeding group, when treated with *S. frutescens* water extracts, showed a significant glucose clearance rate and a maintained serum insulin level compared to the normal diet control group, indicating a possible insulin sensitization and increased glucose uptake. The $^3$H-labeled deoxyglucose uptake test in fat, muscle, liver and kidney tissues of starved Wistar rats under anesthesia indicated significant increases of uptake in muscle and fat by treating with *S. frutescens* extracts in OB/IR diet group, while the in vitro test on rat jejunum reflected a significant inhibition on intestinal glucose uptake for the *S. frutescens* treated OB/IR diet group, and the inhibition was greater than the metformin treatment. These results indicated a hypoglycemic effect of aqueous *S. frutescens* extracts by remitting insulin resistance.

Dyslipidemia is typically shown in type 2 diabetes with elevated triglyceride levels and reduced high density lipoprotein levels (Vijayaraghavan, 2010). High lipid levels may result in insulin resistance by possible accumulation of diacylglycerol which activates protein kinase Cs (PKCs) associated with insulin signaling (Samuel, Petersen *et al.*, 2010; Dasgupta, Bhattacharya *et al.*, 2011). Insulin resistance may be induced by free fatty acids (FFAs), and then results in higher FFAs at a later stage (Imrie, Abbas *et al.*, 2010). Since high caloric food not only raises blood glucose but also plasma FFAs, a recent report by MacKenzie *et al.* showed an insulin resistance remitting effect by *S. frutescens* with proof that it decreased the plasma FFA levels in the high fat diet  (HFD) Wistar rats (MacKenzie, Koekemoer *et al.*, 2009). Plasma insulin was significantly increased in the fasting rat after feeding HFD 12 weeks, while aqueous extracts of *S. frutescens*

significantly lowered the elevated insulin levels from the second week in comparison with the HFD group, indicating similar insulin sensitivity to the normal diet group. In addition to the insulin level, plasma FFA level was significantly increased after two weeks feeding on HFD in comparison with the normal diet group, while compared to HFD group, treating with *S. frutescens* significantly decreased FFA levels even from the first week. Further examination of the levels of triglycerides, cholesterol and low-density lipoprotein/high-density lipoprotein (LDL/HDL) ratio showed that although *S. frutescens* elevated the triglyceride levels in the HFD rats, it exhibited reduction effects on total cholesterol level and LDL/HDL ratio, but this effect only appeared in the long term treatment (after 12 weeks). Interestingly, the reduced FFAs level was significantly lower than the normal diet group after 12 weeks feeding, which is similar to thiazolidinedione type antidiabetic drugs that act on peroxisome proliferator-activated receptor $\gamma$ (PPAR$_\gamma$) to inhibit adipogenic proliferation. Since the effect on elevating triglyceride levels of the extracts was not in accord with that of PPAR$_\gamma$, it seems that a new mode of action may be involved for the antidiabetic effects of *S. frutescens*. Continued work by MacKenzie *et al.* using an insulin resistant (IR) rat model showed a decrease in insulin, FFA and triglyceride levels in blood plasma, liver skeletal muscle and adipose tissues when feeding with HFD and *S. frutescens* (MacKenzie, Koekemoer *et al.*, 2012). The 3 T3-L1 preadipocytes model showed that *S. frutescens* led to a decrease in triglyceride accumulation, and an increase of glucose consumption (glycolysis) and lactate production, indicating that *S. frutescens* could have a direct inhibitory interaction with mitochondrial activity that is possibly caused by the sustained mitochondrial uncoupling in adipose tissue. The unobserved triglyceride accumulation in the treatment of *S. frutescens* for 3 T3-L1 preadipocytes, suggested the mitochondrial dysfunction is unlikely to be related to the glycolytic flux. These studies revealed the insulin resistance prevention activity and insulin

sensitization activity of *S. frutescens* via the modulation of fatty acid biosynthesis.

### 1.3.3.  Anti-oxidant and anti-inflammatory effects

Miscellaneous anti-inflammatory applications of *S. frutescens* have a broad relevance for indigenous people. The anticancer and antidiabetic activities of this plant are to some extent correlated to the anti-oxidant or anti-inflammatory effect.

Tai *et al.* observed that treatment with the ethanolic extract of *S. frutescens* did not show nitric oxide (NO) production suppression or lipopolysaccharide (LPS) induced NO production suppression in RAW 264.7 cells (Tai, Cheung *et al.*, 2004), nor did it display significant inhibition of pro-inflammation cytokines such as IL-1β and TNF-α mRNA, but it did exhibit significant hydroxy free radical scavenging activity in the "Trolox equivalent anti-oxidant capacity (TEAC) assay" in comparison with the potent anti-oxidant agent Trolox (6-hydroxy-2,5,7,8-tetramethylchroman-2-carboxylic acid), as estimated by the equivalency of 0.5 μL of the *Sutherlandia* extract versus 10 μM Trolox. The anti-oxidant potential of the hot water extract of *S. frutescens* was also observed by testing its inhibitory effect on the reactive oxygen species production by L-formyl-L-methionyl-L-leucyl-L-phenylalanine (FMLP) activated human neutrophils, which presented a detectable inhibitory concentration at 10 μg/mL (Fernandes, Cromarty *et al.*, 2004). Moreover, the result was supported by the superoxide and hydrogen peroxide scavenging activity in the cell free system, showing as low as 10 μg/mL extract concentration for inhibition of superoxide anion generation in xanthine/xanthine oxidase system, and as low as 2.5 μg/mL extract concentration for the inhibition of chemiluminescence responded in the hydrogen peroxide/horseradish peroxidase system (Fernandes, Cromarty *et al.*, 2004). Katerere *et al.* reported the anti-oxidant activity of the leaf extract of *S. frutescens* using an assay to

test the scavenging ability of 2,2-diphenylpicrylhydrazyl (DPPH) radical (Katerere and Eloff, 2005). The major activities were shown in acetone and ethyl acetate fractions.

The anti-inflammation potential of the methanol extract of *S. frutescens* was reported using TPA-induced COX-2 expression in MCF10A cells in vitro and in mouse skin in vivo as an inflammation model (Na, Mossanda *et al.*, 2004). The inhibition of the induced COX-2 were postulated as the suppression of DNA binding of NF-κB since the EMSA results indicated that the *S. frutescens* extract attenuated the DNA binding activity to NF-κB in the TPA-induced MCF10A cells. Although in the in vivo ICR mouse skin test, the *S. frutescens* extract didn't show the inhibition on TPA-induced NF-κB activation (Kundu, Mossanda *et al.*, 2005), they did find that other transcription factors such as AP-1 that modulate the COX-2 were inhibited. In addition, although the *S. frutescens* extract didn't show suppression on TPA-induced phosphorylation of ERK1/2, an upstream kinase in the mitogen-activated protein kinases (MAPKs) pathway that regulates the TPA-induced COX-2 expression, inhibiting the phosphorylation of its substrate Elk-1 indicated that the catalytic activity of ERK was suppressed.

### 1.3.4. Anti-infective and immunomodulatory effects

The antibacterial effects of *S. frutescens* have long been implied in the indigenous uses such as dysentery and wounds washing. Katerere *et al.* first reported that the hexane extracts of *S. frutescens* showed antibacterial activity against *Staphylococcus aureus*, *Enterococcus faecalis* and *Escherichia coli* with minimum inhibitory concentrations (MICs) of 0.31, 1.25 and 2.50 mg/mL respectively (Katerere and Eloff, 2005).

Despite the long history of the plant's use as an antimicrobial, *S. frutescens* is notable for the treatment of HIV/AIDS in sub-Saharan Africa, since it has been recommended by the South

African Ministry of Health for HIV management (Mills, Cooper *et al.*, 2005). The known constituents may contribute to the anti-HIV activity. L-Canavanine was suggested to have antiviral activities against retroviruses such as HIV (Mills, Cooper *et al.*, 2005). D-Pinitol showed wasting alleviation potential in AIDS patients (Mills, Cooper *et al.*, 2005). Other anecdotal evidence includes weight gaining, CD4 (cluster of differentiation 4) count improving, virus load decreasing, and mood improving effects for AIDS patients (Harnett, Oosthuizen *et al.*, 2005).

The anti-HIV potential of *S. frutescens* was tested in a study using extracts obtained by different solvents including water, acetone, methanol, ethanol, and dichloromethane (Harnett, Oosthuizen *et al.*, 2005). Although the extracts didn't show significant inhibitions (>50% inhibition) on HIV-II protease at the concentration of 0.2 mg/mL, the HIV-I protease still needs to be tested to exclude the protease target. Promisingly, several extracts of leaves and flowers showed inhibitory activity on reverse transcriptase, with the water extract of leaves being the most active. Similar inhibitory activity retained when sulphated polysaccharides were removed by ethanol precipitation from the aqueous extract of the leaves, indicating that the activity may not be attributable to polysaccharides, which are known to have multiple activities including a universal inhibitory effect on viruses. Addition of bovine serum albumin (BSA) into the test system did reduce the effect on reverse transcriptase, however the retention of around 30% inhibitory activity suggested that tannins are not the only active component that act on the reverse transcriptase. These results led to the conclusion that chemotypes other than tannins and polysaccharides may contribute to the inhibitory activity on reverse transcriptase. In addition to the two popular targets in HIV, most of the *S. frutescens* extracts except the aqueous flower extract showed significant inhibitions on β-glucuronidase. Moreover, the inhibition of glycohydrolases (such as β-glucuronidase) could also contribute to the reduction of HIV virion infectivity (Harnett,

Oosthuizen *et al.*, 2005).

One problem related to drug-herb interaction was noted during the co-administration of the plant material *S. frutescens* and the antiretroviral agents, which caused the loss of therapeutic efficacy due to the potential induction of pregnane xenobiotic receptor (PXR), an orphan nuclear receptor regulating the expression of drug metabolizing enzyme CYP3A4 (Mills, Cooper *et al.*, 2005). Minocha *et al.* demonstrated an induction of the rodent CYP3A by administration of *S. frutescens* extracts for five days caused a raised hepatic clearance of the antiviral agent nevirapine. The inductive components were unlikely to be our newly isolated sutherlandiosides A–D and sutherlandins A–D (Minocha, Mandava *et al.*, 2011). Müller *et al.* found that the *S. frutescens* components influence the absorption and metabolism of a protease inhibitor, atazanavir (Muller, Patnala *et al.*, 2012). The triterpenoid-containing fraction showed an increased atazanavir accumulation effect in human intestinal epithelial cells Caco-2, yet an enhanced atazanavir metabolism by human liver microsomes.

### 1.3.5. Effects on nervous and endocrine systems

*S. frutescens* has been traditionally used for the treatment of neurologically related maladies, including stress, depression, anxiety, seizure, epilepsy, and convulsions. There has been a growing interest in the psychological benefits of the plant in recent years.

The antistress effect was first shown when testing the inhibitory effect of the plant on elevated circulating glucocorticoids. Chronic stress is associated with high levels of glucocorticoids (Prevoo, Smith *et al.*, 2004). The elevation of corticosterone (a major glucocorticoid) of the rats under chronic intermittent immobilization stress was significantly decreased in the *S. frutescens* extract treatment group.

Cytochrome P450 enzymes are involved in the biosynthesis of glucocorticoids. Treatment of ovine adrenocortical microsomes and mitochondria with the *S. frutescens* extracts showed that the binding of cytochrome P450 21-hydroxylase (CYP21), cytochrome P450 11β-hydroxylase (CYP11B1), and cytochrome P450 17-hydroxylase (CYP17) with their substrates such as pregnenolone and progesterone were repressed (Figure 1-1). The inhibition of the conversion of pregnenolone and progesterone was also observed, with a more potent effect by the chloroform extract compared to that of the methanol extract. A further investigation showed that the binding ability of progesterone to CYP17 or CYP21 was notably inhibited by the aqueous and methanol extracts as compared to that of pregnenolone (Prevoo, Swart *et al.*, 2008). The triterpenoid fraction showed significant inhibition on the enzyme-substrate binding between microsomal enzymes and pregnenolone or progesterone. A "type II inhibitor-induced difference spectrum" induced by the triterpenoid fraction was observed, indicating that triterpenoids may bind directly to the heme iron in the active site of the enzymes. Moreover, the metabolism of pregnenolone or progesterone in adrenocortical microsomes was shown to be suppressed by the aqueous extract of *S. frutescens*, which may result in a reduced production of circulating glucocorticoids. This inhibition of the aqueous extract was more significant on CYP21 as compared to CYP17. In COS 1 cells expressing ovine CYP17, the aqueous *S. frutescens* extract limited the metabolism of pregnenolone and progesterone differently, showing a greater inhibitory effect on progesterone than pregnenolone. It was suggested that several active components were involved in the inhibition for the activity of the aqueous extracts (Prevoo, Swart *et al.*, 2008).
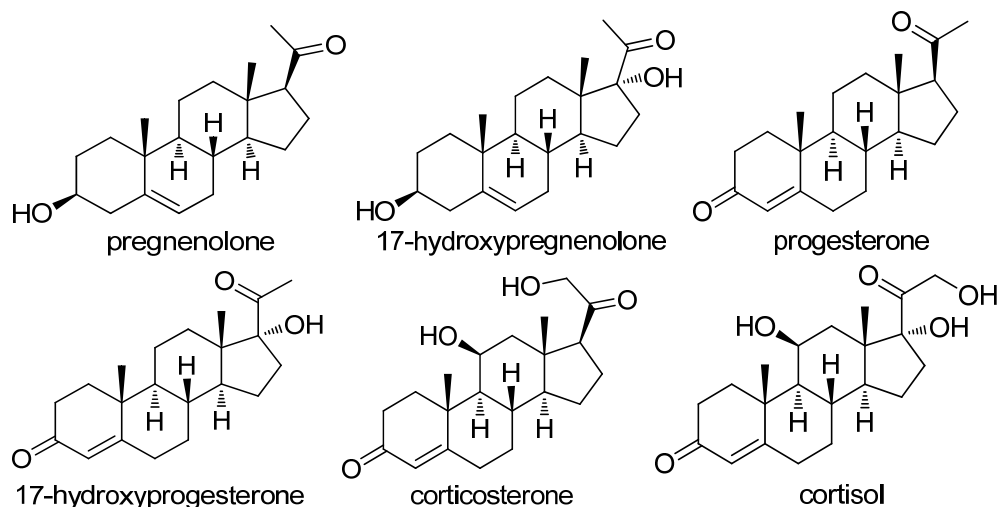
Figure 1-1.  Structures of several glucocorticoids and their precursors.

The anticonvulsant property of the aqueous shoot extract of *S. frutescens* was evidenced in the Ojewole's investigation using drug induced seizures mice models (Ojewole, 2008). Seizures induced by convulsant agents in male *Balb C* mice (*Mus domesticus*) were attenuated by delaying the onset or reducing the duration of the symptoms in the experiment, showing substantial inhibition in the pentylenetetrazole (PTZ) and picrotoxin (PCT) induced mice models and weak inhibition in the bicuculline (BCL) induced mice model. The inhibitory effects observed in the PTZ and PCT induced models were explained as direct or indirect abatement of the defective GABAergic neurotransmission. Although GABA contained in this plant might account for the contribution to its antiseizure effect, the mechanisms were not established yet.

## 1.4.  Toxicity studies

Although products containing *S. frutescens* have been widely used in Southern Africa for

more than a hundred years and were claimed to be safe by traditional healers, the toxicity is a potential concern since L-canavanine was identified in this plant. This compound has long been known as a toxic component in many legume plants (Rosenthal, 1977).

A toxicity study of the *S. frutescens* leaf powder was performed on 16 vervet monkeys (*Chlorocebus aethiops*). No toxicity or side effect was observed at the maximal dose of 81 mg/kg body weight, which was considered to be equivalent to1.62 mg/kg body weight of the water soluble plant extract. (Fernandes, Cromarty *et al.*, 2004). This report from the Medical Research Council of South Africa didn't contain experimental data.

A randomized, double-blind, placebo-controlled human clinical trial was conducted on 25 healthy adult participants in South Africa recently to investigate the safety of the capsules of the leaf powder of *S. frutescens* (Johnson, Syce *et al.*, 2007). The results showed that taking the capsules twice daily (800 mg/day) for three month did not show significant adverse effects, nor did it show significant differences of vital physical hematological, biological, and endocrine parameter changes in the treatment group in comparison to the control group. While each capsule contains about 600 µg of L-canavanine that is equivalent to 1.2 mg consumption per day, it was not possible to detect this known toxic component in the plasma of participants. Other differences such as improved appetite and higher platelet counts were shown in the treatment group, but they were not clinically relevant. It was concluded that the administration of 800 mg per day of the *Sutherlandia* leaf powder was tolerated by healthy adults.


**1.5. Previous phytochemical studies of *S. frutescens* and related bioactivity investigations**

### 1.5.1. Free amino acids

Some free amino acids act as the starting units in the biosynthesis of a number of secondary metabolites, including flavonoids, alkaloids, cyanogenic glycosides, and phenolic compounds. *S. frutescens* has been shown to contain high amounts of free standard amino acids such as L-leucine, L-glutamine, L-phenylalanine, L-proline, L-valine, L-arginine as well as the non-standard amino acids such as L-canavanine.

By testing free amino acid contents in the tablets of *S. frutescens*, which was claimed by the manufacturer, PhytoNova (Cape Town, South Africa), to contain 300 mg of raw herb powder in a 700 mg tablet, Tai *et al.* quantified the contents of L-arginine, L-canavanine, and GABA as 3.0, 3.0, and 0.4 mg/g of the tablet, respectively using HPLC/MS methods (Tai, Cheung *et al.*, 2004). By citing a report published in South Africa, Mills *et al.* pointed out that 30-40 mg/g of L-canavanine and 14 mg/g of GABA were contained in the dried leaves of *S. frutescens*. (Mills, Cooper *et al.*, 2005). According to unpublished data from a research group in South Africa (Van Wyk and Albrecht, 2008), the commercial *S. frutescens* leaves obtained from PhytoNova contained a high level of free amino acids, e.g., 1.6-35.0 mg/g of asparagine, 0.7-7.5 mg/g of proline, and 0.5-6.7 mg/g of arginine. The non-standard amino acid L-canavanine was found ranging from 1.3-3.1 mg/g. A study on the contents of biological active compounds in the "in vitro" and "field" grown leaves, as well as the seeds of *S. frutescens* was performed by HPLC and GC analysis (Shaik, Singh *et al.*, 2011). It showed that 7.29, 3.48, and 1.69 mg/g of GABA, 7.08, 0.35, and 0.02 mg/g of arginine and 0.55, 0.08, and 0.37 mg/g of L-canavanine were contained in the in vitro leaves, field leaves, and seeds, respectively.

Carratù *et al.* determined amino acids in a series of botanicals and their preparations, including *S. frutescens* by an automatic method using precolumn derivatization with

fluorenylmethyl chloroformate (FMOC-Cl) and subsequent separation and quantification of the 22 amino acid derivatives by HPLC analysis using fluorescence and ultraviolet detectors (Carratu, Boniglia *et al.*, 2008). Non-standard amino acids such as ornithine, GABA, and hydroxytryptophan were included, but L-canavanine was not measured. The results showed that *S. frutescens* contains total free amino acids (TFAA) of 7.336 g per 100 g sample extracts "on a wet weight basis", with high levels of leucine, glutamine, phenylalanine, proline, aspartic acid, valine, glutamic acid, which are higher than 500 mg contents equivalent in 100 g sample extracts "on a wet weight basis".  Both arginine and GABA were determined as around 160 mg per 100g sample extracts "on a wet weight basis" (Table 1-1).

Table 1-1.  Reported contents of free amino acids in the dried *S. frutescens* on a wet weight basis.

| free amino acids | content /100g | free amino acids | content /100g |
|---|---|---|---|
| Leucine | 1019 mg | Tyrosine | 292 mg |
| Glutamine | 832 mg | Threonine | 278 mg |
| Phenylalanine | 616 mg | Histidine | 196 mg |
| Proline | 599 mg | GABA | 166 mg |
| Aspartic acid | 572 mg | Arginine | 163 mg |
| Valine | 529 mg | Asparagine | 114 mg |
| Glutamic acid | 500 mg | Lysine | 78 mg |
| Isoleucine | 392 mg | Ornithine | 48 mg |
| Glycine | 324 mg | Alanine | <1 mg |
| Serine | 309 mg | Tryptophan | <1 mg |
| Methionine | 308 mg | Hydroxytryptophan | <1 mg |

*adapted from Carratù *et al.* (Carratu, Boniglia *et al.*, 2008).

1.5.1.1. L-Arginine

L-Arginine was considered to be important in *S. frutescens* because of its detoxifying effect for L-canavanine. Usually contained in certain amounts in many plant seeds, L-arginine was considered to be a nitrogen source for plant growth. Due to the basic property and lone-pair

electrons on nitrogen, the positively charged guanidinium group plays an important role in many physiological activities.

Incorporation of arginine is under the catalysis of arginine-tRNA ligase (EC 6.1.1.19) (also called arginyl-tRNA synthetase). In many plant species, the recognition domain of this enzyme is not specific, causing the misincorporation of its analog such as L-canavanine into the protein synthesis, forming canavanyl proteins.
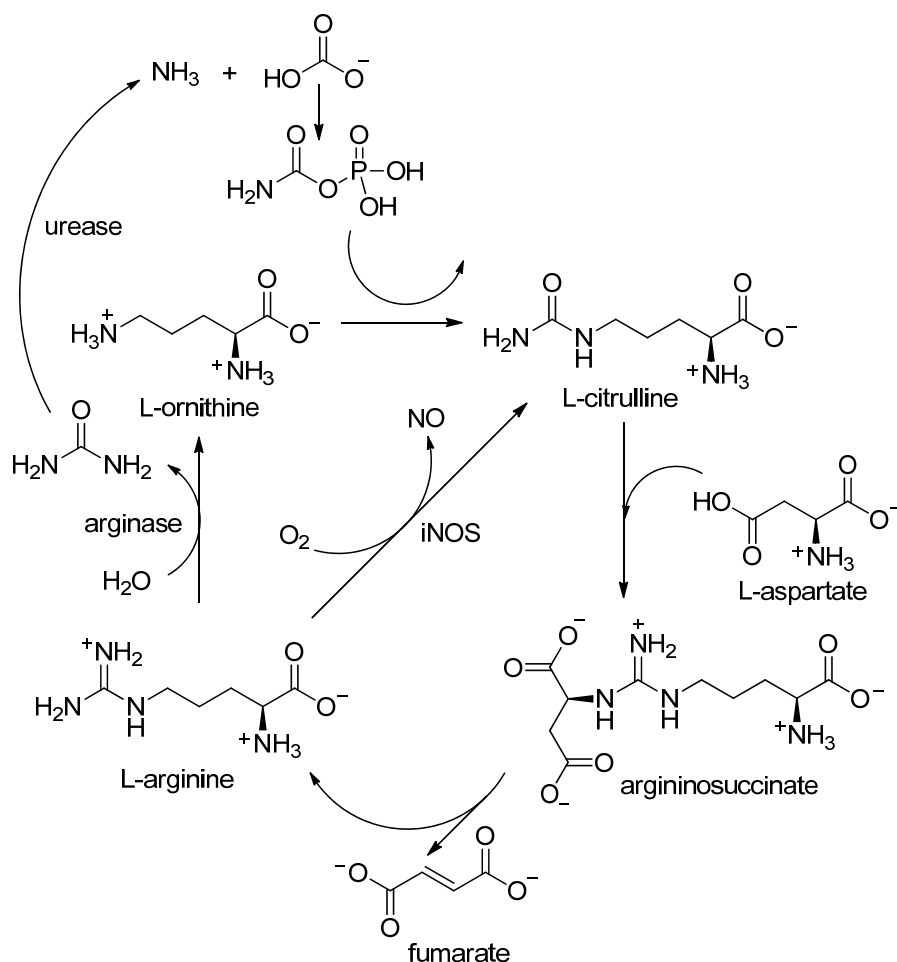


Figure 1-2. Mobilization of ammonia and nitric oxide formation by nitric oxide synthases shown in the urea cycle.

Adapted from Morris SM Jr. (Morris, 2002)

The nitrogen sequestered in the guanidine group can be mobilized by means of an

arginase-mediated hydrolytic formation of urea and subsequent urease catalyzed formation of ammonia (Figure 1-2).

L-Arginine is a source of nitric oxide (NO) in the human body. Arginine-derived nitric oxide synthesis is catalyzed by nitric oxide synthases (NOSs, EC 1.14.13.39) (Figure 1-2).

Therefore, arginine plays a series of physiological activities in the body. Inducible isoform of NOS (iNOS) is related to immune responses (Torre, 2006). Excessively induced NO production is destructive to virus infected tissues through nonspecific oxidative damage by the generation of oxygen radicals from peroxynitrite (ONOO$^-$) (Torre, 2006).

$$\text{L-arginine} + 3/2\ NADPH + H^+ + 2\ O_2 = \text{L-citrulline} + NO + 3/2\ NADP^+$$
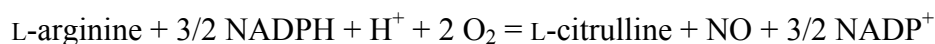
1.5.1.2. L-Canavanine


L-canavanine

L-canaline
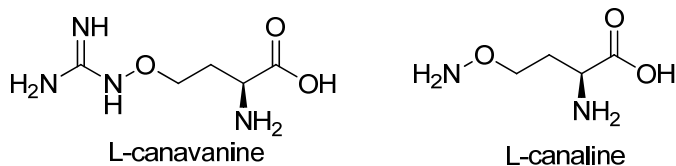
L-Canavanine [L-2-amino-4-(guanidinoxy) butyric acid] is a naturally occurring non-standard amino acid present in beans, clover, onions, seeds, and sprouts of alfalfa. It was first isolated from jack bean, *Canavalia ensiformis* (Kitagawa, 1930), and accounts for up to 5% dry weight of the jack bean seeds (Rosenthal, 1970). With the growth of the germinating seeds, the content of L-canavanine rapidly declines. Therefore, it was thought to be a nitrogen storage metabolite (Rosenthal, 1977). While arginine bears the same nitrogen content per molecule as canavanine, more roles were indicated for the production of this metabolite in plants. Possessing

insecticidal (Janzen, 1971) and bacteriostatic properties (Volcani and Snell, 1948), it functions as a key element of protective allelochemicals (Rosenthal, 1977). L-Canavanine was considered as an anticancer agent in development (Bence, Worthen et al., 2002). It showed antiproliferative and cytotoxic effects against the peripheral blood mononucleocytes, and also showed an enhanced apoptotic effect induced by arginine deprivation (Vynnytska, Mayevska et al., 2011).

The structure of L-canavanine is similar to L-arginine. The oxyguanidino group in L-canavanine is less basic compared to the guanidino group in L-arginine. The toxicity of L-canavanine was attributed to the misincorporation into nascent proteins by arginyl tRNA synthetase (tRNA$^{Arg}$), resulting in the aberrant canavanyl protein production (Bence and Crooks, 2003).

Interestingly, the reported content of L-canavanine in *S. frutescens* varies considerably as described above (Tai, Cheung et al., 2004; Mills, Cooper et al., 2005; Shaik, Singh et al., 2011). Therefore, the toxicity of the plant due to the presence of this compound needs further investigation.

1.5.1.3.  GABA



γ-aminobutyric acid
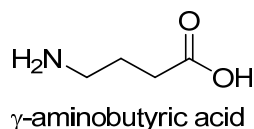
γ-Aminobutyric acid (GABA), as the most abundant inhibitory neurotransmitter in the mammalian central nervous system (CNS), has diverse psychological functions (Henschel, Gipson et al., 2008). GABAergic neurons account for 20% total neurons in the body, and play an

important role in the development and functions of the nervous system. GABAergic drugs (e.g., barbiturates and diazepines) are commonly related to the physiological and pathological functions of the CNS, such as anesthetic, sedative, antiepileptic, and anticonvulsive effects.

The content of GABA in *S. frutescens* was reported in a wide range as described above (Tai, Cheung *et al.*, 2004; Mills, Cooper *et al.*, 2005; Carratu, Boniglia *et al.*, 2008; Shaik, Singh *et al.*, 2011). In addition, it varies in different parts of the plant (Shaik, Singh *et al.*, 2011).

### 1.5.2. Cyclitol and saccharides

The presence of pinitol ((1*R*,2*S*,3*R*,4*S*,5*S*,6*S*)-6-methoxycyclohexane-1,2,3,4,5-pentol, or 3-*O*-methyl-D-chiroinositol), inositol, and monosaccharides in *S. frutescens* was confirmed by Tai *et al.* using an LC/MS method with ESI and negative detection mode, and pinitol was quantified at the "high ppm range" (Tai, Cheung *et al.*, 2004). High levels of undefined polysaccharides were also detected in the leaves of *S. frutescens* (Van Wyk and Albrecht, 2008).

The presence of pinitol (Mills, Cooper *et al.*, 2005) in *S. frutescens* was also reported in the theses at the University of the Free State and University of Johannesburg in South Africa, claiming a level of 14 mg/g of dry weight in the leaves (Van Wyk and Albrecht, 2008). It was considered as the most abundant secondary metabolite in the plant leaves, with 14.75 and 18.17 mg/g in the in vitro cultured and field leaves of *S. frutescens*, respectively (Shaik, Singh *et al.*, 2011).
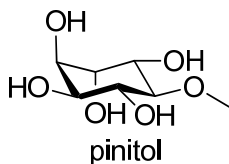


pinitol

Pinitol has been proved to have an insulin-like effect (Bates, Jones *et al.*, 2000). It exhibited protective effect against oxidative stress and elevated pro-inflammatory cytokines induced in streptozotocin-induced diabetic rat models (Sivakumar, Palsamy *et al.*, 2010). It also showed an inflammation inhibitory effect in the carrageenan-induced paw edema in rats (Singh, Pandey *et al.*, 2001). 10 nM pinitol inhibited NO production in LPS-stimulated RAW cells, indicating its anti-oxidant activity (Tai, Cheung *et al.*, 2004). Its targeting the NF-κB activation pathway is also suggested to be related to anti-inflammatory effects and benefits for the inhibition of cancer cell proliferation (Sethi, Ahn *et al.*, 2008).

### 1.5.3. Flavonoids

Flavonoids were found to be present in *S. frutescens* (Van Wyk and Albrecht, 2008). However, no report showed the identification of this type of constituents until our investigation leading to the identification of four new flavonol glycosides (Fu, Li *et al.*, 2010).

A quantitative analysis of components present in different *L. frutescens* extracts showed total flavonoid contents of 7.18, 5.55, and 1.87 mg of rutin equivalents in each gram of dried in vitro cultured leaves, field leaves, and seeds of the plant, respectively (Shaik, Singh *et al.*, 2011).

### 1.5.4. Phenolics

A qualitative analysis by Shaik *et al.* indicated the presence of tannins in the in vitro cultured and field leaves and seeds of *L. frutescens* in addition to flavonoids (Shaik, Singh *et al.*, 2011). Phenolic compounds represent the second highest content of the secondary metabolites next to saponins. The total phenolic compounds were found to be 30.18 mg of gallic acid equivalents in each gram of the in vitro cultured leaves, 15.09 mg/g in the field leaves, and 4.89

mg/g in the seeds, respectively.

### 1.5.5. Triterpene glycosides

Triterpene glycosides (or saponins) were detected in this plant but not identified before our investigation that is described in Chapter 2 (Fu, Li *et al.*, 2008). These compounds represents the major secondary metabolites in *L. frutescens*, with 53.34, 60.00 and 6.00 mg per gram of the in vitro cultured leaves, field leaves, and seeds, respectively (Shaik, Singh *et al.*, 2011). Cardiac glycosides were also found in *L. frutescens* by a Keller-Kiliani test (Shaik, Singh *et al.*, 2011).

One of these components called SU1 was isolated from *S. frutescens* (Sia, 2004), but its structure was not determined. This compound was later proved to be identical (Olivier, 2009) to sutherlandioside B  that is described in Chapter 2 (Fu, Li *et al.*, 2008),
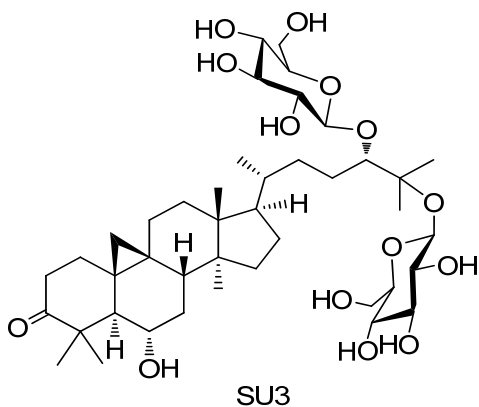


Figure 1-3.  The structure of triterpene diglycoside SU3 from *L. frutescens*.

Olivier *et al.* also reported the isolation of compound SU2 (Olivier, 2009) which is identical to sutherlandioside A that is described in Chapter 2, and the identification of a new triterpene diglycoside named SU3 (Figure 1-3).

26

### 1.5.6. Phytosterols, parabens, fatty acids, and others

GC/MS studies by Tai *et al.* found that γ-sitosterol [(3β, 24*S*)-stigmast-5-en-3-ol], stigmast-4-en-3-one, methyl, and propyl parabens, hexadecanoic acid, and long chain fatty alcohols were contained in the dichloromethane extract of the tablets made from the dried leaf powder by PhytoNova, and methyl and propyl parabens were found in the methanol/water ( 4/1 ) extract of the tablets (Tai, Cheung *et al.*, 2004).
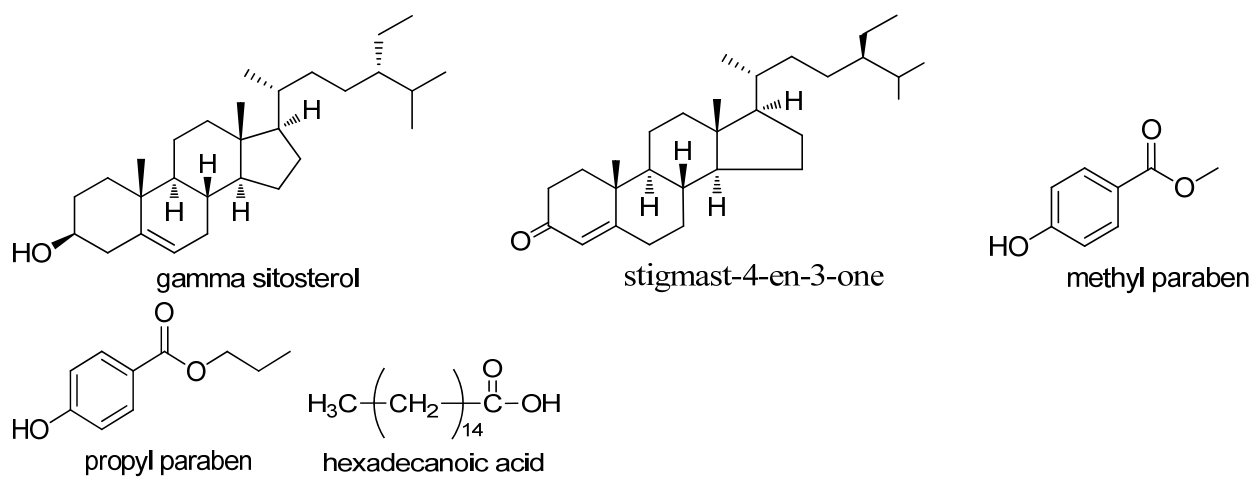


Figure 1-4.  Structures of phytosterols, parabens, and fatty acids from *S. frutescens*.

# CHAPTER 2

## ISOLATION AND STRUCTURE ELUCIDATION OF TRITERPENE AND FLAVONOL GLYCOSIDES FROM *S. FRUTESCENS*

### 2.1. Introduction

The indigenous South African plant *S. frutescens* is known as a multipurpose medicinal plant and has been used by traditional healers to treat cancer, diabetes, inflammation, bacterial infection, AIDS, depression, anxiety, seizure, convulsion, and many other diseases. Various commercial products of the plant are on the market as dietary supplements. As described in Chapter 1, limited literature data are available regarding the chemical constituents of this plant, although a number of biological/pharmacological studies have been done using the crude extracts of the plant material. In order to have a better understanding of the biological activities and toxicities of this plant, and establish authentication and standardization methods for quality control of the commercial products derived from this plant, the primary step is to investigate its chemical constituents. In this chapter, the isolation and structure elucidation of eight new triterpene glycosides and four new flavonol glycosides will be described.

### 2.2. Results and discussion

A total of 12 new compounds (**1-12**) were obtained from the methanol extract of the leaves

of *S. frutescens* in isolated yields of 0.0124, 0.1952, 0.0289, 0.0140, 0.0198, 0.0115, 0.0375, 0.0345, 0.0024, 0.0004, 0.0018, 0.0033 % of the dried plant material, respectively, by repetitive chromatographic techniques as described in the experimental section. Sutherlandiosides A–D (**1**–**4**) (Figure 2-1) represent the major triterpene glycosides. Sutherlandins A–D (**5**–**8**) (Figure 2-27) are the major flavonol glycosides. Sutherlandiosides E–H (**9**–**12**) (Figure 2-45) are minor triterpene glycosides. The structure elucidation of these compounds involving spectroscopic and chemical methods as well as X-ray crystallography is described below.

## 2.2.1.  Structure elucidation of major triterpene glycosides
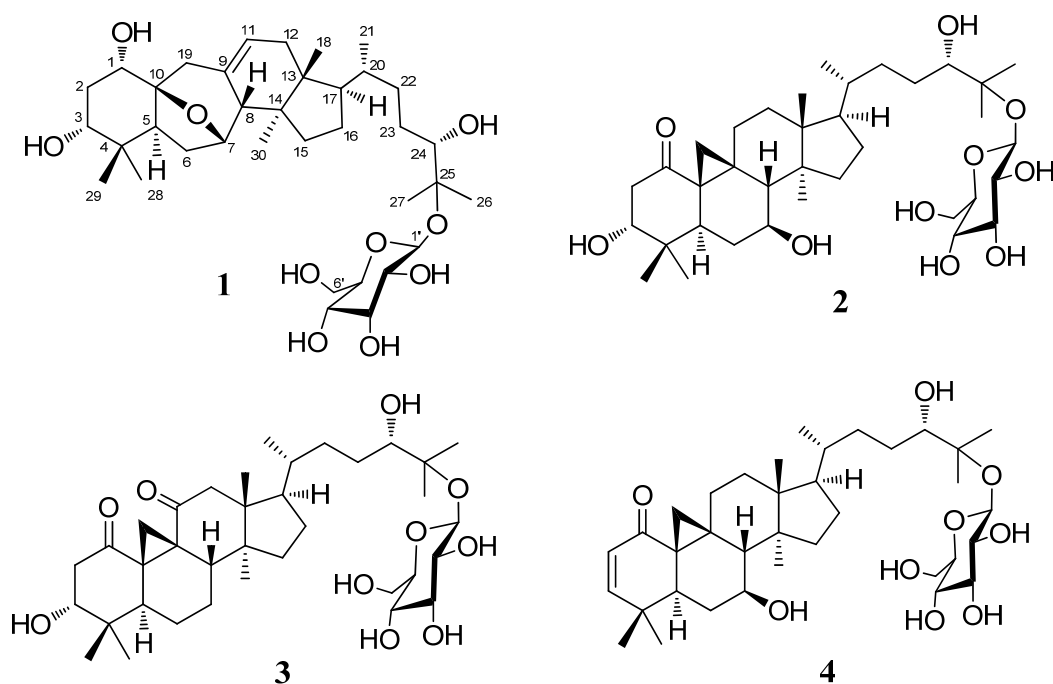


Figure 2-1.  Structures of isolated major triterpene glycosides from *S. frutescens*.

29

## 2.2.1.1. Sutherlandioside A (1)
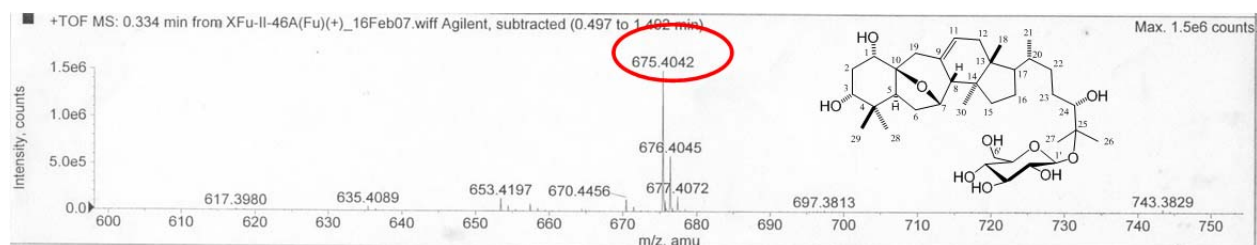


Figure 2-2. HRESIMS spectrum of compound **1**.
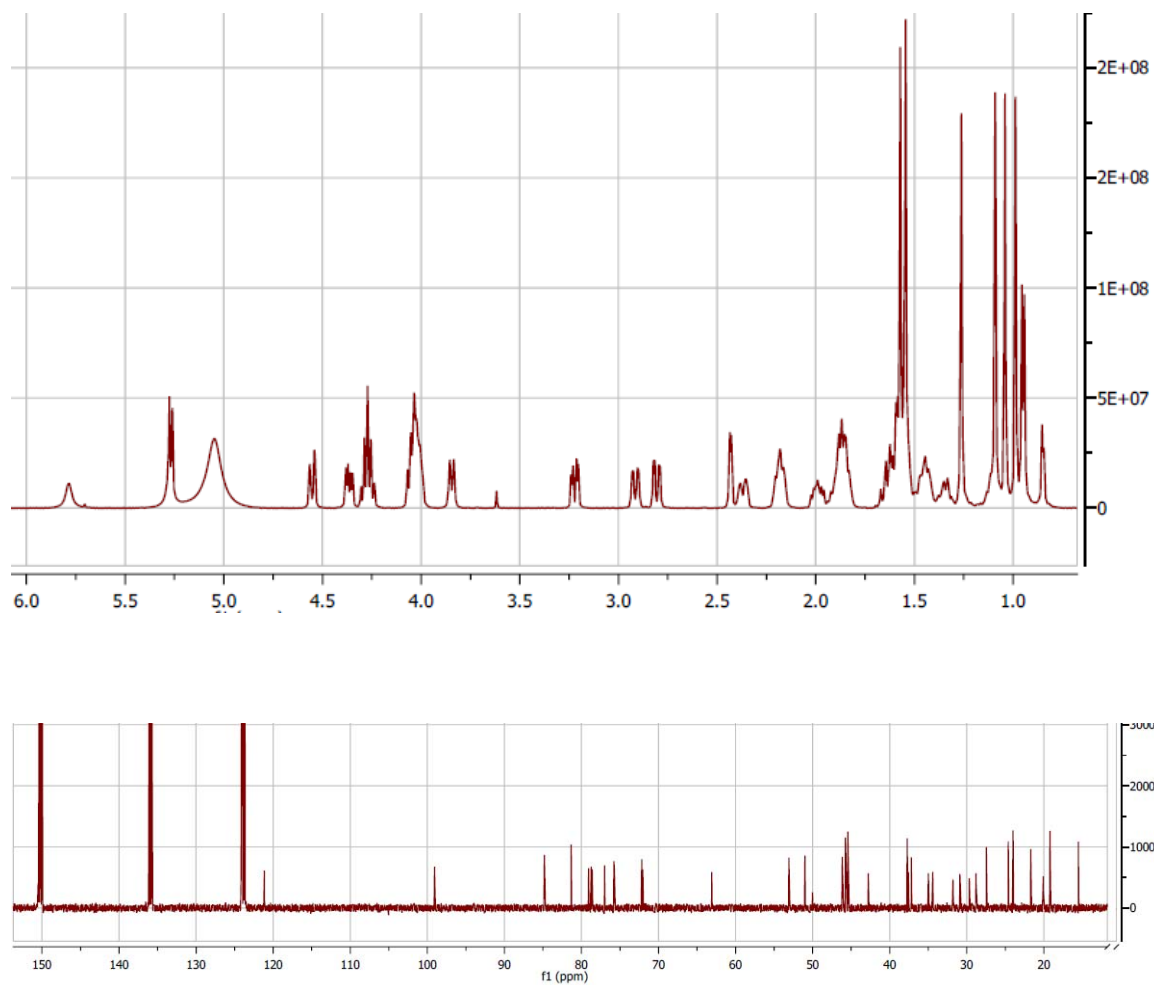


Figure 2-3. $^1$H and $^{13}$C NMR spectra of compound **1** in pyridine-$d_5$.

The molecular formula of sutherlandioside A (**1**) was determined as $C_{36}H_{60}O_{10}$ by HRESIMS which provided a pseudomolecular ion peak at *m/z* 675.4042 [M + Na]$^+$ (Figure 2-2), in conjunction with its $^{13}C$ NMR spectrum presenting 36 resonances. A DEPT NMR experiment permitted differentiation of these 36 resonances into seven methyl, nine methylene, 14 methine, and six quaternary carbons, of which 30 were attributed to a triterpene skeleton and six to a β-glucopyranosyl moiety (Figure 2-3) (Bedir, 2001).

The β configuration of the glucopyranose is evident by its anomeric proton resonance at $\delta_H$ 5.24 (d, *J* = 7.6 Hz, H-1′) in the $^1H$ NMR spectrum (Table 2-1). Regarding the aglycone moiety, typical resonances include six tertiary methyls at $\delta_{H/C}$ 0.71/15.5, 1.57/21.7, 1.54/24.6, 1.17/27.4, 1.03/24.0, 0.75/20.0, one secondary methyl at $\delta_{H/C}$ 0.95/19.2, four oxygenated methines at $\delta_{H/C}$ 3.83 (br, s)/77.0, 3.86 (d, *J* = 9.7 Hz)/78.7, 4.28 (m)/72.0, 4.30 (m)/75.8, two oxygenated quaternary carbons at $\delta_C$ 81.3 and 84.8, and one double bond at $\delta_C$ 135.9 (C) and 121.1 (CH), indicating a polyhydroxylated cycloartane-like triterpene skeleton (Calis, Zor *et al.*, 1996; Bedir, 2001; Ali, Khan *et al.*, 2007).

Unlike most cycloartane compounds that show characteristic proton resonances for H-19 in the extremely upfield region up to $\delta_H$ 0.3 (Ali, Khan *et al.*, 2007), the presence of a significantly downfield shifted H-19 at $\delta_H$ 2.69 and 2.89 with a large coupling constant of 16.1 Hz indicated that **1** is more likely to possess a 9,10-*seco*-cycloartane skeleton (Ali, Khan *et al.*, 2007).

The chemical shifts of a set of carbon resonances, corresponding to the side chain at C-17 (from C-20 to C-27) and the β-glucopyranosyl moiety, are identical to those of known glycosides that possess a 24*S*,25-dihydroxy side chain in which the β-D-glucopyranosyl moiety is attached to the tertiary 25-hydroxy group (Calis, Zor *et al.*, 1996). The location of the hydroxy groups at C-1 and C-3 on the A-ring was indicated by a DQF-COSY experiment showing a coupling network

from H-1 → H-2 → H-3 (Figure 2-7). In the HMBC spectrum of **1**, the characteristic H-19 at $\delta_H$ 2.89 correlated with one oxygenated carbon at $\delta_C$ 84.8 (C), two olefinic carbons at $\delta_C$ 135.9 (C) and 121.1 (CH), and a methine at $\delta_C$ 53.1 that was assumed to be C-8 (Figure 2-5). This indicated that C-10 ($\delta_C$ 84.8) might be oxygenated and a double bond located between C-9 and C-11 (Figure 2-6). The remaining oxygenated tertiary carbon at $\delta_C$ 75.8 correlated with the proton at $\delta_H$ 4.30 in the HMQC spectrum (Figure 2-4). This proton showed cross peaks with an olefinic carbon at $\delta_C$ 135.9 (C) and the quaternary carbon at $\delta_C$ 84.8 (C-10) in the HMBC spectrum (Figure 2-5), establishing the location of an oxygen atom at C-7 on the B-ring, and also the formation of an oxygen bridge between C-7 and C-10 (Figure 2-6). The presence of the epoxy group, instead of free hydroxy groups at C-7 and C-10, is consistent with the HRESIMS data (Figure 2-2). All other HMBC correlations that provide key C-C connectivity information support the two-dimensional structure of compound **1**.
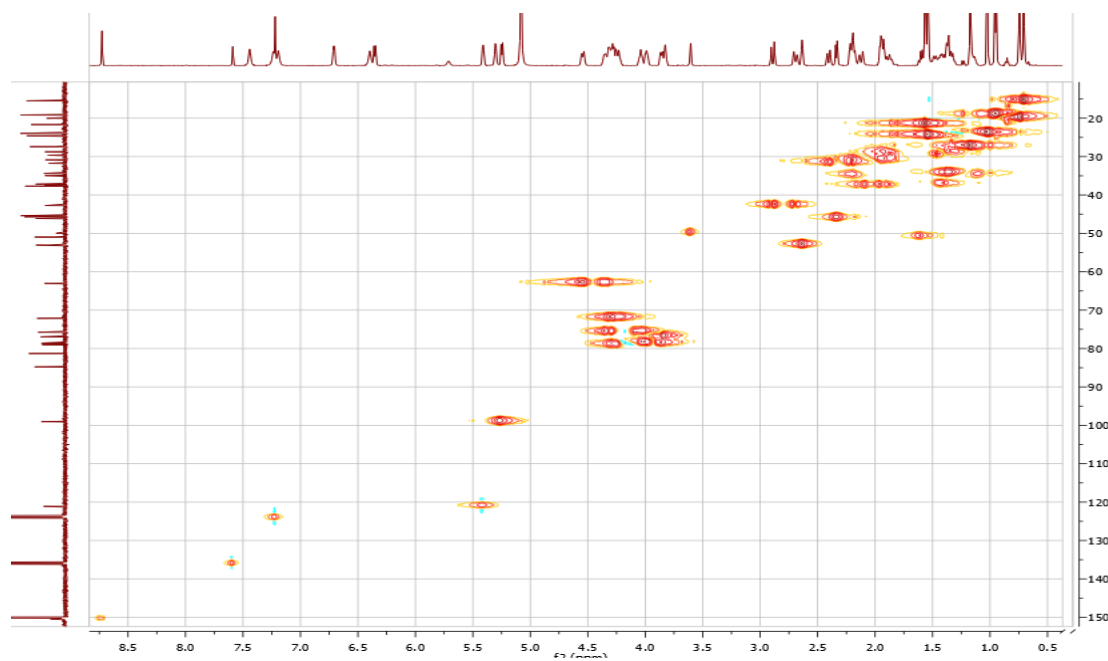


Figure 2-4. HMQC spectrum of compound **1** in pyridine-$d_5$.
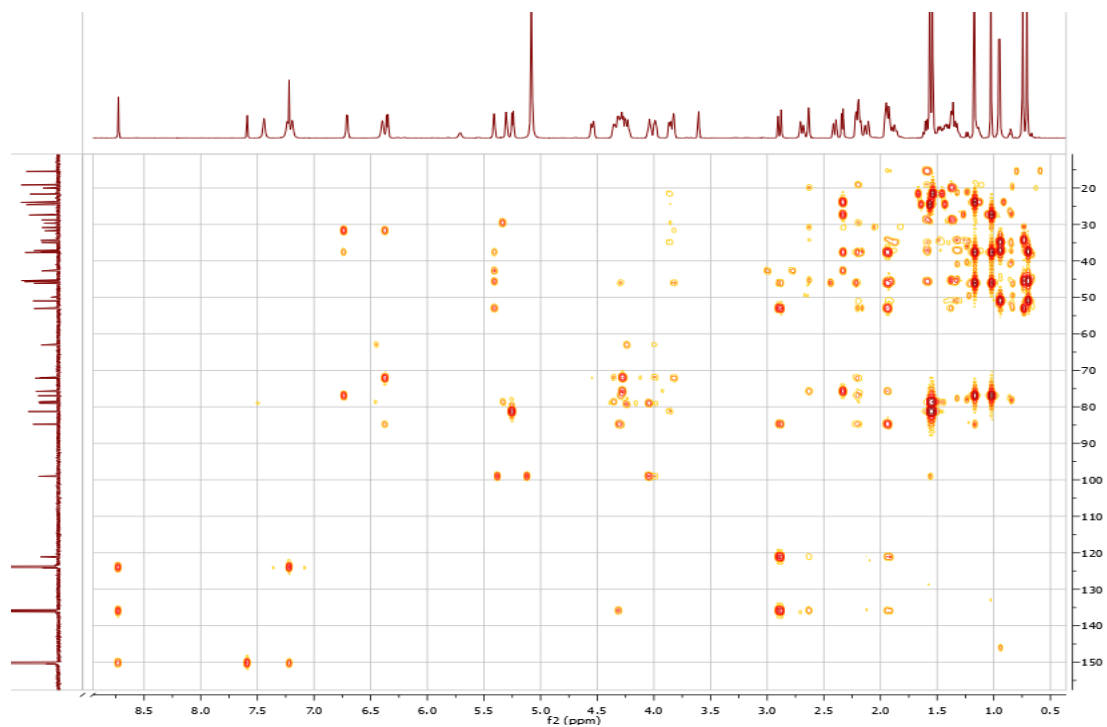
Figure 2-5. HMBC spectrum of compound **1** in pyridine-$d_5$.
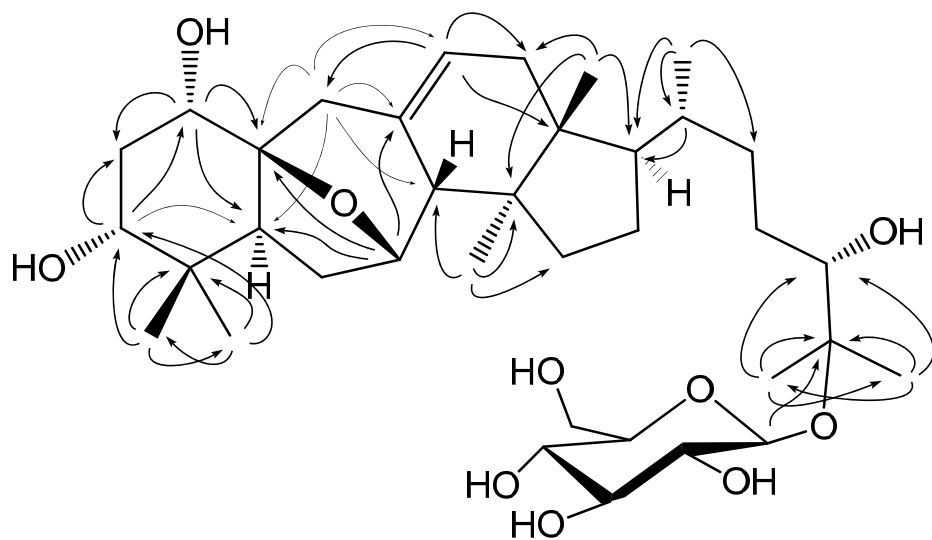


Figure 2-6. Key HMBC correlations (→) of **1**.

The two C-2 geminal protons in the $^1$H NMR spectrum have very small couplings with H-1 and H-3 since H-2 shows a broad doublet at $\delta_H$ 2.20 ($J$ = 14.0 Hz) and 2.40 ($J$ = 14.0 Hz), respectively (Figure 2-3). This indicates that both H-1 and H-3 are equatorially oriented, positioned between the two geminal protons and thus the hydroxy groups at C-1 and C-3 should be α-oriented. Further evidence is derived from the NOE correlation between H-1 and H-19β and between H-3 and both Me-28 (weaker) and Me-29 (stronger) in the ROESY spectrum of **1** (Figure 2-10).

The epoxy group between C-7 and C-10 was deduced to be β-oriented based on the NOE correlations between H-7 and Me-30, between H-6α and Me-30, and between H-5 and Me-28 and H-19α (Figure 2-9). Other key NOE correlations include H-8β and Me-18 as well as anomeric H-1′ and Me-26/Me-27 (Figure 2-9). A comprehensive analysis of the 2D NMR data of **1** facilitates the assignments of the proton and carbon resonances, which are shown in Tables 2-1 and 2-2. The configuration of **1** including the sugar moiety was eventually established by X-ray crystallographic analysis (The experimental result is described in Section 2.3.4). A collection of anomalous X-ray scattering from the oxygen atoms confirmed the absolute configuration. The Flack absolute parameter was 0.06(16), where a value ranging from 0 to 1 represents the correct structure when close or equal to zero (Flack, 1983). Also, the deviation parameter $u$, being 0.016, satisfies the requirement that "u < 0.04 implies a strong inversion-distinguishing power" (Flack and Bernardinelli, 2000). Its structure was thus characterized as 1$S$, 3$R$, 24$S$, 25-tetrahydroxy-7$S$, 10$S$-epoxy-9,10-*seco*-9, 19-cyclolanost-9(11)-ene 25-$O$-β-D-glucopyranoside.
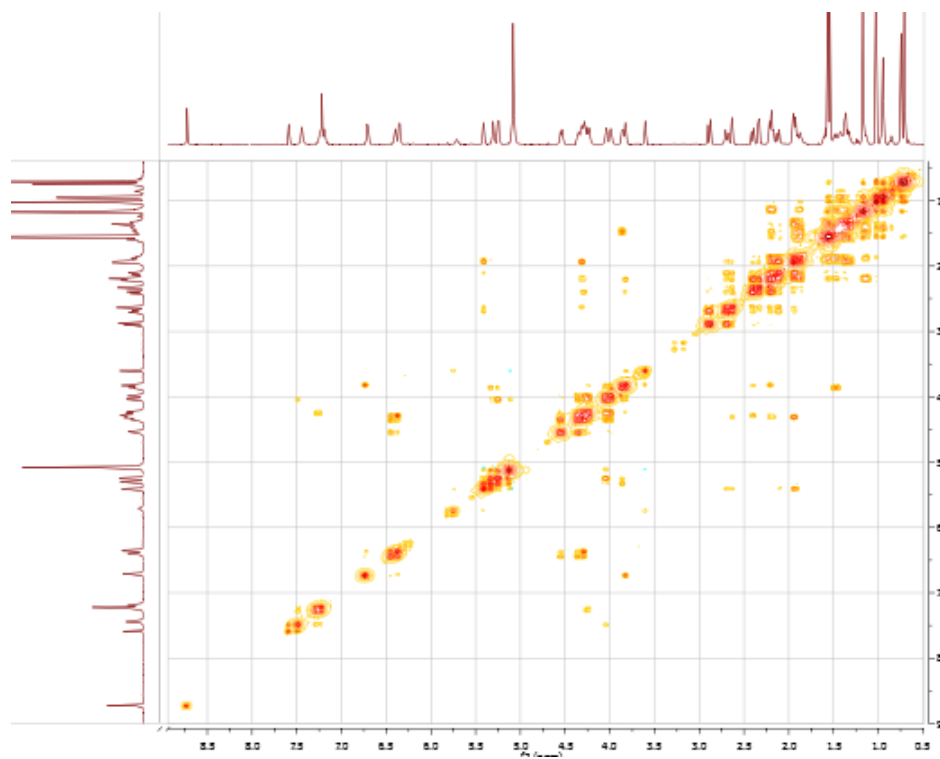
Figure 2-7. COSY spectrum of compound **1** in pyridine-$d_5$.
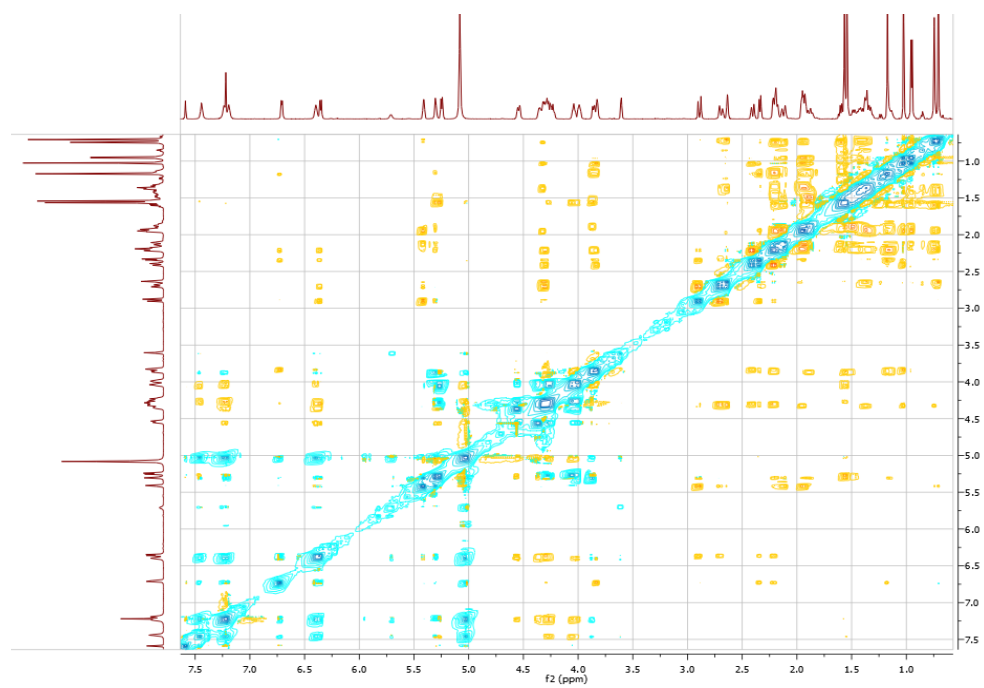


Figure 2-8. ROESY spectrum of compound **1** in pyridine-$d_5$.
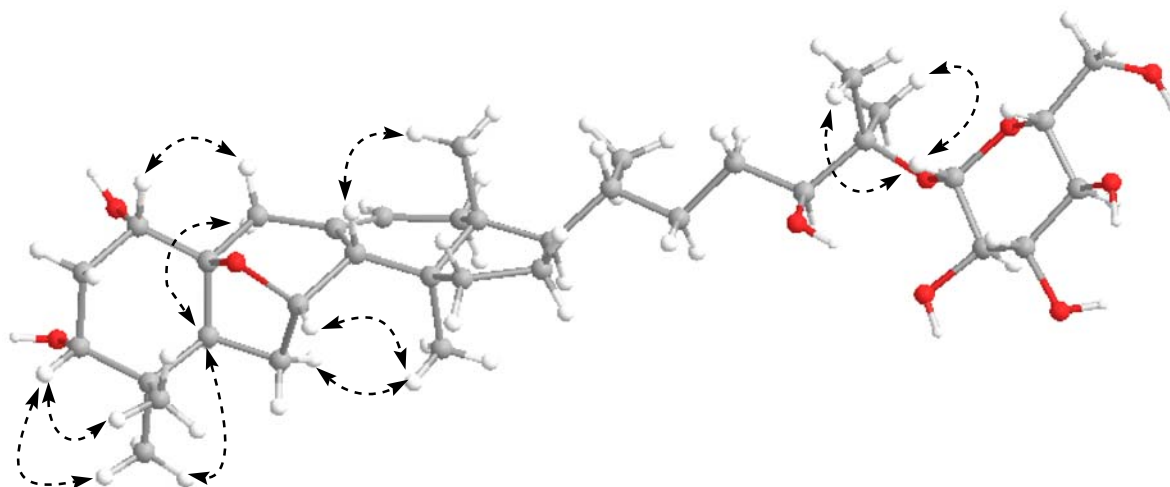
Figure 2-9.  Key ROESY correlations (↔) of **1**.
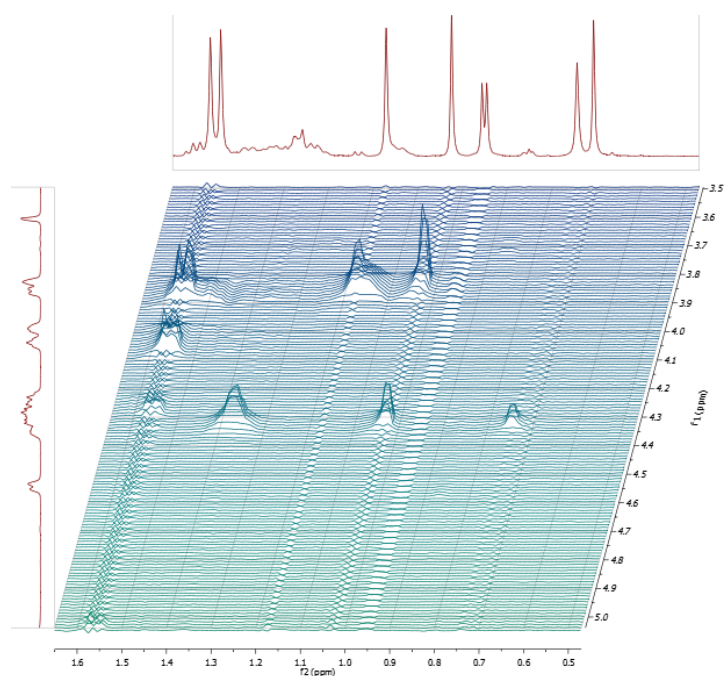


Figure 2-10.  Key signal intensities shown in a 3D stacked plot of the ROESY spectrum of **1** in pyridine-$d_5$.

## 2.2.1.2. Sutherlandioside B (**2**)

Sutherlandioside B (**2**) was obtained as colorless needles via recrystallization in methanol. Its molecular formula was determined as $C_{36}H_{60}O_{10}$ by $^{13}C$ NMR data and HRESIMS. A DEPT NMR experiment permitted differentiation of the 36 resonances into seven methyl, 10 methylene, 12 methine, and seven quaternary carbons. The presence of a β-glucopyranosyl moiety in compound **2** is clear by comparison of its $^1H$- and $^{13}C$ NMR data with those of compound **1** (Tables 2-1 and 2-2).

The characteristic resonances due to the aglycone moiety were observed for an isolated methylene of the cyclopropane system at $\delta_{H/C}$ 0.86,1.60/24.4, six tertiary methyls at $\delta_{H/C}$ 0.99/16.0, 1.04/21.7, 1.09/18.9, 1.26/25.6, 1.54/24.6, 1.57/21.6, and a secondary methyl at $\delta_{H/C}$ 0.95/19.3, indicating a cycloartane-type triterpene skeleton (Calis, Zor *et al.*, 1996; Bedir, 2001; Li, Jacob *et al.*, 2006; Ali, Khan *et al.*, 2007).

The side chain at C-17 including the β-glucopyranosyl moiety attached to the 25-hydroxy group in **2** is the same as that of compound **1** since their $^1H$ and $^{13}C$ NMR chemical shifts are identical (Tables 2-1 and 2-2). This suggests the difference between **1** and **2** lies in their aglycone moieties.

The presence of a carbonyl group in **2** is evident from the absorption at $v_{max}$ 1686 cm$^{-1}$ in its IR spectrum and the carbon resonance at $\delta_C$ 210.7 in its $^{13}C$ NMR spectrum.
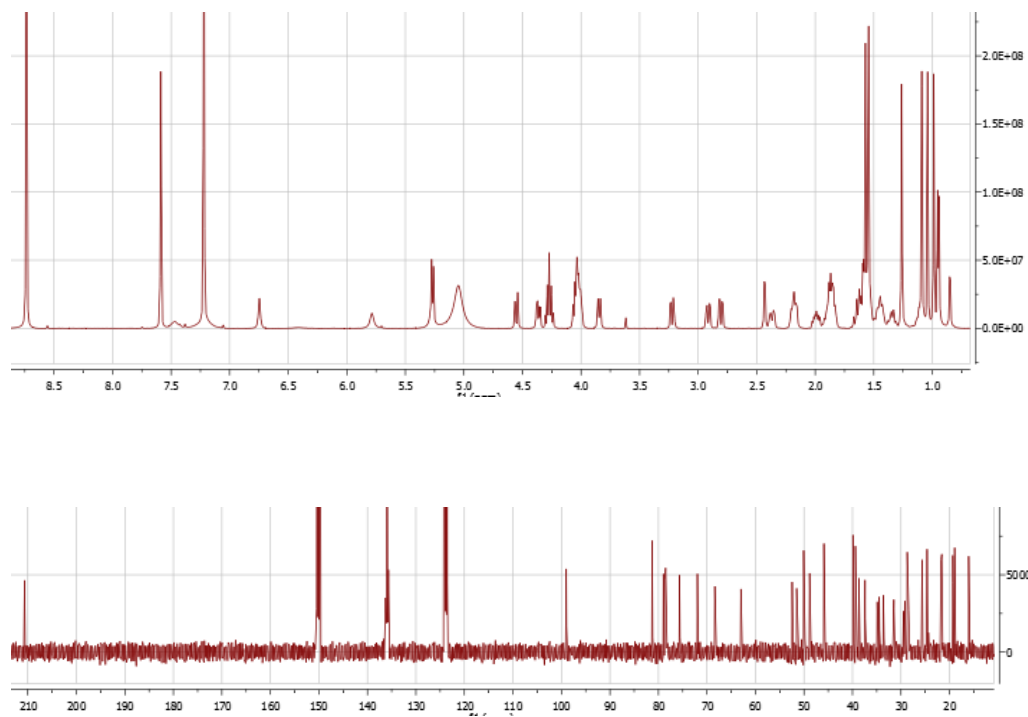
Figure 2-11.  $^1$H and $^{13}$C  NMR spectra of compound **2** in pyridine-$d_5$.



Figure 2-12.  HMQC spectrum of compound **2** in pyridine-$d_5$.
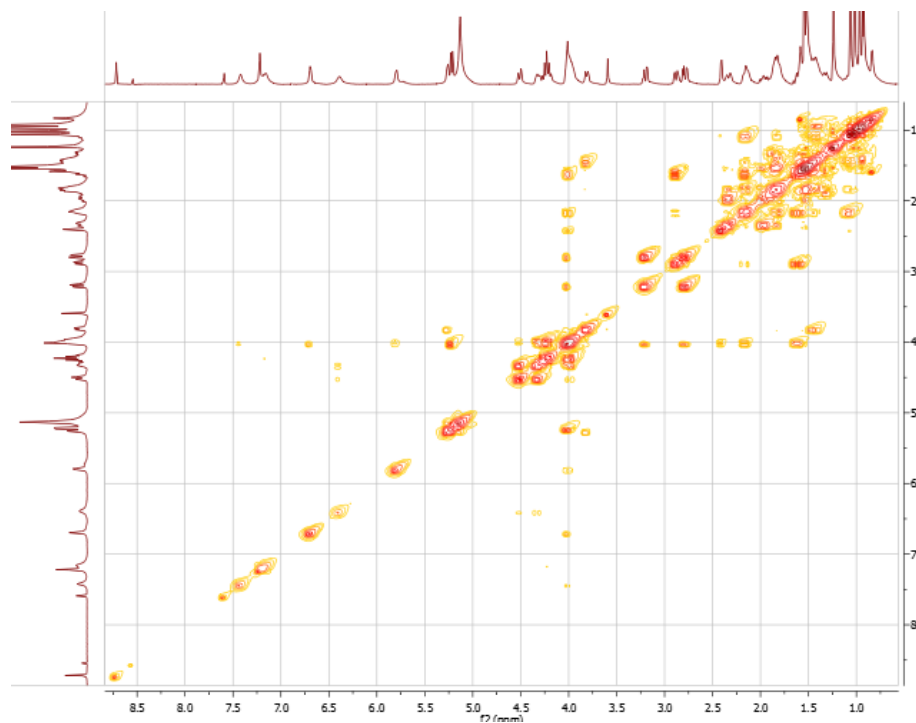
Figure 2-13. COSY spectrum of compound **2** in pyridine-$d_5$.

The carbonyl is located at C-1 since it shows an HMBC correlation with H-19. Instead of the correlation with two olefinic carbons at $\delta_C$ 135.9 (C) and 121.1 (CH), the protons at $\delta_H$ 0.86 and 1.60 show correlations with a methylene group at 29.2, suggesting the absence of a double bond between C-9 and C-11 in compound **2**. The location of hydroxy groups at C-3 and C-7 was confirmed by relevant HMBC correlations such as H-2 and C-3 and H-8 and C-7 (Figure 2-14).
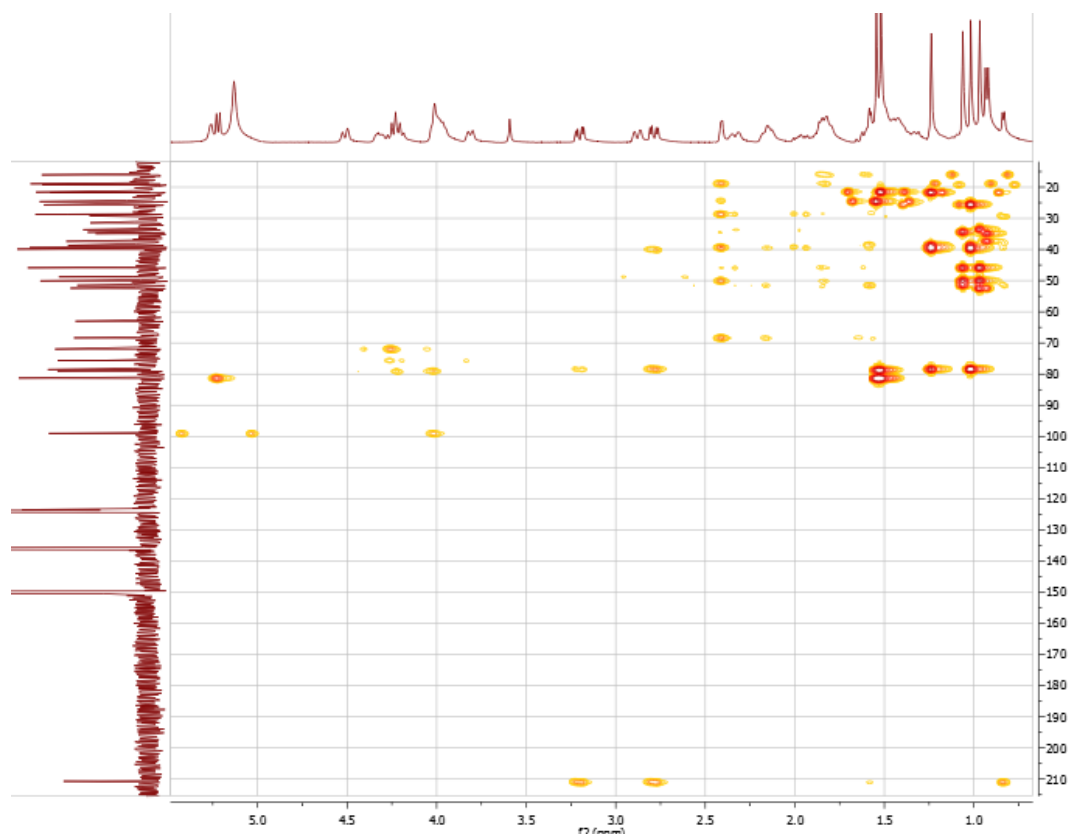
Figure 2-14.  HMBC spectrum of compound **2** in pyridine-$d_5$.

The orientation of the hydroxy groups was determined by NOE evidence showing α at C-3 and β at C-7, respectively. H-3 has a weak correlation with the α-orientated Me-28 and a strong correlation with the β-orientated Me-29, while H-7 has a strong correlation with Me-30. Other NOE correlations support the structure shown and facilitated the NMR signal assignments of **2**.
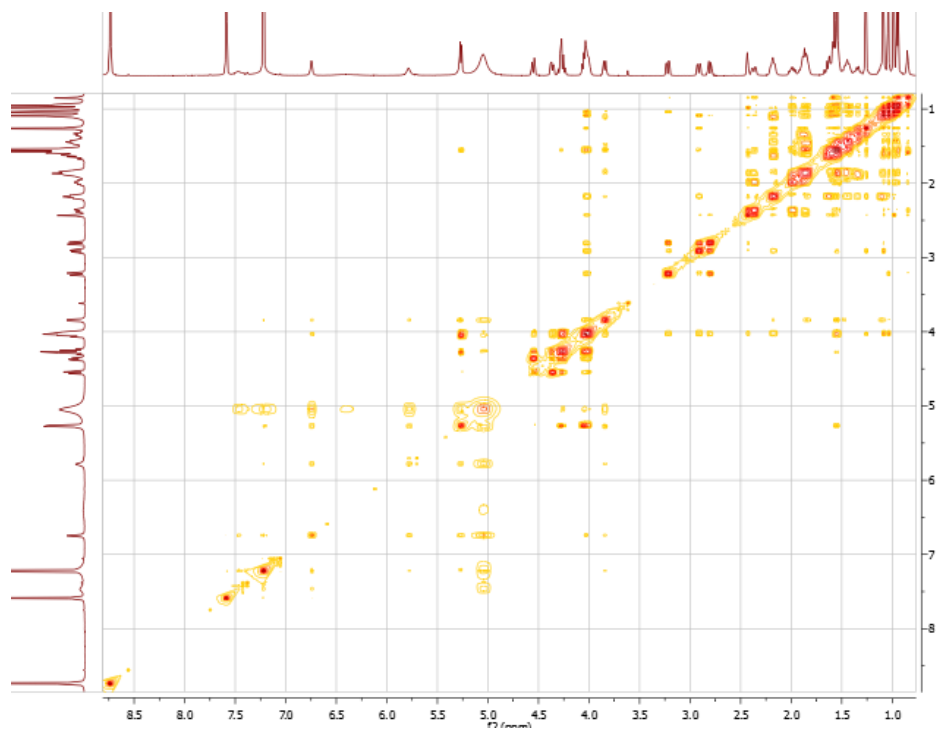
Figure 2-15. ROESY spectrum of compound **2** in pyridine-$d_5$.
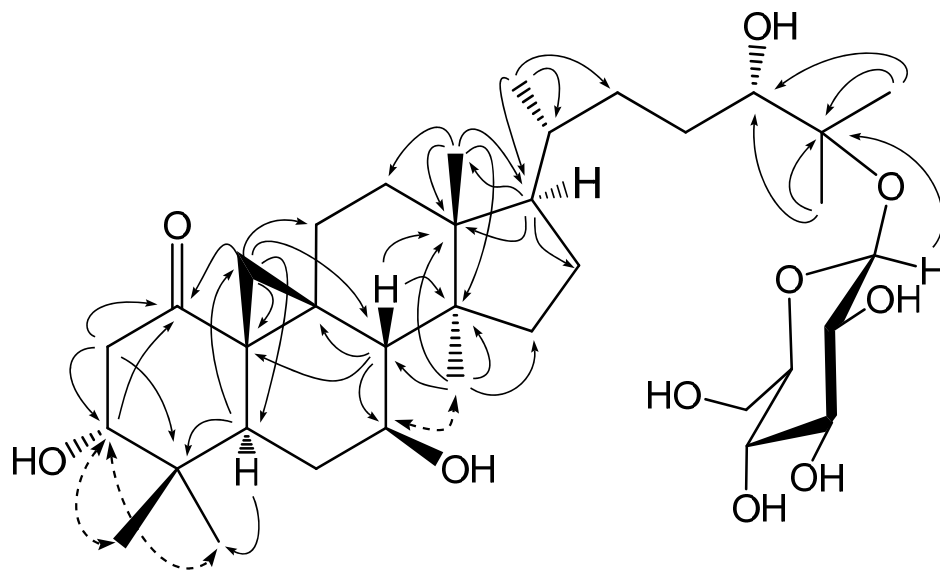


Figure 2-16. Key HMBC (→) and ROESY correlations (↔) of **2**.

The structure of **2** is defined as 3*R*,7*S*,24*S*,25-tetrahydroxycycloartan-1-one 25-*O*-β-D-glucopyranoside, together with the absolute configuration determination of the sugar moiety by acid hydrolysis (Section 2.3.5). The conformation of the A-ring of compound **2** could be slightly different from that of compound **1**. This is indicated by the C-2 geminal protons showing similar coupling constants (~4 Hz) with equatorially oriented H-3, which is different from the A-ring coupling pattern of compound **1**.

2.2.1.3.  Sutherlandiosides C (**3**)

Sutherlandioside C (**3**) had a molecular formula of $C_{36}H_{58}O_{10}$ deduced from its ^{13}C NMR data and HRESIMS. The NMR data of **3** resembled those of **2** (Tables 2-1 and 2-2). Typical differences are the presence of an additional carbonyl group and one fewer oxygenated carbon in **3**. The two carbonyls gave IR absorption at 1708 and 1671 cm$^{-1}$. The HMBC spectrum indicated that the additional carbonyl was positioned at C-11 since both the C-19 protons at $\delta_H$ 1.32 and 2.26 showed correlations with both carbonyls at $\delta_C$ 205.6 and 209.3. In addition, the C-11 carbonyl caused the neighboring H-12 to shift downfield at $\delta_H$ 2.72 and 2.88 (ABq, *J* = 16.4 Hz) when compared to H-12 at $\delta_H$ 1.54 (m) and 1.84 (m) in **2** (Figure 2-17). This was also confirmed by the HMBC spectrum showing that both the C-12 protons ($\delta_H$ 2.72 and 2.88) are correlated with the carbonyl carbon at $\delta_C$ 209.3 and with C-13 at $\delta_C$ 46.7 and Me-18 at $\delta_C$ 17.0. The absence of the C-7 hydroxy group in **3** was confirmed by 2D NMR data, which supports its structure as 3*R*,24*S*,25-trihydroxycycloartane-1,11-dione 25-*O*-β-D-glucopyranoside.
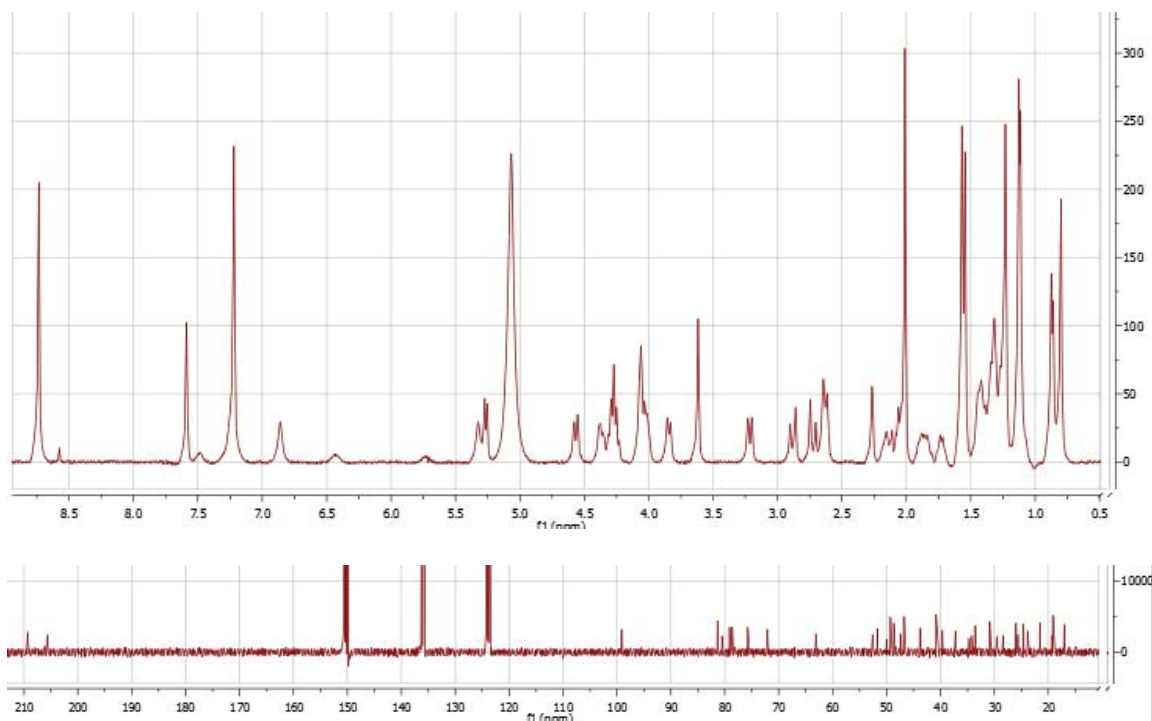
Figure 2-17. $^{1}$H and $^{13}$C NMR spectra of compound **3** in pyridine-$d_5$.

### 2.2.1.4. Sutherlandioside D (**4**)

Sutherlandioside D (**4**) had a molecular formula of $C_{36}H_{58}O_9$ on the basis of its $^{13}$C NMR data and HRESIMS. The $^{1}$H and $^{13}$C NMR spectra of **4** (Figure 2-18) were similar to those of **2** (Figure 2-11). The noticeable difference between these two compounds lies in that compound **4** possesses an α,β-unsaturated carbonyl system indicated by the NMR [$\delta_C$ 129.6, 159.1, 200.9, (Table 2-4); $\delta_H$ 6.11, 6.59 (1H each, d, $J = 10$ Hz), (Table 2-3)], IR ($v_{max}$ 1655 cm$^{-1}$), and UV ($\lambda_{max}$ 222 nm) data. It appears that this system is located in the A-ring since the NMR data for the remaining protons and carbons are superimposable on those of **2** (Tables 2-1 and 2-2).
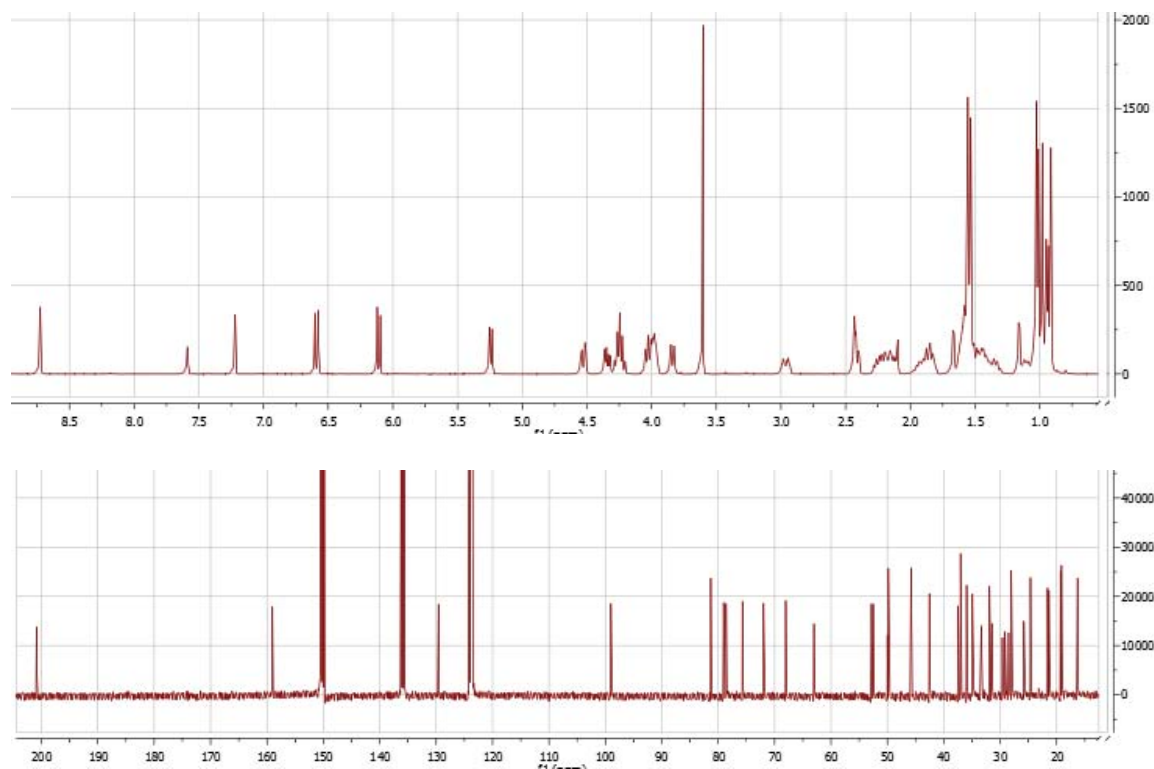
Figure 2-18. $^1$H and $^{13}$C NMR spectra of compound **4** in pyridine-$d_5$.
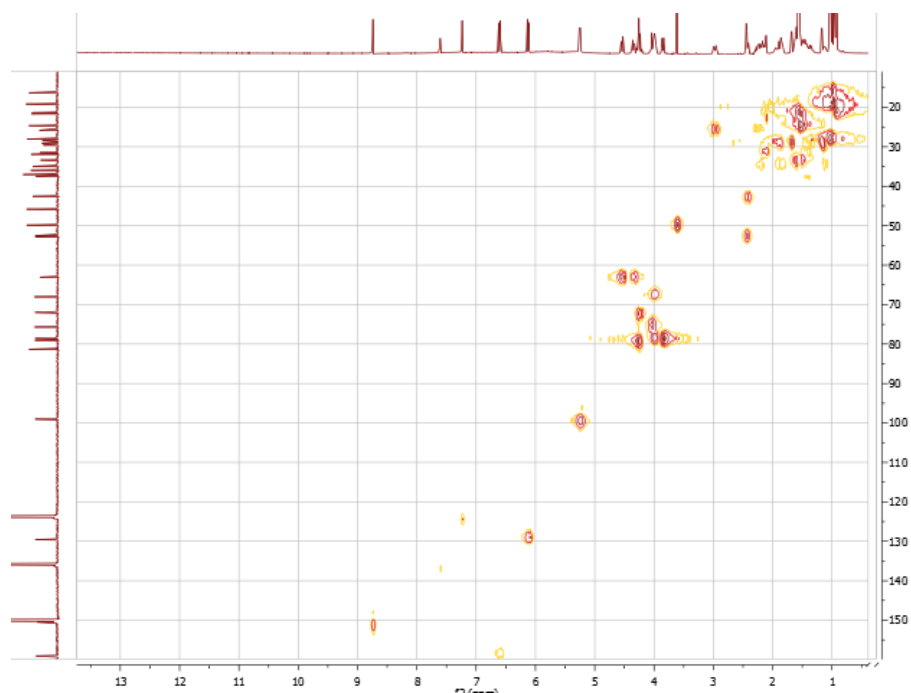
Figure 2-19. HMQC spectrum of compound **4** in pyridine-$d_5$.
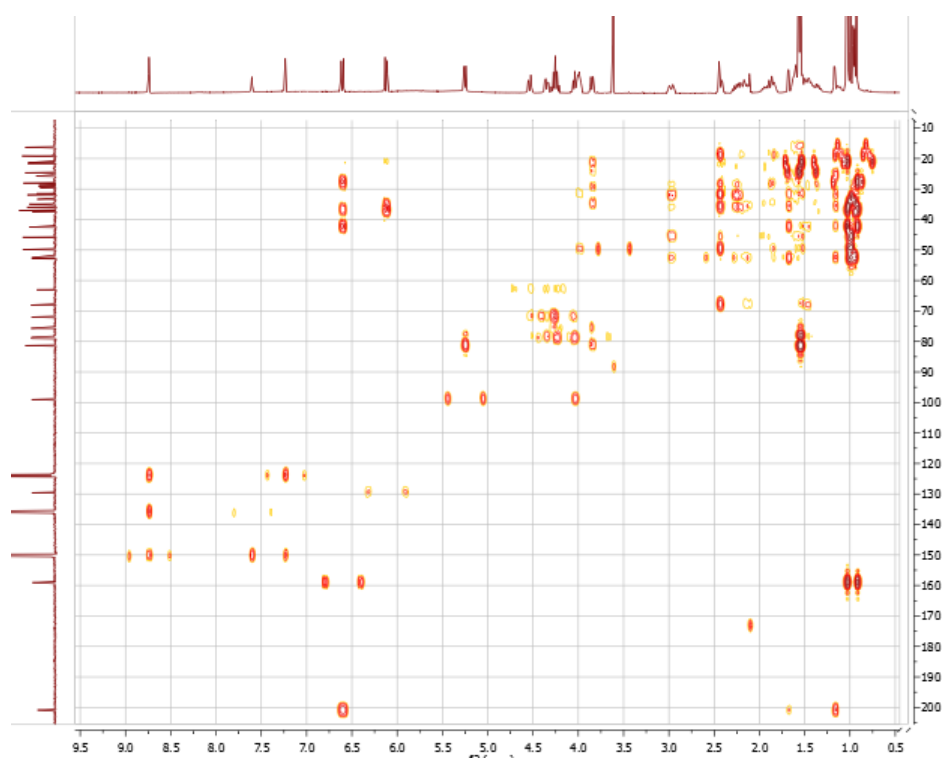


Figure 2-20. HMBC spectrum of compound **4** in pyridine-$d_5$.
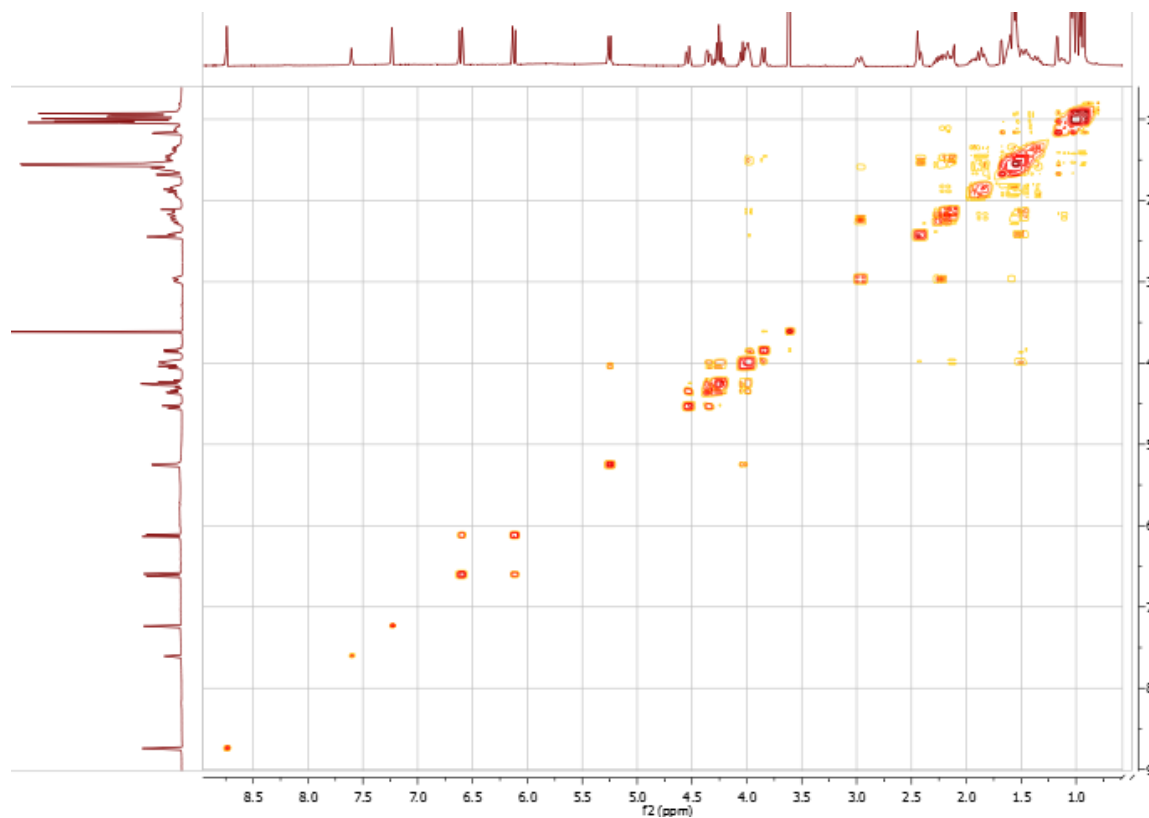
Figure 2-21. COSY spectrum of compound **4** in pyridine-$d_5$.

The position of this double bond is further confirmed by the HMBC spectrum showing H-3 at $\delta_H$ 6.59 correlated with the carbonyl carbon at $\delta_C$ 200.9 and with C-4 ($\delta_C$ 37.0) and C-5 ($\delta_C$ 42.5). All the NMR data of **4**, assigned by DQF-COSY, HMQC and HMBC, and the result of sugar analysis by acid hydrolysis are satisfactorily consistent with the structure shown as 7*S*,24*S*,25-trihydroxycycloart-2-en-1-one 25-*O*-β-D-glucopyranoside.

Table 2-1. $^1$H NMR data for compounds **1–4** in pyridine-$d_5$ and **16** in chloroform-$d$.

| # | 1 | 2 | 3 | 4 | 16 |
|---|---|---|---|---|---|
| 1 | 4.28 | - | - | - | - |
| 2a | 2.20 m α | 2.81 dd (13.6, 4.4) α | 2.63 [*] | 6.11 d (9.6) | 5.81 d (10.1) |
| 2b | 2.40 br d (14.1) β | 3.23 dd (13.8, 4.2) β | 3.22 dd (12.0, 2.8) | | |
| 3 | 3.83 br s | 4.03 [*] | 4.06 m | 6.59 d (9.6) | 6.54 d (9.7) |
| 5 | 2.34 br d (8.5) | 2.90 dd (13.4, 3.4) | 2.64 [*] | 2.41 dd (11.6, 3.8) | 1.56 [*] |
| 6a | 1.95 β [*] | 1.66 β [*] | 2.01 [*] | 1.48 [*] | 1.51 [*] |
| 6b | 2.20 α [*] | 2.17 α [*] | 2.01 [*] | 2.10 [*] | 1.66 [*] |
| 7 | 4.30 [*] | 3.97 [*] | 1.22 [*] | 4.00 [*] | 3.90 m |
| | | | 1.43 [*] | | |
| 8 | 2.64 br s | 2.43 d (4.0) | 2.06 [*] | 2.42 d (4.4) | 2.12 [*] |
| 10 | - | - | - | - | 2.23 dt, (12.8, 4.8) |
| 11a | 5.41 d (2.3) | 1.99 m β | - | 2.25 dd (16.4, 7.6) | 5.53br t (2.42) |
| 11b | | 2.37 dd (12.8, 2.8) α | | 2.96 dt (15.2, 4.0) | |
| 12a | 1.94 d (13.5) β | 1.54 [*] | 2.72 d (16.4) | 1.60 [*] | 1.94 d (4.8) |
| 12b | 2.12 d (17.0) α | 1.84 [*] | 2.88 d (16.4) | 1.83 [*] | 2.06 m |
| 15a | 1.30 [*] | 1.55 [*] | 1.24 [*] | 1.53 [*] | 1.50 [*] |
| 15b | 1.36 [*] | 1.86 [*] | 1.27 [*] | 1.55 [*] | 1.60 [*] |
| 16a | 1.36 [*] | 1.36 t (14.0) | 1.22 [*] | 1.06 [*] | 1.35 m |
| 16b | 1.94 [*] | 1.84 [*] | 1.34 [*] | 1.89 [*] | 1.89 m |
| 17 | 1.60 [*] | 1.60 [*] | 1.73 [*] | 1.58 [*] | 1.53 [*] |
| 18 | 0.71 s | 0.99 s | 0.80 s | 0.98 s | 0.68 s |
| 19a | 2.69 d (16.1) β | 0.86 d (4.4) α | 1.32 [*] | 1.16 d (3.6) | 2.58 dd (14.8, 4.8) |
| 19b | 2.89 d (16.1) α | 1.60 d (4.0) β | 2.26 d (3.6) | 1.67 d (4.0) | 2.67 dd (14.4, 3.2) |
| 20 | 1.43 [*] | 1.46 [*] | 1.34 [*] | 1.45 [*] | 1.37 [*] |
| 21 | 0.95 d (6.2) | 0.95 d (6.0) | 0.87 d (6.1) | 0.94 d (6.0) | 0.87 d (6.0) |
| 22a | 1.14 *pro-R* [*] | 1.12 [*] | 1.14 [*] | 1.11 [*] | 1.72 [*] |
| 22b | 2.20 *pro-S* [*] | 2.17 [*] | 2.13 [*] | 2.16 [*] | 2.02 [*] |
| 23a | 1.48 [*] | 1.46 [*] | 1.44 [*] | 1.33 [*] | 0.96 [*] |
| 23b | 1.87 [*] | 1.83 [*] | 1.84 [*] | 1.94 [*] | 1.78 [*] |
| 24 | 3.86 br d (9.7) | 3.84 br d (9.2) | 3.84 br d (10.4) | 3.84 br d (9.6) | 3.24 dd (10.0, 1.6) |
| 26 | 1.57 s | 1.57 s | 1.57 s | 1.55 s | 1.12 s |
| 27 | 1.54 s | 1.54 s | 1.54 s | 1.53 s | 1.17 s |
| 28 | 1.17 s | 1.26 s | 1.23 s | 1.03 s | 1.11 s |
| 29 | 1.03 s | 1.04 s | 1.11 s | 0.91 s | 1.00 s |
| 30 | 0.75 s | 1.09 s | 1.12 s | 1.01 s | 0.83 s |
| 1′ | 5.25 d (7.9) | 5.24 d (7.6) | 5.26 d (8.0) | 5.24 d (8.0) | - |
| 2′ | 4.05 t (7.1) | 4.04 t (7.4) | 4.03 [*] | 4.03 [*] | - |
| 3′ | 4.27 [*] | 4.28 [*] | 4.27 [*] | 4.26 [*] | - |
| 4′ | 4.26 [*] | 4.22 [*] | 4.25 [*] | 4.22 [*] | - |
| 5′ | 3.99 [*] | 4.03 [*] | 4.01 [*] | 3.98 [*] | - |
| 6′a | 4.35 dd (11, 5.5) | 4.34 dd (11.6, 5.2) | 4.37 dd (11.5, 5.1) | 4.33 dd (11.6, 5.4) | - |
| 6′b | 4.54 br d (11) | 4.54 br d (10.8) | 4.57 br d (11.3) | 4.52 dd (12.0, 2.0) | |

Data ($\delta$, ppm) recorded at 600 MHz for **1**, 400 MHz for **2–4** and **16**. Assignments were based on 2D NMR including DQF-COSY, HMQC, HMBC, and ROESY. Well-resolved couplings are expressed with coupling patterns and coupling constants in Hz in parenthesis. [*] signal partially obscured.

Table 2-2. $^{13}$C NMR data for compounds **1–4** in pyridine-$d_5$ and **16** in chloroform-$d$.

| # | 1 | | 2 | | 3 | | 4 | | 16 | |
|---|------|---|-------|---|-------|---|-------|---|-------|---|
| 1 | 72.0 | d | 210.7 | s | 205.6 | s | 200.9 | s | 200.6 | s |
| 2 | 31.8 | t | 48.8 | t | 47.3 | t | 129.6 | d | 126.3 | d |
| 3 | 77.0 | d | 78.5 | d | 80.5 | d | 159.1 | d | 159.8 | d |
| 4 | 37.7 | s | 39.9 | s | 40.8 | s | 37.0 | s | 36.8 | s |
| 5 | 46.1 | d | 38.7 | d | 43.8 | d | 42.5 | d | 44.8 | d |
| 6 | 30.9 | t | 31.5 | t | 30.8 | t | 31.5 | t | 35.3 | t |
| 7 | 75.8 | d | 68.4 | d | 23.8 | t | 68.0 | d | 72.0 | d |
| 8 | 53.1 | d | 51.5 | d | 39.6 | d | 52.8 | d | 55.4 | d |
| 9 | 135.9 | s | 28.7 | s | 33.5 | s | 31.9 | s | 133.5 | s |
| 10 | 84.8 | s | 39.4 | s | 48.6 | s | 35.9 | s | 47.1 | d |
| 11 | 121.1 | d | 29.2 | t | 209.3 | s | 25.8 | t | 127.3 | d |
| 12 | 37.6 | t | 33.6 | t | 52.6 | t | 34.9 | t | 37.7 | t |
| 13 | 45.7 | s | 45.9 | s | 46.7 | s | 45.8 | s | 45.5 | s |
| 14 | 45.4 | s | 50.1 | s | 49.3 | s | 49.8 | s | 48.4 | s |
| 15 | 34.4 | t | 34.5 | t | 34.2 | t | 33.4 | t | 28.9 | t |
| 16 | 28.8 | t | 28.4 | t | 28.4 | t | 29.6 | t | 28.5 | t |
| 17 | 51.0 | d | 52.4 | d | 51.7 | d | 52.5 | d | 50.4 | d |
| 18 | 15.5 | q | 16.0 | q | 17.0 | q | 16.3 | q | 15.2 | q |
| 19 | 42.8 | t | 24.4 | t | 25.6 | t | 29.1 | t | 33.8 | t |
| 20 | 37.2 | d | 37.4 | d | 37.2 | d | 37.5 | d | 36.6 | d |
| 21 | 19.2 | q | 19.3 | q | 19.3 | q | 19.3 | q | 18.7 | q |
| 22 | 35.0 | t | 34.9 | t | 34.7 | t | 34.9 | t | 39.4 | t |
| 23 | 29.6 | t | 29.5 | t | 29.6 | t | 28.5 | t | 33.7 | t |
| 24 | 78.7 | d | 78.7 | d | 78.6 | d | 78.7 | d | 79.7 | d |
| 25 | 81.3 | s | 81.3 | s | 81.3 | s | 81.3 | s | 73.4 | s |
| 26 | 21.7 | q | 21.6 | q | 21.7 | q | 21.6 | q | 23.4 | q |
| 27 | 24.6 | q | 24.6 | q | 24.6 | q | 24.6 | q | 26.7 | q |
| 28 | 27.4 | q | 25.6 | q | 26.0 | q | 28.0 | q | 27.9 | q |
| 29 | 24.0 | q | 21.7 | q | 21.5 | q | 21.4 | q | 20.0 | q |
| 30 | 20.0 | q | 18.9 | q | 19.1 | q | 19.1 | q | 18.4 | q |
| 1' | 99.0 | d | 99.0 | d | 99.1 | d | 99.0 | d | | |
| 2' | 75.7 | d | 75.7 | d | 75.7 | d | 75.7 | d | | |
| 3' | 79.0 | d | 79.0 | d | 79.1 | d | 79.0 | d | | |
| 4' | 72.1 | d | 72.0 | d | 72.1 | d | 72.0 | d | | |
| 5' | 78.6 | d | 78.4 | d | 78.7 | d | 78.6 | d | | |
| 6' | 63.1 | t | 63.0 | t | 63.1 | t | 63.0 | t | | |

Spectra were acquired at 150 MHz for **1** and 100 MHz for **2–4** and **16**. Multiplicity was obtained from DEPT spectra. ($\delta$, ppm)

2.2.1.5.  Proposed biogenesis of sutherlandioside A (**1**) from sutherlandioside B (**2**)

Acid hydrolysis of compound **2** afforded compound **16** and D-glucose, providing important information for us to propose the possible biogenesis of the unique oxygen bridge formation in compound **1** (Figure 2-26).



**16**
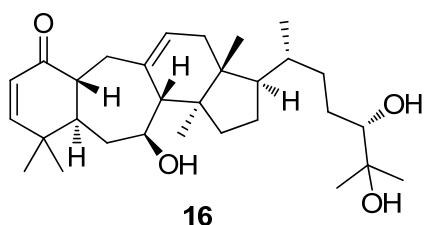
The molecular formula of compound **16** ($C_{30}H_{48}O_4$) determined by ^{13}C NMR (Figure 2-22) and HRESIMS data indicates that it is an artifact of the aglycone with a loss of one molecule of water. The major differences of the chemical shift values in ^{1}H (Table 2-1) and ^{13}C NMR spectra (Table 2-2) between **2** and **16** are shown in the A- and B-rings. The change in the A-ring indicates the formation of an α,β-unsaturated carbonyl system by losing the C-3 hydroxy group, and the B-ring change indicates ring expansion via the opening of the cyclopropane ring. These changes were further confirmed by 2D NMR spectra (Figures 2-23 and 2-24).
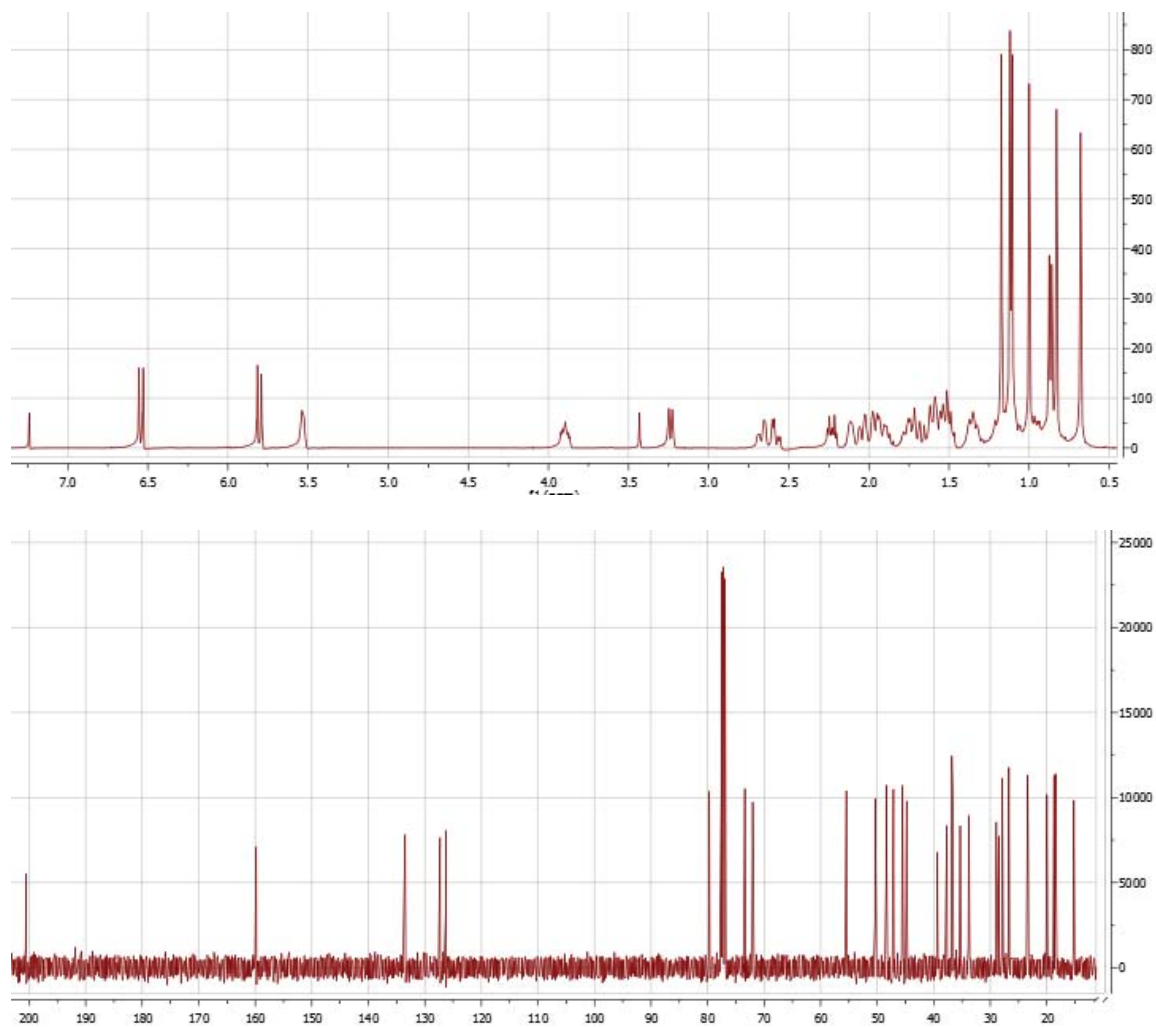
Figure 2-22. $^1$H and $^{13}$C NMR spectra of compound **16** in pyridine-$d_5$.
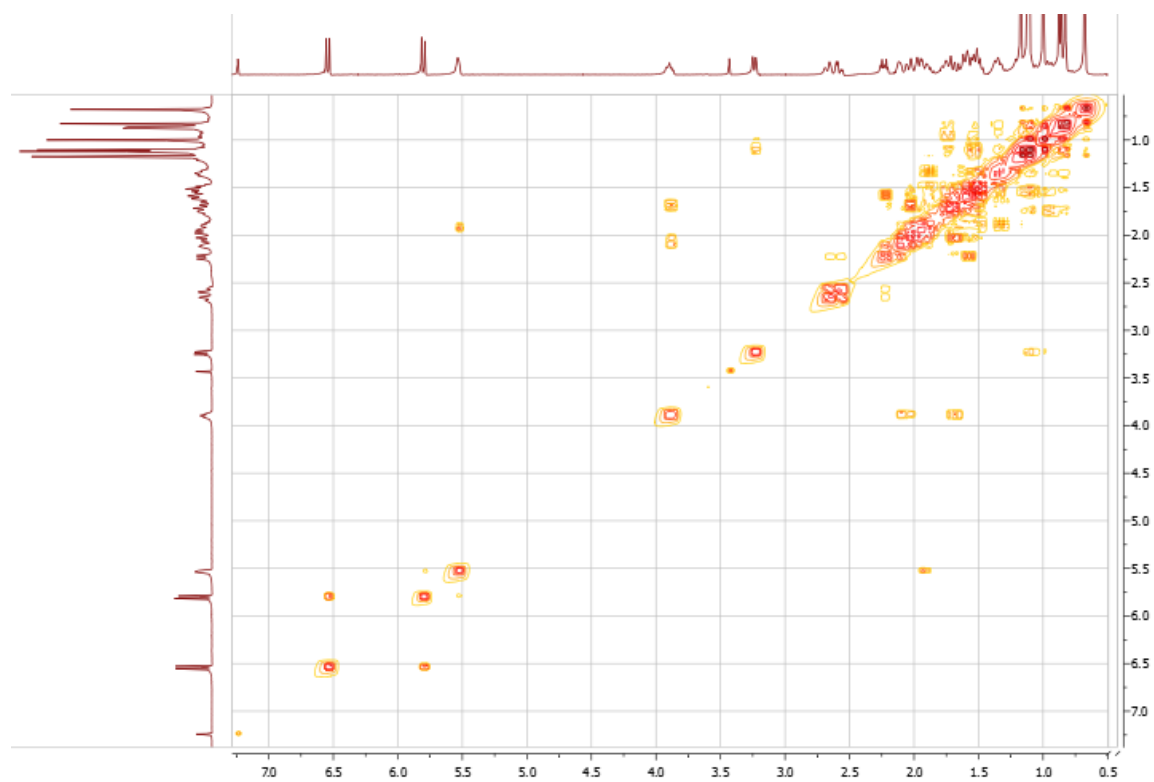
Figure 2-23.  COSY spectrum of compound **16** in pyridine-$d_5$.
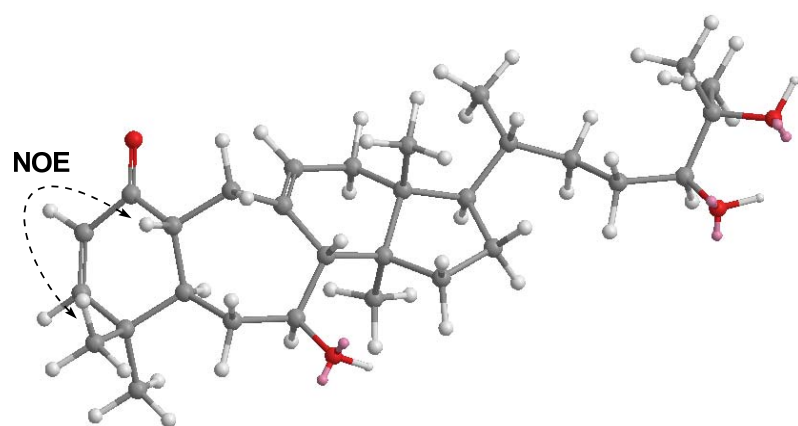


Figure 2-24.  Conformation of compound **16** according to key NOE correlations.

The conformationally optimized model of **16** obtained from Chem3D ultra 10.0 (Figure 2-24) shows that the β orientated H-10 forms the similar dihedral angles with both of the geminal protons on C-19, which is in accordance with the similar vicinal coupling constants of H-19s (3.2 and 4.8 Hz) observed in the $^1$H NMR spectrum (Table 2-1). The structure of **16** was finally established by the analysis of its IR, HRESIMS and NMR data including COSY, HMQC, HMBC and ROESY as 7*S*,24*S*,25-trihydroxy-9,10*R*-seco-9,19-cyclolanosta-2(3),9(11)-diene. The possible mechanism for the formation of **16** was proposed as shown in Figure 2-25.
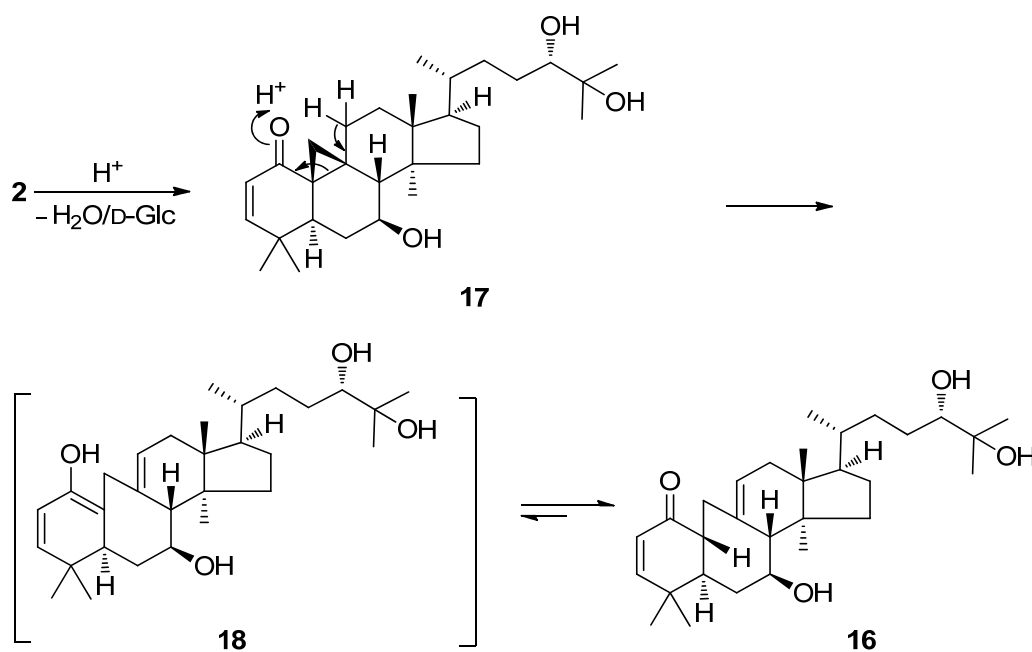


Figure 2-25. Putative mechanism for the formation of **16**.

Thus, compound **2** was subjected to acid-catalyzed dehydration between C-2 and C-3 and the cleavage of the glucosyl unit at the hydroxy group of C-25 to afford intermediate **17**. The intermediate **17** underwent ring opening to generate two double bonds in the key intermediate **18**,

which underwent stereoselective keto-enol tautomerism to furnish **16**.
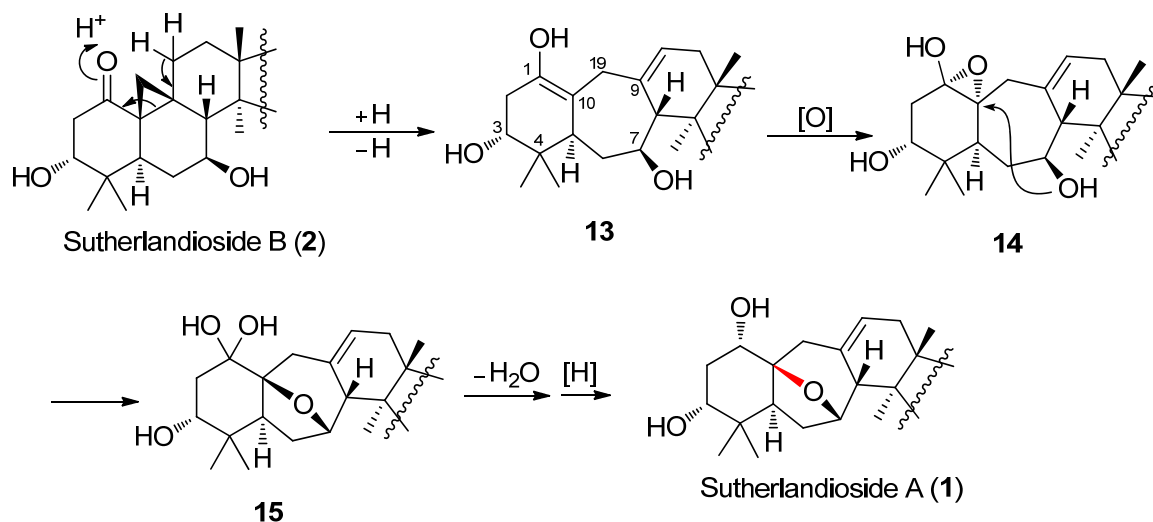


Figure 2-26.  Putative mechanism for the formation of **1**.

With the information that the opening of the cyclopropane ring in sutherlandioside B (**2**) can be chemically achieved, the possible biogenesis of sutherlandioside A (**1**) from sutherlandioside B was proposed as shown in Figure 2-26.

Compound **1** may derive from compound **2**, which undergoes a ring opening between C-9 and C-10, generating two unsaturated $C_9$-$C_{11}$ and $C_1$-$C_{10}$ bonds in the presumed intermediate **13**. Epoxidation of the $C_1$-$C_{10}$ double bond in **13** affords **14**. An intramolecular nucleophilic attack of the C-7 hydroxy group in **14** to the epoxide at C-10 forms the oxygen bridge in **15** (Figure 2-26). Dehydration of **15** followed by reduction at C-1 affords **1**. This could explain the retention of the C-7 configuration in **1**.

## 2.2.2. Structure elucidation of major flavonol glycosides

Sutherlandins A–D (**5**–**8**, see Figure 2-27) presented typical UV and IR spectroscopic data of flavonoid derivatives as shown in the Experimental Section 2.3.3 (Mabry, Markham *et al.*, 1970).

A general analysis of their $^1$H and $^{13}$C NMR spectroscopic data (Tables 2-3 and 2-4) indicated that **5** and **6** were quercetin 3-*O*-diglycosides, while **7** and **8** were kaempferol 3-*O*-diglycosides (Mabry, Markham *et al.*, 1970). For example, the presence of the quercetin aglycone in **5** was evident by the $^1$H NMR resonances at $\delta_H$ 6.20 (br s, H-6), 6.40 (br s, H-8) for a 5,7-dihydroxylated A-ring, and at $\delta_H$ 7.65 (br s, H-2'), 6.88 (d, $J$ = 8.3, H-5'), and 7.62 (d, $J$ = 8.3 Hz, H-6') for an ABX coupling pattern in the B-ring (Hubner, Wray *et al.*, 1999; Kazuma, Noda *et al.*, 2003; Lee, Chen *et al.*, 2008). The presence of the kaempferol aglycone in **7** derived from the $^1$H NMR resonances at $\delta_H$ 6.19 (br s, H-6), 6.41 (br s, H-8), 6.89 (br s, H-3' and H-5'), and 8.05 (d, $J$ = 5.2 Hz, H-2' and H-6') and $^{13}$C NMR data (Hubner, Wray *et al.*, 1999; Kazuma, Noda *et al.*, 2003). The base peak of *m/z* 303 for **5** and **6** and the base peak of *m/z* 287 for **7** and **8** is also shown the presence of quercetin aglycone and kaempferol aglycone, respectively.

A common feature of the four glycosides was the ester absorption (1711 cm$^{-1}$) in their IR spectra and typical proton resonances around $\delta_H$ 1.20 and 2.44 in the upfield regions of their $^1$H NMR spectra. In conjunction with related carbon resonances identified by HMQC and HMBC, e.g., at $\delta_C$ 27.7, 45.6, 46.3, 70.9, 172.6, and 175.2 in compound **5**, the presence of a 3-hydroxy-3-methylglutaroyl (HMG) moiety in compounds **5**–**8** was confirmed (Semmar, Fenet *et al.*, 2002).

Further analysis of their NMR spectra revealed that **5** and **7** possessed the same sugar moiety attached to an HMG moiety, and **6** and **8** had the same sugar moiety attached to an HMG

moiety. The linkages of the sugar and HMG moieties in these glycosides were further determined

as follows.
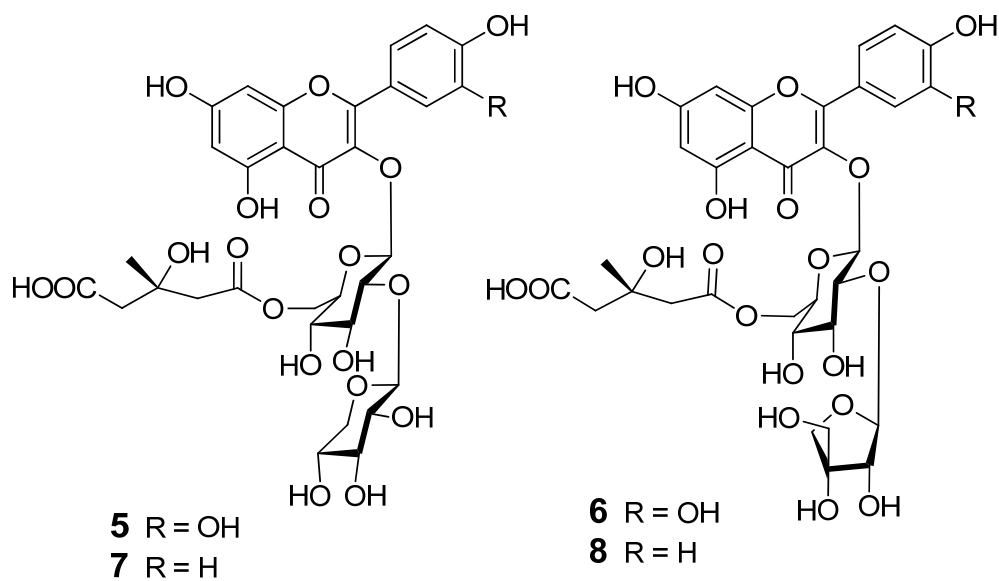


Figure 2-27.  Structures of isolated major flavonol glycosides from *S. frutescens*.
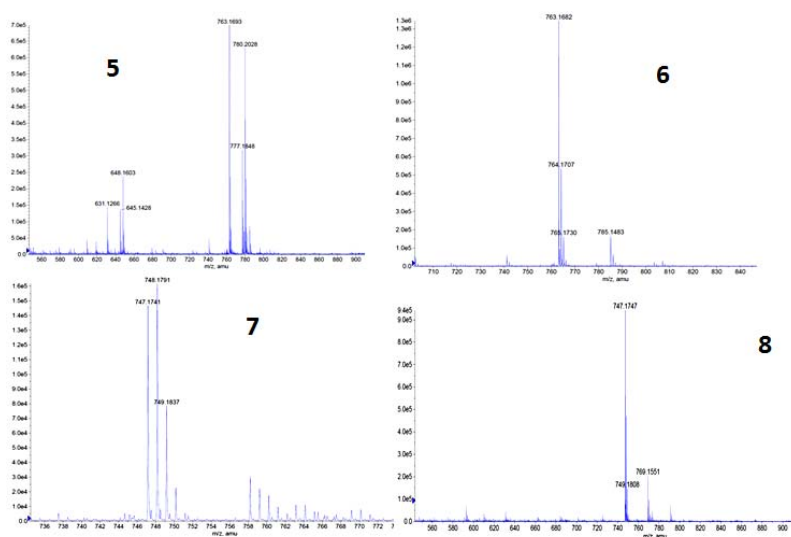


Figure 2-28.  HRESIMS spectra of compounds **5**–**8**.

## 2.2.2.1. Sutherlandin A (**5**)

The HRESIMS of compound **5** exhibited pseudomolecular ion peaks at *m/z* 763.1693 [M + Na]$^+$ and 741.1887 [M + H]$^+$, consistent with the molecular formula $C_{32}H_{36}O_{20}$. The fragment ion at *m/z* 609.1467 [M + H − 132 (pentose)]$^+$ indicated that a pentose is located at the terminal position in the sugar chain.
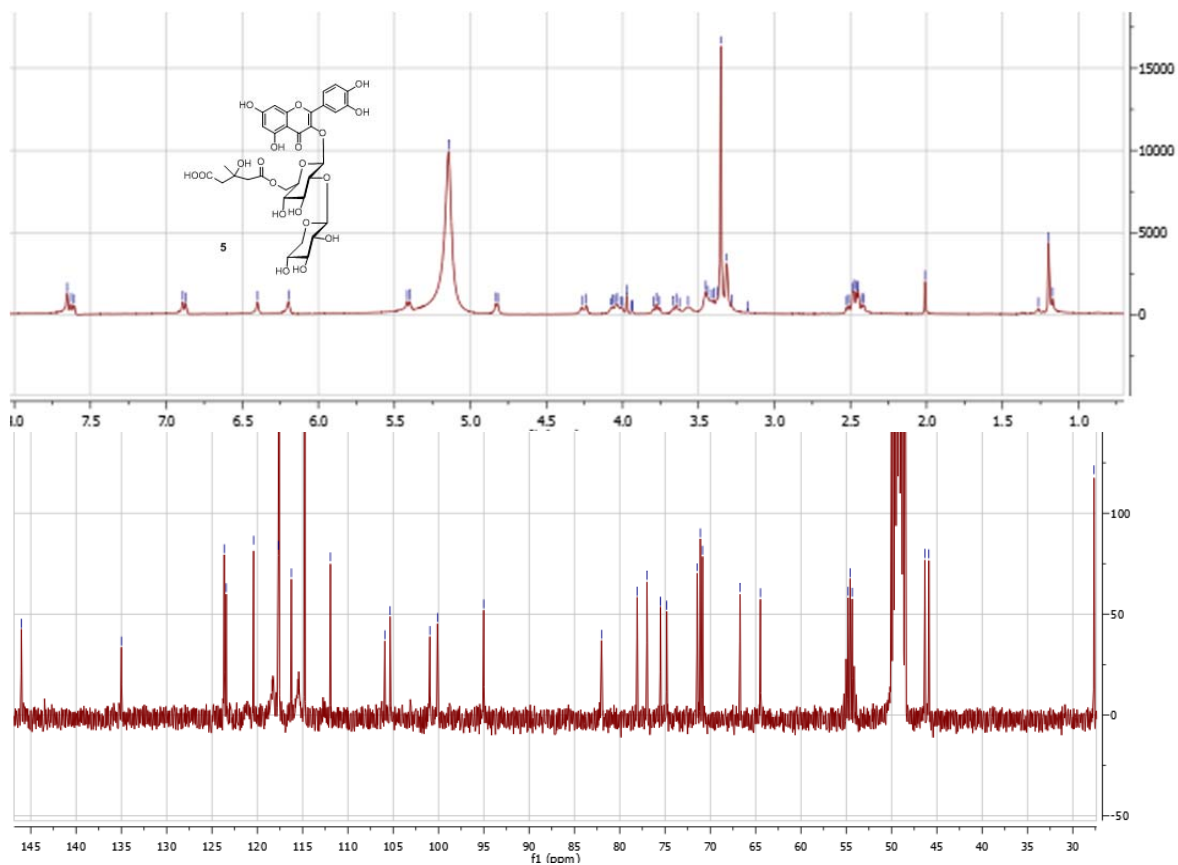


Figure 2-29. $^1$H and $^{13}$C NMR spectra of compound **5** in methanol-$d_4$.

Two anomeric protons at $\delta_H$ 5.41 (d, *J* = 7.5 Hz) and 4.83 (d, *J* = 5.5 Hz) in the $^1$H NMR

spectrum and two sets of $^{13}$C NMR resonances at $\delta_C$ 105.4 (C-1'''), 74.8 (C-2'''), 77.0 (C-3'''), 71.1

(C-4'''), and 66.7 (C-5''') corresponding to a terminal β-xylopyranosyl unit, and at $\delta_C$ 101.0 (C-1''),

82.0 (C-2''), 78.1 (C-3''), 71.5 (C-4''), 75.5 (C-5'') and 64.5 (C-6'') corresponding to a

β-glucopyranosyl unit indicated that the sugar moiety of **5** is composed of a β-xylopyranosyl and

β-glucopyranosyl units (Kinjo, Araki *et al.*, 1992). This disaccharide moiety is attached to the C-3

hydroxy group of the aglycone based on the HMBC correlation between the anomeric proton of

the glucosyl unit at $\delta_H$ 5.41 (H-1'') and C-3 of the aglycone at $\delta_C$ 135.0. A three-bond HMBC

correlation between the anomeric proton of the xylosyl unit at $\delta_H$ 4.83 (H-1''') and C-2 of the

glucosyl unit at $\delta_C$ 82.0 suggested a 1→2 linkage from the xylosyl unit to the glucosyl unit.



Figure 2-30.  HMQC spectrum of compound **5** in methanol-$d_4$.

57
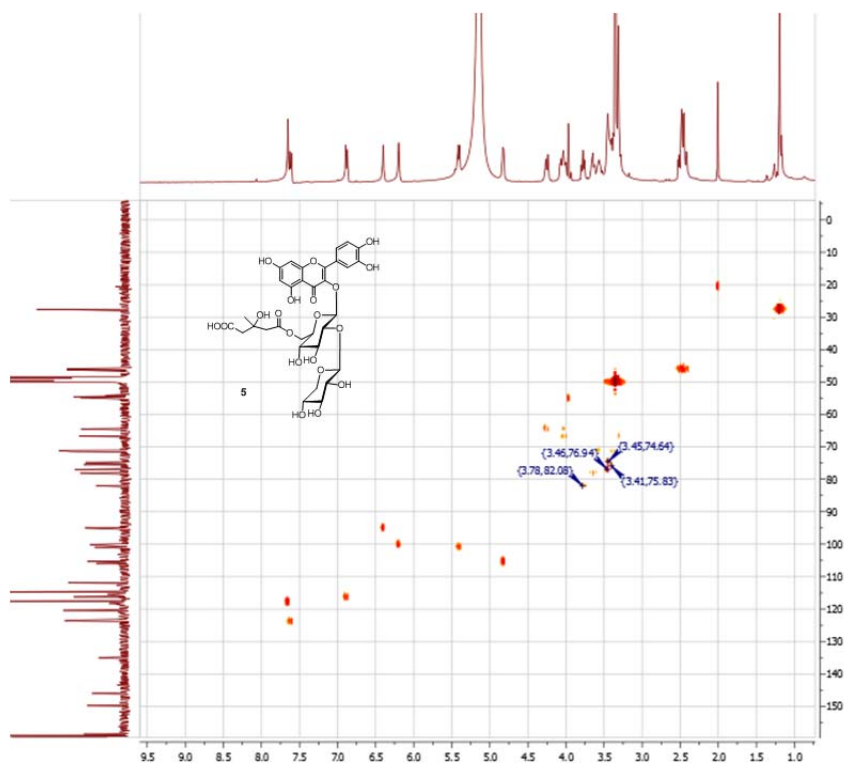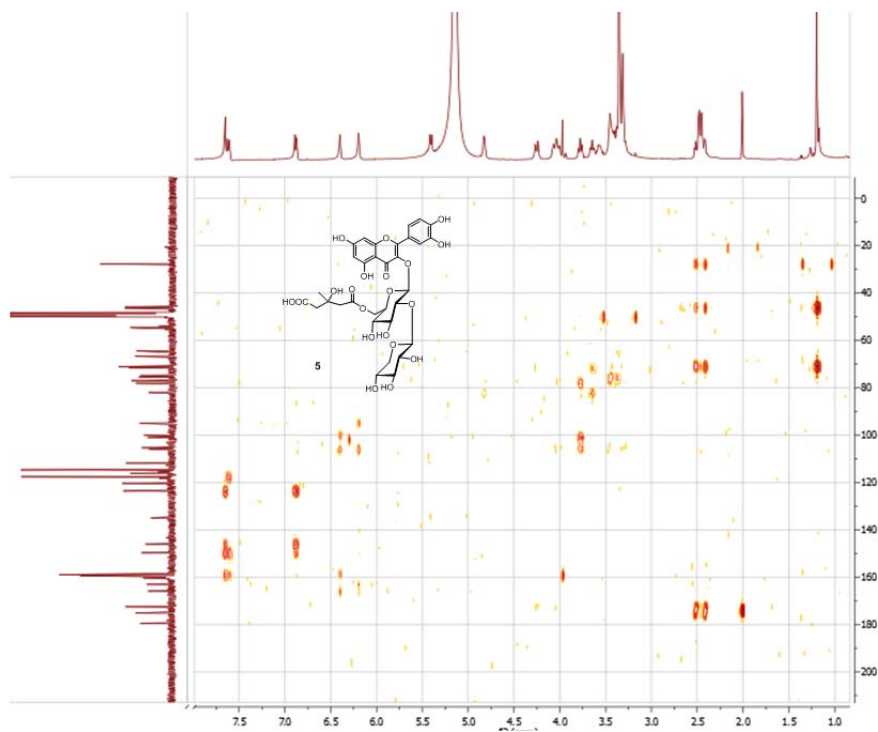
Figure 2-31.  HMBC spectrum of compound **5** in methanol-$d_4$.
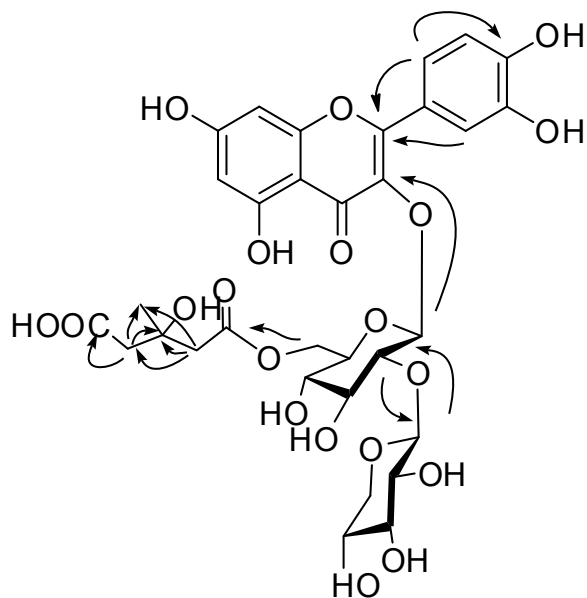


Figure 2-32.  Selected key HMBC correlations of **5**.
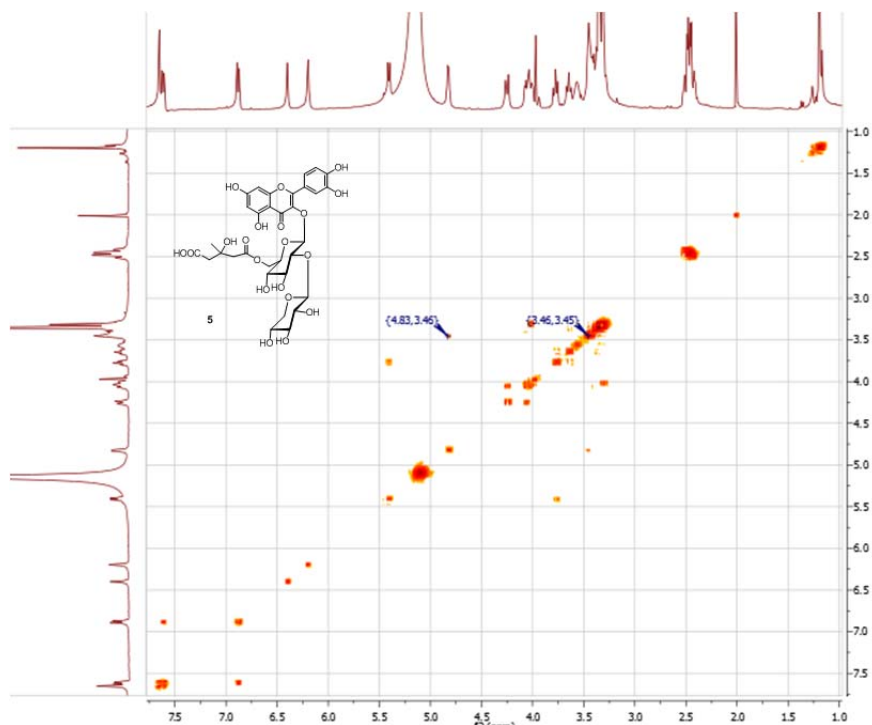
Figure 2-33. COSY spectrum of compound **5** in methanol-$d_4$.

The three-bond HMBC correlations between H-6'' ($\delta_H$ 4.06 and $\delta_H$ 4.25) and the ester carbonyl group at $\delta_C$ 172.5 confirmed the linkage of the HMG moiety to the C-6 hydroxy group of the glucosyl unit. The esterification at this position generally leads to an upfield shift and a downfield shift for C-5 and C-6, respectively, of the glucosyl unit (Semmar, Fenet *et al.*, 2002).

Although the absolute configuration of the stereogenic center in HMG group was not determined yet, (3*S*)-HMG moiety would be the most probable since it would be consistent with the biosynthetic pathway through esterification from naturally occurring (3*S*)-HMG-CoA (Bergot, Baker *et al.*, 1979). Reports using Hirai's method to determine the *R*-configuration of the stereogenic center of HMG were later revised to a (3*S*)-HMG moiety using a more reliable method (Fujimoto, Nakamura *et al.*, 2001; Kamo, Hirai *et al.*, 2004). Thus, the structure of compound **5**

was characterized as quercetin 3-*O*-β-D-xylopyranosyl(1→2)-[6-*O*-(3-hydroxy-3-methylglutaroyl)]-β-D-glucopyranoside.

## 2.2.2.2. Sutherlandin B (**6**)

The molecular formula of compound **6**, $C_{32}H_{36}O_{20}$, was determined by HRESIMS showing pseudomolecular ion peaks at *m/z* 763.1682 [M + Na]$^+$, and *m/z* 741.1941 [M + H]$^+$. The $^1$H and $^{13}$C NMR spectra resembled those of **5** except for the anomeric proton at $\delta_H$ 5.50 (br s) and a set of carbon resonances at $\delta_C$ 110.7 (d, C-1'''), 78.2 (d, C-2'''), 81.1 (s, C-3'''), 75.8 (t, C-4''') and 66.5 (t, C-5''') corresponding to a β-D-apiofuranosyl unit (Kitagawa, Hori *et al.*, 1993; Semmar, Fenet *et al.*, 2002) in **6** instead of the presence of a β-D-xylopyranosyl unit in **5**. Its HRESIMS displayed the same fragmentation pattern as **5**, indicating that the β-D-apiofuranosyl unit was located at the terminal position of the sugar moiety. The interglycosidic linkage of the apiosyl unit to the C-2 hydroxy group of the glucosyl unit was confirmed by an upfield shift of approximately 3 ppm and a downfield shift of approximately 2 ppm for C-1 and C-2, respectively, of the glycosyl unit (Kazuma, Noda *et al.*, 2003).

The attachment of the HMG moiety to the C-6 hydroxy group of the glucosyl unit was supported by the similar chemical shifts of C-6″ at $\delta_C$ 64.2 and H-6″ at $\delta_H$ 4.00 (br d, *J* = 9.4 Hz), 4.22 (br d, *J* = 11.7 Hz), in comparison to those of compound **5**. Thus, the structure of **6** was characterized as quercetin 3-*O*-β-D-apiofuranosyl(1→2)-[6-*O*-(3*S*-hydroxy-3*S*-methylglutaroyl)]-β-D-glucopyranoside.
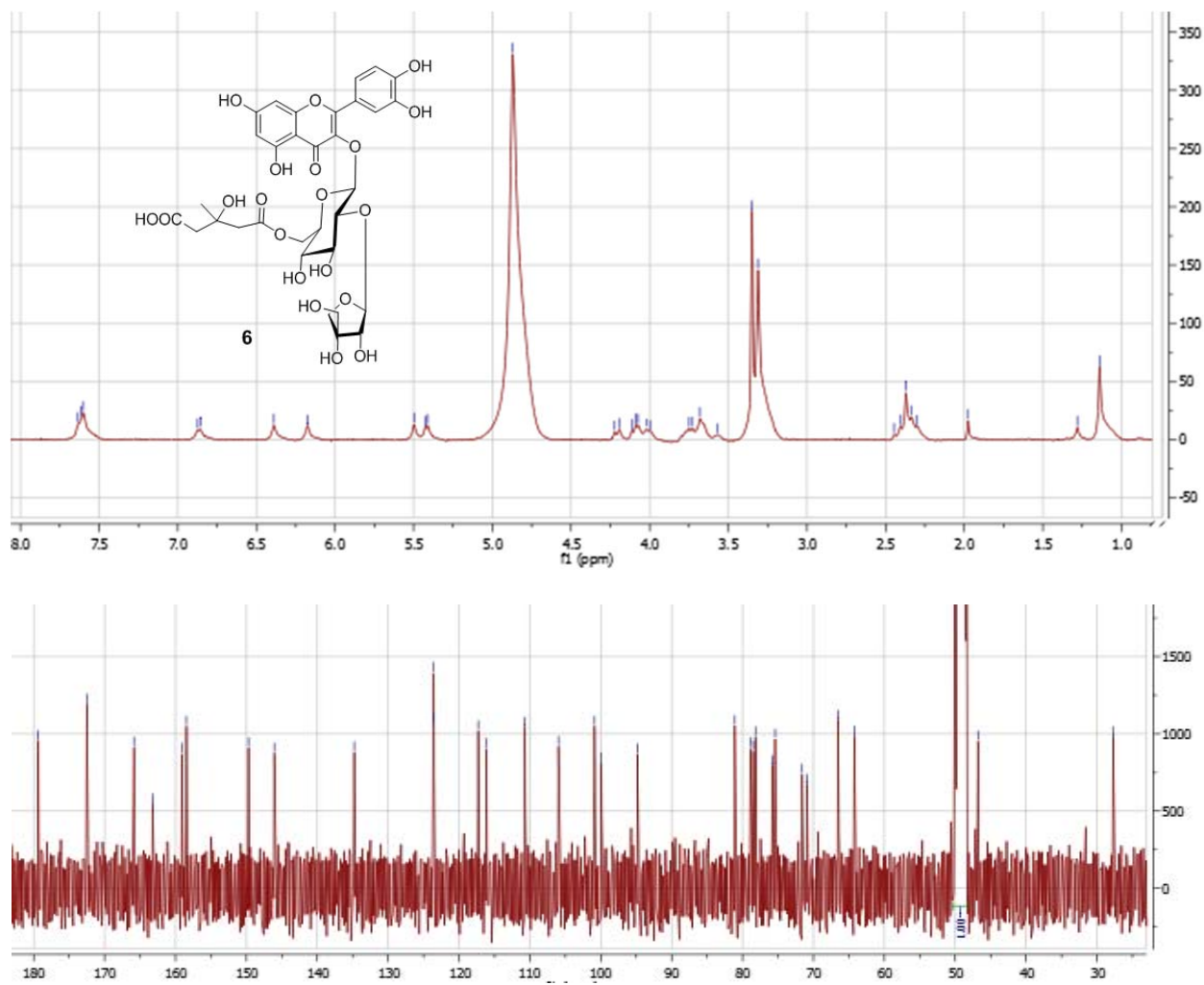
Figure 2-34. $^1$H and $^{13}$C NMR spectra of compound **6** in methanol-$d_4$.

## 2.2.2.3. Sutherlandin C (**7**)

The molecular formula of compounds **7** was determined as $C_{32}H_{36}O_{19}$ by a combination of HRESIMS, exhibiting pseudomolecular ion peaks at *m/z* 747.1741 $[M + Na]^+$ (calcd 747.1748), together with and $^{13}C$ NMR data. The $^1H$ and $^{13}C$ NMR spectra of **7** due to the sugar and acyl moieties showed exactly the same chemical shifts as those of compound **5** (Tables 2-3 and 2-4).
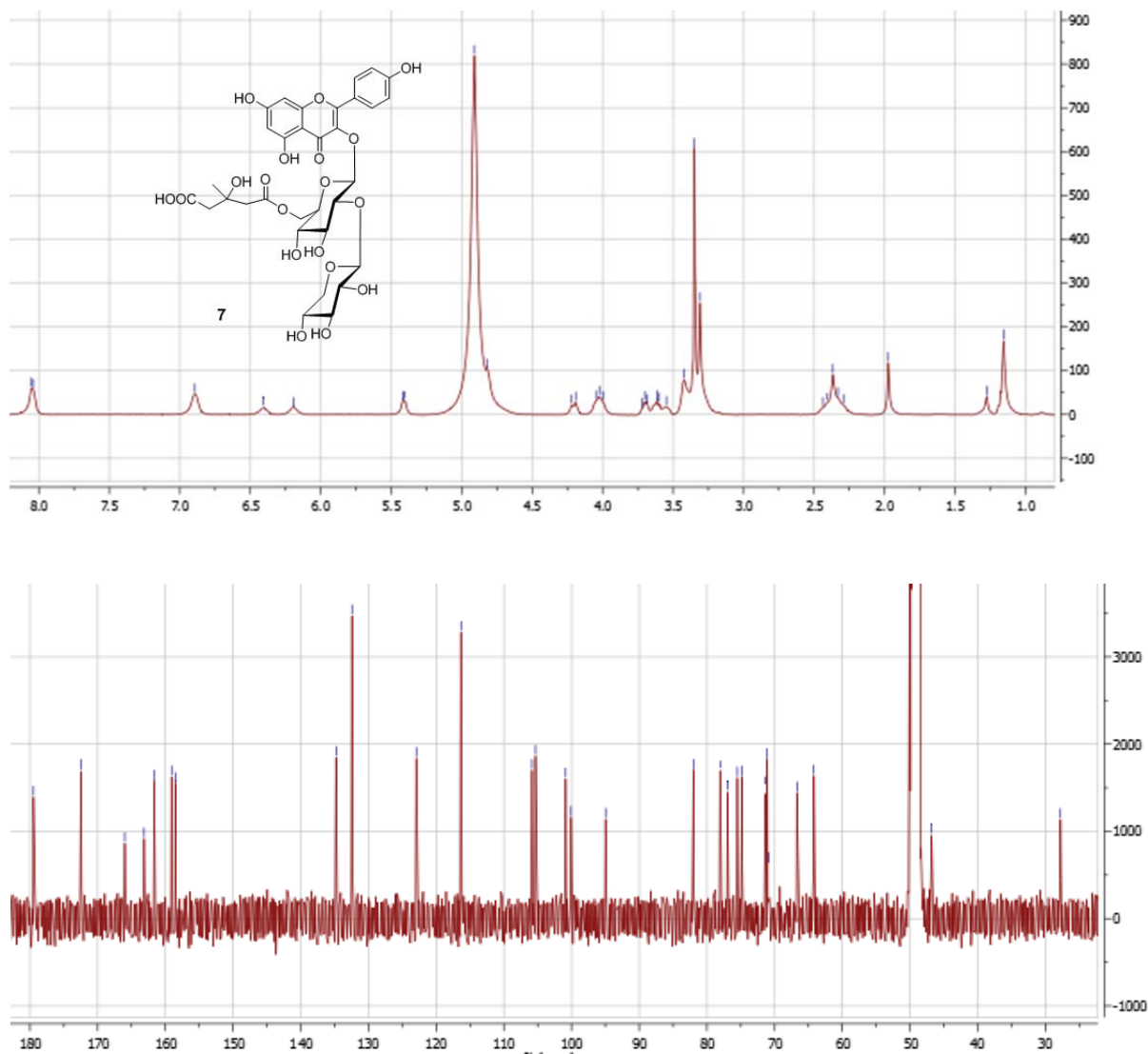


Figure 2-35. $^1H$ and $^{13}C$ NMR spectra of compound **7** in methanol-$d_4$.
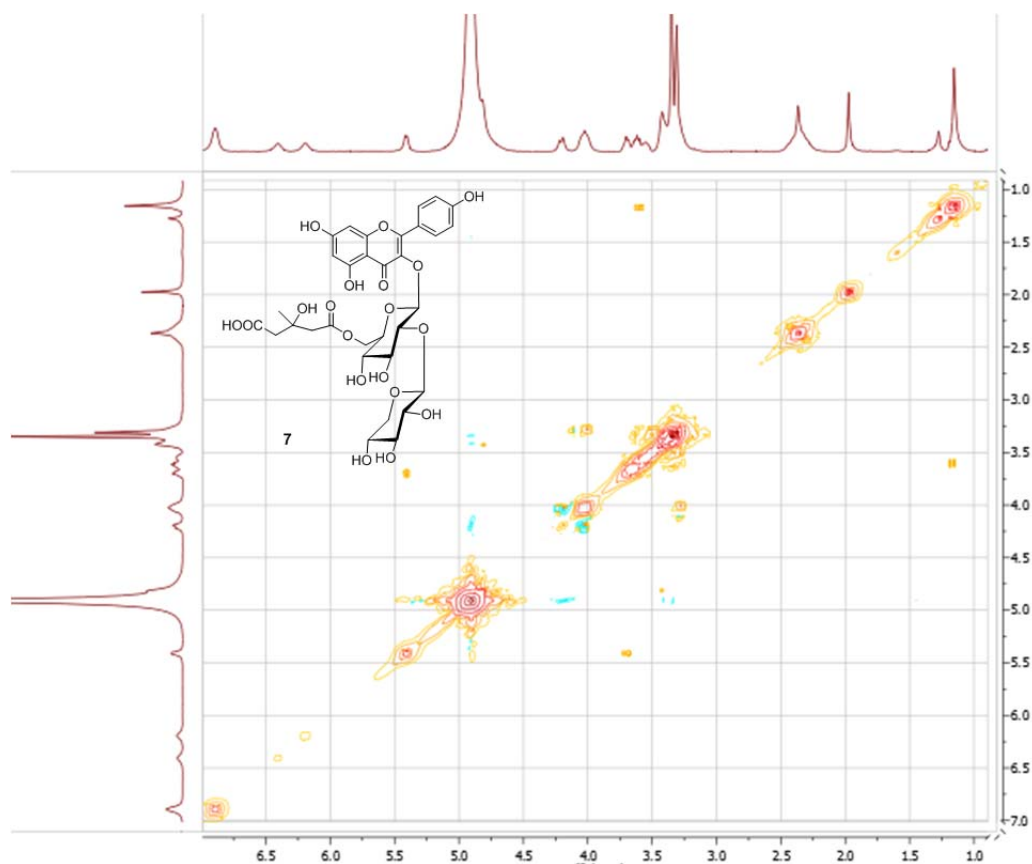
Figure 2-36.  COSY spectrum of compound **7** in methanol-$d_4$.

In combination with the 2D NMR data, the structure of **7** was established as kaempferol 3-*O*-β-D-xylopyranosyl(1→2)-[6-*O*-(3-hydroxy-3-methylglutaroyl)]-β-D-glucopyranoside.

### 2.2.2.4.  Sutherlandin D (**8**)

The molecular formula of compounds **8** was determined as $C_{32}H_{36}O_{19}$ by a combination of HRESIMS and ^{13}C NMR data (Table 2-4). The ^{1}H and ^{13}C NMR spectra of **8** due to the sugar and acyl moieties (Figure 2-37) showed identical chemical shifts as those of compounds **6** (Figure 2-34).
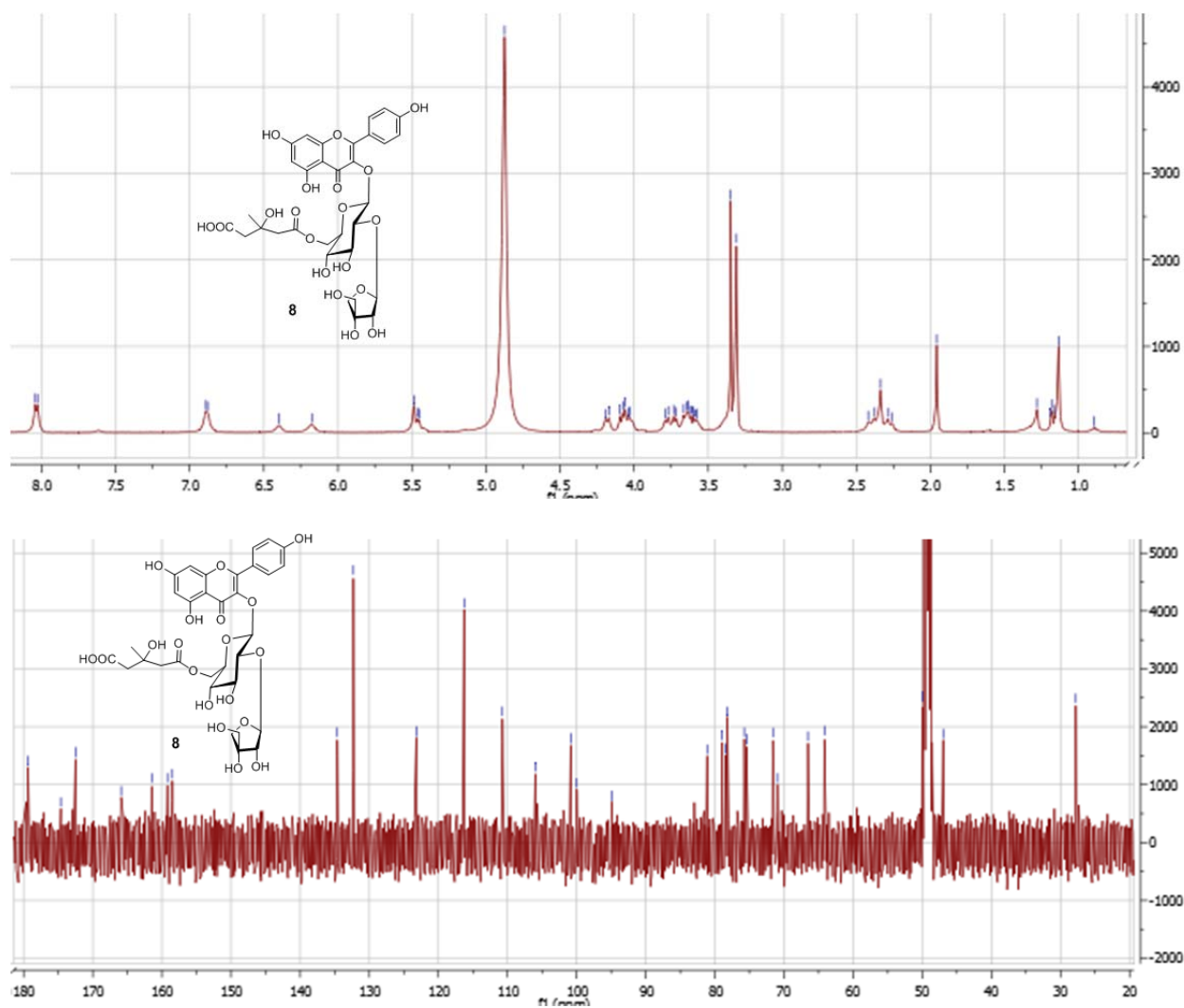
Figure 2-37. $^1$H and $^{13}$C NMR spectra of compound **8** in methanol-$d_4$.

In addition, 2D NMR spectra including HMBC (Figures 2-38, 2-39, 2-40, and 2-41) were used to confirm the structure of **8**. Therefore, the structure of **8** was readily established as kaempferol 3-*O*-β-D-apiofuranosyl(1→2)-[6-*O*-(3*S*-hydroxy-3*S*-methylglutaroyl)]-β-D-glucopyranoside.

64
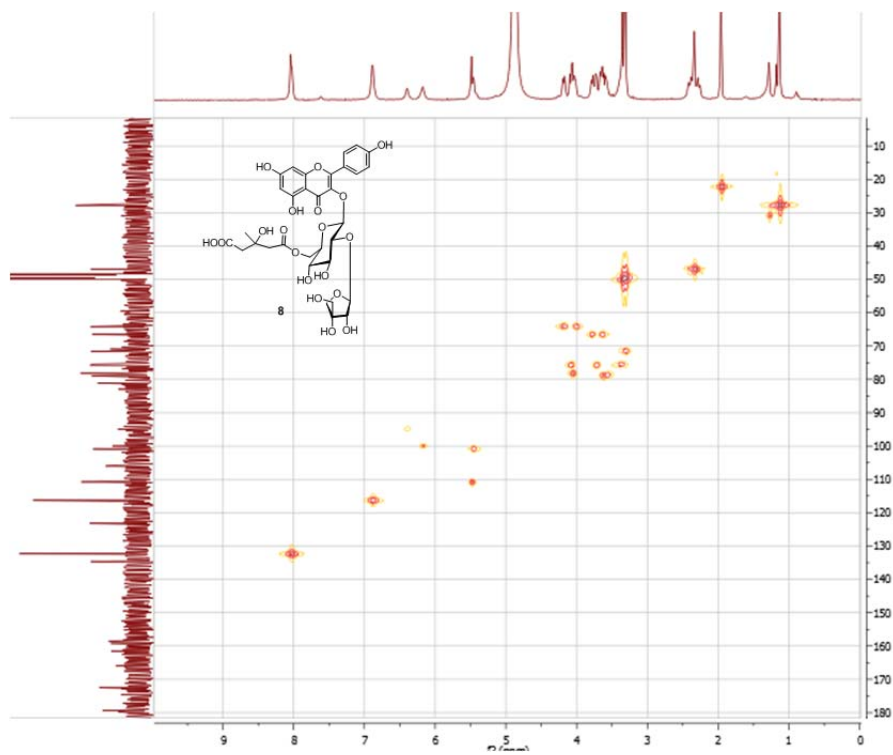
Figure 2-38.  HMQC spectrum of compound **8** in methanol-$d_4$.
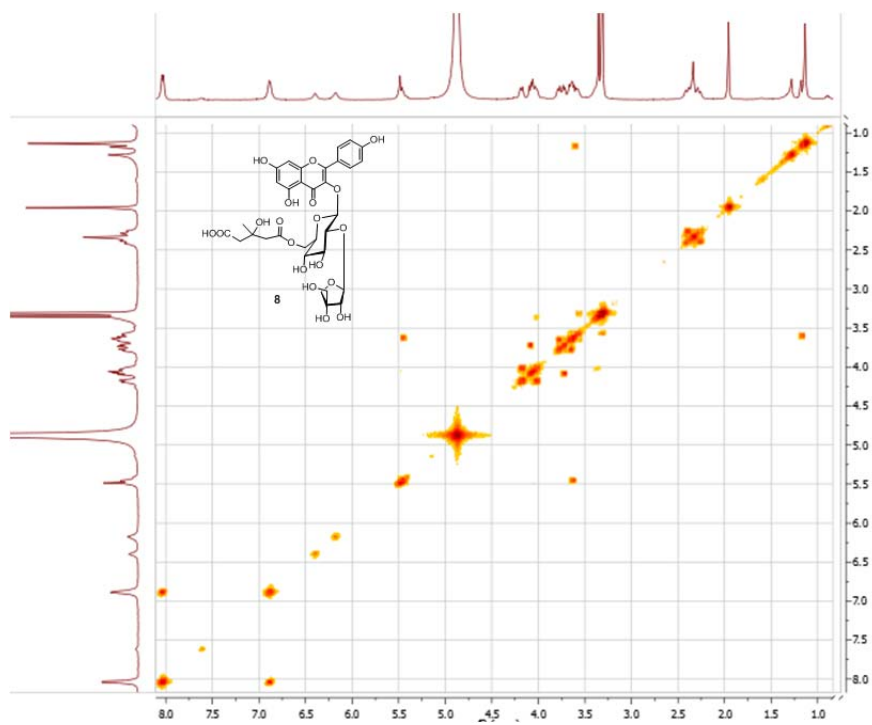


Figure 2-39.  COSY spectrum of compound **8** in methanol-$d_4$.

65
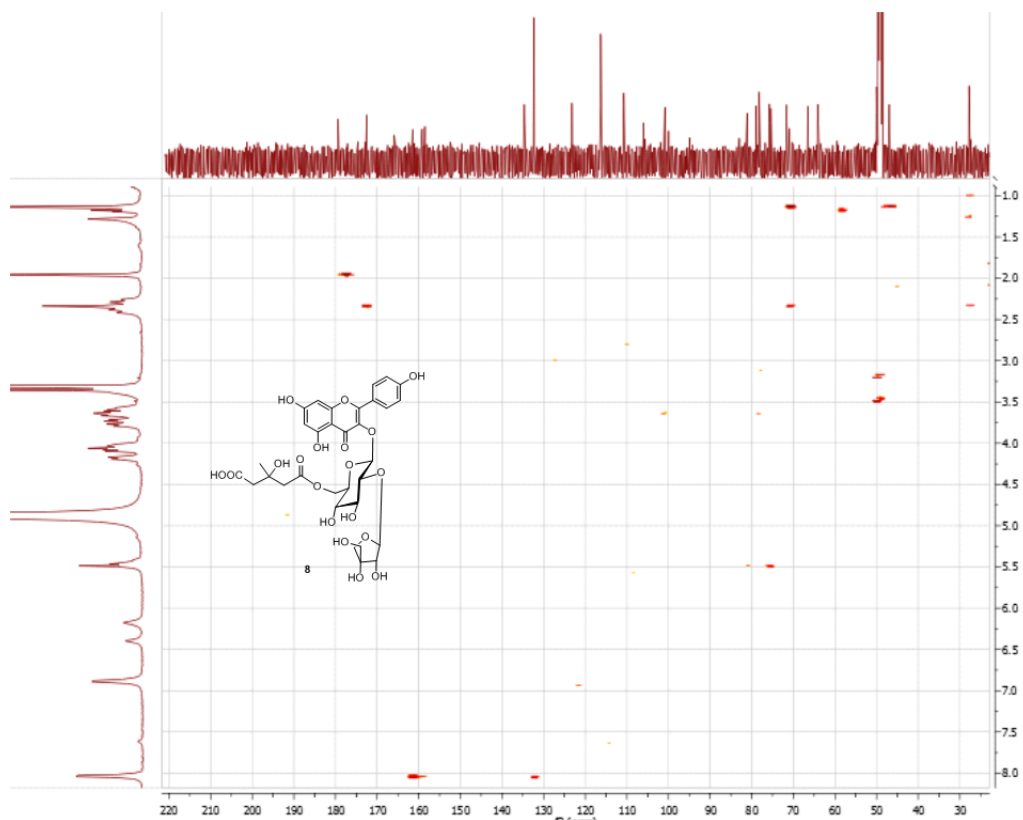
Figure 2-40. HMBC spectrum of compound **8** in methanol-$d_4$.
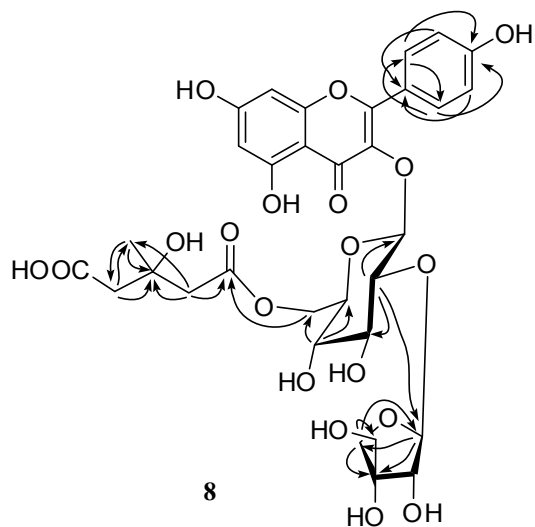


Figure 2-41. Selected key HMBC correlations of **8**.

Table 2-3.  $^1$H NMR data for compounds **5**–**8** in methanol-$d_4$.

| | 5 | 6 | 7 | 8 |
|---|---|---|---|---|
| 6 | 6.20 br s | 6.17 br s | 6.19 br s | 6.17 br s |
| 8 | 6.40 br s | 6.39 br s | 6.41 br s | 6.39 br s |
| 2' | 7.65 br s | 7.63 $^b$ | 8.05 br d (5.6 Hz) | 8.03 d (8.0 Hz) |
| 3' | | | 6.89 br s | 6.88 d (6.6 Hz) |
| 5' | 6.88 d (8.3 Hz) | 6.87 d (6.9 Hz) | 6.89 br s | 6.88 d (6.6 Hz) |
| 6' | 7.62 d (8.4 Hz) | 7.59 t (8.3 Hz) | 8.05 br d (5.6 Hz) | 8.03 d (8.0 Hz) |
| **Glc** | | | | |
| 1" | 5.41 d (7.5 Hz) | 5.42 d (7.1 Hz) | 5.41 d (6.4 Hz) | 5.46 d (7.1 Hz) |
| 2" | 3.78 t (8.5 Hz) | 3.63 $^b$ | 3.70 t (8.7 Hz) | 3.62 $^b$ |
| 3" | 3.65 t (8.5 Hz) | 3.57 $^b$ | 3.62 t (7.2 Hz) | 3.58 $^b$ |
| 4" | 3.39 $^b$ | 3.25 $^b$ | 3.40 $^b$ | 3.30 $^b$ |
| 5" | 3.41 $^b$ | 3.35 $^b$ | 3.40 $^b$ | 3.38 $^b$ |
| 6" | 4.06 dd (12.0 Hz, 5.0 Hz); 4.25 $^b$ | 4.00 br d (9.4 Hz); 4.22 br d (11.7 Hz) | 4.04 $^b$; 4.21 br d (11.6) | 4.00 $^b$; 4.20 br d (11.1 Hz) |
| **Xyl** | | | | |
| 1''' | 4.83 d (5.5 Hz) | \ | 4.82 $^b$ | \ |
| 2''' | 3.45 $^b$ | \ | 3.42 $^b$ | \ |
| 3''' | 3.46 $^b$ | \ | 3.42 $^b$ | \ |
| 4''' | 3.57 $^b$ | \ | 3.55 $^b$ | \ |
| 5''' | 3.31 $^b$; 4.02 dd(12.0 Hz, 4.1 Hz) | \ | 3.31 $^b$; 4.00 $^b$ | \ |
| **Api** | | | | |
| 1''' | \ | 5.50 br s | \ | 5.48 br s |
| 2''' | \ | 4.08 $^b$ | \ | 4.06 $^b$ |
| 4''' | \ | 3.74 d (9.0 Hz); 4.10 d (9.3 Hz) | \ | 3.72 d (9.5 Hz); 4.08 d (9.5 Hz) |
| 5''' | \ | 3.64 $^b$; 3.78 d (11.8 Hz) | \ | 3.64 $^b$; 3.78 d (11.1 Hz) |
| **HMG** | | | | |
| 2'''' | 2.43 d (14.5 Hz); 2.50 d (14.5 Hz); | 2.37 $^b$ | 2.37 $^b$ | 2.34 $^b$ |
| 4'''' | 2.44 d (15.1 Hz); 2.51 d (15.1 Hz) | 2.37 $^b$ | 2.37 $^b$ | 2.34 $^b$ |
| 6'''' | 1.20 s | 1.14 s | 1.16 s | 1.13 s |

($\delta$, ppm)

Table 2-4. $^{13}$C NMR data for compounds **5**–**8** in methanol-$d_4$.

|  | 5 | 6 | 7 | 8 |
|---|---|---|---|---|
| 2 | 158.5 s | 158.5 s | 159.1 s | 159.2 s |
| 3 | 135.0 s | 134.8 s | 134.8 s | 134.6 s |
| 4 | 179.6 s | 179.4 s | 179.5 s | 179.4 s |
| 5 | 163.1 s | 163.2 s | 163.1 s | 163.2 s |
| 6 | 100.1 d | 99.9 d | 100.1 d | 100.0 d |
| 7 | 166.0 s | 165.9 s | 166.0 s | 165.9 s |
| 8 | 95.0 d | 94.8 d | 95.0 d | 94.9 d |
| 9 | 159.0 s | 159.1 s | 158.5 s | 158.5 s |
| 10 | 105.9 s | 106.0 s | 105.9 s | 106.0 s |
| 1' | 123.4 s | 123.6 s | 122.9 s | 123.2 s |
| 2' | 117.7 d | 117.3 d | 132.4 d | 132.3 d |
| 3' | 146.0 s | 146.1 s | 116.3 d | 116.3 d |
| 4' | 149.8 s | 149.7 s | 161.6 s | 161.5 s |
| 5' | 116.2 d | 116.2 d | 116.3 d | 116.3 d |
| 6' | 123.7 d | 123.6 d | 132.4 d | 132.3 d |
| **Glc** | | | | |
| 1" | 101.0 d | 100.9 d | 100.9 d | 100.9 d |
| 2" | 82.0 d | 78.9 d | 82.0 d | 78.9 d |
| 3" | 78.1 d | 78.5 d | 78.1 d | 78.5 d |
| 4" | 71.5 d | 71.6 d | 71.4 d | 71.6 d |
| 5" | 75.5 d | 75.4 d | 75.5 d | 75.4 d |
| 6" | 64.5 t | 64.2 t | 64.2 t | 64.2 t |
| **Xyl** | | | | |
| 1''' | 105.4 d | / | 105.3 d | / |
| 2''' | 74.8 d | / | 74.8 d | / |
| 3''' | 77.0 d | / | 77.0 d | / |
| 4''' | 71.1 d | / | 71.1 d | / |
| 5''' | 66.7 t | / | 66.7 t | / |
| **Api** | | | | |
| 1''' | / | 110.7 d | / | 110.8 d |
| 2''' | / | 78.2 d | / | 78.2 d |
| 3''' | / | 81.1 s | / | 81.1 s |
| 4''' | / | 75.8 t | / | 75.8 t |
| 5''' | / | 66.5 t | / | 66.5 t |
| **HMG** | | | | |
| 1'''' | 172.6 s | 172.5 s | 172.5 s | 172.5 s |
| 2'''' | 46.3 t | 46.8 t | 46.8 t | 47.0 t |
| 3'''' | 70.9 s | 70.9 s | 70.9 s | 70.9 s |
| 4'''' | 45.9 t | 46.8 t | 46.8 t | 47.0 t |
| 5'''' | 175.2 s | | | |
| 6'''' | 27.7 q | 27.7 q | 27.8 q | 27.8 q |

($\delta$, ppm)

2.2.2.5. Determination of the absolute configuration of the monosaccharide units of sutherlandins

      C (**7**) and D (**8**)

To confirm the absolute configuration of the monosaccharide moieties in sutherlandins C (**7**) and D (**8**), an HPLC-based method recently developed by Tanaka *et al.* for sugar analysis (Tanaka, Nakashima *et al.*, 2007) was employed. The advantage of using a liquid chromatographic method is that this type of experiment can be conveniently conducted in a general laboratory that is simply equipped with an HPLC-UV instrument. Using D-glucose as an example (Figure 2-42), the monosaccharide residue is reacted with L-cysteine methyl ester in pyridine to give a thiazolidine derivative, which is then incubated with phenyl isothiocyanate to form a phenylthiocarbamate derivative for HPLC analysis.
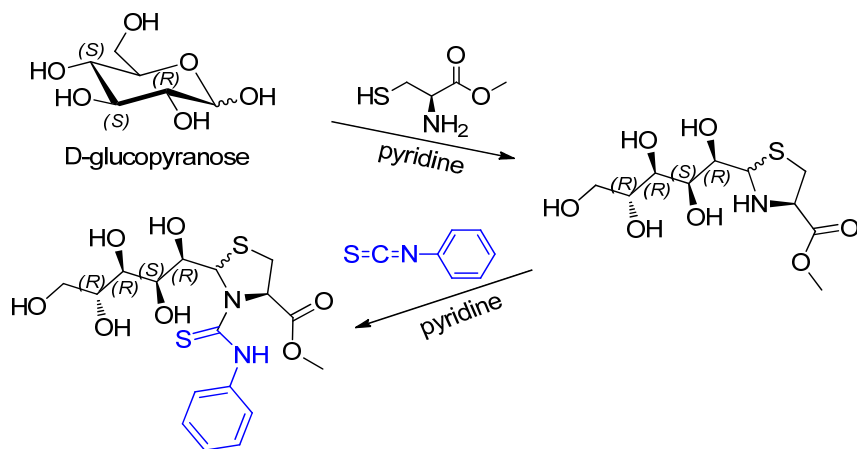


Figure 2-42. Chemical reactions involved in the sugar analysis using D-glucose as an example. Based on the reported method (Tanaka, Nakashima *et al.*, 2007).

As shown in Figures 2-43 and 2-44, each pair of the enantiomers of D /L- glucoses and D /L-

xyloses was able to be clearly discriminated in the HPLC chromatograms after chiral derivatization. L-Apiose was not included in the experiment due to unavailability of an authentic sample. However, similar derivatization of the enantiomers showed significant difference of retention time ($\Delta t_R$) between D- and L- apiose (> 12 minutes) in the reversed-phase HPLC separation, while the $\Delta t_R$ between the enantiomers of glucose and xylose were moderate (< 2 minutes) (Tanaka, Nakashima *et al.*, 2007). In addition, no interference peaks was shown among D- / L-glucose, D- / L-xylose, and D-apiose in the developed chromatographic condition.
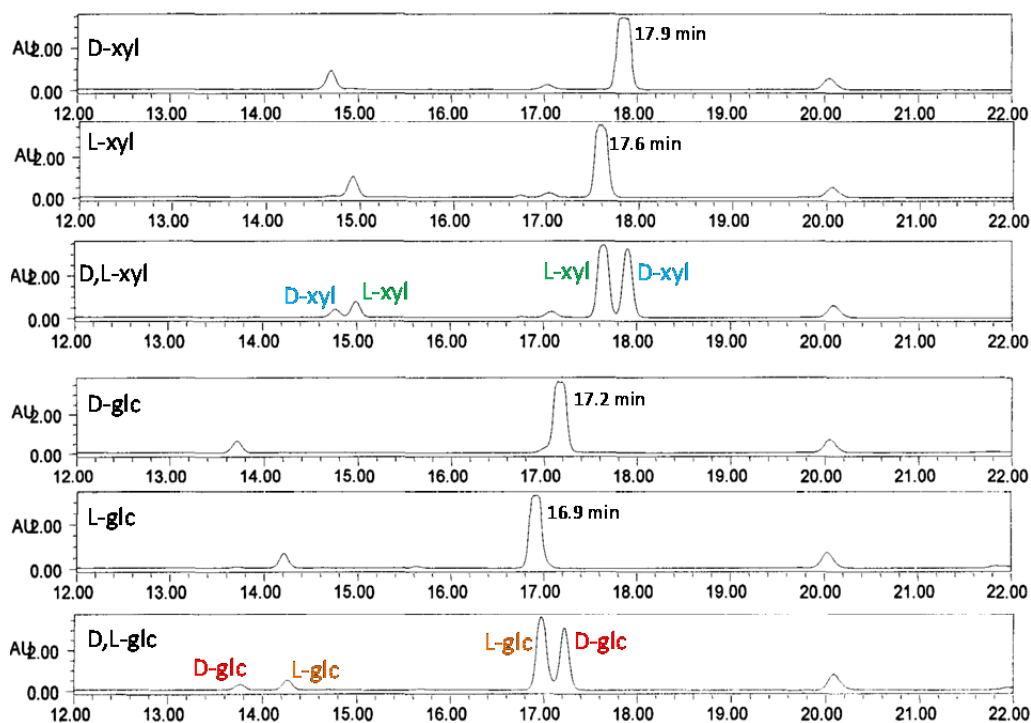


Figure 2-43.  HPLC chromatograms of the derivatives of enantiomers of glucoses and xyloses.

The retention times for each monosaccharide were determined as: D-glucose: 17.2 min,

L-glucose: 16.9 min, D-xylose: 17.9 min, L-xylose: 17.6 min, D-apiose: 19.3 min. The monosaccharides resulting from the acid hydrolyses of sutherlandins C (**7**) and D (**8**) were treated similarly and determined as D-glucose, D-xylose, and D-apiose by comparison of the retention times with those authentic standard monosaccharide derivatives (Figure 2-44).
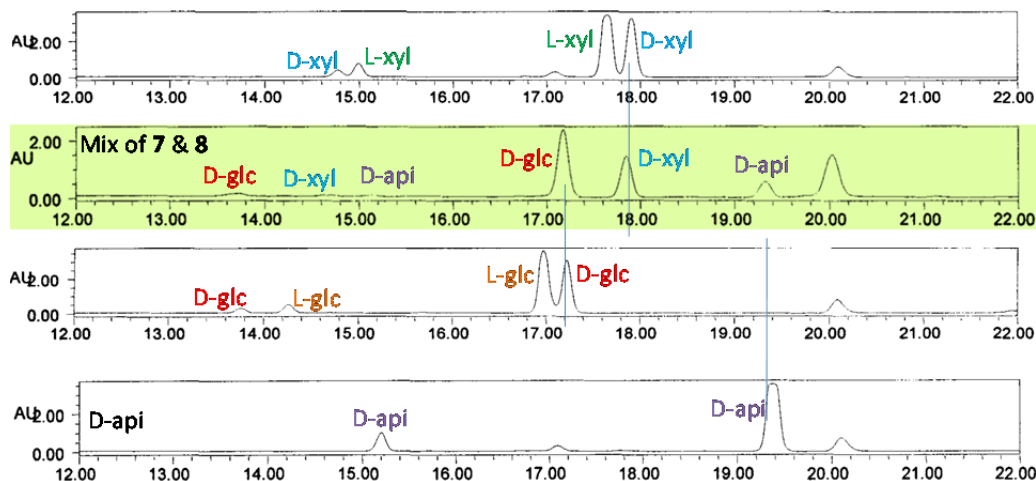


Figure 2-44.  HPLC chromatograms of the derivatives of mixed enantiomers and test samples.

It is also discernible from Figure 2-44 that a series of weak characteristic peaks of the sugar derivatives with shorter retention times were also shown at 14.7 min, 14.9 min, 13.7 min, 14.2 min, and 15.2 min for D-xylose, L-xylose, D-glucose, L-glucose, and D-apiose, respectively. This could be due to the coexistences of artifactual epimeric products formed in the thiazolidine ring closure process during the derivatization.  Interestingly, these types of minor peaks were not shown in the GC based experiments and in our established LC-UV/MS method for simultaneous analysis of multiple monosaccharides (see Section 3.2).  Broadened peaks were observed in the GC-based analysis and were explained as possible coexistence of two epimers (Hara, Okabe *et al.*, 1987).

71

## 2.2.3. Structure elucidation of minor triterpene glycosides
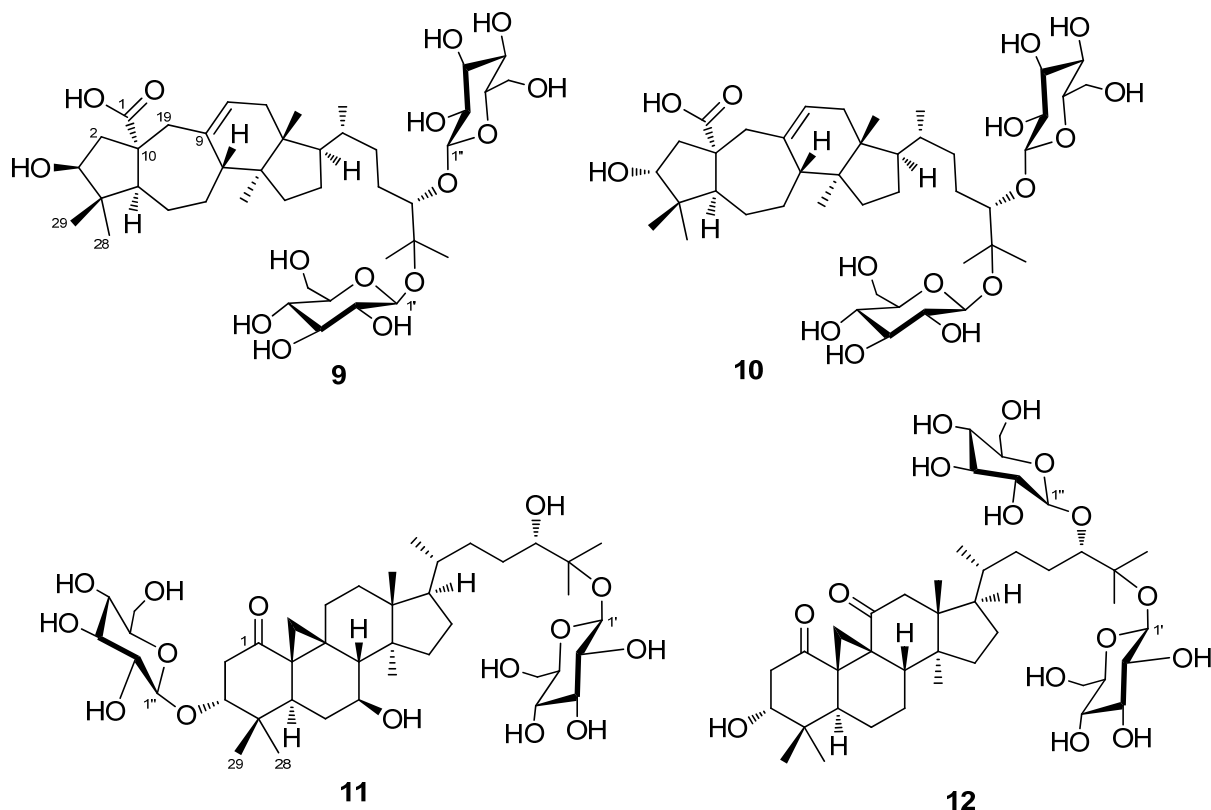


Figure 2-45. Structures of isolated minor triterpene glycosides from *S. frutescens*.

### 2.2.3.1. Sutherlandiosides E (**9**) and F (**10**)

The molecular formula of both compounds **9** and **10** were determined as $C_{42}H_{70}O_{15}$ by combination of HRESIMS and $^{13}C$ NMR data. The $^{1}H$ NMR spectrum showed 30 resonances due to the aglycone moiety (Figure 2-46), including six tertiary methyl groups that resemble those of the cycloartane-type monoglycosides **1**–**4** (Table 2-1).

Compared to the $^{13}C$ NMR spectra displaying 36 carbon signals in compounds **1**–**4**, a set of six additional carbon signals in the spectra of **9** and **10** (one typical anomeric carbon at $\delta_C$ 105.2

(C-1″), four oxygenated tertiary carbons, and one oxygenated secondary carbon) were attributed to an extra terminal glucopyranosyl moiety. The resonance of the additional anomeric proton at $\delta_H$ 5.53 (d, $J$ = 7.8 Hz, H-1″) in $^1$H NMR spectrum of **9** evidenced the β-configuration of the glucopyranosyl moiety. The linkage of the additional glucopyranosyl unit to the C-24 hydroxy group is evident from the upfield shift of C-24 at $\delta_C$ 86.9 (Table 2-7) as well as the correlation from the anomeric proton to C-24 in the HMBC spectrum (Figure 2-49). The absolute configuration of the glucose in **9** was determined as D-form as described in the Experimental Section 2.3.7.

The resonances of the C-19 methylene protons of compound **9** are shown at $\delta_H$ 2.69 and 2.89, which are exactly the same as those protons of **1** in spite of a slightly decreased $J$ value at 13.8 Hz, indicating that compound **9** possesses an expanded B-ring system by the opening of the cyclopropane ring (Fu, Li *et al.*, 2008). Similar to compound **1**, two olefinic carbons at $\delta_C$ 138.5 (C) and 126.5 (CH) are positioned between C-9 and C-11, with the evidence of HMBC correlations between C-19 protons and C-11, and between C-11 protons and C-8 as well as C-13 (Figure 2-49).

It is noticeable that a downfield carbonyl carbon at $\delta_C$ 181.0 (Table 2-7) was shown in the $^{13}$C NMR spectrum of the aglycone moiety instead of a ketocarbonyl as compared to those of other cycloartane-type glycosides bearing a carbonyl at C-1 (e.g., sutherlandiosides B–D, see Table 2-2). This implies that compound **9** may have a terminal carboxy group at C-1 in a converted A-ring system. A contracted five-membered A-ring was confirmed by the HMBC spectra (Figure 2-48), showing the correlations from H-5 ($\delta_H$ 3.03, br d  9.0 Hz), H-2 ($\delta_H$ 2.11), and H-19 (2.69, d 13.8 Hz) to the C-1 carbonyl carbon at $\delta_C$ 181.0 (Figure 2-49).
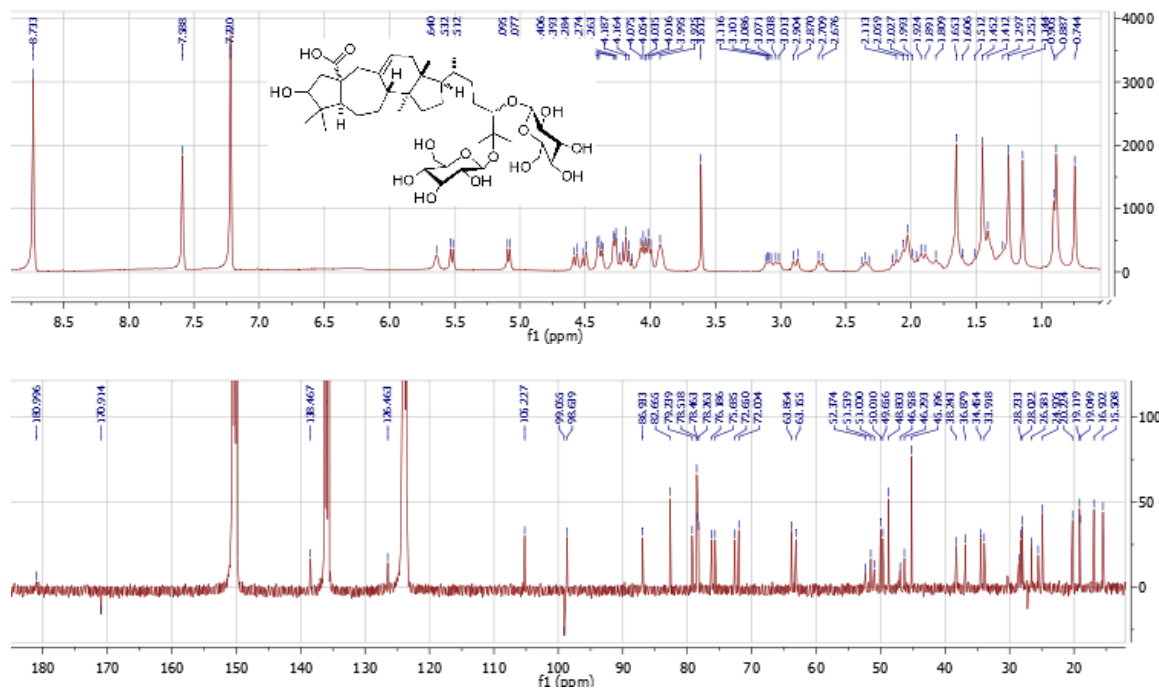
Figure 2-46. $^1$H and $^{13}$C NMR spectra of compound **9** in pyridine-$d_5$.
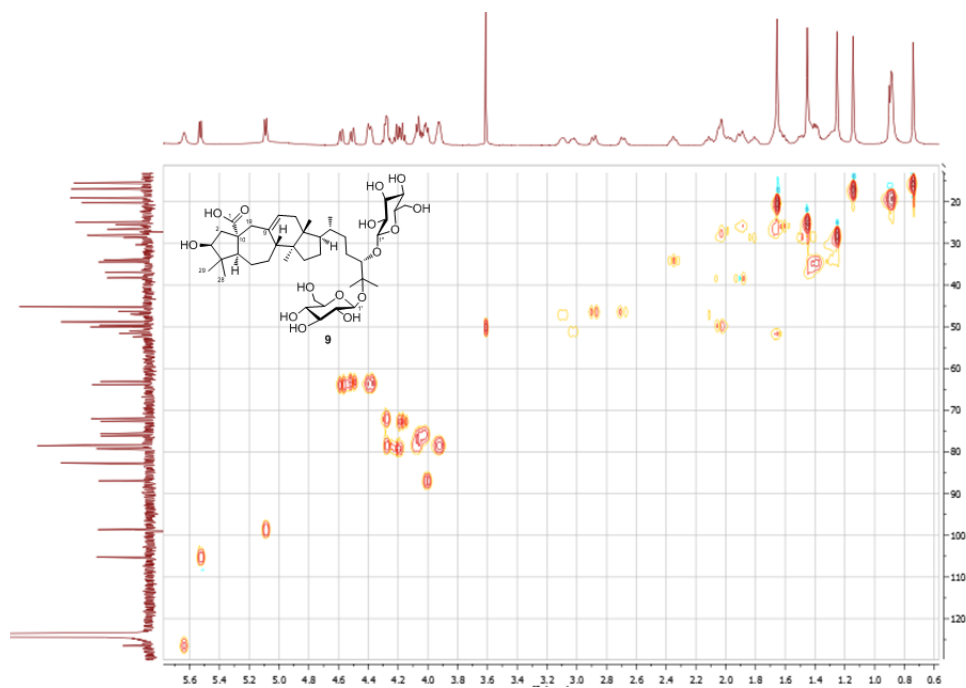


Figure 2-47. HMQC spectrum of compound **9** in pyridine-$d_5$.
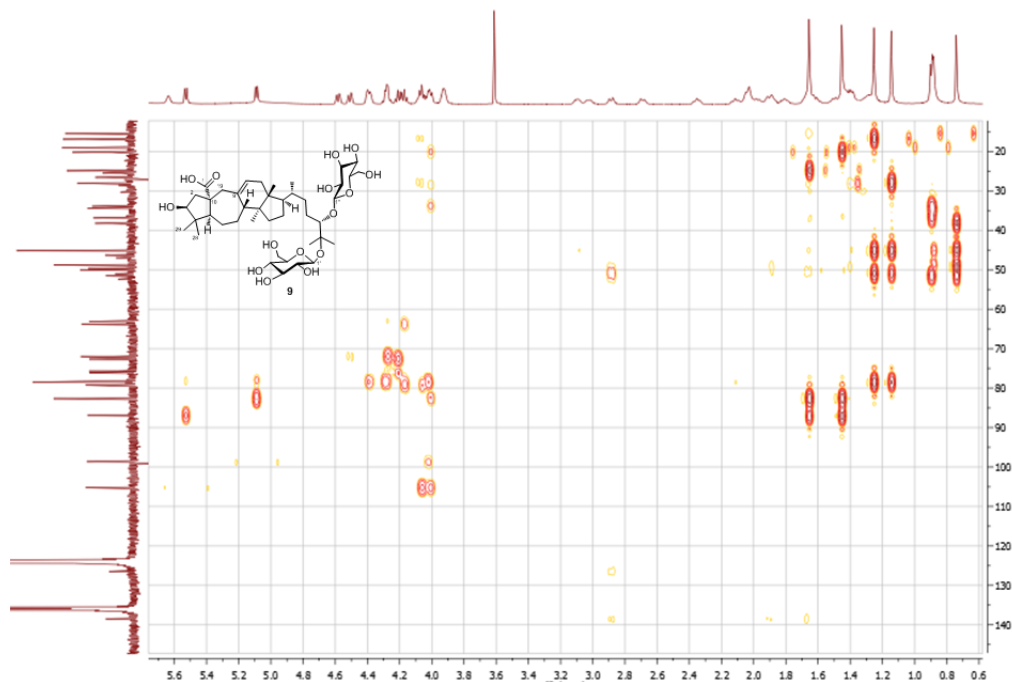
Figure 2-48.  HMBC spectrum of compound **9** in pyridine-$d_5$.



Figure 2-49.  Selected key HMBC correlations of **9**.
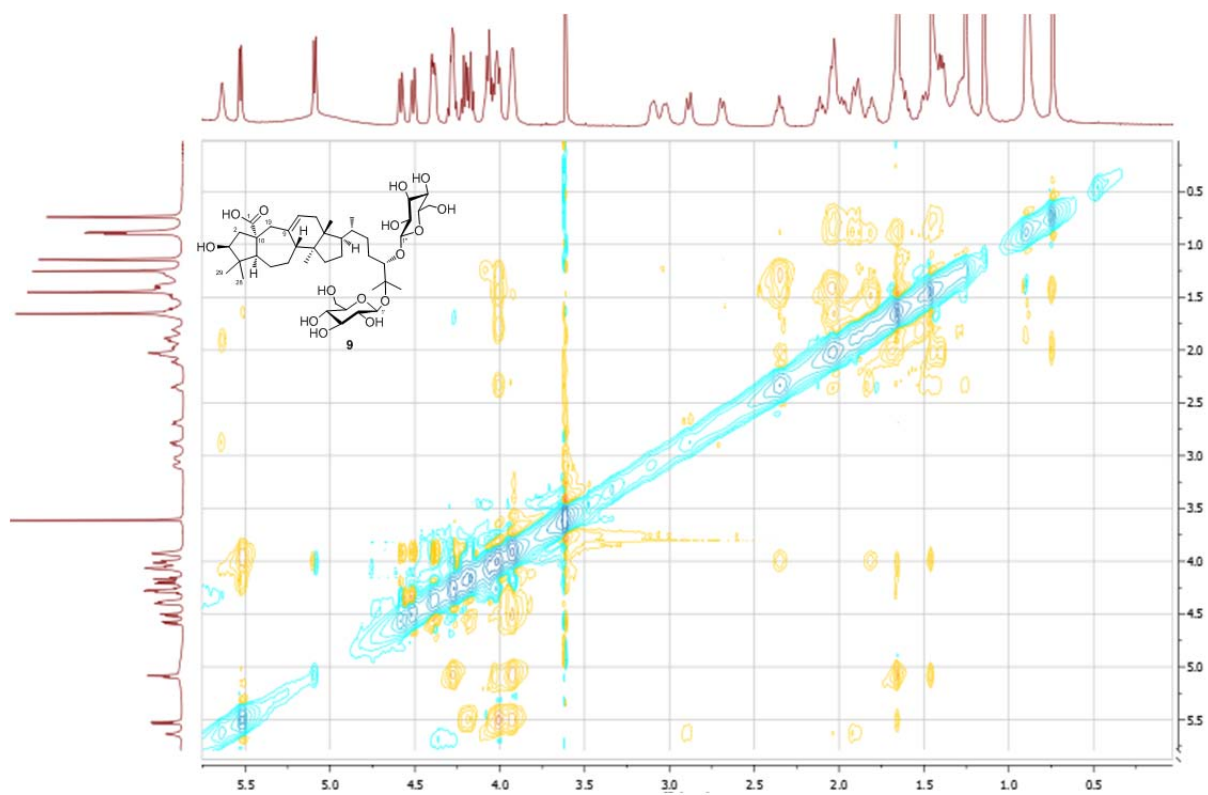
Figure 2-50. ROESY spectrum of compound **9** in pyridine-$d_5$.

In combination with other 1D and 2D spectral data, the two-dimensional structure of **9** was confirmed as an A-ring rearranged 9,10-*seco*-cycloartane-type diglycoside bearing an unprecedented 5/7/6/5 ring skeleton.
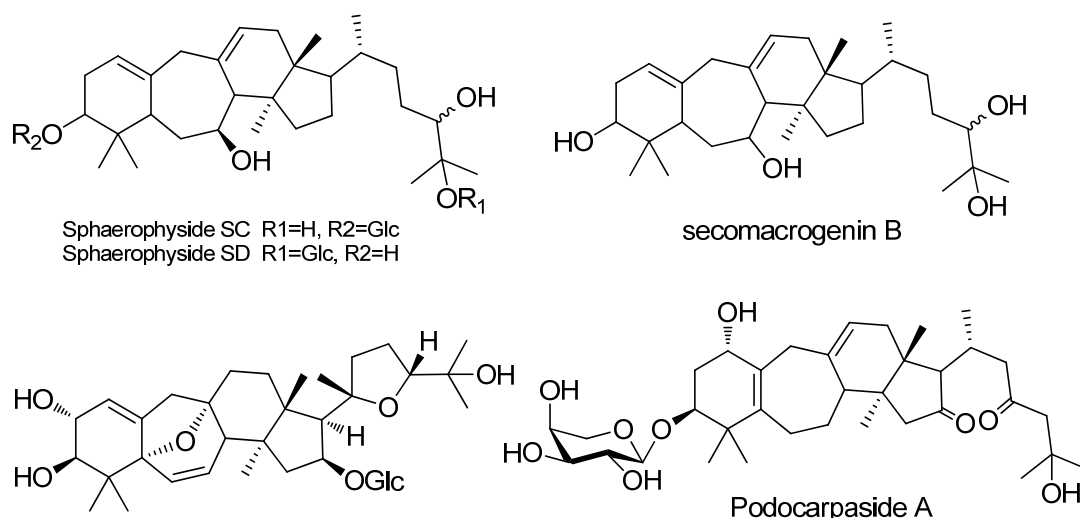
Figure 2-51. Reported examples of triterpenoids with an expanded B-ring.

(Bedir, 2001; Ma, Wang *et al.*, 2006; Ali, Khan *et al.*, 2007; Isaev, 2010)

Cycloartane-type triterpenoids with an expanded B-ring system occur in nature, which constitute a group of 9,10-*seco*-cycloartane-type compounds. Examples of this type of metabolites are shown in Figure 2-51. Compared to the B-ring expanded products, a few cases of the A-ring contracted naturally occuring triterpenoids in nature were reported as shown in Figure 2-52.
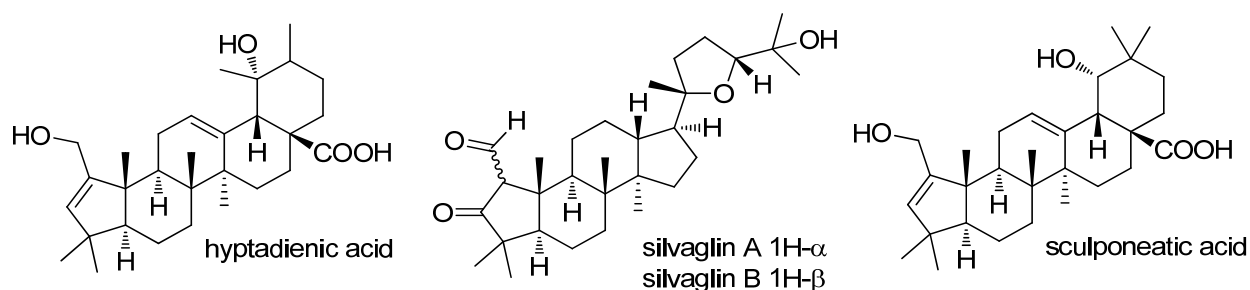


Figure 2-52. Reported examples of triterpenoids with a contracted A-ring.

(Raja Rao, 1990; Pointinger, Promdang *et al.*, 2008; Wang, Li *et al.*, 2009).

77
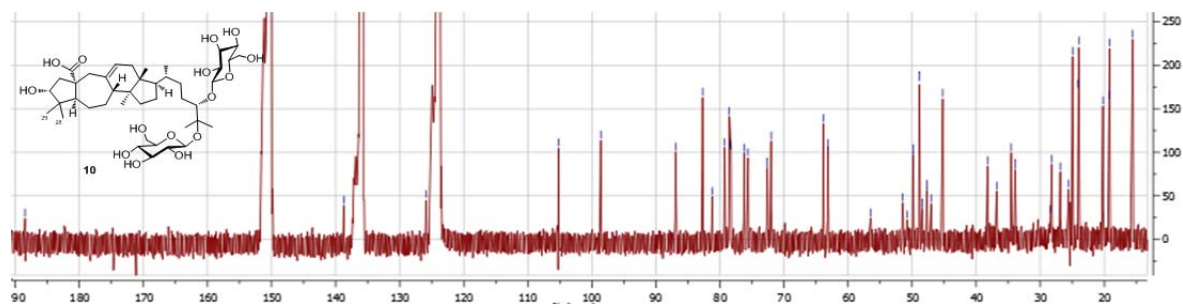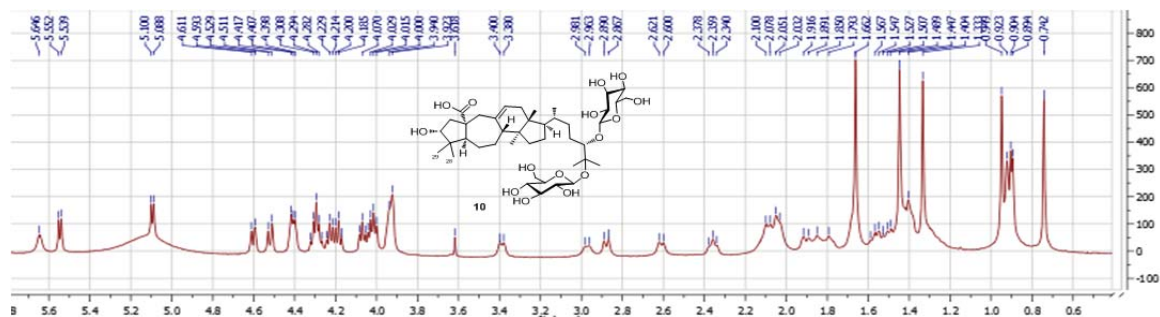
Figure 2-53. $^1$H and $^{13}$C NMR spectra of compound **10** in pyridine-$d_5$.
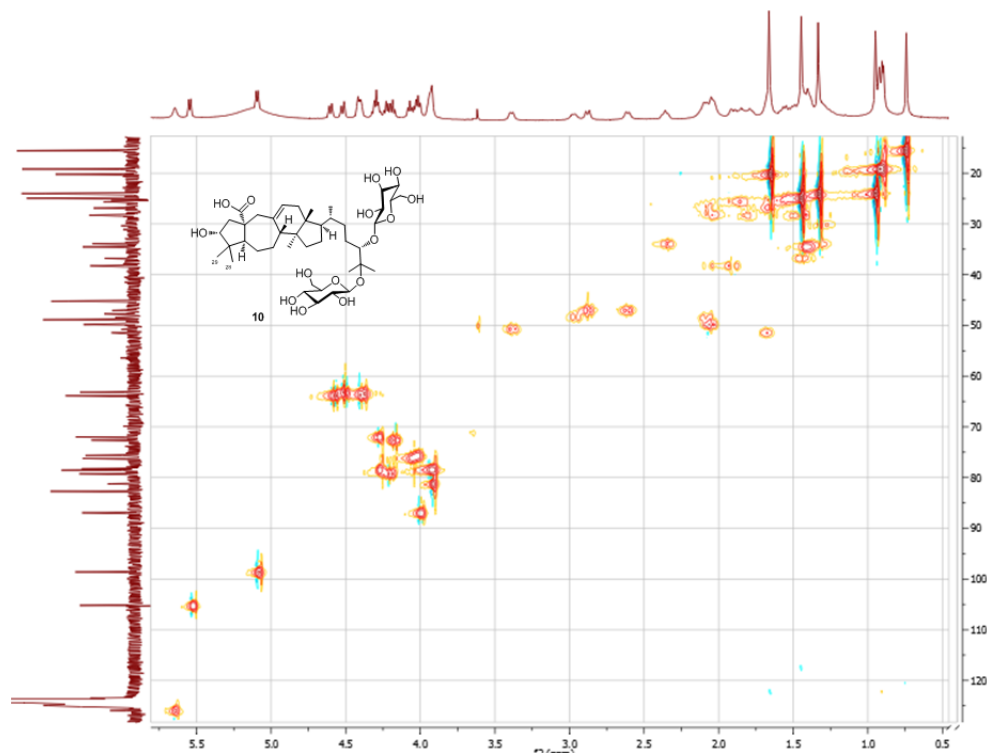


Figure 2-54. HMQC spectrum of compound **10** in pyridine-$d_5$.
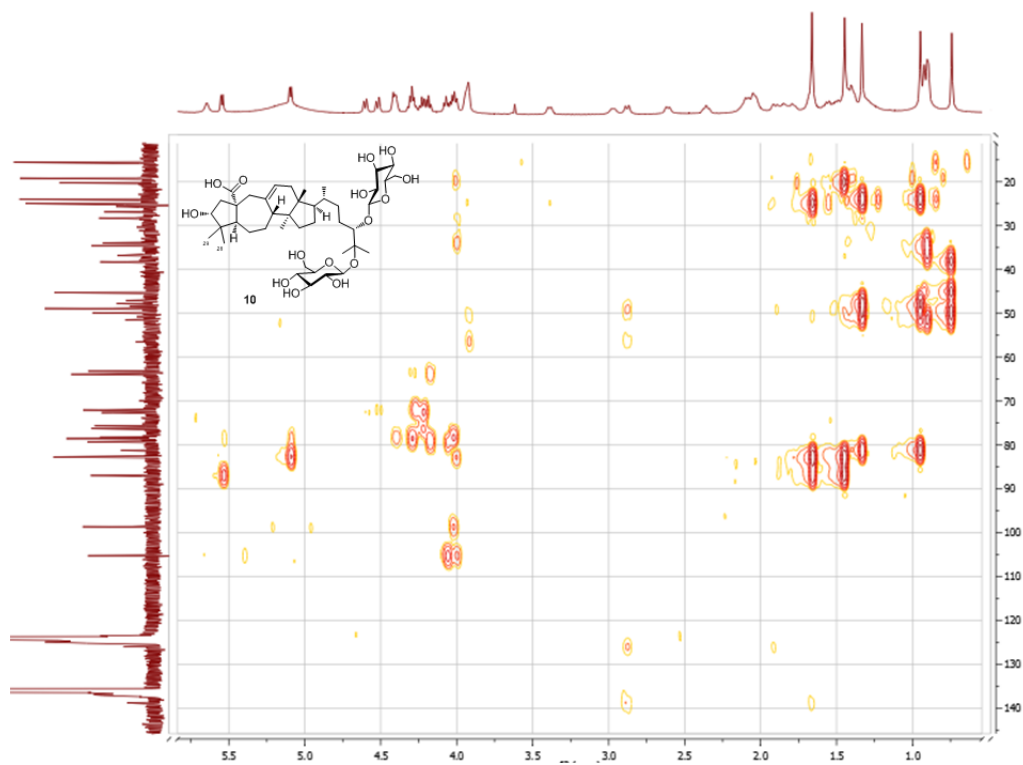
Figure 2-55.  HMBC spectrum of compound **10** in pyridine-$d_5$.
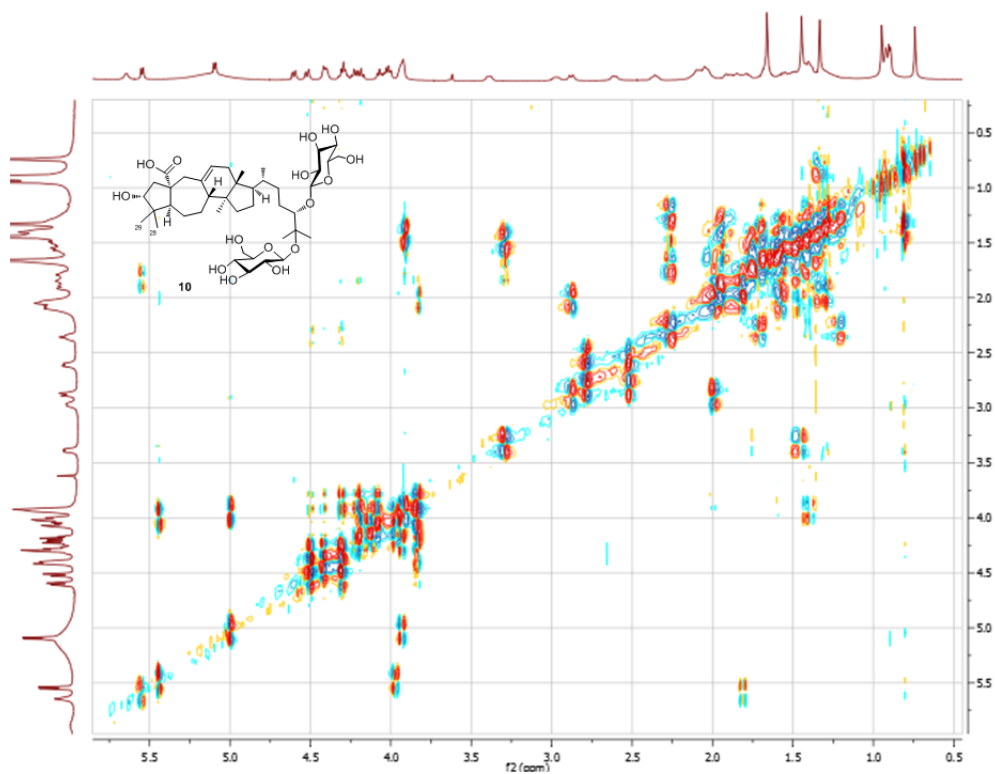


Figure 2-56.  COSY spectrum of compound **10** in pyridine-$d_5$.
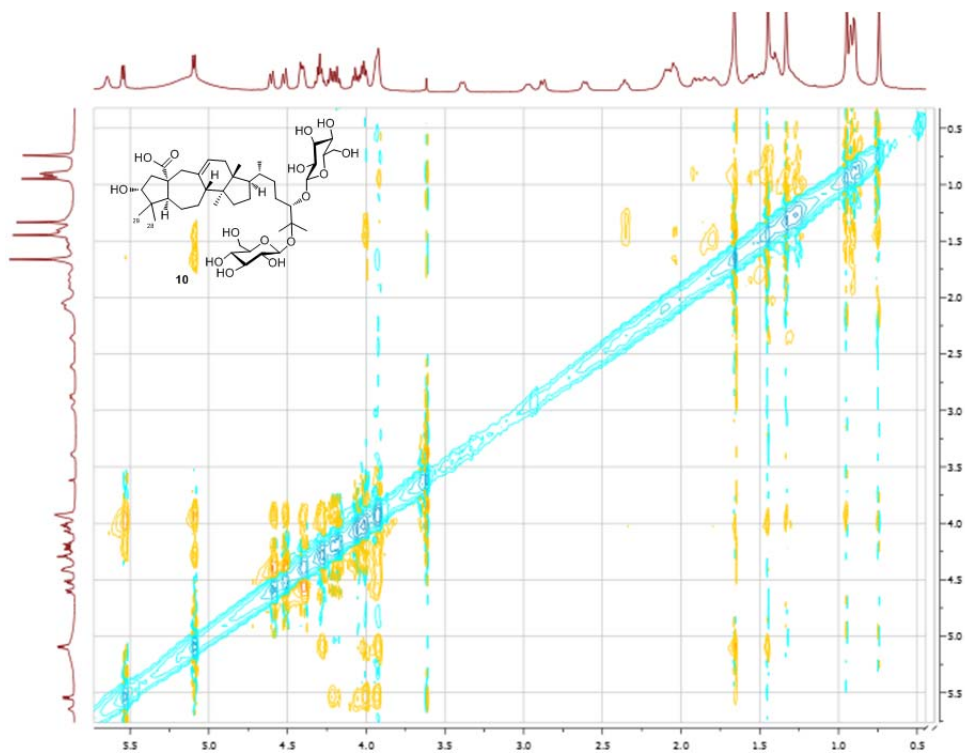
Figure 2-57. ROESY spectrum of compound **10** in pyridine-$d_5$.

Compounds **9** and **10** share the same two-dimensional structure based on the analyses of 1D and 2D NMR spectroscopic data indicating that both compounds have identical C-C connections. However, 1D NMR spectra of these two compounds are not superimposable. The major differences in the $^1$H NMR spectra of **9** and **10** are shown within three regions between $\delta_H$ 0.9-1.5, $\delta_H$ 2.6-3.4, and $\delta_H$ 3.9-4.1, involving the resonances of two methyl, two methylene, and one methine protons (Figure 2-58). The major differences of chemical shift values ($\Delta\delta$) in the $^{13}$C NMR spectra of **9** and **10** were at C-3 ($\Delta\delta_C$ 2.7), C-4 ($\Delta\delta_C$ 2.5), and C-10 ($\Delta\delta_C$ 4.0), suggesting the structural variances between **9** and **10** are restricted to the A-ring (Table 2-5).
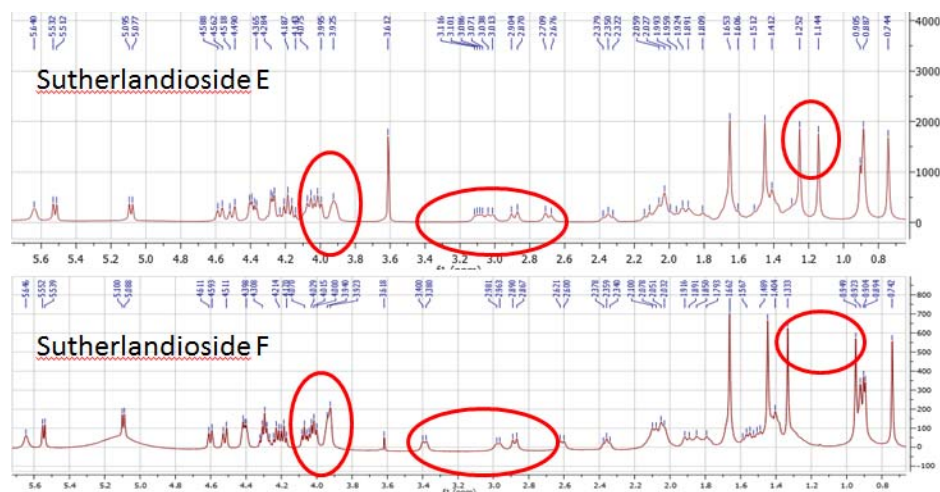
Figure 2-58. Comparison of the $^{1}$H NMR spectra of **9** and **10**.

(The differences are circled in red.)

Table 2-5. Comparison of $^{13}$C NMR chemical shift differences ($\Delta\delta_C$) in the A-ring of **9** and **10**.

| position | $\delta_C$ (**9**) | $\delta_C$ (**10**) | $\Delta\delta_C$ |
|----------|--------|--------|--------|
| 2 | 47.0 | 48.4 | 1.4 |
| 3* | 78.5 | 81.2 | 2.7 |
| 4 | 45.2 | 47.7 | 2.5 |
| 5* | 51.0 | 50.8 | 0.2 |
| 10* | 52.4 | 56.4 | 4.0 |

Recorded in pyridine-$d_5$ at 125 MHz.
* indicates a stereogenic center.

The large differences of $\delta_C$ values at C-3 and C-10 imply that **9** and **10** may be a pair of diastereomers with inversed configurations most probably at these two stereogenic centers.

The C-3 hydroxy group was identified as β-orientated for compound **9**, and α-orientated for compound **10** by showing the NOE correlation of H-3 with the oppositely orientated methyl groups, Me-28 and Me-29, respectively (H-3 at $\delta_H$ 4.06 with H-28 at $\delta_H$ 1.25 in **9**, and H-3 at $\delta_H$ 3.92 with H-29 at $\delta_H$ 0.95 in **10**).

Since the C-1 carboxy group and its vicinal quaternary carbon (C-10) have no connection

with any non-exchangeable proton, H-H based NOE correlation is not available for directly observing the orientation of the carboxy group from the ROESY spectrum. Alternatively, an NOE correlation between H-19β and the protons on Me-29 provides indirect but otherwise important information to determine the orientation of the C-10 carboxy group for compounds **9** and **10**.
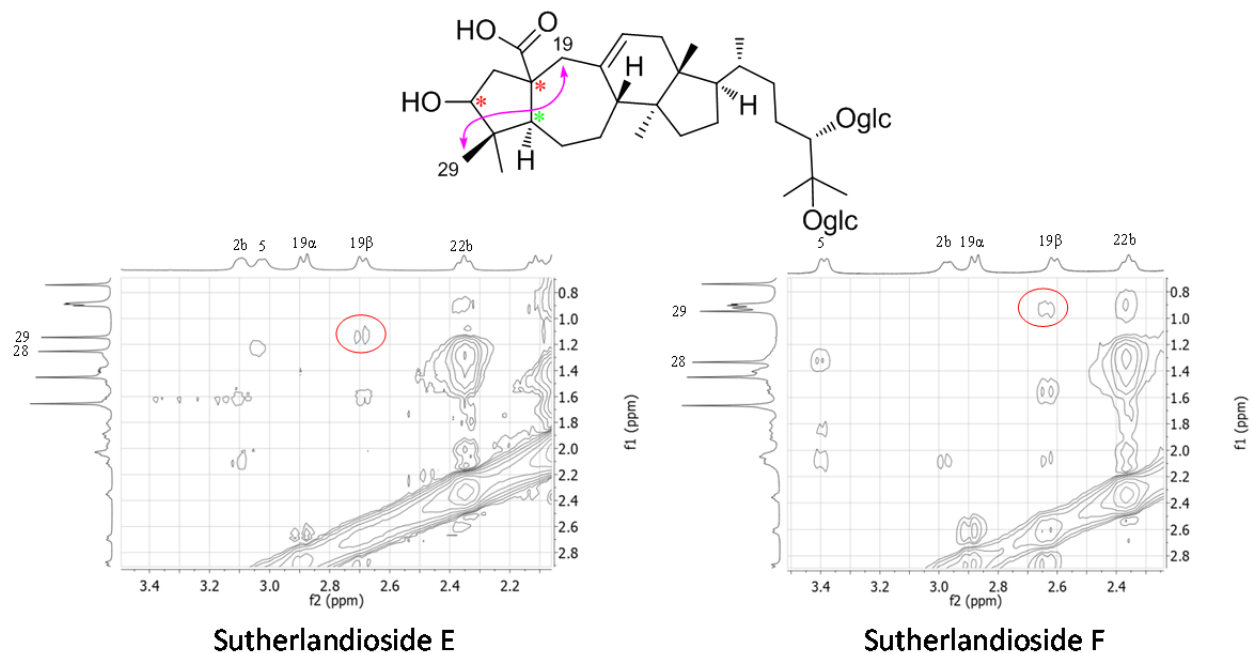


Figure 2-59. Comparison of core correlations in the ROESY spectra of **9** and **10**. (Core correlation between H-19β and the protons of Me-29 for **9** and **10** are circled in red.)

Although H-19β and Me-29 have a 6-bond distance range in compounds **9** and **10**, the through-space coupling implies that the protons on this two positions are spatially close with the actual distance no more than 4.5 Å (Silverstein, Webster *et al.*, 2005).
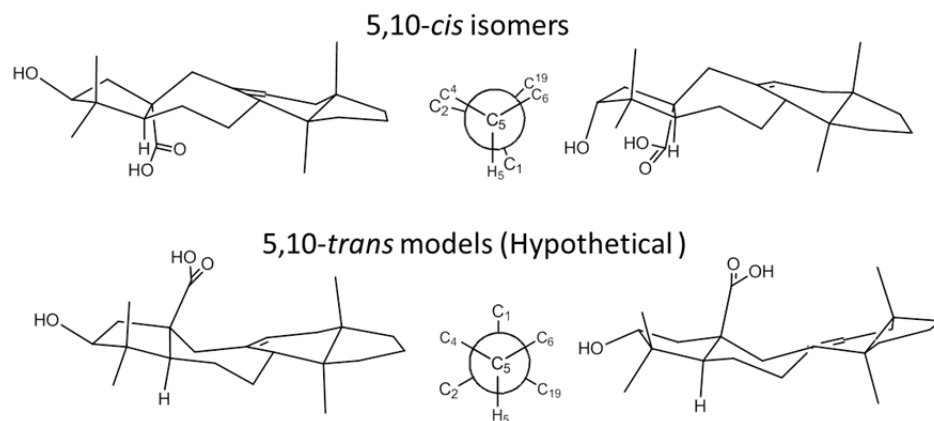
Figure 2-60.  Minimum-energy geometries of 5,10-*cis*- and *trans*- models.

(5,10-*Cis*- and *trans*- models with MM2 energy minimization shows the different conformational conditions for our studied 5/7/6/5 fused ring system.)

The aglycone moieties of **9** and **10** and their hypothetical C-10 inversed epimers constitute two types of models for a configurational and conformational study based on two different fusion styles for the A/B-rings. Both H-5 and the C-10 carboxy group have α-orientation in the 5,10-*cis* model. In the other type of model (5,10-*trans*), H-5 is α-orientated while the C-10 carboxy group has β-orientation, as shown in Figure 2-60. However, the ring fusion in such 5/7-membered ring system restricts the conformational changes of the molecule. The minimum-energy geometry of the 5,10-*cis* model shows an eclipsed conformation for the C-5—C-10 bond,  while 5,10-*trans* model has a staggered conformation for this bond. Similar minimum-energy geometries are also shown in a more simplified bicyclo[3.5.0] decane system (Figure 2-61).
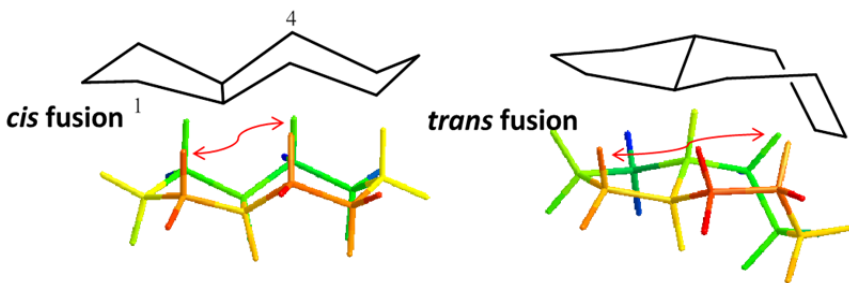
Figure 2-61. Minimum-energy geometries of *cis*- and *trans*-bicyclo[3.5.0] decane.

In the hypothetical 5,10-*trans* model, the distance between H-19β and Me-29 is longer than that of the 5,10-*cis* model. This model is subject to less torsional strain with the $C_5$-$C_{10}$ bond in a staggered conformation, but the *trans*-position of H-5 and the C-10 carboxy group causes the carboxy group protruding between H-19β and Me-29. The steric strain due to the close distance of two bulky groups (Me-29 and the carboxy) may allow a slight rotation of the carboxy on $C_5$-$C_{10}$ bond to avoid the repulsion. This rotation will lead to increased distance between H-19β and Me-29.



3β-5,10-*trans* model          3α-5,10-*trans* model
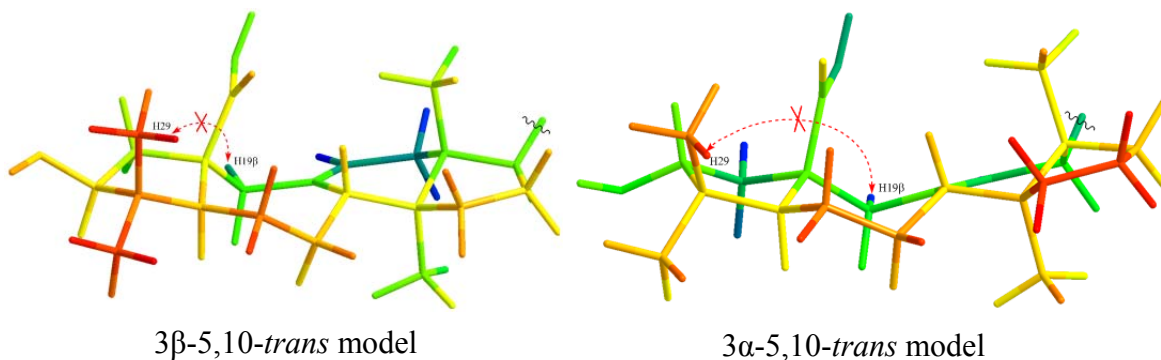
Figure 2-62. Hypothetical 5,10-*trans* model rendered in stick display mode.

(Elongated distances between H-19β and H-29 are marked with a red dashed line and arrow in 3β- and 3α-5,10-*trans* models.)

The shortest distance between H-19β and the protons on Me-29 was measured as 4.86 Å in the MM2 minimized 3β-5,10-*trans* model, and 5.41 Å in the 3α-5,10-*trans* model, which are unlikely to be observed in the ROESY spectrum.
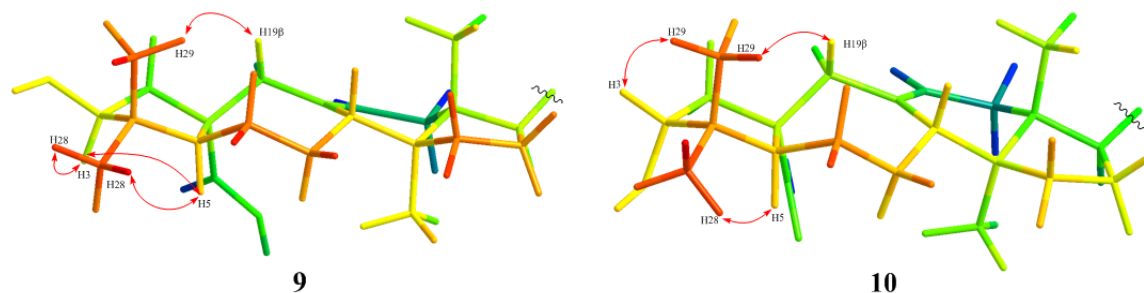


Figure 2-63.  Key NOE correlations for compounds **9** and **10** shown in optimized structural models.

On the other hand, the conformations of 5,10-*cis* model show much shorter distance between H-19β and the protons on Me-29 than that of 5,10-*trans* model,  which is in a range of having NOE effect. Both H-19β and Me-29 assume axial positions. The shortest measured distances between H-19β and the protons on Me-29 in the MM2 energy minimized models are 2.76 Å for the 3β isomer (**9**), and 2.40 Å for the 3α isomer (**10**), which are close enough to be observed in the ROESY spectra. As a result, we concluded that the NOE correlations marked in Figure 2-59 were generated from 5,10-*cis* isomers instead of 5,10-*trans* isomers.

Based on the conformational analysis, the orientations on C-3 hydroxy and C-10 carboxy were clearly determined for compound **9** as 3β,10α, and for compound **10** as 3α,10α.

## 2.2.3.2. Sutherlandioside G (11)

The molecular formula of compound **11** was determined as $C_{42}H_{70}O_{15}$ by combination of HRESIMS which provided a pseudomolecular ion peak $[M + Na]^+$ at *m/z* 837.4505 (calculated as 837.4607) and $^{13}C$ NMR spectroscopic data.
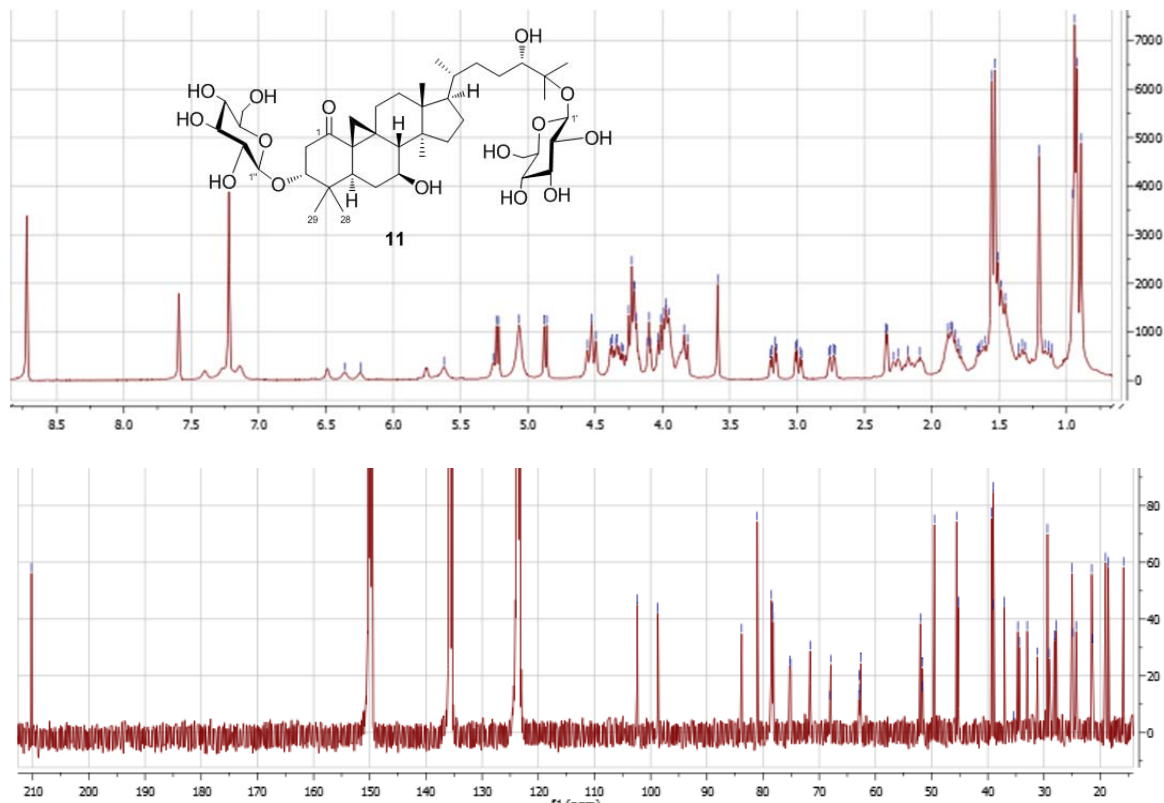


Figure 2-64. $^1H$ and $^{13}C$ NMR spectra of compound **11** in pyridine-$d_5$.

Its $^{13}C$ NMR spectrum resembles compound **2** including 30 signals from the aglycone moiety and six carbon signals from a glucosyl moiety. The additional six carbon signals at $\delta_C$ 98.7, 78.5, 78.2, 75.1, 71.6, and 62.9 (Table 2-7), along with the anomeric proton at $\delta_H$ 5.22 (d, *J* = 7.6 Hz, H-1″), allowed us to recognize the presence of a β-glucopyranosyl unit. The linkage of the glucosyl unit to the C-3 hydroxy group was revealed by an upfield shift of C-3 at $\delta_C$ 83.8 in the $^{13}C$

NMR spectrum as compared to that of compound **2** ($\delta_C$ 78.5), and confirmed by the HMBC spectrum with the correlation of the anomeric proton to C-3 at $\delta_C$ 83.8.

Also, an unexpected on-column deglucosylation of **11** during the purification process was observed (Figure 2-79). The decomposed product was identified as compound **4** (Figure 2-65). This confirms the connection of the gluycosyl unit at C-3.
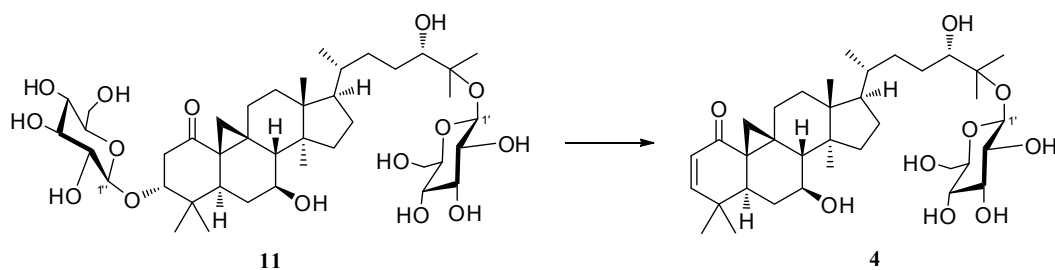


Figure 2-65.  On-column decomposition of compound **11** to form **4**.
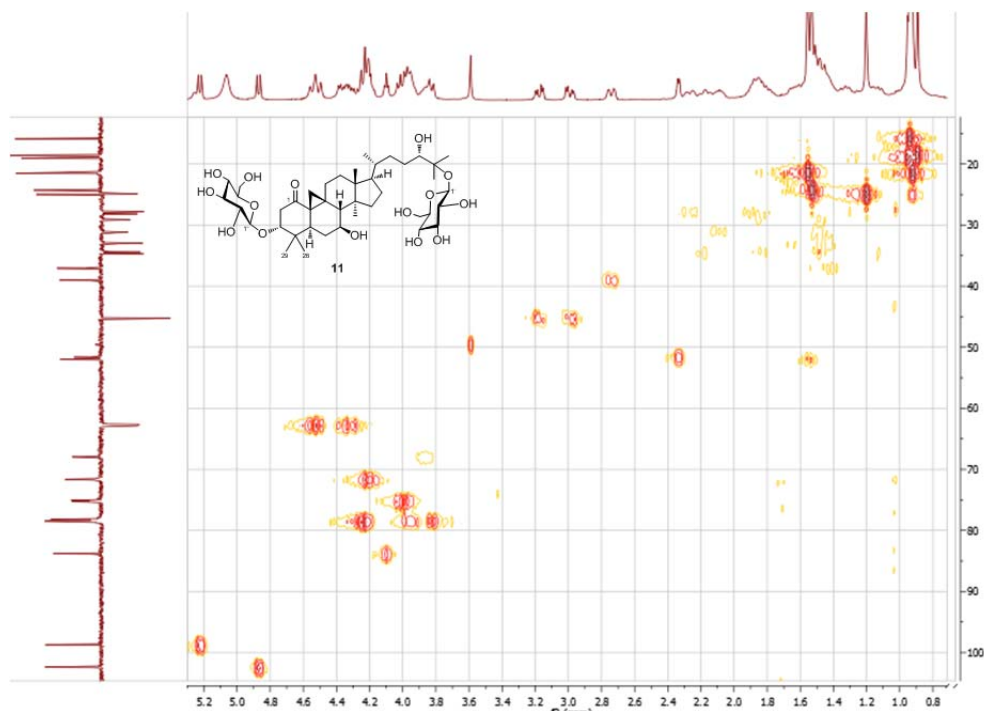


Figure 2-66.  HMQC spectrum of compound **11** in pyridine-$d_5$.
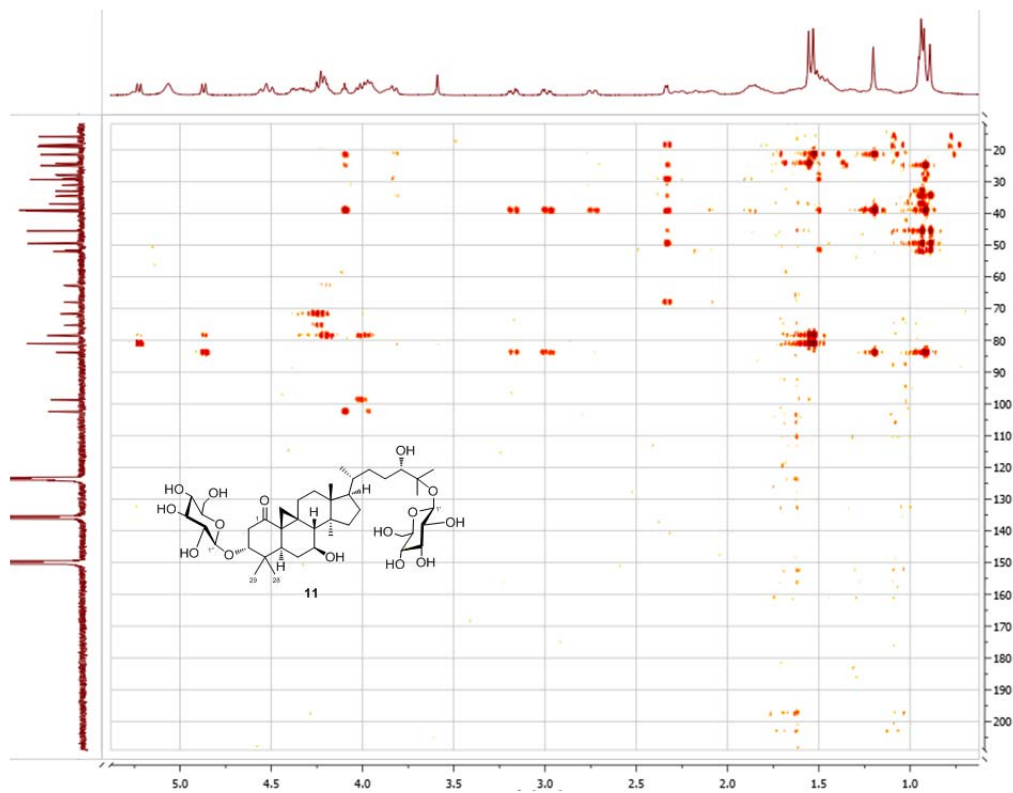
Figure 2-67. HMBC spectrum of compound **11** in pyridine-$d_5$.
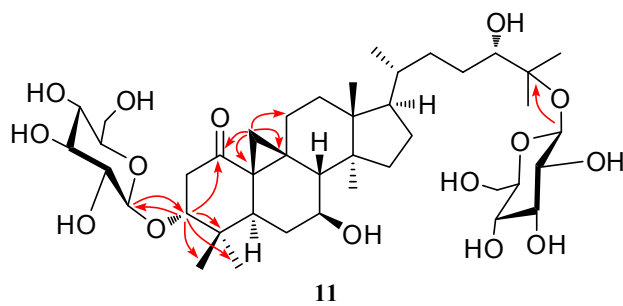


Figure 2-68. Selected key HMBC correlations of **11**.
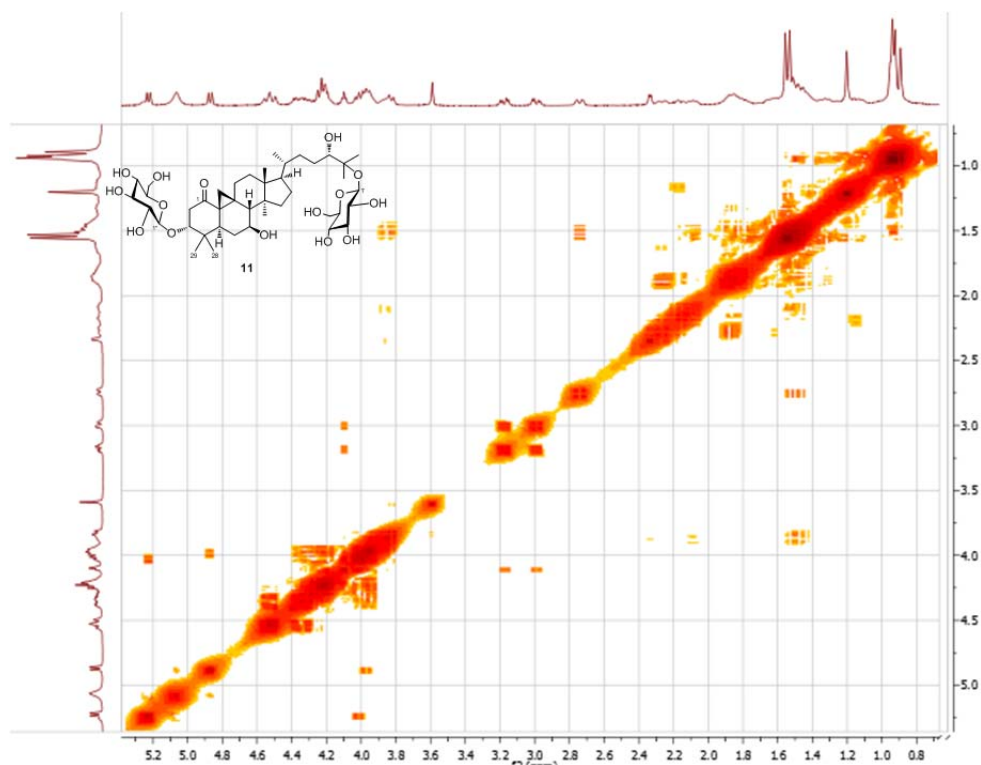
Figure 2-69.  COSY spectrum of compound **11** in pyridine-$d_5$.
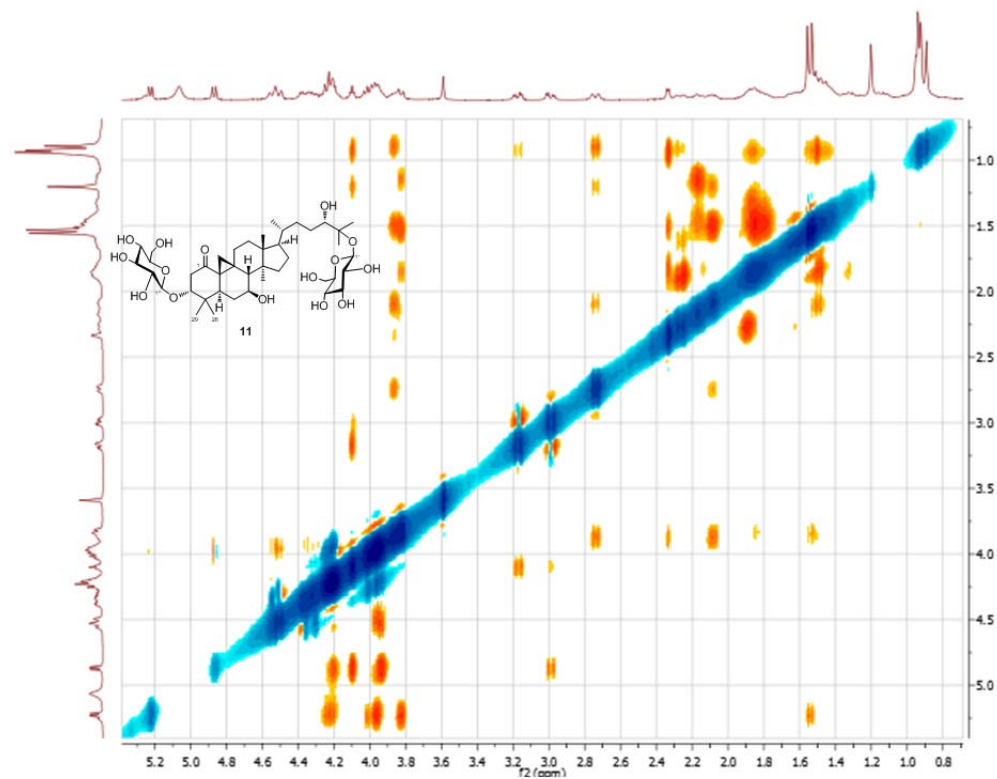


Figure 2-70.  ROESY spectrum of compound **11** in pyridine-$d_5$.

## 2.2.3.3. Sutherlandioside H (**12**)

The molecular formula of compound **12** was determined as $C_{42}H_{68}O_{15}$ by a combination of HRESIMS which provided a pseudomolecular ion peak $[M + Na]^+$ at *m/z* 835.4607 (calculated as 835.4450) , and $^{13}C$ NMR spectroscopic data. The $^1H$ and $^{13}C$ NMR spectra are almost the same as those of compound **3** except for six additional carbon signals that belong to a β-glucopyranosyl unit. The linkage of this glucosyl unit to C-24 was evidenced by an upfield shift of C-24 at $\delta_C$ 86.9 and its 3-bond HMBC coupling with anomeric proton at $\delta_H$ 5.52 (d, *J* = 8.0 Hz, H-1″).
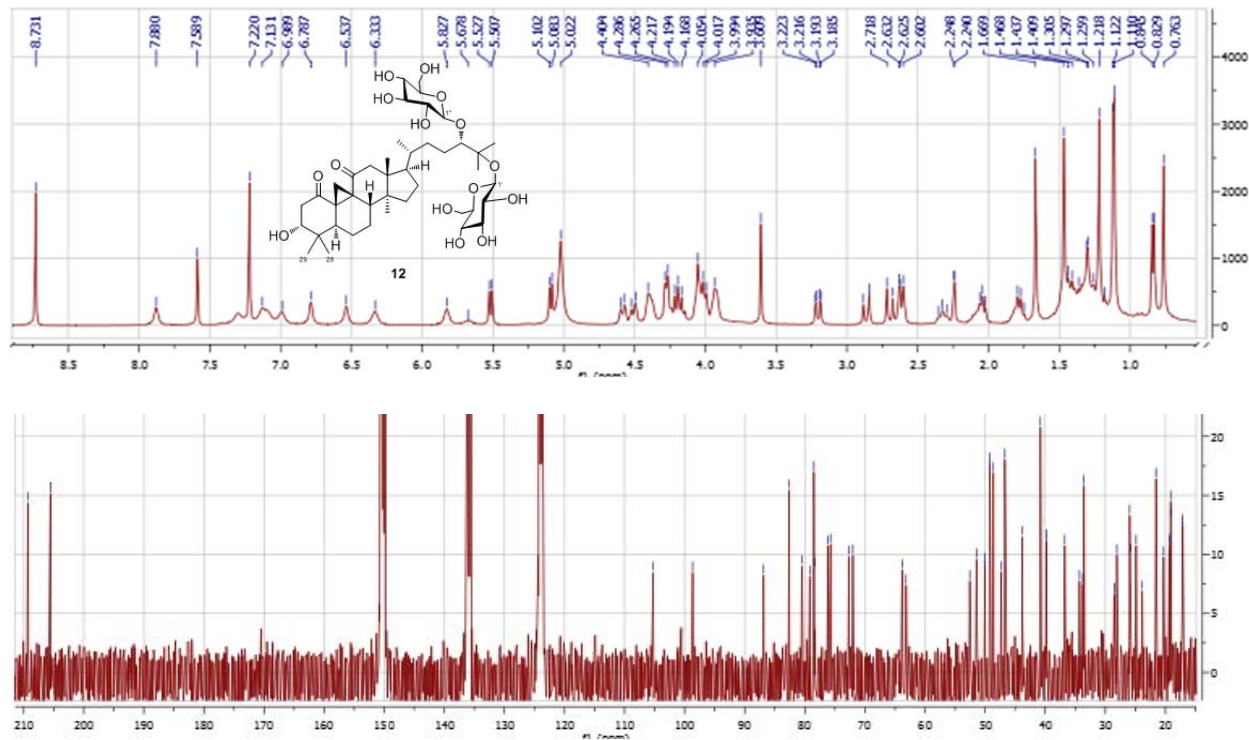


Figure 2-71. $^1H$ and $^{13}C$ NMR spectra of compound **12** in pyridine-$d_5$.
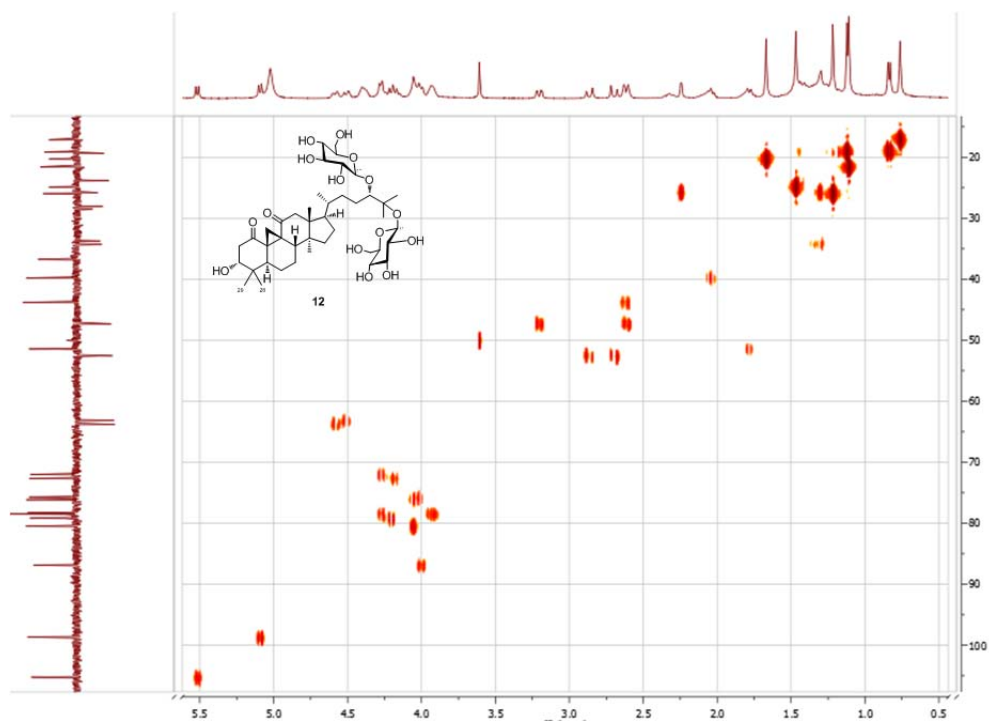
Figure 2-72.  HMQC spectrum of compound **12** in pyridine-$d_5$.



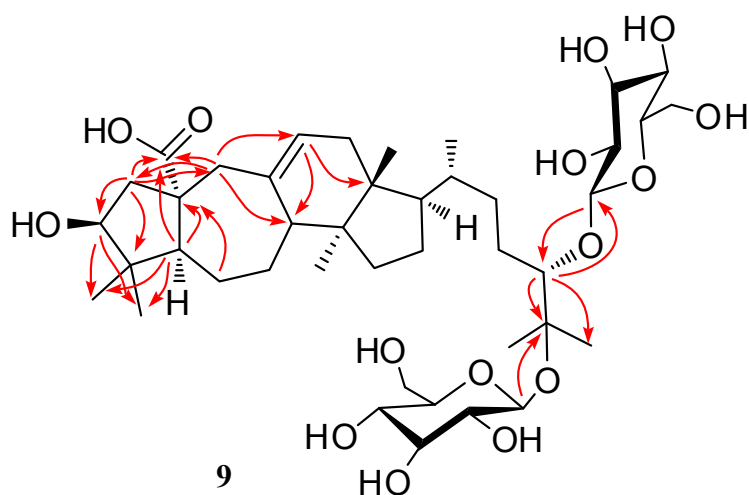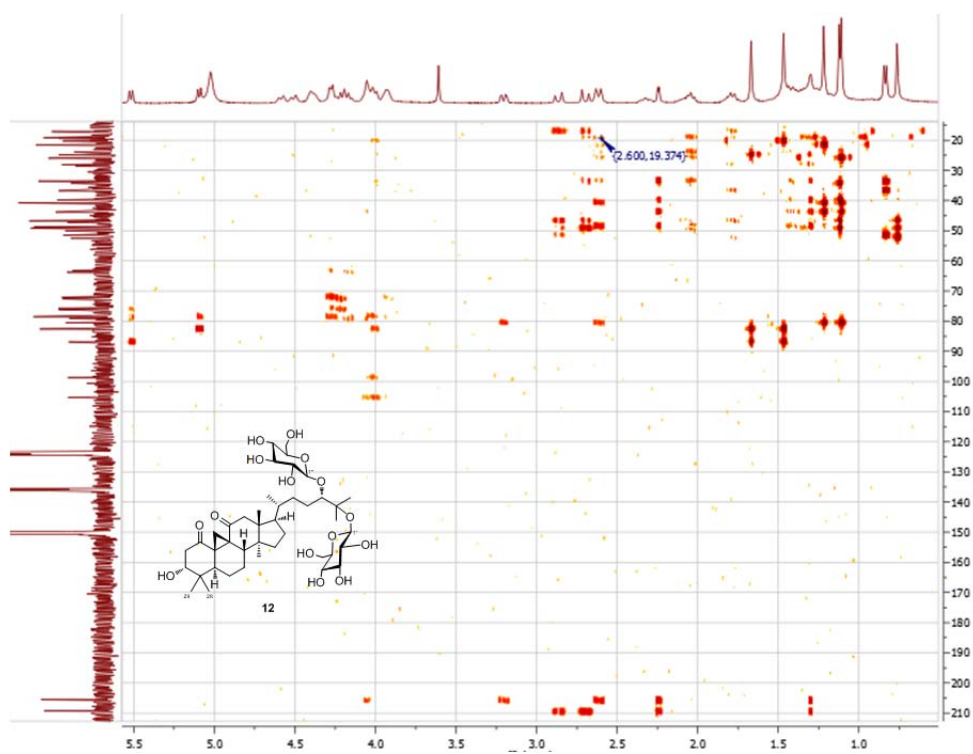Figure 2-73.  HMBC spectrum of compound **12** in pyridine-$d_5$.
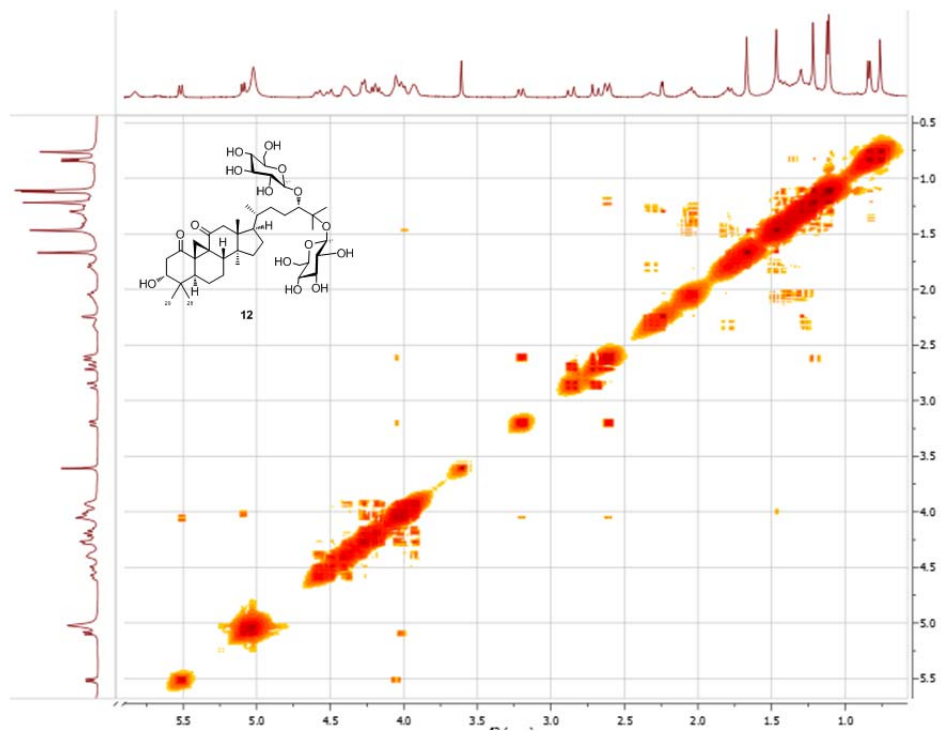
Figure 2-74. COSY spectrum of compound **12** in pyridine-$d_5$.
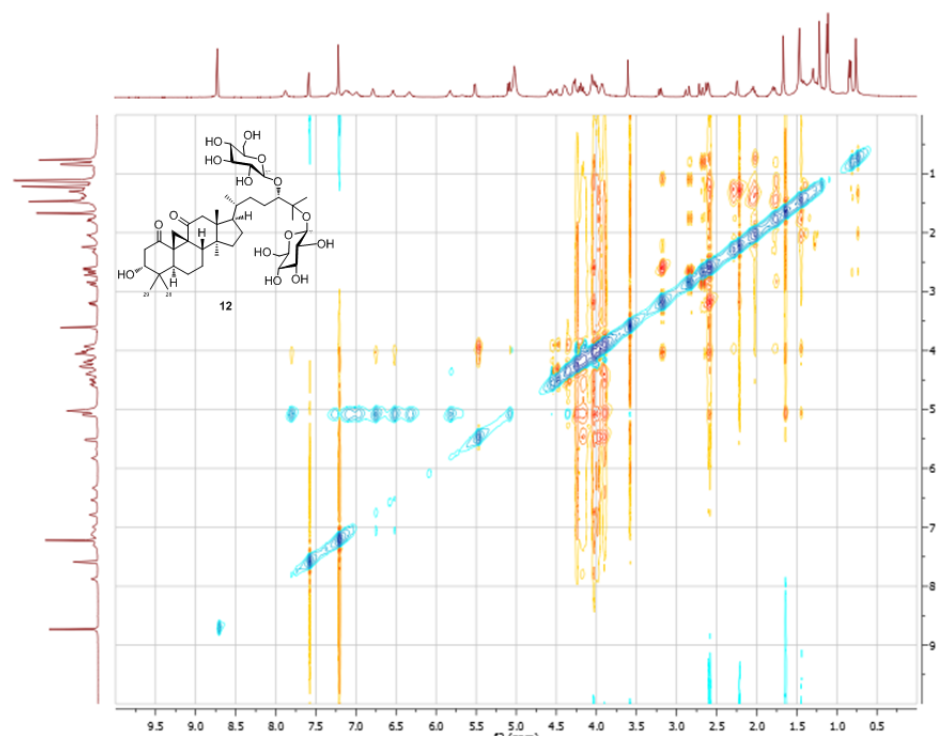


Figure 2-75. ROESY spectrum of compound **12** in pyridine-$d_5$.

Table 2-6. $^1$H NMR data for compounds **9–12** in pyridine-$d_5$.

| # | 9 | 10 | 11 | 12 |
|---|---|---|---|---|
| 1 | \ | \ | \ | \ |
| 2 | 2.11,<br>3.09 | 2.09, α<br>2.96 d (10.8) β | 2.99 dd (14.0, 4.7),<br>3.17 dd (14.0, 4.8) | 2.62,<br>3.20 dd (12.4, 3.2) |
| 3 | 4.06 | 3.92 | 4.10 | 4.05 br s |
| 5 | 3.03 br d (9.0) | 3.39 br d (12.0) | 2.74 dd (13.3, 3.3) | 2.62 dd (12.1, 3.2) |
| 6 | 1.61, 1.89 | 1.55 β , 1.85 α | 1.49, 2.09 | 1.22, 1.44 |
| 7 | 1.63, 1.97 | 1.67 β , 2.09 α | 3.86 | 1.23, 1.45 |
| 8 | 2.03 | 2.06 | 2.33 d (4.4) | 2.04 |
| 11 | 5.64 br s | 5.65 br s | 2.24, 2.29 | \ |
| 12 | 1.90, 2.09 | 1.90, 2.08 | 1.41, 1.66 | 2.68, 2.88 |
| 15 | 1.40 | 1.38, 1.42 | 1.49, 1.83 | 1.28, 1.33 |
| 16 | 1.81, 2.05 | 2.03 | 1.83, 1.90 | 2.05 |
| 17 | 1.66 | 1.68 | 1.55 | 1.78 d |
| 18 | 0.74 | 0.74 | 0.94 | 0.76 |
| 19 | 2.69 d (13.8), β<br>2.89 d (13.8) α | 2.61 d (12.6), β<br>2.88 d (13.8) α | 0.92,<br>1.49 | 1.30,<br>2.25 |
| 20 | 1.45 | 1.45 | 1.41 | 1.35 |
| 21 | 0.90 d (6.0) | 0.90 (6.0) | 0.95 | 0.83 |
| 22 | 1.29, 2.35 | 1.29, 2.35 | 2.16, 2.20 | 1.33, 2.32 |
| 23 | 1.49 | 1.48, 1.79 | 1.47, 1.84 | 1.80 |
| 24 | 4.00 | 4.01 | 3.82 | 4.00 d (9.2) |
| 26 | 1.66 | 1.66 | 1.56 | 1.67 |
| 27 | 1.45 | 1.45 | 1.53 | 1.46 |
| 28 | 1.25 | 1.33 | 1.20 | 1.22 |
| 29 | 1.15 | 0.95 | 0.92 | 1.11 |
| 30 | 0.88 | 0.92 | 0.89 | 1.12 |
| 1' | 5.09 d (7.2) | 5.09 d (7.2) | 4.87 d (7.6) | 5.09 d (7.6) |
| 2' | 4.02 | 4.02 | 4.02 | 4.02 |
| 3' | 3.92 | 4.27 | 4.23 | 4.27 d (8.4) |
| 4' | 4.29 | 4.29 | 4.23 | 4.27 d (8.4) |
| 5' | 3.93 | 3.92 | 3.96 | 3.91 |
| 6' | 4.39 br d (11.4),<br>4.51 dd (12.0, 1.8) | 4.40,<br>4.52 br d (10.8) | 4.31,<br>4.51 | 4.39,<br>4.51 d (11.2) |
| 1" | 5.53 d (7.8) | 5.55 d (7.8) | 5.22 d (7.6) | 5.52 d (8.0) |
| 2" | 4.05 | 4.07 | 3.97 | 4.04 |
| 3" | 4.20 | 4.21 | 4.23 | 4.20 |
| 4" | 4.17 | 4.18 | 4.23 | 4.18 |
| 5" | 4.26 | 3.92 | 3.96 | 3.91 |
| 6" | 4.39 br d (11.4),<br>4.58 dd (10.8, 1.8) | 4.40,<br>4.60 br d (10.8) | 4.34,<br>4.54 | 4.39,<br>4.58 d (11.0) |

Recorded ($\delta$, ppm) in pyridine-$d_5$ at 400 MHz. Well resolved couplings are expressed with coupling patterns (s, singlet; d, doublet; dd, doublet of doublets; br, broad) and coupling constants in Hz in parentheses. For overlapped signals, only chemical shift values are given.

Table 2-7. $^{13}$C NMR data for compounds **9**–**12** in pyridine-$d_5$.

| # | 9 | 10 | 11 | 12 |
|---|---|---|---|---|
| 1 | 181.0 s | 181.5 s | 210.2 s | 205.6 s |
| 2 | 47.0 t | 48.4 t | 45.3 t | 47.3 t |
| 3 | 78.5 d | 81.2 d | 83.8 d | 80.5 d |
| 4 | 45.2 s | 47.7 s | 39.3 s | 40.8 s |
| 5 | 51.0 d | 50.8 d | 39.0 d | 43.8 d |
| 6 | 25.5 t | 25.6 t | 31.2 t | 23.9 t |
| 7 | 26.6 t | 26.9 t | 68.0 d | 19.4 t |
| 8 | 49.7 d | 49.9 d | 51.6 d | 39.8 d |
| 9 | 138.5 s | 138.7 s | 29.4 s | 33.6 s |
| 10 | 52.4 s | 56.4 s | 35.5 s | 48.6 s |
| 11 | 126.5 d | 125.9 d | 27.8 t | 209.3 s |
| 12 | 38.2 t | 38.3 t | 33.0 t | 52.6 t |
| 13 | 45.2 s | 45.2 s | 45.6 s | 46.7 s |
| 14 | 48.8 s | 48.9 s | 49.5 s | 49.2 s |
| 15 | 34.5 t | 34.5 t | 34.4 t | 34.3 t |
| 16 | 28.2 t | 28.3 t | 28.2 t | 28.1 t |
| 17 | 51.5 d | 51.5 d | 52.0 d | 51.4 d |
| 18 | 15.5 q | 15.5 q | 15.9 q | 17.1 q |
| 19 | 46.3 t | 47.1 t | 24.9 t | 25.8 t |
| 20 | 36.9 d | 36.8 d | 37.1 d | 36.8 d |
| 21 | 19.1 q | 19.2 q | 19.0 q | 19.1 q |
| 22 | 33.9 t | 33.9 t | 34.7 t | 33.7 t |
| 23 | 28.6 t | 28.5 t | 29.1 t | 28.5 t |
| 24 | 86.9 d | 86.9 d | 78.4 d | 86.9 d |
| 25 | 82.7 s | 82.7 s | 81.0 s | 82.6 s |
| 26 | 20.2 q | 20.2 q | 21.4 q | 20.3 q |
| 27 | 24.9 q | 25.0 q | 24.3 q | 24.9 q |
| 28 | 28.0 q | 24.1 q | 25.0 q | 26.0 q |
| 29 | 16.9 q | 24.0 q | 21.5 q | 21.6 q |
| 30 | 19.05 q | 19.24 q | 18.6 q | 19.0 q |
| 1' | 98.6 d | 98.6 d | 102.4 d | 98.7 d |
| 2' | 75.7 d | 75.6 d | 75.3 d | 75.7 d |
| 3' | 78.46 d | 78.5 d | 78.5 d | 78.3 d |
| 4' | 72.0 d | 72.0 d | 71.6 d | 72.0 d |
| 5' | 78.3 d | 78.3 d | 78.2 d | 78.5 d |
| 6' | 63.2 t | 63.2 t | 62.6 t | 63.2 t |
| 1" | 105.2 d | 105.2 d | 98.7 d | 105.3 d |
| 2" | 76.2 d | 76.2 d | 75.1 d | 76.2 d |
| 3" | 79.2 d | 79.3 d | 78.5 d | 79.2 d |
| 4" | 72.7 d | 72.6 d | 71.6 d | 72.7 d |
| 5" | 78.5 d | 78.4 d | 78.2 d | 78.5 d |
| 6" | 63.9 t | 63.9 t | 62.9 t | 63.8 t |

Recorded ($\delta$, ppm) in pyridine-$d_5$ at 100 MHz.

2.2.3.4.  Proposed biogenesis of sutherlandiosides E (**9**) and F (**10**)


Sutherlandiosides E (**9**) and F (**10**) are a pair of epimers bearing an unusual 5/7/6/5-membered ring system with an inversed stereogenic center at C-3. They represent an unprecedented carbon skeleton. Since the epimers are structurally similar to the major sutherlandiosides B (**2**), we hypothesize that the formation of the two compounds are from the cycloartane-type precursor **17** via a B-ring expansion and an A-ring contraction processes.

Epoxidation has been proposed to be involved in  the biogenesis of many ring contracted natural products such as carotenoids (Ito, Yamano *et al.*, 2009). For example, an epoxidation-mediated ring contraction mechanism was proposed to explain the formation of capsanthin from β-carotene (Dewick, 2002). In this process, the epoxidation of the endocyclic double bond in the six-membered ring was revealed to facilitate the formation of the carbocation intermediate during the formation of the contracted five-membered ring (Figure 2-76).
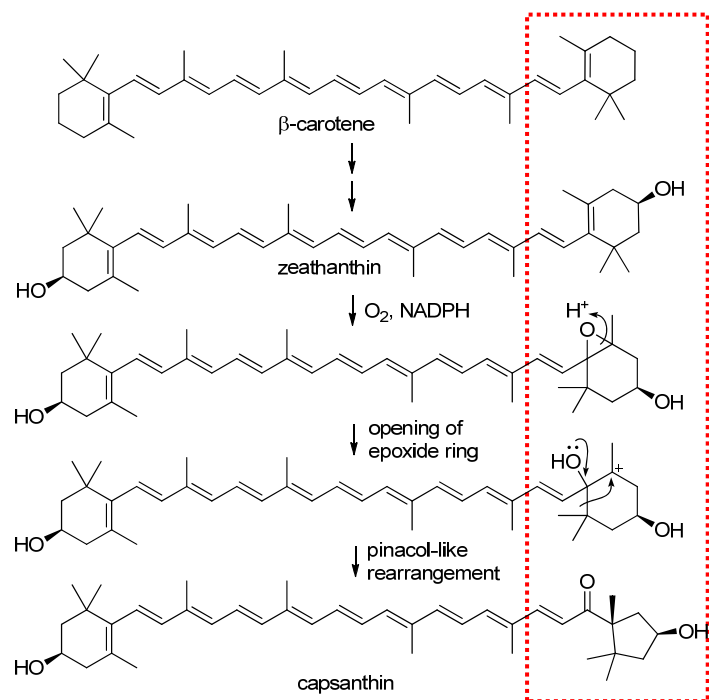
Figure 2-76. Biogenesis of capsanthin from β-carotene via a ring contraction process. Adapted from Dewick (Dewick, 2002).

A mechanism of B-ring expansion was formerly proposed in Section 2.2.1.5 to explain the possible biogenesis of **1** from **2** (Figure 2-26). The ring expansion for **9** and **10** could be similar to that for compound **1** from the cycloartane triterpenoid precursor **17**. The cyclic carbonyl group at C-1 facilitates the deprotonation of C-11 and the opening of the cyclopropane ring by cleavage of the C-C bond between C-9 and C-10, forming a B-ring expanded intermediate **18**. Stereoselective epoxidation of the enolic double bond and oxidation of the C-3 hydroxy group in **18** afford the other two key intermediates **19** and **20**.

Unlike forming the oxygen bridge in **1** from intermediate **14** via an intramolecular nucleophilic attack from the C-7 hydroxy group, the enolic C-1 hydroxy group induces a 1,2-alkyl shift of C-2 toward C-10 via a concerted $S_N2$-like mechanism, forming the rearranged α-carboxy

derivatives **10** and **21**. The stereoselective reduction of the ketone in **21** affords 3β-OH product **9**.
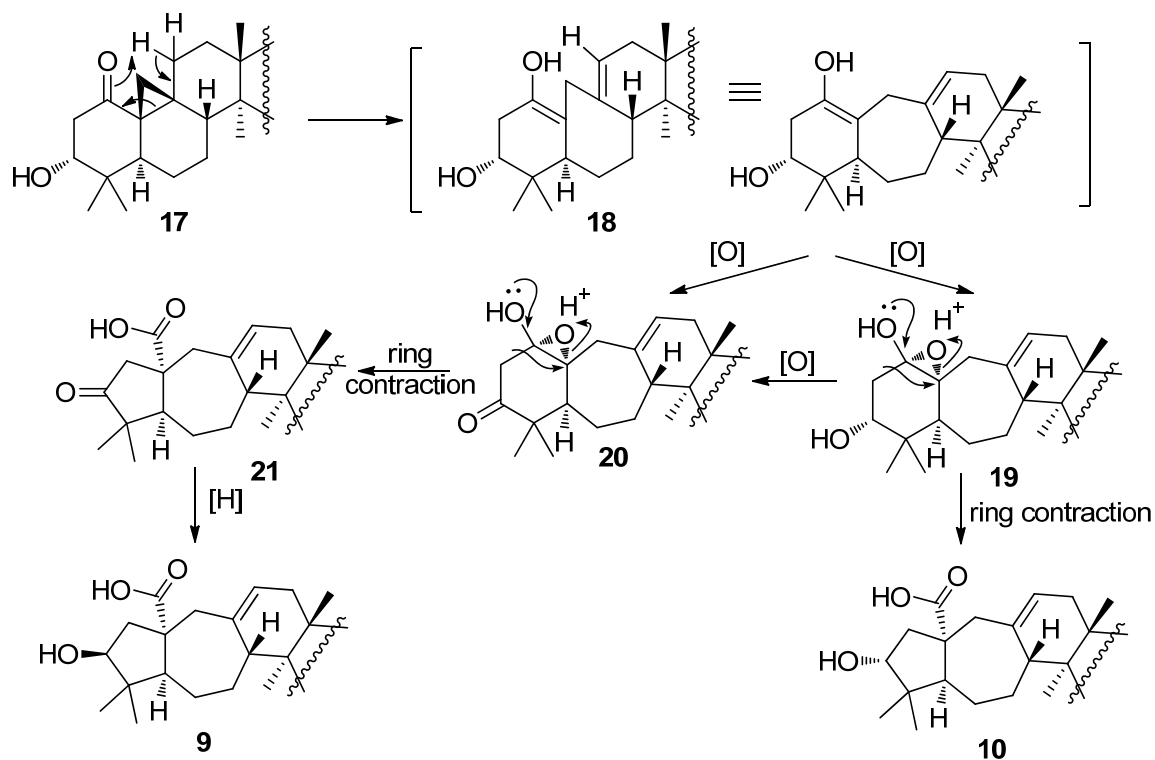


Figure 2-77. Proposed mechanism for the formation of sutherlandiosides E (**9**) and F (**10**).

## 2.3. Experimental section

### 2.3.1. General procedures

The 1D and 2D NMR (DQF-COSY, HMQC, HMBC, NOESY, ROESY) proton and carbon spectra were recorded on a Varian Oxford AS400 spectrometer operating at 400 ($^1$H) and 100 ($^{13}$C) MHz, Varian Unity Inova 600 spectrometer operating at 600 ($^1$H) and 150 ($^{13}$C) MHz, or on a Bruker Avance DRX 500 FT spectrometer operating at 500 ($^1$H) and 125 ($^{13}$C) MHz. The

chemical shift values ($\delta$) are relative to the solvent with the reference values given in ppm. The coupling constants ($J$) are given in Hz.

High-resolution mass spectra (HRESIMS) were obtained on an Agilent Series 1100 SL mass spectrometer.

UV spectra were acquired on a Varian 50 Bio UV spectrophotometer.

IR spectra were recorded on a Bruker, Tensor 27 FT-IR spectrometer, or on a PerkinElmer Spectrum 100 FT-IR spectrometer.

Optical rotations were measured on an Autopol IV polarimeter (Rudolph Research Analytical, Flanders, NJ) with a sodium lamp (589 nm) and a 1 cm microcell.

Column chromatography was performed using normal-phase silica gel (J. T. Baker, 40 μm) and reversed-phase silica gel (RP-18, J. T. Baker, 40 μm). Semi-preparative HPLC was conducted on a Waters Model 2695 Alliance Separation Module Phenomenex® Prodigy ODS column (250 × 10 mm, 10 μm) or Gemini $C_{18}$ column (250 × 10 mm, 10 μm, Phenomenex®, Torrance, CA, USA) using UV detector. Analytical HPLC system consisted of a Model 2695 Alliance Separations Module equipped with a 2996 photodiode array detector, and a computerized data station equipped with Waters Empower 2 software (Waters, Milford, MA).

TLC was performed on silica gel sheets (Alugram® Sil G/UV$_{254}$, Macherey-Nagel, Germany) and reversed-phase plates (RP-18 F$_{254S}$, Merck, Germany). Spots were visualized by: 10% $H_2SO_4$ followed by heating.

### 2.3.2. Plant material

The leaves of *S. frutescens* were collected in December 2005 in the Eastern Cape region of South Africa. The plant was identified by Dr. Vaishali Joshi. A voucher specimen was deposited at

the National Center for Natural Products Research, the University of Mississippi (voucher specimen No. 3222).

### 2.3.3. Extraction and isolation procedures

The air dried leaves (2 kilograms) were extracted with MeOH at room temperature (3.0 L × 24 hr × 4). The combined extracts were concentrated under reduced pressure to obtain a dried MeOH extract (433.6 grams), a portion of which (102.0 grams) was suspended in water, and extracted consecutively with hexanes, chloroform, and $n$-butanol (saturated with water). The $n$-butanol phase was evaporated to dryness *in vacuo* under 45 °C to give a brown residue (29.8 grams). The residue was subjected to silica gel chromatography (silica gel 560 grams; column 30 × 10 cm) using a stepwise gradient mixture of $CHCl_3$: MeOH: $H_2O$ (9:1:0, 6:1:0 and 7:3:0.5, 50.5 L) as eluent, to give 20 fractions (Fractions A through T).

Fraction E (1.07 g) was applied to an RP-18 column using 60%-70% MeOH to give sub-fractions E1- E18 and compound **1** (58.3 mg). Fraction H was recrystallized from MeOH to yield compound **2** (919.3 mg). Sub-fraction E7 was subjected to reversed-phase (ODS) semi-preparative HPLC using 30% acetonitrile in $H_2O$ (2 mL/min), yielding compounds **3** (12.0 mg, $t_R$ = 11.8 min) and **4** (5.8 mg, $t_R$ = 9.6 min) as shown in Figure 2-78.

The flavonoid-containing fraction O (942.6 mg) eluted by $CHCl_3$: MeOH: $H_2O$ = 7:3:0.5 (0.25 L) was first chromatographed on an RP-18 column (reverse phase silica gel 170 grams; column 48 × 4 cm) using 50% MeOH in $H_2O$ (0.8 L) to afford a mixture of two compounds (336.1 mg), 12.0 mg of which was subjected to reversed-phase (ODS) semi-preparative HPLC (0.15 mg for each injection) using 23% acetonitrile in $H_2O$ with 0.1% acetic acid at the flow rate of 2 mL/min to yield compounds **7** (6.3 mg, $t_R$ = 23.5 min) and **8** (5.8 mg, 26.8 min). Another

flavonoid-containing Fraction S (571.0 mg) was chromatographed on an RP-18 column (reverse phase silica gel 80 grams; column 26 × 3.5 cm;) using 50% MeOH in $H_2O$ (0.4 L) to afford a mixture of two compounds (198.7 mg), 19.4 mg of which was subjected to reversed-phase (ODS) semi-preparative HPLC (0.2 mg for each injection) using 22% acetonitrile in $H_2O$ with 0.1% acetic acid at the flow rate of 2 mL/min to furnish compounds **5** (9.1 mg, $t_R$ = 27.8 min) and **6** (5.3 mg, $t_R$ = 30.4 min).

**ISOLATION SCHEME FOR COMPOUNDS 1- 8**

Dried leaves and stems (2000 g)

| Extracted with MeOH

MeOH ext. (433.2 g)

102.0 g

| Partitioning

Hexanes | $CHCl_3$ | *n*-BuOH | $H_2O$

Hexanes Ext. (44.0 g)   $CHCl_3$ Ext. (0.7 g)   *n*-BuOH Ext. (29.8 g)   $H_2O$ Ext. (44.3 g)

Silica gel CC
$CHCl_3$-MeOH-$H_2O$

E (1.0747 g)   H (3.416 g)   O (942.6 mg)   S (571 mg)

RP18 column MeOH-$H_2O$   Recrystalization   RP18 column 50% MeOH/$H_2O$   RP18 column 50% MeOH/$H_2O$

**1** (58.3 mg)   E7 (227 mg) 20.0 mg   **2** (0.9193 g)   O1 (336.1 mg) 12.0 mg   S1 (198.7 mg) 19.4 mg

HPLC   HPLC   HPLC

**3** (12.0 mg)   E7-1 (8.7 mg)   **7** (6.3 mg)   **8** (5.8 mg)   **5** (9.1 mg)   **6** (5.3 mg)

| HPLC

**4** (5.8 mg)

Figure 2-78.  Isolation scheme of triterpene and flavonol glycosides from *S. frutescens*.

The remaining portion of the methanol extracts (331.2 grams) was suspended in water, and consecutively extracted with hexanes, chloroform, and water saturated *n*-butanol. The *n*-butanol phase was evaporated to dryness *in vacuo* under 45 °C to yield 128.5 grams of brown residue, a portion of which (60.0 grams) was subjected to silica gel chromatography (silica gel 560 grams; column 30 × 10 cm) using gradient mixtures of $CHCl_3$: MeOH: $H_2O$ (9:1:0, 6:1:0 and 7:3:0.5) as eluent, to give 16 fractions (Fractions A through P). Fraction K (14.6 grams) was subjected to a second silica gel chromatography (silica gel 595 grams; column 60 × 7 cm) to give 21 fractions $K_1$ through $K_{21}$.

Fraction $K_{17}$ (882.0 mg) was subjected to reversed-phase silica gel chromatography (Biotage RP-18, 40 grams) eluting with 55% MeOH in $H_2O$ to give 21 sub-fractions, $K_{17}$-A through $K_{17}$-U, and one purified compound **12** (23.3 mg).

Sub-fraction $K_{17}$-B (170.3 mg) was chromatographed on silica gel (Biotage Flash12+M, 9.0 grams) using a mixture of $CHCl_3$: MeOH: $H_2O$ (4:1:0.1) as eluent. However, the clogged column due to a technical problem caused a rapid on-column decomposition of sutherlandioside G (**11**) in this nearly pure fraction within two hours. Further purification of the recovered sample (138.4 mg) by reversed-phase silica gel chromatography (reverse phase silica gel 18.7 grams, column 30 × 1.5 cm) with 55% MeOH in $H_2O$ afforded compound **11** (12.8 mg) as well as the major decomposed product which was proved to be compound **4** (77.7 mg).

Sub-fraction $K_{17}$-M (56.4 mg) was further purified on a reversed-phase column (reverse phase silica gel 18.7 grams, column 30 × 1.5 cm) eluting with 68% MeOH in $H_2O$ to yield 29.7 mg major fraction, a portion of which (14.1 mg) was further purified on a reversed-phase (ODS) semi-preparative HPLC column using 85% MeOH in $H_2O$ (3 mL/min), yielding compound **9** (8.1 mg).

Sub-fraction K$_{17}$-S (7.1 mg) was purified on a reversed-phase (ODS) semi-preparative HPLC using 85 % MeOH in H$_2$O (3 mL/min), yielding compounds **10** (3.0 mg).

## ISOLATION SCHEME FOR COMPOUNDS 9- 12

Dried leaves and stems (2000 g)

| Extracted with MeOH

MeOH ext. (433.2 g)

331.2 g

| Partitioning

Hexanes / CHCl$_3$ / *n*-BuOH / H$_2$O

| Hexanes Ext. (47.9 g) | CHCl$_3$ Ext. (12.5 g) | *n*-BuOH Ext. (128.5 g) | H$_2$O Ext. (155.0 g) |

60.0 g

| Silica gel CC
| CHCl$_3$-MeOH-H$_2$O

K
(14.6 g)

Silica gel CC
CHCl$_3$-MeOH-H$_2$O

K$_{17}$
(882.0 mg)

Biotage RP18 40M
MeOH-H$_2$O

| K$_{17}$-B (170.3 mg) | **12** (23.3 mg) | K$_{17}$-M (56.4 mg) | K$_{17}$-S (7.1 mg) |

Biotage 12+M
CHCl$_3$/MeOH/H$_2$O

K$_{17}$-B'
(138.4 mg)

RP18 column
55% MeOH/H$_2$O

RP18 column
68% MeOH/H$_2$O

K$_{17}$-M'
(29.7 mg)
14.1 mg

| HPLC

HPLC

**10**
(3.0 mg)

| **11** (12.8 mg) | **4** (77.7 mg) |

**9**
(8.1 mg)

Figure 2-79. Isolation scheme of minor saponin diglycosides from *S. frutescens*.

**Sutherlandioside A (1)**: Colorless needles (from EtOH), m.p. 210-220 °C, $[\alpha]_D^{20}$ +17.8 (*c* 1.00, MeOH); IR (NaCl) $\nu_{max}$ 3344, 2915, 2358 cm$^{-1}$; $^1$H and $^{13}$C NMR data: Tables 2-1 and 2-2; HRESIMS *m/z* 675.4042 (calculated for $[C_{36}H_{60}O_{10} + Na]^+$, 675.4079).

**Sutherlandioside B (2)**: Colorless needles (from MeOH), m.p. 158 °C, $[\alpha]_D^{20}$ -26.8 (*c* 1.00, MeOH); IR (NaCl) $\nu_{max}$ 3279, 2950, 2362, 1686 cm$^{-1}$; $^1$H and $^{13}$C NMR data: Tables 2-1 and 2-2; HRESIMS *m/z* 675.4112 (calculated for $[C_{36}H_{60}O_{10} + Na]^+$, 675.4079).

**Sutherlandioside C (3)**: White powder, $[\alpha]_D^{20}$ +15.0 (*c* 0.41, MeOH); IR (NaCl) $\nu_{max}$ 3389, 2933, 2361, 1708, 1671 cm$^{-1}$; $^1$H and $^{13}$C NMR data: Tables 2-1 and 2-2; HRESIMS *m/z* 673.3961 (calculated for $[C_{36}H_{58}O_{10} + Na]^+$, 673.3922), 651.4143 (calculated for $[C_{36}H_{58}O_{10} + H]^+$, 651.4103).

**Sutherlandioside D (4)**: White powder, $[\alpha]_D^{20}$ +58.0 (*c* 0.79, MeOH); IR (NaCl) $\nu_{max}$ 3405, 2955, 2361, 1655 cm$^{-1}$; UV (MeOH): $\lambda_{max}$ (logε) 222 (4.04) nm; $^1$H and $^{13}$C NMR data: Tables 2-1 and 2-2; HRESIMS *m/z* 657.4116 (calculated for $[C_{36}H_{58}O_9 + Na]^+$, 657.3973), 635.4194 (calculated for $[C_{36}H_{58}O_9 + H]^+$, 635.4154).

**Sutherlandin A (5)**: amorphous yellow powder; $[\alpha]_D^{25}$ -34.5 (c 0.43, MeOH); UV (MeOH) $\lambda_{max}$ (log ε) 256 (4.28), 356 (4.20) nm; IR $\nu_{max}$ 3229, 2924, 1711, 1654, 1603, 1356, 1166 cm$^{-1}$; HRESIMS *m/z* 763.1693 (calculated for $[M + Na]^+$, 763.1692). $^1$H and $^{13}$C NMR data: see Tables 2-3 and 2-4.

**Sutherlandin B (6)**: amorphous yellow powder; $[\alpha]_D^{25}$ -3.5 (c 0.35, MeOH); UV (MeOH) $\lambda_{max}$ (log ε) 257 (4.24), 358 (4.15) nm; IR $\nu_{max}$ 3233, 2924, 1715, 1651, 1600, 1357, 1139 cm$^{-1}$; HRESIMS *m/z* 763.1682 (calculated for $[M + Na]^+$, 763.1692). $^1$H and $^{13}$C NMR data: see Tables 2-3 and 2-4.

**Sutherlandin C (7)**: amorphous orange powder; $[\alpha]_D^{25}$ -57.6 (c 0.25, MeOH); UV (MeOH) $\lambda_{max}$

(log ε) 266 (4.45), 349 (4.38) nm; IR $\nu_{max}$ 3229, 2929, 1717, 1654, 1561, 1357, 1176 cm$^{-1}$; HRESIMS $m/z$ 747.1741 (calculated for $[M + Na]^+$, 747.1748). $^1$H and $^{13}$C NMR data: see Tables 2-3 and 2-4.

**Sutherlandin D (8)**: amorphous orange powder; $[\alpha]_D^{25}$ -77.1 (c 0.24, MeOH); UV (MeOH) $\lambda_{max}$ (log ε) 266 (4.32), 350 (4.25) nm; IR $\nu_{max}$ 3218, 2927, 1717, 1654, 1564, 1357, 1175 cm$^{-1}$; HRESIMS $m/z$ 747.1747 (calculated for $[M + Na]^+$, 747.1748). $^1$H and $^{13}$C NMR data: see Tables 2-3 and 2-4.

### 2.3.4. X-ray crystallography of sutherlandioside A (1)

Colorless needles of **1** were obtained from slow evaporation of a solution in EtOH. A single crystal, approximate dimensions of 0.18 × 0.16 × 0.10 mm, was used for data collection on a Bruker Smart Apex II system (APEX II, 2005), using Cu $K_\alpha$ radiation with a graphite monochromator, fine-focus sealed tube. The crystal was kept at 100 K under a stream of cooled nitrogen gas from a KRYO-FLEX low temperature device.
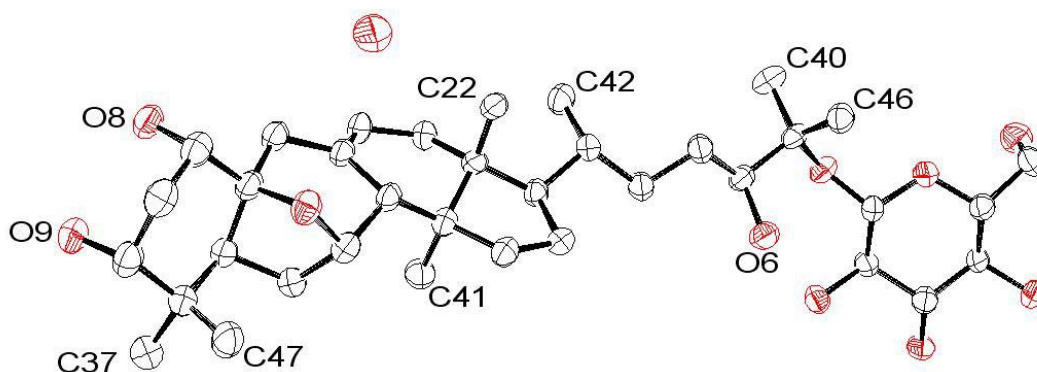


Figure 2-80. ORTEP projections of **1**.

104

Sutherlandioside A (**1**), $C_{36}H_{60}O_{10} \cdot H_2O$, MW = 670.87, crystallized with one molecule of water in the asymmetric unit, monoclinic space group $P2_1$, $a$ = 13.4595 (2) Å, $b$ = 6.78720 (10) Å, $c$ = 20.1461 (3) Å, $\beta$ = 104.7850 (10)°, $V$ = 1779.46 (5) Å$^3$, $Z$ = 2. Goodness of fit (GooF) = 1.024, Flack Parameter = 0.06(16), determined from the refinement of 2658 Friedel pairs.

Data collection, indexing and initial cell refinements were all carried out using APEX II software. Frame integration and final cell refinements were done using SAINT software (SAINT, 2003). The final cell parameters were determined from least-squares refinement on 8837 reflections, with R value = 0.0669, $wR(F^2)$ = 0.091. Structure solution, refinement, graphics and generation of publication materials were performed by using SHELXTL, V6.12 software (SHELXTL, 2002). Hydrogen atoms were placed at their expected chemical positions using the HFIX command and were included in the final cycles of least squares with isotropic $U_{ij}$ 's related to the atom's ridden upon.

The crystallographic data are accessible from The Cambridge Crystallographic Data Centre with a reference number CCDC 673458 (www.ccdc.cam.ac.uk/data_request/cif).

### 2.3.5. Acid hydrolysis of sutherlandioside B (2)

Compound **2** (31.0 mg) in 2 N hydrochloric acid/dioxane was refluxed at 100 °C for two hours. After cooling, the reaction mixture was diluted with water and then extracted with chloroform (4 × 5 mL). The combined chloroform extracts were evaporated to dryness to yield a residue (23.2 mg). The residue was subjected to silica gel chromatography using the isocratic $CHCl_3$:MeOH (49:1) solvent system as eluent to give compound **16** (6.6 mg).

**Compound 16** is a white powder; $[\alpha]_D^{20}$ 83.6 (*c* 0.35, MeOH); IR (NaCl) $\nu_{max}$ 3337, 2960, 2360, 1663 cm$^{-1}$; UV (MeOH) $\lambda_{max}$ 224 nm; NMR data: see Tables 2-1 and 2-2; HRESIMS *m/z*

473.3679 (calculated for $[C_{30}H_{48}O_4 + H]^+$, 473.3636).

The water layer of the hydrolysate allowed the absolute configuration determination for the glucosyl unit in compound **2** by comparison the optical rotation with that of the standard D/L-glucose. The water layer was passed through an Amberlite MB-150 column eluting with water, and the eluent was concentrated to dryness to afford 5.9 mg D-glucose: $[\alpha]_D^{20}$ +43.2 (c 0.45, $H_2O$).

### 2.3.6. Determination of the absolute configuration of the monosaccharides in sutherlandins C (7) and D (8)

A mixture of compounds **7** and **8** (5.2 mg) was dissolved in 1 N hydrochloric acid (dioxane : water 1:1, 1 mL) and incubated at 100 °C for 2.5 hrs. After cooling, the mixture was diluted with 1 mL water, and followed by extraction with 2 mL chloroform four times. The combined chloroform layers were evaporated to dryness to yield 0.6 mg yellow powder, which showed the same $R_f$ value as that of kaempferol on normal phase silica gel TLC (solvent system: $CHCl_3$ : MeOH : $H_2O$ = 8:5:1, $R_f$ = 0.79).

The water layer was neutralized by passing through an Amberlite MB-150 column eluting with water. The collected eluent was concentrated to dryness to afford 1.5 mg residue for monosaccharide analysis following a published procedure (Tanaka, Nakashima *et al.*, 2007).

The residue was dissolved in 250 μL anhydrous pyridine, 50 μL of which and 50 μL of 60 μM L-cysteine methyl ester hydrochloride in pyridine were mixed and incubated at 60-70 °C for 1 hr, and then 100 μL of 36.8 μM phenyl isothiocyanate in pyridine was added and reacted at 60-70 °C for another 1 hr. Standard sugars including D/L-glucose, D/L-xylose, and D-apiose were treated in the same way.

Separation was achieved on a Gemini $C_{18}$ 110 Å column ($150 \times 4.6$ mm I.D.; 5 μm particle size; Phenomenex Inc., Torrance, CA, USA) and operated at 30 °C. The column was equipped with a 2 cm LC-18 guard column (Phenomenex Inc., Torrance, CA, USA). The mobile phase consisted of water (A) and acetonitrile (B), both containing 0.1% acetic acid. The solvents were applied in the following gradient elution: 0-20 min, 95% A/ 5% B to 60% A/ 40% B; 20-25 min, 60% A/ 40% B to 100% B. The total run time was 25 minutes, and the flow rate was 1.0 mL/min. Each run was followed by a 5 min wash with 100% acetonitrile and an equilibration period of 15 min. The peaks were assigned based on their retention times and UV spectra. Detection wavelengths were used at 254 nm. The injection volume was 10 μL.

## 2.3.7. Determination of the absolute configuration of the monosaccharides in sutherlandiosides E–H (9–12)

Compounds **9–12** (2.8, 1.6, 3.4, and 4.0 mg, respectively) were dissolved in 1 N hydrochloric acid (dioxane : water 1:1, 1 mL) and heated at 100 °C for 2.5 hours, followed by the sequential extraction with 2 mL chloroform ($4 \times 2$ mL). The aqueous layer was neutralized by Amberlite MB-150 column eluting with water. The eluents were dried to afford the monosaccharide resides, which were derivatized and analyzed by HPLC using the method described in Section 2.3.6. The monosaccharides contained in compounds **9–12** were all identified as D-glucose by comparison of the retention times with those of the standard derivatives of D- and L- glucoses.

# CHAPTER 3

# AN IMPROVED UPLC-UV/MS BASED METHOD TO DETERMINE ABSOLUTE CONFIGURATION OF MONOSACCHARIDES

## 3.1. Introduction

Carbohydrates are widely distributed in nature. They are indispensable components in many bioactive molecules such as polysaccharides, nucleic acids, glycolipids, and glycoproteins. Monosaccharides are the basic structural units of carbohydrates. A large number of secondary metabolites exist as glycosides of terpenoids, steroids, flavonoids, etc., of which the sugar moieties are generally composed of monosaccharides. Monosaccharides are polyhydroxylated compounds which often exist predominantly in cyclic hemiacetal form in nature. Determination of the absolute configuration of these optically active compounds is important (Tanaka, Nakashima *et al.*, 2007; Lopes and Gaspar, 2008). A variety of techniques involving gas chromatography (GC)(Hara, Okabe *et al.*, 1987), capillary electrophoresis (CE) (Hongda, Taga *et al.*, 1997), HPLC (Tanaka, Nakashima *et al.*, 2007) and chiral HPLC (Lopes and Gaspar, 2008; Ilisz, Berkecz *et al.*, 2009) have been used for this purpose. As shown in Chapter 2, the absolute configuration of the monosaccharide residues in sutherlandins C and D was determined by comparison of the chromatographic retention times of the derivatized diastereomers with those of corresponding standard sugar derivatives by HPLC. In this Chapter, we demonstrate that a UPLC-UV/MS based method has shown improved detection in this regard, allowing separation and characterization of

16 monosaccharides in a single injection. The method was also successfully applied to determine the absolute configurations of sugar units contained in naturally occurring glycosides of triterpenoids, steroids, and flavonoids.

## 3.2.  UPLC-UV/MS method development for simultaneous analysis of 16 monosaccharides

The advantage of the method developed by Tanaka *et al.* for sugar analysis (Tanaka, Nakashima *et al.*, 2007) is in that this type of experiment can be conveniently conducted in a general laboratory that is simply equipped with HPLC-UV instrument. With the wide application of UPLC-MS in analytical and natural products chemistry laboratories in recent years, we attempted to take advantage of the high sensitivity of MS detection to analyze complex multiple monosaccharide components.

Sixteen standard monosaccharides included D-/L-glucose, D-/L-galactose, D-/L-allose, D-/L-arabinose, D-/L-xylose, D-/L-fucose, L-rhamnose, 2-deoxy-D-glucose, 6-deoxy-D-glucose, and 2-deoxy-D-galactose. The derivatization of monosaccharides followed the reported method (Tanaka, Nakashima *et al.*, 2007), in which enantiomeric aldoses were converted to diastereomeric phenylthiocarbamate derivatives (Figure 3-1). In the reaction, monosaccharide samples were condensed with L-cysteine methyl ester during the first step to give thiazolidine derivatives. When treated with phenyl isothiocyanate in pyridine, the thiazolidine derivatives were coupled with phenyl isothiocyanate to afford the final products. The phenylthiocarbamate derivatives were reported to be unstable at room temperature (Tanaka, Nakashima *et al.*, 2007). However, the reaction mixture was found to be stable for up to eight months when keeping in a −20 °C refrigerator with no apparent influence on the analysis of the sugar derivatives.

Phenylisothiocyanate derivatives contain a phenyl group that provides an excellent chromophore for UV detection after conjugation with monosaccharides. The stereogenic center of L-cysteine was introduced into the derivatives of monosaccharide enantiomers, making possible for chromatographic separation of the diastereomeric derivatives. Figure 3-1 demonstrates the separation of D- and L-glucose on UPLC and their ESI-MS spectra. The maximum UV absorptions of D- and L-glucose were observed at 250 and 246 nm, respectively. In the ESI-MS spectra, D- and L-glucose derivatives gave both $[M + H]^+$ and $[M + Na]^+$ ions at $m/z$ 433 and 455, respectively (Figure 3-1). Fragment ions were observed at $m/z$ 320, 298, 262, 178, 160, and 136 corresponding to the ions $[455 - C_7H_5NS]^+$, $[433 - C_7H_5NS]^+$, $[298 - 2H_2O]^+$, $[298 - C_4H_8O_4]^+$, $[178 - H_2O]^+$, and $[C_7H_6NS]^+$, respectively.
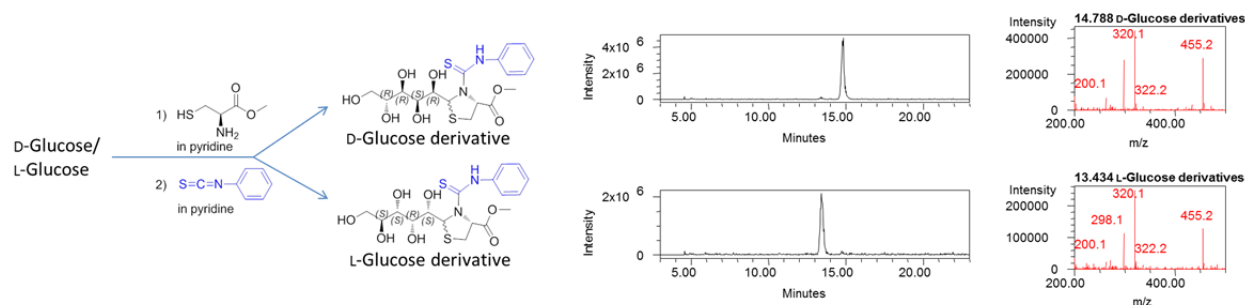


Figure 3-1. Selected ion chromatograms of $[M + Na]^+$ for D-/ L-glucose derivatives at $m/z$ 455.

In a preliminary test for the discrimination of sugar enantiomers, sugar derivatives were analyzed on several different 1.7 μm UPLC columns in order to optimize the separation. The tested columns included Acquity UPLC BEH $C_{18}$ (50 mm × 2.1 mm I.D., 1.7 μm), BEH Shield RP18 (50 mm × 2.1 mm I.D., 1.7 μm), BEH $C_{18}$ (100 mm × 2.1 mm I.D., 1.7 μm), and BEH Shield RP18 (100 mm × 2.1 mm I.D., 1.7 μm). The best separation and peak shape were achieved when using a 100 mm × 2.1 mm BEH $C_{18}$ column.

Several gradient eluting systems were tested to determine the optimal separation conditions for the analysis of the 16 monosaccharide derivatives, including acetonitrile/water, methanol/water, methanol/ acetonitrile/ water, and methanol/ isopropanol/ acetonitrile/ water. Optimal chromatographic conditions were found with methanol/ isopropanol/ acetonitrile (25 : 25 : 50, v/v/v) plus 0.05% formic acid and water containing 0.05% formic acid as the mobile phase. Formic acid was used as a modifier because it improved peak shapes and separation. It also enhanced the sensitivity of the mass spectrometer when operated in the positive ion mode.

The chromatograms of 16 monosaccharide derivatives are shown in Figure 3-2. The retention times and major fragment ions of each tested monosaccharide derivative are listed in Table 3-1. In a single injection of a mixture of sugar derivatives, 16 monosaccharide products were identified within 23 minutes by comparison of their retention times as well as selected ion chromatograms (SICs). Although coelution occurred between derivatives of L-allose and 2-deoxy-D-glucose that were marked as peaks (1) and (7), and between D-glucose and L-xylose that were marked as peaks (5) and (13) in the chromatograms (Figure 3-2), both pairs of coeluting derivatives were able to be distinguished by SICs at *m/z* 455, 439, and 425 daltons.
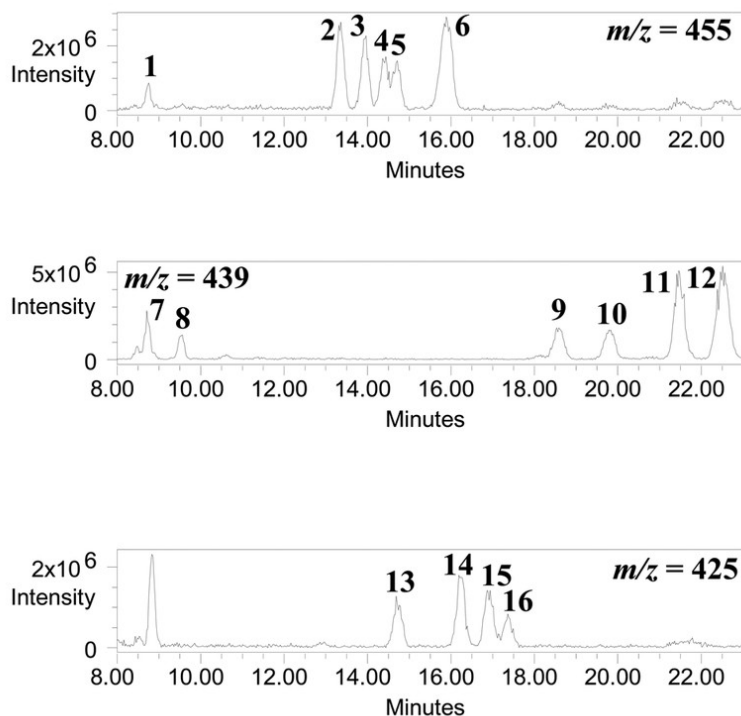
Figure 3-2.  Selected ion chromatograms of 16 monosaccharide derivatives.

Hexose subgroup at *m/z* = 455: (1) L-allose, (2) L-glucose, (3) D-galactose, (4) L-galactose, (5) D-glucose, and (6) D-allose; deoxy hexose subgroup at *m/z* = 439: (7) 2-deoxy-D-glucose, (8) 2-deoxy-D-galactose, (9) D-fucose, (10) L-fucose, (11) 6-deoxy-D-glucose, and (12) L-rhamnose, pentose subgroup at *m/z* = 425: (13) L-xylose, (14) D-xylose, (15) L-arabinose, and (16) D-arabinose.

Since high sensitivity of the detection provides the decreased quantity of test samples required for accurate sugar analysis, this method is especially useful in natural products research considering the structures of naturally occurring metabolites are generally complicated and the quantities obtained from labor intensive purification are often limited. In this experiment less than 50 ng of monosaccharide derivatives were used to differentiate via single injection on the UPLC column. The sensitivity of identification on the UPLC column was 12-30 times higher than that of the reported methods using GC and HPLC methods (Hara, Okabe *et al.*, 1987; Tanaka, Nakashima *et al.*, 2007).

Based on the structural differences, the examined monosaccharides can be generally categorized into three different subgroups: pentoses, hexoses, and deoxy hexoses, each of which produce characteristic fragment ions at *m/z* 425, 455, and 439 respectively. Consequently, they can be observed in their related SICs separately. Table 3-1 also summarizes the *m/z* ratios of the observed fragment ions for each subgroup.

Table 3-1. Retention times (t$_R$) and major fragment ions of individual sugar derivatives by a UPLC-MS method.

| Sub-group | Peak number | analyzed sugar name | t$_R$ (min) | Fragment ions (*m/z*) |
|---|---|---|---|---|
| Hexose | 1 | L-allose | 8.7 | 455, 433, 320, 298, 160, 136 |
| | 2 | L-glucose | 13.3 | 455, 433, 320, 298, 262, 178, 160, 136 |
| | 3 | D-galactose | 13.9 | 455, 433, 320, 298, 262, 178, 160, 136 |
| | 4 | L-galactose | 14.4 | 455, 433, 320, 298, 262, 178, 160, 136 |
| | 5 | D-glucose | 14.7 | 455, 433, 320, 298, 262, 178, 160, 136 |
| | 6 | D-allose | 15.8 | 455, 433, 320, 298, 262, 178, 160, 136 |
| Deoxy hexose | 7 | 2-deoxy-D-glucose | 8.6 | 439, 304, 239, 136 |
| | 8 | 2-deoxy-D-galactose | 9.5 | 439, 304, 239, 136 |
| | 9 | D-fucose | 18.5 | 439, 417, 304, 282, 160, 136 |
| | 10 | L-fucose | 19.7 | 439, 417, 304, 282, 160, 136 |
| | 11 | 6-deoxy-D-glucose | 21.4 | 439, 304, 178, 160, 136 |
| | 12 | L-rhamnose | 22.4 | 439, 417, 304, 282, 178, 160, 136 |
| Pentose | 13 | L-xylose | 14.8 | 425, 403, 290, 268, 232, 178, 160, 136 |
| | 14 | D-xylose | 16.2 | 425, 403, 290, 268, 232, 178, 160, 136 |
| | 15 | L-arabinose | 16.9 | 425, 403, 290, 268, 232, 178, 160, 136 |
| | 16 | D-arabinose | 17.4 | 425, 403, 290, 268, 232, 178, 160, 136 |

As far as the eluting sequences are concerned, the retention times of tested sugar derivatives didn't result in any preferences of elution orders on the $C_{18}$ column for certain enantiomeric type (such as D- or L-sugars) monosaccharides as compared to its enantiomeric counterpart, and hence the eluting sequence of certain sugar derivative is not related to its underivatized D- or L- form. For instance, the derivatives of D-enantiomers were retained longer on the $C_{18}$ column than those of L-enantiomeric counterparts in the case of glucose, xylose, allose, and arabinose, while the derivatives of L-enantiomers were eluted longer on the $C_{18}$ column than those of D-enantiomeric counterparts in the case of galactose and fucose. However, when the retention times were examined with the stereogenic centers of the related aldoses, it appeared that the absolute configuration at C-3′ of the aldoses has a significant influence on the elution order for all the derivatives of the selected monosaccharides. In the current data sets, a sugar derivative with an *R*-configuration at C-3′ of the aldose showed a longer retention time than that of the epimeric derivative with 3′*S*-configuration of the aldose.

## 3.3. Application of the method to determine absolute configuration of monosaccharides in naturally occurring glycosides

This analytical method was employed to determine the absolute configurations of the sugar components in the selected glycosides of triterpenoids, steroids, and flavonoids. For triterpene glycosides cauloside G and ciwujianoside A1 isolated from the medicinal plant Blue cohosh (*Caulophyllum thalictroides*), it was determined that 1 mole of cauloside G or ciwujianoside A1 is composed of 3 moles of glucose, 1 mole of arabinose, and 1 mole of rhamnose as was reported

from the previous study (Ali and Khan, 2008). The hydrolysate of the glycosides was treated as described in Section 3.4 and examined by UPLC-MS.



Cauloside G

Ciwujianoside A1

20-hydroxyecdysone-3-O-β-D-glucopyranoside

20-hydroxy-(25-acetyl)-ecdysone-3-O-β-D-glucopyranoside

rutin
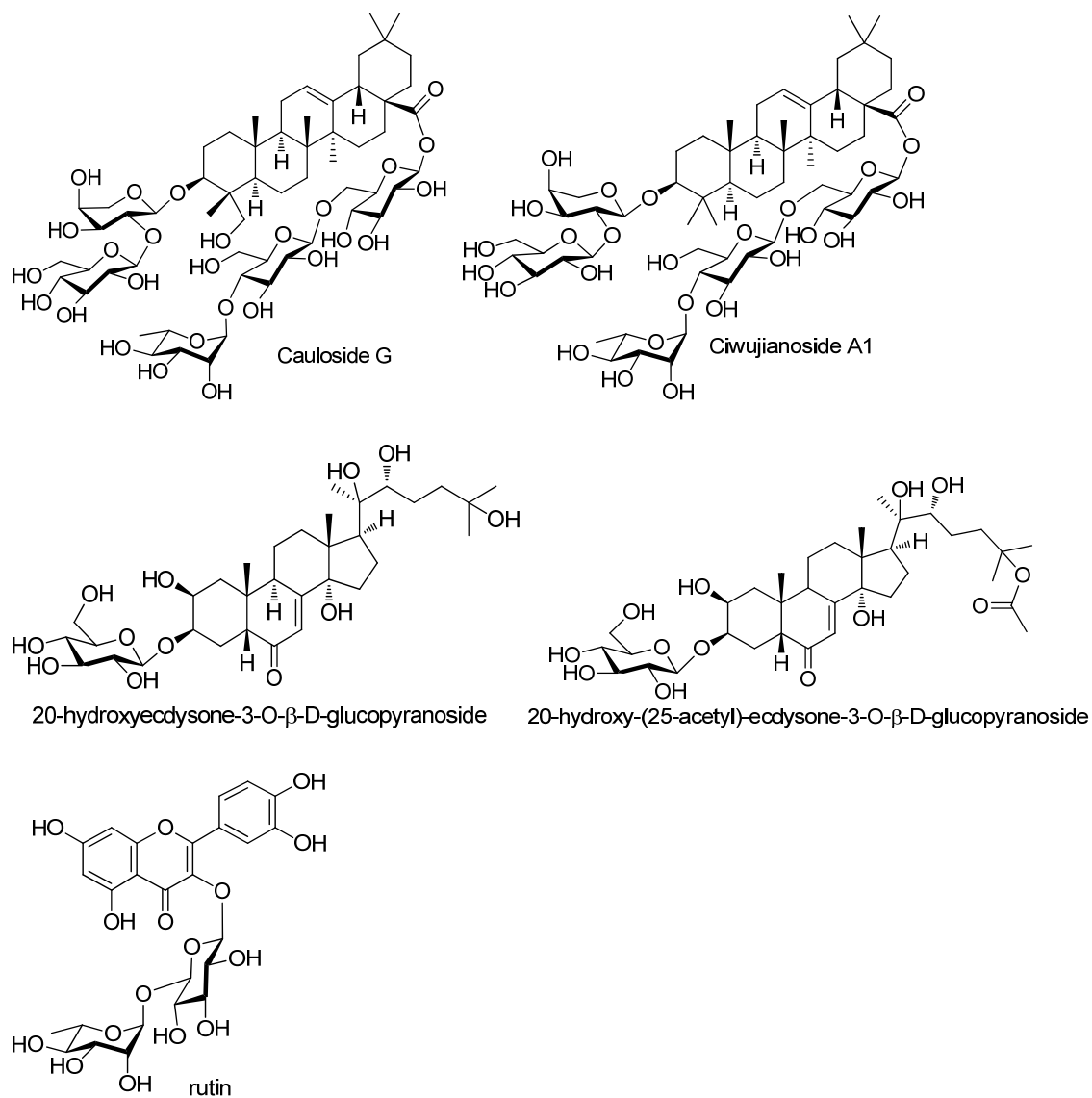
Figure 3-3. Structure of triterpene, steroids, and flavonol glycosides used in the UPLC-based sugar analysis.

Glucose, arabinose, and rhamnose were readily identified from the chromatograms and mass spectra of derivatives of either cauloside G or ciwujianoside A1. By comparison of retention

time values and mass spectra of each sample with that of standard compounds, the absolute configurations of the sugar components were determined to be D- for glucose, and L- for arabinose and rhamnose respectively.

The developed method was also successfully applied for steroid and flavonoid glycosides. For the steroid glycosides 20-hydroxyecdysone-3-$O$-β-D-glucopyranoside and 20-hydroxy-(25-acetyl)-ecdysone-3-$O$-β-D-glucopyranoside isolated from *Sida rhombifolia*. The absolute configuration of the glucose was identified as D that was in agreement with the reported results (Jadhav, Pawar *et al.*, 2007). For the flavonoid glycoside rutin, the sugar components were characterized to be D-glucose and L-rhamnose.

## 3.4. Experimental section

### 3.4.1. Samples and materials

All analyses were performed on a Waters Acquity UPLC™ system (Waters Corp.) that included a binary solvent manager, sample manager, heated column compartment, photodiode array (PDA) detector, and a single quadrupole detector (SQD). The instrument was controlled by Waters Empower 2 software. An Acquity UPLC™ BEH C$_{18}$ column (100 mm × 2.1 mm I.D., 1.7 µm) also from Waters was used. The column temperature was maintained at 35 °C. The eluent consisted of water with 0.05% formic acid (A) and acetonitrile/methanol/isopropanol (50 : 25 : 25, v/v) with 0.05% formic acid (B). Analysis was performed using the following gradient elution at a flow rate of 0.30 mL/min: 14% B to 16.5% B in 22 min, and increasing B to 100% B in next 0.5 min. The composition of mobile phase was changed linearly. The analysis was followed by a 2.5-min washing procedure with 100% B and re-equilibration period of 3.5 min. All solutions were

filtered through 0.20-μm membrane filters, and the injection volume was 2 μL. The total run time for analysis was 23 minutes. The PDA detection wavelength was 254 nm.

The ESI source was used in the positive mode. Mass spectrometer conditions were optimized to obtain maximal sensitivity. The source and desolvation gas temperatures were maintained at 150 and 350 °C, respectively. The probe voltage (capillary voltage), cone voltage, and extractor voltage were fixed at 3.0 kV, 45 V, and 3.0 V, respectively. Nitrogen was used as the desolvation gas (650 L/hr) and drying gas (25 L/hr). Analyte identity was confirmed in selected ion recording (SIR) mode. Mass spectra were obtained at a dwell time of 0.1 s in SIR and 500 Da/sec of the scan rate.

Monosaccharide standards including D-/L-glucose, D-/L-galactose, D-/L-allose, D-/L-arabinose, D-/L-xylose, D-/L-fucose, L-rhamnose, 2-deoxy-D-glucose, 6-deoxy-D-glucose, and 2-deoxy-D-galactose, as well as flavonoid glycoside rutin were purchased from Sigma Chemical Company (St Louis, Missouri). The purity of monosaccharide standards was labeled in the range 97-99%. Triterpene glycosides cauloside G and ciwujianoside A1, and steroid glycosides 20-hydroxyecdysone-3-O-β-D-glucopyranoside and 20-hydroxy-(25-acetyl)-ecdysone-3-O-β-D-glucopyranoside were isolated from blue cohosh (*Caulophyllum thalictroides*) (Ali and Khan, 2008) and *Sida rhombifolia* L. (Jadhav, Pawar *et al.*, 2007), respectively, at the NCNPR, the University of Mississippi, MS, USA. Acetonitrile, methanol, isopropanol, water, hydrogen chloride, and formic acid are HPLC grade and were purchased from Fisher Scientific Company. Phenyl isothiocyanate, L-cysteine methyl ester, ammonium hydroxide, and pyridine were purchased from Sigma Chemical Company.

### 3.4.2. Hydrolyses of triterpene glycosides and derivatization of the resultant monosaccharides

About 1 mg of glycoside sample, such as cauloside G and ciwujianoside A1 was dissolved in 200 µL of 2 M HCl and heated at 90 °C for 2 hrs. After hydrolysis, the reaction mixture was neutralized with 200 µL of 9 M NH$_4$OH, and dried with high purity N$_2$ gas.

About 1 mg of each monosaccharide or hydrolyzed glycoside sample was dissolved in 120 µL of 0.3 M L-cysteine methyl ester in pyridine. After mixing thoroughly, the reaction mixture was incubated at 90 °C for 1 hr. 160 µL of 0.69 M phenyl isothiocyanate in pyridine was added as the chiral reagent, and the solution was heated for another hour. The final solution was further diluted 20-200 times before UPLC-MS analysis.

# CHAPTER 4

# BIOLOGICAL ACTIVITIES OF TRITERPENE AND FLAVONOL GLYCOSIDES

# FROM *S. FRUTESCENS*

## 4.1. Introduction

*S. frutescens* has long been used for the treatment of a variety of diseases in South Africa. The ethanol and water extracts of this plant showed activities through recent biological /pharmacological investigations, including anticancer, antidiabetic, anti-oxidant, anti-inflammatory, antibacterial and antiviral effects, as has been described in Chapter 1. However, due to the limited phytochemical studies, the active principles of this multipurpose medicinal plant are still not fully understood. The limited number of known components such as L-canavanine and γ-aminobutyric acid cannot sufficiently explain the multiple beneficial effects from this plant. The isolation of the 12 new glycosides (described in Chapter 2) has made it possible to evaluate the biological activities of other chemotypes of compounds, which may provide helpful scientific information for this medicinally important plant. In this Chapter, the antimicrobial, antiviral, antiprotozoal activities, and cytotoxicities of the 12 purified compounds and the crude ethanol extracts of *S. frutescens* were evaluated. It is noticeable that the major compound sutherlandioside B showed antiviral activity against the Epstein-Barr virus.

## 4.2. Results and discussion

### 4.2.1. In vitro antimicrobial activity

Compounds **1–12** were tested for antimicrobial activity against *Candida albicans, C. glabrata, C. krusei, Cryptococcus neoformans, Aspergillus fumigatus, Staph. aureus,* MRS, *E. coli, P. aeruginosa,* and *M. intracellulare*, along with the crude methanol extract and subsequent partitioning fractions including hexanes, chloroform, *n*-butanol, and water soluble portions. Sutherlandiosides G (**11**) and H (**12**) showed marginal activities against *Staph. aureus* with $IC_{50}$s 2.29 and 1.59 µg/mL, respectively, and against MRS with $IC_{50}$ values at the level of 6.79 and 1.86 µg/mL, respectively. The positive control ciprofloxacin gave $IC_{50}$s of 0.1 and 0.08 µg/mL against *Staph. aureus* and MRS, respectively. No activities were observed for others at the highest test concentration of 20 µg/mL.

Table 4-1. Antifungal activities of samples from *S. frutescens*.

| sample | $IC_{50}$ (µg/mL) | | | | |
| --- | --- | --- | --- | --- | --- |
| | *C. albicans* | *C. glabrata* | *C. krusei* | *A. fumigatus* | *Crypto. neoformans* |
| Sutherlandioside A | NA | ND | ND | NA | NA |
| Sutherlandioside B | NA | ND | ND | NA | NA |
| Sutherlandioside C & D | NA | ND | ND | NA | NA |
| Sutherlandins A & B | NA | ND | ND | NA | NA |
| Sutherlandins C & D | NA | ND | ND | NA | NA |
| Sutherlandioside E | NA | NA | NA | NA | NA |
| Sutherlandioside F | NA | NA | NA | NA | NA |
| Sutherlandioside G | NA | NA | NA | NA | NA |
| Sutherlandioside H | NA | NA | NA | NA | NA |
| Amphotericin B | 1.26 | 0.84 | 1.4 | 1.22 | 0.2 |

NA = not active; ND = no data or not determined.

Table 4-2. Antibacterial activities of samples from *S. frutescens*.

| sample | IC$_{50}$ (µg/mL) | | | | |
|---|---|---|---|---|---|
| | *Staph. aureus* | **MRS** | *E. coli* | *P. aeruginosa* | *M. intracellulare* |
| Sutherlandioside A | ND | NA | NA | NA | NA |
| Sutherlandioside B | ND | NA | NA | NA | NA |
| Sutherlandioside C & D | ND | NA | NA | NA | NA |
| Sutherlandins A & B | ND | NA | NA | NA | NA |
| Sutherlandins C & D | ND | NA | NA | NA | NA |
| Sutherlandioside E | NA | NA | NA | NA | NA |
| Sutherlandioside F | 10.26 | 8.03 | NA | NA | NA |
| Sutherlandioside G | 2.29/NA* | 6.79/NA* | NA | NA | NA |
| Sutherlandioside H | 1.59/NA* | 1.86/NA* | NA | NA | NA |
| Ciprofloxacin | 0.1 | 0.08 | 0.005/0* | 0.07 | 0.22 |

NA = not active; ND = no data or not determined; * data from Tertiary Screen.

## 4.2.2. In vitro antiviral activity

The major secondary metabolite, sutherlandioside B, was submitted to the NIAID for antiviral testing. A series of viruses, including measles, SARS, EBV, Rift Valley fever, Tacaribe, WNV, adenovirus, Flu A (H1N1), Flu A (H3N2), Flu A (H5N1), Flu B, rhinovirus type 2 were cultured in different cells. The anti-EBV activity was evaluated by DNA hybridization assay. Other antiviral activities were evaluated by determining the infected cell viabilities using neutral red and visual light based assays.

Sutherlandioside B exhibited anti-EBV activity with a CC$_{50}$ value at 0.4 µM, an EC$_{50}$ value higher than 0.16 µM, and the SI value lower than 2.5. The EC$_{50}$ of the positive control drug acyclovir was 0.35 µM.

The activities of this compound against other tested viruses were not significant. It showed only a moderate activity against Tacaribe virus in a visual light test with an EC$_{50}$ at 10 µg/mL, but

it didn't show activity in the neutral red based assay.

Table 4-3. Antiviral activities of sutherlandioside B against a panel of respiratory and biodefense related viruses.

| Virus | Virus Strain | Cell Line | Assay | EC$_{50}$ (μg/mL) | IC$_{50}$ (μg/mL) | SI |
|---|---|---|---|---|---|---|
| Measles | Chicago | Vero 76 | NR | 32 | 37 | 1.2 |
| Measles | Chicago | Vero 76 | Visual | 32 | 100 | 3.1 |
| SARS | Urbani | Vero 76 | NR | >100 | >100 | 0 |
| SARS | Urbani | Vero 76 | Visual | >100 | >100 | 0 |
| Adeno | 65089/Chicago | A-549 | NR | >100 | >100 | 0 |
| Adeno | 65089/Chicago | A-549 | Visual | >100 | >100 | 0 |
| Flu A (H1N1) | Solomon Islands/03/2006 | MDCK | NR | >100 | >100 | 0 |
| Flu A (H1N1) | Solomon Islands/03/2006 | MDCK | Visual | >100 | >100 | 0 |
| Flu A (H3N2) | Wisconsin/67/2005 | MDCK | NR | >100 | >100 | 0 |
| Flu A (H3N2) | Wisconsin/67/2005 | MDCK | Visual | >100 | >100 | 0 |
| Flu A (H5N1) | Vietnam/1203/2004H | MDCK | NR | >100 | >100 | 0 |
| Flu A (H5N1) | Vietnam/1203/2004H | MDCK | Visual | >100 | >100 | 0 |
| Flu B | Malaysia/2506/2004 | MDCK | NR | >100 | >100 | 0 |
| Flu B | Malaysia/2506/2004 | MDCK | Visual | >100 | >100 | 0 |
| Rhinovirus Type 2 | HGP | HeLa Ohio-1 | NR | >100 | >100 | 0 |
| Rhinovirus Type 2 | HGP | HeLa Ohio-1 | Visual | >100 | >100 | 0 |
| Rift Valley Fever | MP-12 | Vero 76 | NR | >100 | 100 | 0 |
| Rift Valley Fever | MP-12 | Vero 76 | Visual | >100 | 100 | 0 |
| Tacaribe | TRVL 11573 | Vero 76 | NR | >100 | >100 | 0 |
| Tacaribe | TRVL 11573 | Vero 76 | Visual | 10 | >100 | >10 |
| WNV | New York isolate | Vero 76 | NR | >100 | >100 | 0 |

### 4.2.3. In vitro cytotoxicity

Compounds **9**–**11** were tested for cytotoxicity against tumorigenic cell lines SK-MEL, KB, BT-549, SK-OV-3, and normal cell lines Vero and LLC-PK$_{11}$. None of the test samples was found cytotoxicity at the level of 25 μg/mL.

Table 4-4.  Cytotoxicity of samples from *S. frutescens*.

| Sample | IC$_{50}$ (μg/mL) | | | | | |
|---|---|---|---|---|---|---|
| | **SK-MEL** | **KB** | **BT-549** | **SK-OV-3** | **Vero** | **LLC-PK$_{11}$** |
| Sutherlandioside E | NA | NA | NA | NA | NC | NC |
| Sutherlandioside G | NA | NA | NA | NA | NC | NC |
| Sutherlandioside H | NA | NA | NA | NA | NC | NC |
| Doxorubicin | 0.6 | 1.4 | 1.1 | 1.4 | NC | 0.75 |

NA = not active; NC = not cytotoxic.

### 4.2.4. In vitro antiprotozoal activity

A mixture of compounds **9** and **10** in a ratio of nearly 1:1 showed a weak antimalarial activity against the W2 strain parasite with an IC$_{50}$ value of 4.76 μg/mL, but didn't show activity against the D6 strain parasite. Other samples including extracts, partitioning fractions and compounds didn't show activity against both strains of parasites.

Table 4-5. Antimalarial activities of samples from *S. frutescens*.

| Sample | P. falciparum D6 I% | P. falciparum D6 IC$_{50}$ (ng/mL) | D6 SI | P. falciparum W2 IC$_{50}$ (ng/mL) | W2 SI | Vero IC$_{50}$ (ng/mL) |
|---|---|---|---|---|---|---|
| Ex (MeOH) | 31 | \ | \ | \ | \ | \ |
| Pt (Hexanes) | 25 | \ | \ | \ | \ | \ |
| Pt (CHCl$_3$) | 27 | \ | \ | \ | \ | \ |
| Pt (BuOH) | 11 | \ | \ | \ | \ | \ |
| Pt (H$_2$O) | 32 | \ | \ | \ | \ | \ |
| Sutherlandioside B | \ | NA | - | NA | - | NC |
| Sutherlandiosides C & D | \ | NA | - | 4760 | >1 | NC |
| Sutherlandioside A | \ | NA | - | NA | - | NC |
| Sutherlandins C & D | \ | NA | - | NA | - | NC |
| Sutherlandins A & B | \ | NA | - | NA | - | NC |
| Sutherlandioside E | \ | NA | - | NA | - | NC |
| Sutherlandioside F | \ | NA | - | NA | - | NC |
| Sutherlandioside G | \ | NA | - | NA | - | NC |
| Sutherlandioside H | \ | NA | - | NA | - | NC |
| Artemisinin | \ | 5.5 | ND | 4.9 | ND | NC |
| Chloroquine | 99 | 7 | ND | 100 | ND | NC |

Ex, extract; Pt, partition; NA = not active; NC = not cytotoxic; ND = no data or not determined.


The partitioning water extract showed a weak inhibitory activity against *L. donovani* with IC$_{50}$ and IC$_{90}$ of 9.0 and 4.9 μg/mL, respectively, compared to the drug control amphotericin B with IC$_{50}$ and IC$_{90}$ of 0.13 and 0.24 μg/mL, respectively. Other extracts and compounds didn't show inhibitory activities. This result indicated that the water extracts of *S. frutescens* could contain some antileishmanial components against *L. donovani*. Further investigation of the water extract may lead to the discovery of new antileishmanial compounds.

Table 4-6.  Antileishmanial activities of samples from *S. frutescens*.

| Sample | *L. donovani* IC$_{50}$ (μg/mL) | *L. donovani* IC$_{90}$ (μg/mL) |
|---|---|---|
| Ex (MeOH) | NA | NA |
| Pt (Hex) | NA | NA |
| Pt (CHCl$_3$) | 60 | NA |
| Pt (BuOH) | NA | NA |
| Pt (H$_2$O) | 9 | 4.9 |
| Sutherlandioside B | NA | NA |
| Sutherlandioside A | NA | NA |
| Sutherlandiosides C & D | NA | NA |
| Sutherlandins C & D | NA | NA |
| Sutherlandins A & B | NA | NA |
| Sutherlandioside E | NA | NA |
| Sutherlandioside F | NA | NA |
| Sutherlandioside G | NA | NA |
| Sutherlandioside H | NA | NA |
| Pentamidine | 0.73 | 1.92 |
| Amphotericin B | 0.13 | 0.24 |

Ex, extract; Pt, partition; NA = not active.

## 4.3.  Experiment

### 4.3.1.  Samples and materials

All used microorganisms, including five fungi and five bacteria, were obtained from the American Type Culture Collection (Manassas, VA).  The involved fungi were *Candida albicans* ATCC 90028, *C. glabrata* ATCC 90030, *C. krusei* ATCC 6258, *Cryptococcus neoformans* ATCC 90113, and *A. fumigatus* ATCC 204305,  and the bacteria were *Staph. aureus* ATCC 29213, methicillin-resistant *Staph. aureus* ATCC 33591 (MRS), *E. coli* ATCC 35218, *Pseudomonas aeruginosa* ATCC 27853, and *Mycobacterium intracellulare* ATCC 23068.

A panel of mammalian origin normal and solid tumor cell lines, including Vero (African green monkey kidney fibroblasts), LLC-PK$_{11}$ (pig kidney epithelial cells), HepG2 (human hepatocellular carcinoma), SK-MEL (human malignant melanoma), KB (human epidermal carcinoma, oral), BT-549 (human breast carcinoma), and SK-OV-3 (human ovary carcinoma) were obtained from ATCC (Manassas, VA).

Alamar Blue™ was from BioSource International, Camarillo, CA. RPMI 1640 were obtained from Cellgro. Mueller-Hinton agar was obtained from Difco Laboratories. 3-($N$-morpholino)propanesulfonic acid (MOPS) was obtained from Sigma-Aldrich, St. Louis, MO. Ciprofloxacin and amphotericin B were obtained from ICN Biomedicals, Ohio. Fetal calf serum (FCS) was obtained from Gibco Chemical Company. Type-A human red blood cells and human serum were obtained from Interstate Blood Bank, Memphis, TN. Amikacin was obtained from Sigma, St. Louis, MO. Malstat™ reagent was obtained from Flow Inc., Portland, OR. Nitro blue tetrazolium/phenazine ethosulfate (NBT/PES) solution was purchased from Sigma-Aldrich, St. Louis, MO.

### 4.3.2.  Experimental methods

4.3.2.1.  Antimicrobial activity test

Assays for antimicrobial activity were conducted at the NCNPR. Antimicrobial test were performed on a panel of 10 pathogenic microbes including five fungi (Yang, Zhang *et al.*, 2006) and five bacteria (Ma, Khan *et al.*, 2004). All organisms were tested using modified versions of the CLSI (formerly NCCLS) methods.  Optical density (OD) was used to monitor growth (NCCLS,

2002; NCCLS, 2006) for all organisms excluding *M. intracellulare* and *A. fumigatus*. Media supplemented with 5% Alamar Blue™ was utilized for growth detection of *M. intracellulare* (Franzblau, Witzig *et al.*, 1998; NCCLS, 2003) and *A. fumigatus* (NCCLS, 2002). Briefly, samples (dissolved in DMSO) were serially-diluted in 20% DMSO/saline and transferred (10 µL) in duplicate to 96-well flat bottom microplates. Inocula were prepared by correcting the $OD_{630}$ of microbe suspensions in incubation broth, including RPMI 1640/ 0.2% dextrose/ 0.03% glutamine/ MOPS at pH 6.0 (Cellgro) for *Candida spp.*, Sabouraud dextrose for *C. neoformans*, cation-adjusted Mueller-Hinton (Difco) at pH 7.3 for *Staph. spp.*, *E. coli*, and *P. aeruginosa*, 5% Alamar Blue™ in Middlebrook 7H9 broth with OADC enrichment, pH = 7.0 for *M. intracellulare*, and 5% Alamar Blue™/ RPMI 1640 broth (0.2% dextrose, 0.03% glutamine, buffered with 0.165 M MOPS at pH 7.0) for *A. fumigatus* to afford an assay volume of 200 µL final target inocula. The seeding densities are *Candida spp.* and *C. neoformans.*: $1.5 \times 10^3$, *M. intracellulare*: $2.0 \times 10^6$, *Staph. spp.*, *E. coli*, *P. aeruginosa*: $5.0 \times 10^5$ CFU/mL, and *A. fumigatus*: $2.7 \times 10^4$ CFU/mL. Final tested sample concentrations were 1/100th of the stock concentration in DMSO. Ciprofloxacin was used in each assay as the positive control for antibacterial assays, while Amphotericin B was used for the positive control of antifungal tests.

All organisms were read at either 530 nm using the Biotek Powerwave XS plate reader (Bio-Tek Instruments, Vermont) or 544ex/590em, (for *M. intracellulare, A. fumigatus*) using the Polarstar Galaxy plate reader (BMG LabTechnologies, Germany). The incubation conditions are: *Candida spp.* at 35 °C for 46-50 hours; *Staph. spp.*, *E. coli*, and *P. aeruginosa* at 35 °C for 16-20 hours; *C. neoformans* at 35 °C for 70-74 hours; *A. fumigatus* at 35 °C for 46-50 hours; *M. intracellulare* at 37 °C and 10% $CO_2$ for 70-74 hours.

$IC_{50}$ is defined as a test concentration that affords 50% inhibition of the microbe relative to

negative and positive controls. It was calculated by XL*fit* 4.2 software (IDBS, Alameda, CA) using fit model 201. The MIC is defined as the lowest test concentration that allows no detectable growth (for *M. intracellulare* and *A. fumigatus*, no color change from blue to pink). Even though the growth of the organism was completely inhibited at the MIC, some cells could be alive without growing. To verify such condition, an aliquot from the MIC and above was transferred to a fresh media. Cells that grow in the fresh media were shown the survival. The minimum fungicidal or bactericidal concentrations (MFCs or MBCs respectively) were therefore determined. The MFC and MBC are defined as the lowest test concentration that kills the organism (without growth).

A three-step screening (primary/ secondary/ tertiary) was performed according to the purity of samples. Crude extracts were initially tested against all 10 strains in a Primary Screen at 50 μg/mL in duplicate, and percent inhibitions were calculated relative to negative and positive controls. Samples in a Secondary Screen were tested in duplicate at three test concentrations of 5-fold dilutions, including the extracts showing inhibitions higher than 50% in the Primary Screen, first-run pure compounds, and column fractions. Crude extracts and column fractions were dissolved to 20 mg/mL and tested at 50, 10 and 2 μg/mL. Pure compounds and column fractions in high purity were dissolved to 2 mg/mL and tested at 20, 4 and 0.8 μg/mL. Extracts from the Secondary Screen showing an $IC_{50}$ of lower than 2 μg/mL were tested in a Tertiary Screen in duplicate at six concentrations (5-fold dilutions): 50, 10, 2, 0.4, 0.08, 0.016 μg/mL. Pure compounds having $IC_{50}$s of lower than 7 μg/mL were tested in a Tertiary Screen at a series of two-fold diluted concentrations from 20 to 0.02 μg/mL. In addition to the $IC_{50}$s, the MIC was assigned. MFCs or MBCs were determined by removing 5 μL from each clear (or blue) well, transferring to fresh media for incubation.

4.3.2.2. In vitro antiviral activity test

Assays for antiviral activity were conducted by National Institute of Allergy and Infectious Diseases (NIAID). The inhibitory activities against a series of virus were tested, including a human herpesvirus and a panel of eight respiratory and three biodefense related viruses.

Epstein-Barr virus (EBV) was cultivated in the Burkitt's lymphoma cell line Akata and was used for antiviral test in a DNA Hybridization Assay.

A series of respiratory viruses were cultured in the infected cells for antiviral activities. The Chicago strain of measles virus and Urbani strain of SARS virus were grown in African green monkey kidney cell line Vero 76, and the cell viabilities were tested by neutral red and visual based assays. Adenovirus (65089/Chicago) was grown on A-549 cell line and cell viability was tested by Neutral Red and Visible Light assays. Influenza viruses A including the subtypes of H1N1 (Solomon Islands/03/2006), H3N2 (Wisconsin/67/2005), and H5N1 (Vietnam/1203/2004H), and influenza virus B (Malaysia/2506/2004) were grown in MDCK cell line, and cell viability was examined by Neutral Red and Visible Light assays. The HGP strain of rhinovirus Type 2 was grown in HeLa Ohio-1 cell line, and cell viability was measured by Neutral Red and Visible Light assays.

For a panel of three biodefense viruses, the MP-12 strain of Rift Valley Fever virus (RVFV) and the TRVL 11573 strain of Tacaribe virus (TCRV, arenavirus) were grown in a line of Vero 76 cell and the cell viability were determined by neutral red based and visual based assays. A New York isolate of West Nile virus (WNV) was grown on Vero 76 cell line was determined the cell viability by Neutral Red Assay.

Acyclovir was used as the positive control in the experiment. Four concentrations were

used in the neutral red based assay to determine the half effective concentration ($EC_{50}$), $IC_{50}$, and half cytotoxic concentration ($CC_{50}$) from the dose-response curve. $EC_{50}$ was defined as the concentration of the compound needed to inhibit the cytopathic effect to 50% of the control value. $CC_{50}$ was defined as the concentration of the compound that reduces cell viability to 50%. The selectivity index (SI) values were thus calculated as the ratio of $CC_{50}$ to the $EC_{50}$.

4.3.2.3.  In vitro cytotoxicity test

The samples were tested for their in vitro cytotoxicity against a panel of normal cell lines in the NCNPR, including Vero and LLC-PK$_{11}$, and against a panel of solid tumor cell lines, including SK-MEL, KB, BT-549, and SK-OV-3 (Mustafa, Khan *et al.*, 2004).  Cells were grown in RPMI 1640 medium supplemented with 10% bovine calf serum (BCS) and amikacin (60 mg/L). HepG2 cells were grown in DMEM-F12 medium supplemented with 10% fetal bovine serum (FBS).

Each type of cells (25,000 cells per well) was seeded in the well of a 96-well plate and incubated for 24 hours. Samples were then added and followed by incubation for 48 hours. The number of viable cells was determined based on a modified version of neutral red (NR) assay procedure using a supravital dye neutral red (Borenfreund, Babich *et al.*, 1990). Briefly, the cells were washed with saline and incubated with a solution of NR dye for 3 hrs. After the incubation, the cells were washed again to remove extracellular dye. The incorporated dye from viable cells can be liberated by dissolving the dye in an acidified ethanol solution. The absorbance of the NR solution was read at 450 nm. $IC_{50}$ values were determined from logarithmic graphs of growth inhibition versus concentration. Doxorubicin was used as a positive control, while DMSO was used as the negative control.

### 4.3.2.4. Antiprotozoal activity test

The antimalarial and antileishmanial assays were conducted at the NCNPR for testing the antiprotozoal activities of samples isolated from *S. frutescens*.

An in vitro antimalarial assay examined samples for their ability to inhibit *Plasmodium falciparum* using chloroquine-sensitive D6 clone and chloroquine-resistant W2 clone protozoans. The antimalarial activity was evaluated by comparison of the plasmodial lactate dehydrogenase (LDH) activities with those of the controls (Makler and Hinrichs, 1993; Makler, Ries *et al.*, 1993). Briefly, D6 or W2 clone was adjusted with uninfected $A^+$ red blood cells and RPMI 1640 medium supplemented with 10% human serum and 60 mg/mL amikacin to yield a 2% of hematocrit and 2.0% of parasitemia. The infected cells in a volume of 200 µL were seeded to 96-well plates. After adding 10 µL samples with a series of diluted concentrations to the plate in duplicate, the cells were incubated in a modular incubation chamber (Billups-Rothenberg, CA) flushed with a gas mixture of 90% $N_2$, 5% $O_2$, and 5% $CO_2$ at 37 °C for 72 hours. Parasitic LDH activity was measured by mixing 20 µL of the cell incubation mixture with 100 µL of Malstat™ reagent at room temperature for 30 min, and then adding 20 µL NBT/PES (1:1) mixture and continue incubating in the dark for 1 hr. The reaction was then quenched by adding 100 µL of 5% acetic acid solution. The plate was read at 650 nm using the EL-340 Biokinetics Reader (Bio-Tek Instruments, Vermont). The antimalarial drugs chloroquine and artemisinin were used as positive controls, and DMSO was used as negative control. $IC_{50}$ is defined as the test concentration that affords 50% inhibition of the protozoan relative to negative and positive controls, and was obtained based on the dose-response curves. $IC_{50}$ values were calculated using the XL*fit* software

131

for curve-fitting. In addition to the *P. falciparum* strains, samples are tested in Vero cell line as an indicator of general cytotoxicity. The selectivity indices (SIs) (the $IC_{50}$ ratios of Vero to D6 or W2) were thus calculated.

A two-step screen was conducted for extracts, fractions and purified components. The extracts are initially tested against the D6 strain of *P. falciparum* in a Primary Screen at 15.867 µg/mL in duplicate. The percent inhibitions were calculated relative to negative and positive controls and the extracts with inhibition values higher than 50% proceed to a Secondary Screen with a series of diluted sample concentrations of 4.7600, 1.5867, and 0.5289 µg/mL. Pure compounds and fractions in high purity were tested in the Secondary Screen at the concentrations of 4760, 1587, and 529 ng/mL against both the D6 and W2 strains, and the $IC_{50}$s were calculated according to the dose-response curves.

An in vitro antileishmanial assay was conducted using a culture of promastigotes and axenic amastigotes parasite for testing the inhibitory activity of samples against *Leishmania donovani*, a fly-borne protozoan causing visceral leishmaniasis (Ma, Khan *et al.*, 2004). Briefly, the promastigotes of *L. donovani* were grown in RPMI 1640 medium supplemented with 10% fetal calf serum at 26°C. After three days culture, the diluted promastigotes were seeded into a 96-well plate at a density of $5 \times 10^5$ cells/mL. The compounds were added to the inoculated parasites at six concentrations. Each sample was tested in duplicate. The plates were incubated at 26 °C for 72 hours (37 °C for amastigote). The growth of promastigotes and amastigotes of *L. donovani* were determined by Alamar blue assay (Mikus and Steverding, 2000). $IC_{50}$ and 90% inhibition concentration ($IC_{90}$) values are defined as the test concentrations that afford 50% and 90% inhibition of the protozoan relative to controls, respectively. The $IC_{50}$ and $IC_{90}$ were calculated based on the growth inhibition curves. Pentamidine and amphotericin B were used as the standard

antileishmanial agents. The compounds were simultaneously tested for cytotoxicity on Vero cell line by Neutral Red assay (Babich and Borenfreund, 1991).

Crude extracts were initially tested against *L. donovani* in a Primary Screen in duplicate at the concentration of 80 µg/mL, and percentage inhibitions were calculated based on the comparison of OD values to that of negative and positive controls. The extracts showing inhibitions of higher than 50% were subjected to a Secondary Screen. Samples were tested at 40, 8.0 and 1.6 µg/mL in the Secondary Screen. The $IC_{50}$ and $IC_{90}$ are defined as test concentrations that afford 50% and 90% inhibition of the protozoan relative to controls, respectively. They were calculated based on the dose-response curve with line fitting by XL*fit* 4.2 software. The Tertiary Screen was carried out when the samples showed $IC_{50}$ lower than 1.6 µg/mL in the Secondary Screen. Samples were tested at a series of diluted concentrations of 40, 8, 1.6, 0.32, 0.064, 0.0128 µg/mL, and $IC_{50}$ and $IC_{90}$ values were calculated from the dose-response curve based on the tested concentrations in the Tertiary Screen.

# CHAPTER 5

## ANALYSIS OF TRITERPENE AND FLAVONOL GLYCOSIDES IN *S. FRUTESCENS* AND DIETARY SUPPLEMENTS BY LC-UV/ ELSD

### 5.1. Introduction

As a popular medicinal plant in South Africa, a variety of herbal products or dietary supplements containing *S. frutescens* are commonly seen on the market. Without proper quality control methods, adulteration could be a serious problem particularly when the supplies fall short of the demands. An important goal of this project is to develop an analytical method to quantify the characteristic compounds in the plant and related commercial products.

Eight major compounds including four cycloartane-type triterpene glycosides, sutherlandiosides A–D (**1–4**, see Figure 2-1), and four flavonol glycosides, sutherlandins A–D (**5–8**, see Figure 2-27) isolated from the plant were used as chemical markers.

Owing to the lack of conjugating system, the four triterpene glycosides show very weak UV absorption and thus evaporative light scattering detector (ELSD) was used for detection. The flavonoid-type compounds were analyzed by LC-UV method at 260 nm wavelength. This work established the analytical method for the first time for quantitatively determination of eight newly identified triterpenoids **1–4** and flavonoids **5–8** (Avula, Wang *et al.*, 2010). The analytical method was also applied to commercial products claimed to contain *S. frutescens*.

## 5.2. Results and discussion

### 5.2.1. Chromatographic conditions

Several types of columns providing different stationary phases have been assessed, including Luna 5 μm $C_{18}$(2), Luna 5 μm $C_8$(2), Synergi 4 μm Max-RP 80 Å, Lichrospher 5 RP18, Discovery $C_{18}$, and Gemini 5 μm $C_{18}$. The best results were obtained on the Discovery $C_{18}$ stationary phase from Supelco.

Compounds **1** and **4** coeluted on most of the columns (Luna 5 μm $C_{18}$(2), Luna 5 μm $C_8$(2), Synergi 4 μm Max-RP 80 Å, Lichrospher 5 RP18, and Gemini 5 μm $C_{18}$) using a variety of eluting systems. However, the resolution of the test compounds was achieved on the Discovery $C_{18}$ column at a higher degree of column temperature (e.g., 43 °C) resulted in a base line separation of the compounds and reduced the separation time. Compounds were monitored using an ELS detector considering the weak UV absorption for **1**–**4**. Optimal chromatographic conditions were obtained after running different mobile phases on the Discovery $C_{18}$ column. The mobile phase contained an acidic system to improve the peak symmetry of all compounds. Acidic conditions also improved the sensitivity and protons enhancement.
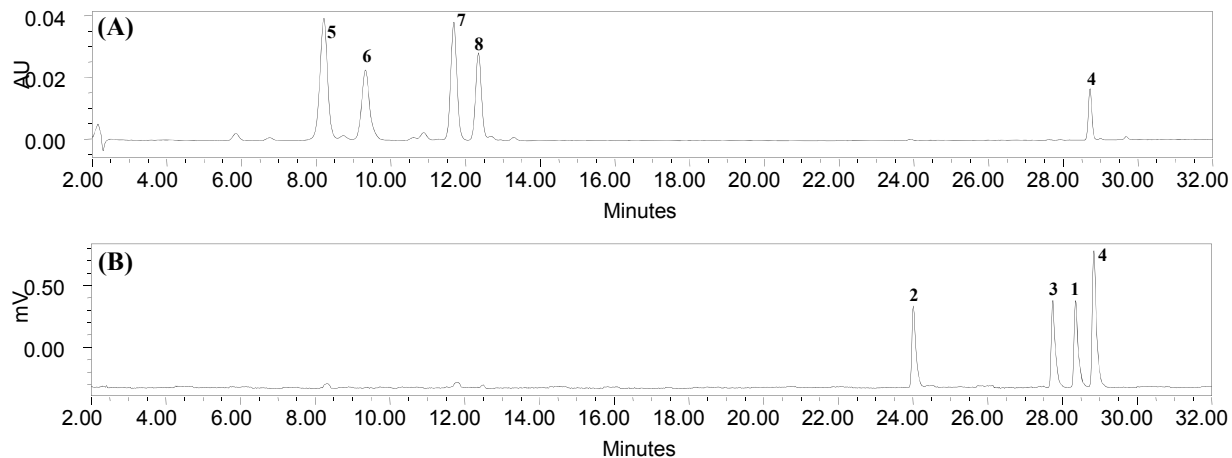
Figure 5-1. HPLC chromatograms of standard mixtures of **4**–**8** (A) and **1**–**4** (B) at 260 nm by LC-UV and ELSD methods.

The column condition was then established using a flow rate of 1.0 mL/min at a column temperature of 40 °C, and with an injection volume of 10 μL. The chromatograms of the mixtures of the cycloartanol glycosides **1**–**4** and flavonoids **5**–**8** from *S. frutescens* of the LC-UV/ELSD methods are shown in Figures 5-1 and 5-2.
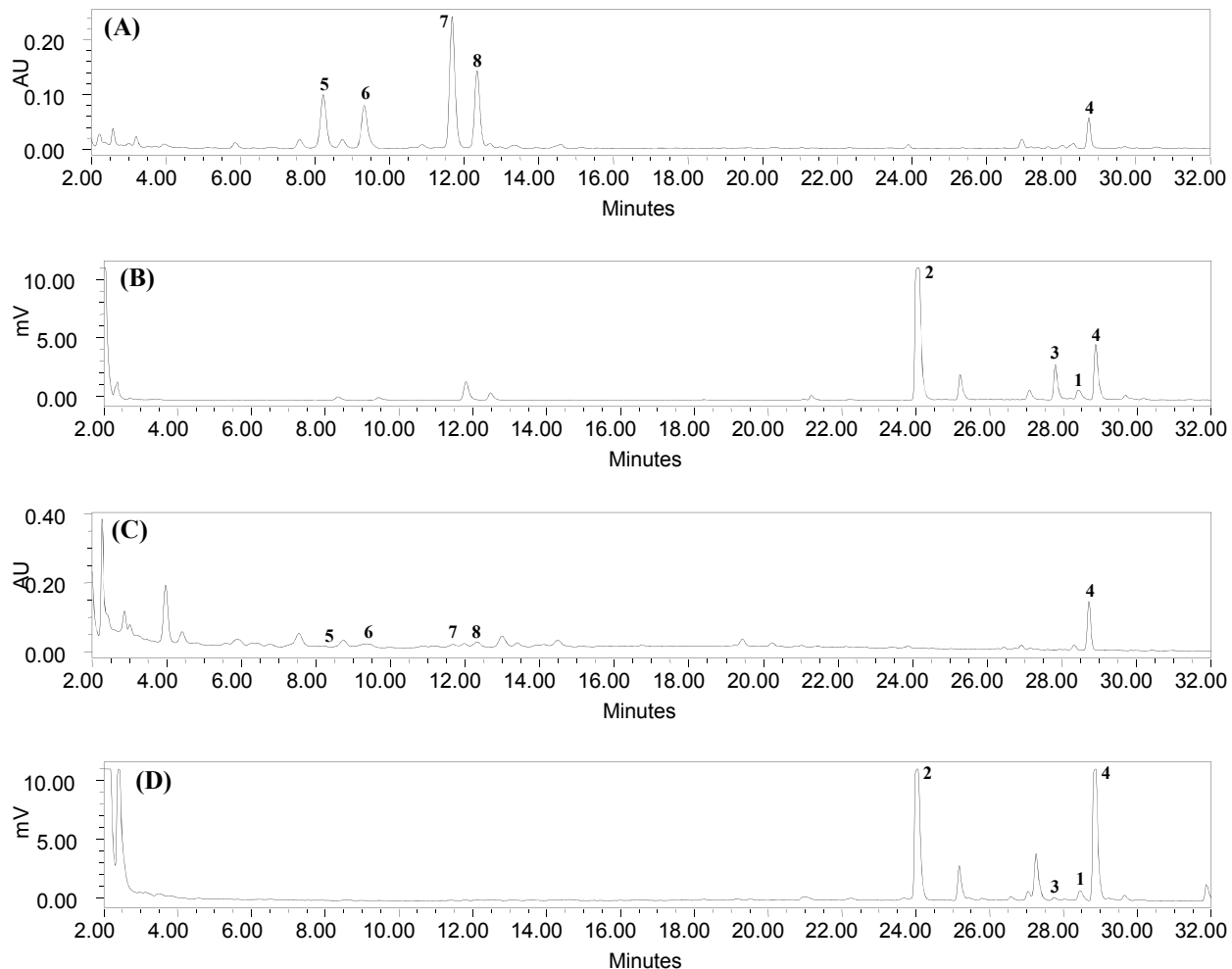
Figure 5-2. HPLC chromatograms of plant sample and dietary supplements by LC-UV at 260 nm and LC-ELSD methods.

(A) Plant sample by UV detection; (B) plant sample by ELSD detection; (C) dietary supplements by UV detection; (D) dietary supplements by ELSD detection;

### 5.2.2. Validation of analytical procedures

Five-point calibration curves for the eight compounds showed a linear relationship between concentration and peak area over the working concentration ranges. Calibration data indicated a good linearity ($r^2 > 0.998$) of the detector response for all standard compounds (Table

5-1). The limits of detection (LOD) and limits of quantification (LOQ) were found to be in the range from 0.1 to 7.5 μg/mL and from 0.5 to 25 μg/mL, respectively (Table 5-1) for the eight standard compounds **1**–**8**. The LOD and LOQ were defined, respectively, as signal-to-noise ratio equal to 2 or 3 and 10.

Table 5-1. Regression equation, correlation coefficient ($r^2$), LOD, and LOQ by LC-UV/ ELSD method for analysis of triterpenoids **1**–**4** and flavonoids **5**–**8** from *S. frutescens*.

| analyte | regression equation | $r^2$ | LOD (μg/mL) | LOQ (μg/mL) |
|---------|--------------------|-------|-------------|-------------|
| **1** | $Y = (1.62\mathrm{e}{+}000)x + (1.05\mathrm{e}{+}000)$ | 0.9986 | 5 | 15 |
| **2** | $Y = (1.78\mathrm{e}{+}000)x + (7.41\mathrm{e}{-}001)$ | 0.9996 | 5 | 10 |
| **3** | $Y = (1.71\mathrm{e}{+}000)x + (5.60\mathrm{e}{-}001)$ | 0.9998 | 7.5 | 25 |
| **4** | $Y = (1.67\mathrm{e}{+}000)x + (9.01\mathrm{e}{-}001)$ | 0.9990 | 7.5 | 25 |
| **5** | $Y = (7.75\mathrm{e}{+}003)x - (1.02\mathrm{e}{+}004)$ | 0.9996 | 0.35 | 1.0 |
| **6** | $Y = (7.35\mathrm{e}{+}003)x - (5.48\mathrm{e}{+}003)$ | 0.9998 | 0.35 | 1.0 |
| **7** | $Y = (9.87\mathrm{e}{+}003)x - (3.10\mathrm{e}{+}003)$ | 0.9997 | 0.1 | 0.5 |
| **8** | $Y = (9.68\mathrm{e}{+}003)x + (1.56\mathrm{e}{+}002)$ | 0.9997 | 0.1 | 0.5 |

All standard compounds and samples were injected in triplicate. Multiple injections showed that the results are highly reproducible and presented low standard error. The accuracy of the method was confirmed by performing a recovery experiment. Intra- and inter-day variation of the assay was determined showing the ratio lower than 3.0%, with a maximum relative standard deviation (RSD) value of 2.29% (Table 5-2). It was performed three times on three different days and each concentration point was injected in triplicate.

The intra- and inter-day precision and accuracy values were determined by analyzing samples spiked with standard compounds **1**–**8** at two different concentrations of 25 and 50 μg/mL

for cycloartanol glycosides **1**–**4** and 5 and 10 µg/mL for flavonoids **5**–**8** (Table 5-2).

Table 5-2. Intra- and inter-day accuracy analyses for cycloartanol glycosides **1**–**4** and flavonoids **5**–**8** from *S. frutescens*.

| Analyte | Concentration (µg/mL) | Intra-day (*n* = 3) | | | Inter-day (*n* = 9) | | |
|---|---|---|---|---|---|---|---|
| | | Found (µg/mL) | RSD (%) | Accuracy* (%) | Found (µg/mL) | RSD (%) | Accuracy* (%) |
| **1** | 25.0 | 25.13 | 0.34 | 100.52 | 25.21 | 0.34 | 100.84 |
| | 50.0 | 50.23 | 0.06 | 100.46 | 50.11 | 0.11 | 100.22 |
| **2** | 25.0 | 25.35 | 0.11 | 101.4 | 24.76 | 0.19 | 99.04 |
| | 50.0 | 50.05 | 0.11 | 100.1 | 49.95 | 0.23 | 99.90 |
| **3** | 25.0 | 24.27 | 0.17 | 97.08 | 25.11 | 0.23 | 100.44 |
| | 50.0 | 50.15 | 0.11 | 100.3 | 49.89 | 0.28 | 99.7 |
| **4** | 25.0 | 24.77 | 0.17 | 99.08 | 24.43 | 0.17 | 97.72 |
| | 50.0 | 49.64 | 0.09 | 99.28 | 50.13 | 0.16 | 100.26 |
| **5** | 5.0 | 5.12 | 0.42 | 102.4 | 5.11 | 0.28 | 102.2 |
| | 10.0 | 10.23 | 0.28 | 102.3 | 10.15 | 0.63 | 101.5 |
| **6** | 5.0 | 5.09 | 0.14 | 101.8 | 5.03 | 0.56 | 100.6 |
| | 10.0 | 10.29 | 0.82 | 102.9 | 10.05 | 0.70 | 100.5 |
| **7** | 5.0 | 5.19 | 0.55 | 103.8 | 5.10 | 0.83 | 102.0 |
| | 10.0 | 10.31 | 0.21 | 103.1 | 10.25 | 0.69 | 102.5 |
| **8** | 5.0 | 4.89 | 1.16 | 97.8 | 4.95 | 2.29 | 99.0 |
| | 10.0 | 10.11 | 0.49 | 101.1 | 10.19 | 0.56 | 101.9 |

* Accuracy (%) = 100% × mean of measured concentration/nominal concentration.

The intra-day coefficient of variations (CVs) for the replicates of cycloartanol glycosides **1**–**4** and flavonoids **5**–**8** (*n* = 3) at two different concentrations were between 0.06 and 1.16% for compounds, respectively (Table 5-2). The CVs for the day to day replicates of compounds **1**–**8** (*n* = 9) at different concentrations were between 0.11% and 2.29%, respectively. The accuracy of the HPLC method for analytes **1**–**8** was found to be higher than 97% at all concentration levels (Table 5-2).

### 5.2.3. Analysis of samples from plant material and plant containing products

In addition to ELS detection, the UV spectra from the PDA detector provided spectrometric information for these compounds (Figure 5-3).
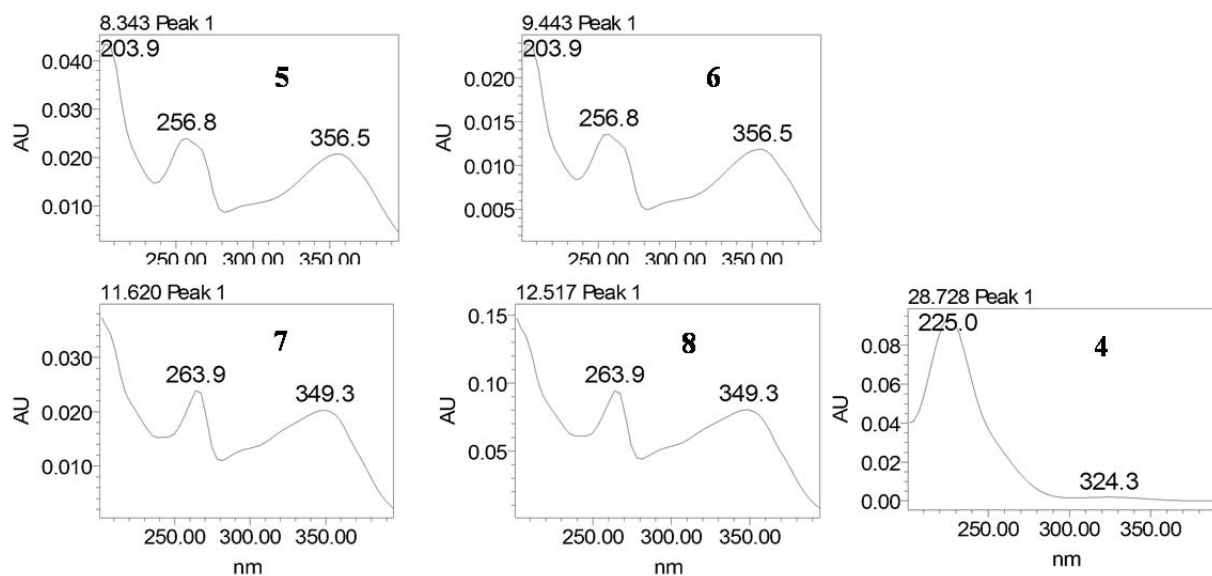


Figure 5-3. UV spectra of sutherlandins A–D and sutherlandioside D.

After exhaustive extraction ($\times$ 4) and drying, samples containing *S. frutescens* materials were spiked with known amounts of the standard compounds at two concentration levels for both flavonoids and cycloartanol glycosides, and then analyzed under optimized conditions.

One plant sample and six commercial dietary supplements named SF-1 to SF-6 were analyzed for contents of triterpenoids **1**–**4** and flavonoids **5**–**8**. The identification of these compounds in the *S. frutescens* sample was based on the retention times and by comparison of UV spectra with those of authentic standards. Spiked samples with reference compounds were conducted as a confirmation assay. The developed method was used for analysis of eight compounds in the leaves of *S. frutescens* and commercial samples consisting of the plant as one of

the ingredients.

Variations in concentrations of the triterpenoids and flavonoids in one plant sample of *S. frutescens*, and commercial products containing *S. frutescens* are shown in Tables 5-3, 5-4, and 5-5. The content (*w/w*) of compounds **1**–**8** in plant sample were 0.61, 2.75, 0.22, 0.64, 0.53, 0.49, 0.94, and 0.54%, respectively.

Table 5-3.  Content (%, *w/w*) of standard compounds **1**–**8** from *S. frutescens* sample by LC-UV/ ELSD methods.

| Compound # | content% of standards (*g/100 g*, in 302.4 mg plant sample ) |
|:---:|:---:|
| 1 | 0.606 ± 1.267 |
| 2 | 2.75 ± 0.234 |
| 3 | 0.221 ± 0.312 |
| 4 | 0.644 ± 0.524 |
| 5 | 0.531 ± 0.821 |
| 6 | 0.485 ± 0.047 |
| 7 | 0.943 ± 1.544 |
| 8 | 0.542 ± 0.524 |

Mean values (*n* = 3) ± standard deviations.

Sutherlandioside B (**2**), a major cycloartanol glycoside was present in the range of 5.224 to 1.099 mg/average weight of capsule or tablet content in the tested samples. The amounts of other cycloartanol glycosides [sutherlandiosides A (**1**), C (**3**) and D (**4**)] were in the range of 0.064 to 1.149, 0.083 to 0.568, 0.079 to 3.894 mg/average weight of capsule or tablet content (Table 5-4).

Table 5-4.  Content (%, *w/w*) of triterpenoids **1–4** from *S. frutescens* sample and commercial dietary supplements SF-1 through SF-6 by LC-UV/ELSD method.

| Extractions | Weight (mg) | content of standard(mg) in average weight of product form | | | |
|---|---|---|---|---|---|
| | | 1 | 2 | 3 | 4 |
| SF-1 | 384.2 | 0.473 ± 0.367 | 5.224 ± 0.132 | 0.568 ± 0.426 | 3.894 ± 1.191 |
| SF-2 | 331.2 | 1.149 ± 0.149 | 4.619 ± 0.144 | 0.099 ± 0.174 | 0.488 ± 0.356 |
| SF-3 | 237.2 | 0.064 ± 0.344 | 1.561 ± 0.187 | 0.083 ± 0.227 | 0.691 ± 0.288 |
| SF-4 | 515.6 | 0.178 ± 0.001 | 1.099 ± 0.321 | 0.109 ± 0.075 | 0.306 ± 0.384 |
| SF-5 | 504.9 | 0.287 ± 0.261 | 1.179 ± 0.313 | 0.116 ± 0.342 | 0.458 ± 0.423 |
| SF-6 | 394.6 | 0.760 ± 0.813 | 2.713 ± 0.275 | 0.146 ± 0.302 | 0.079 ± 0.361 |

Mean values (*n* = 3) ± standard deviations.

The contents of **5**–**8** were present in the levels from 0.041 to 0.498, 0.023 to 1.128, 0.021 to 1.537 and 0.115 to 0.645 mg/average weight of capsule or tablet, respectively, in six dietary supplements claiming to contain *S. frutescens* (Table 5-5).

Table 5-5.  Content (%, *w/w*) of flavonoids **5**–**8** from *S. frutescens* sample and commercial dietary supplements SF-1 through SF-6 by LC-UV/ELSD method.

| Extractions | Weight (mg) | content of standard (mg) in average weight of product form | | | |
|---|---|---|---|---|---|
| | | 5 | 6 | 7 | 8 |
| SF-1 | 384.2 | 0.498 ± 0.419 | 0.437 ± 0.440 | 0.063 ± 0.238 | 0.148 ± 0.281 |
| SF-2 | 331.2 | 0.209 ± 0.213 | 0.398 ± 0.400 | 1.537 ± 0.384 | 0.645 ± 0.216 |
| SF-3 | 237.2 | 0.049 ± 0.128 | 0.111 ± 0.119 | 0.021 ± 0.205 | 0.124 ± 0.249 |
| SF-4 | 515.6 | 0.041 ± 0.125 | 0.023 ± 0.204 | 0.0517 ± 0.202 | 0.162 ± 0.545 |
| SF-5 | 504.9 | 0.176 ± 0.288 | 0.057 ± 0.218 | 0.243 ± 0.219 | 0.115 ± 0.449 |
| SF-6 | 394.6 | 0.054 ± 0.225 | 1.128 ± 0.273 | 0.558 ± 0.549 | 0.312 ± 0.457 |

Mean values (*n* = 3) ± standard deviations.

This method involved the use of selected ion monitoring (SIM). The $[M + H]^+$ and $[M + Na]^+$ ions in the positive ion mode and $[M − H]^−$ in the positive ion mode were selected. In the positive ion mode, the protonated species $[M + H]^+$ at *m/z* 653.4267, 653.4257, 651.4134, 635.4189, 741.1887, 741.1941, 725.1918, 725.1961, and sodiated species $[M + Na]^+$ at *m/z*

675.4112, 675.4117, 673.3968, 657.3998, 763.1739, 763.1749, 747.1773, 747.1791, for

compounds **1–8** were observed (Table 5-6). In the negative ion mode, the deprotonated species [M

− H]$^-$ at *m/z* 651.4108, 651.4108, 649.3952, 633.4003, 739.1705, 739.1725, 723.1745, 723.1784,

for compounds **1–8** were observed (Table 5-6).

Table 5-6. Selected pseudomolecular ions in the mass spectra of compounds **1–8** identified using
LC-ESI-MS in positive and negative scan mode.

| Analyte | negative ion (*m/z*) | positive ions (*m/z*) |
|---|---|---|
| 1 | 651.4108 [M − H]$^-$ | 653.4267 [M + H]$^+$, 675.4112 [M + Na]$^+$ |
| 2 | 651. 4108 [M − H]$^-$ | 653.4257 [M + H]$^+$, 675.4117 [M + Na]$^+$ |
| 3 | 649.3952 [M − H]$^-$ | 651.4134 [M + H]$^+$, 673.3968 [M + Na]$^+$ |
| 4 | 633.4003 [M − H]$^-$ | 635.4189 [M + H]$^+$, 657.3998 [M + Na]$^+$ |
| 5 | 739.1705 [M − H]$^-$ | 741.1887 [M + H]$^+$, 763.1739 [M + Na]$^+$ |
| 6 | 739.1725 [M − H]$^-$ | 741.1941 [M + H]$^+$, 763.1749 [M + Na]$^+$ |
| 7 | 723.1745 [M − H]$^-$ | 725.1918 [M + H]$^+$, 747.1773 [M + Na]$^+$ |
| 8 | 723.1784 [M − H]$^-$ | 725.1961 [M + H]$^+$, 747.1791 [M + Na]$^+$ |

In addition, the observed fragmentation patterns in the mass spectrum were helpful for the

characterization of the compounds.

Compounds **1** and **2** showed characteristic fragments of [aglycones + H]$^+$ (*m/z* 491.3696 &

491.3718), [aglycones + H − H$_2$O]$^+$ (473.3582 & 473.3631), [aglycones + H − 2 H$_2$O]$^+$ (455.3477

& 455.3541), [aglycones + H − 3 H$_2$O]$^+$ (437.3368 & 437.3397), [aglycones + H − 4 H$_2$O]$^+$

(419.3264 & 419.3287). Compound **3** showed characteristic fragments at *m/z* 489.3592 [aglycone

+ H]$^+$ and 471.3511 [aglycone + H − H$_2$O]$^+$ while compound **4** showed fragment ions at *m/z*

473.3647 [aglycone + H]$^+$, 455.3544 [aglycone + H − H$_2$O]$^+$, 437.3437 [aglycone + H − 2 H$_2$O]$^+$

and 419.3333 [aglycone + H − 3 H$_2$O]$^+$. These ions were recognized as the loss of sugar and water

from the cycloartane-type skeleton (Table 5-7).

Table 5-7. Key fragment analysis of pure standard compounds **1-4** by the LC-ESI-TOF method.

| Particle | 1 | 2 | 3 | 4 |
|---|---|---|---|---|
| Exact mass | 652.4186 | 652.4186 | 650.4030 | 634.4081 |
| $[M + H]^+$ | 653.4265 | 653.4265 | 651.4143 | 635.4194 |
| $[M + H - glu]^+$ | 491.3696 | 491.3718 | 489.3592 | 473.3647 |
| $[M + H - H_2O]^+$ | 635.4094 | 635.4118 | 633.3996 | 617.4078 |
| $[M + H - H_2O - glu]^+$ | 473.3582 | 473.3631 | 471.3511 | 455.3544 |
| $[M + H - 2\ H_2O]^+$ | 617.3987 | 617.4018 | | 599.3977 |
| $[M + H - 2\ H_2O - glu]^+$ | 455.3477 | 455.3541 | | 437.3437 |
| $[M + H - 3\ H_2O]^+$ | 599.3881 | 599.3913 | | 581.3703 |
| $[M + H - 3\ H_2O - glu]^+$ | 437.3368 | 437.3397 | | 419.3333 |
| $[M + H - 4\ H_2O - glu]^+$ | 419.3264 | 419.3287 | | |

Compounds **5** and **6** showed characteristic fragments at $m/z$ 609.1467 and 609.1447 that indicated the loss of the terminal pentose moiety, and the base peaks at $m/z$ 303.0508 and 303.0495 that indicated the aglycone part as quercetin. Compounds **7** and **8** showed characteristic fragments at $m/z$ 593.1484 and 593.1480 that indicated the presence of a terminal pentose unit. The base peaks at $m/z$ 287.0545 and 287.0547 indicated the presence of the kaempferol-type aglycone (Table 5-8).

Table 5-8. Key fragment analysis of pure standard compounds **5-8** by the LC-ESI-TOF method.

| Particle | 5 | 6 | 7 | 8 |
|---|---|---|---|---|
| Exact mass | 740.1800 | 740.1800 | 724.1851 | 724.1851 |
| $[M + Na]^+$ | 763.1748 | 763.1748 | 747.1817 | 747.1817 |
| $[M + H]^+$ | 741.1928 | 741.1928 | 725.1986 | 725.1986 |
| $[M + H - pentose]^+$ | 609.1467 $[M + H - 132]^+$ | 609.1447 $[M + H - 132]^+$ | 593.1484 $[M + H - 132]^+$ | 593.1480 $[M + H - 132]^+$ |
| Base peak | 303.0508 (quercetin) | 303.0495 (quercetin) | 287.0545 (kaempferol) | 287.0547 (kaempferol) |

The extracted ion chromatograms (XICs) in positive ion mode for the standard sample are shown in Figure 5-4. The retention times and mass spectra of plant sample and products (not shown) exactly matched those of the corresponding standard compounds.
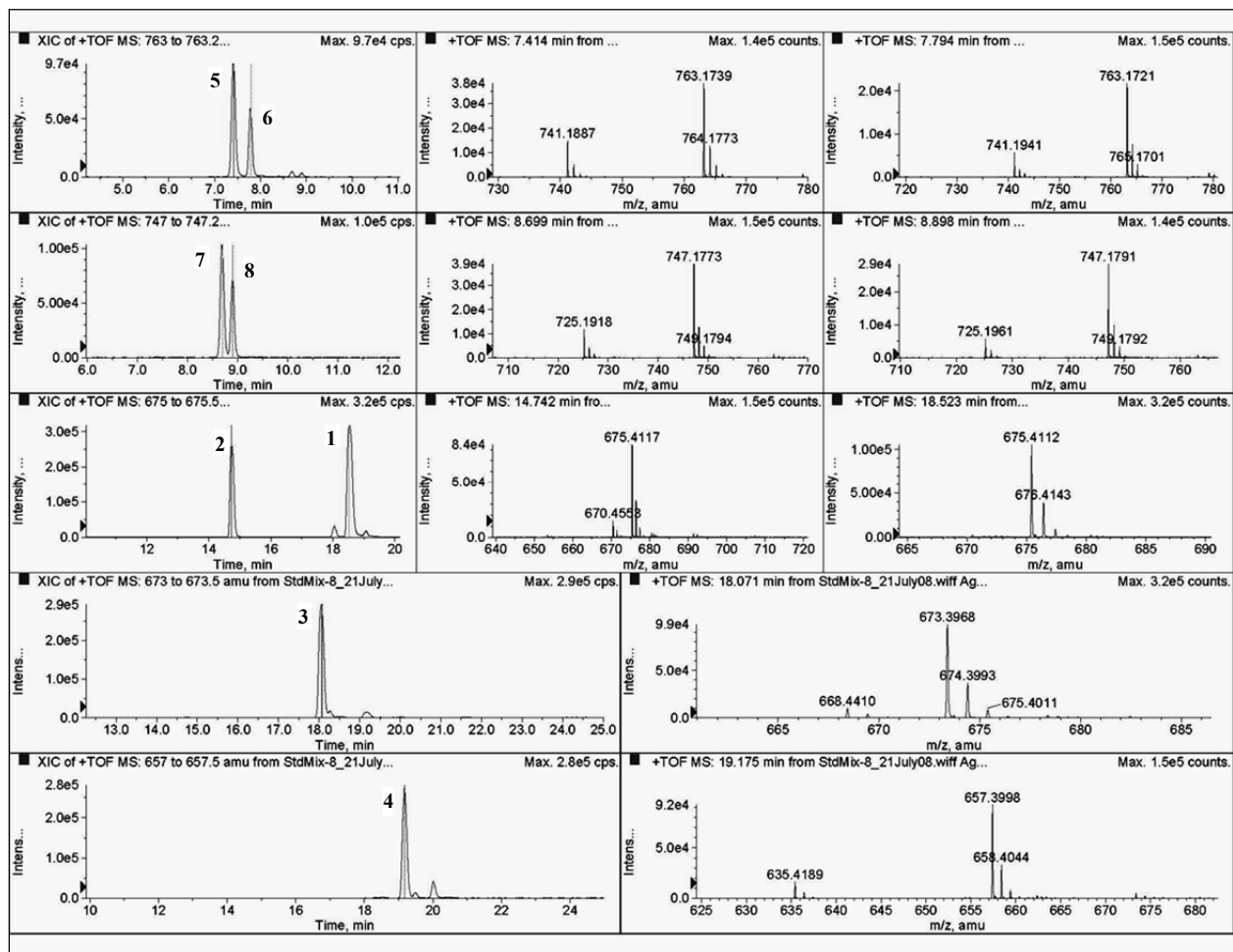


Figure 5-4. Extracted ion chromatograms and mass spectra of standard compounds **1–8**.

## 5.3. Experimental section

### 5.3.1. Chemicals and materials

The standard compounds sutherlandiosides A–D (**1–4**) and sutherlandins A–D (**5–8**) were isolated as described in Chapter 2. The identity and purity were confirmed by chromatographic (TLC and HPLC) methods and by the analysis of the spectroscopic data (IR, 1D- and 2D-NMR and HRESIMS). The purity was 98.34, 98.73, 99.10, 98.53, 93.33, 94.81, 96.65, and 93.46% for compounds **1–8**, respectively.

Acetonitrile and formic acid were HPLC grade, and purchased from Fisher Scientific (Fair Lawn, NJ, USA). Water for the HPLC mobile phase was purified using a Milli-Q system (Millipore).

Leaves and stems of *S. frutescens* were collected from Riversdale, South Africa in November 2006. The plants were identified by Kersten Paulse, a consulting botanist for the pharmaceutical manufacturer Afriplex. A voucher specimen (voucher # PSM 602) is deposited in Parceval Laboratories, Paarl, South Africa.

### 5.3.2. Instrumentations and chromatographic conditions

#### 5.3.2.1. LC-UV analysis

The HPLC system consisted of Waters Alliance 2695 HPLC system, equipped with a 996 photodiode array detector (Waters Corp., Milford, MA, USA). A computerized data station was equipped with Waters Empower 2 software. A Discovery $C_{18}$ column (150 mm × 4.6 mm; 5 μm

particle size) from Supelco (Bellefonte, PA, USA) was used as the stationary phase and the column temperature was maintained at 40 °C. The column was equipped with a 2 cm LC-18 guard column (Phenomenex, Torrance, CA, USA). The mobile phase consisted of water (0.1% acetic acid) (A), and acetonitrile (0.1% acetic acid) (B) at a flow rate of 1.0 mL/min. Analysis was performed using the following gradient elution: 85% A / 15% B to 35% A / 65% B over 35 minutes using a slightly concave gradient profile (Waters curve type 7). Each run was followed by a five minutes' wash with 100% B and an equilibration period of 15 minutes. The ELS detector was set up to a probe temperature of 43 °C, at gain 10.0 and the nebulizer gas (Nitrogen) was adjusted to 4.1 bar. The detection wavelength was 260 nm for flavonoids. Ten microliters of sample was injected and peaks were assigned by spiking the samples with standard compounds and comparison of the UV spectra with those of standards.

5.3.2.2. Liquid chromatography/mass spectrometry (LC-ESI-TOF)

The liquid chromatograph used for the experiment was an Agilent Series 1100 comprised of the following modular components: quaternary pump, a vacuum solvent microdegasser and an autosampler with 100-well tray. The mass spectrometric analysis was performed by using the LC-TOF (Model #G1969A, Agilent Technologies, Palo Alto, CA, USA) equipped with an ESI source. All acquisitions were performed under positive ionization mode with a capillary voltage of 3000 V. Nitrogen was used as the nebulizer gas (35 psig) as well as the drying gas at a flow rate of 13 L/min at a temperature of 350 °C. The voltage of PMT, fragmentor and skimmer was set at 850, 100 and 60 V, respectively. Full scan mass spectra were acquired from $m/z$ 100 to 1300. Data acquisition and processing was done using the Analyst™ QS software (Agilent Technologies, Palo

Alto, CA, USA).

Separation was achieved on a Discovery $C_{18}$ column; 150 mm × 4.6 mm I.D.; 5 μm particle size (Phenomenex, Torrance, CA, USA). The column was equipped with a guard column (Supelco, Bellefonte, PA, USA). The mobile phase consisted of water with 0.1% formic acid (A), and acetonitrile with 0.1% formic acid (B) at a flow rate of 0.5 mL/min, with the following gradient elution: 0 min, 80% A / 20% B to 60% A / 40% B over 20 min. Each run was followed by a five minutes' wash with 100% B and an equilibration period of 11 minutes with 80% A / 20% B. The total run time for analysis was 20 minutes.

Ten microliters of the sample was injected and peaks were assigned with respect to the mass of the compounds and comparison of the retention times.

### 5.3.3. Standard solutions

Individual stock solutions of standard compounds were prepared at a concentration of 1.0 mg/mL in methanol. The calibration curves were prepared at five different concentration levels. The range of the calibration curves was 25-250 μg/mL for sutherlandiosides A, C and D and 10-100 μg/mL for sutherlandioside B by LC-ELSD method, 0.5-60 μg/mL for sutherlandins A and B and 1.0-60.0 μg/mL for sutherlandins C and D by LC-UV method at 260 nm.

The LC-UV calibration data, the calculated limits of detection (LODs), and limits of quantitation (LOQs) for each method are shown in Table 5-1.

### 5.3.4. Sample preparation

Dried plant sample of 300 mg and dietary supplements (equivalent of 0.3-0.5 grams of the capsule content or the tablet weight) were sonicated in 2.5 mL methanol for 30 minutes followed

148

by centrifugation for 15 minutes at 3500 rpm. The supernatant was transferred to a 10 mL volumetric flask. The procedure was repeated thrice and respective supernatants were combined. The final volume was adjusted to 10.0 mL with methanol and mixed thoroughly. Prior to injection, an adequate volume (ca. 2 mL) was filtered through a nylon membrane with 0.45 μm pore size. The first 1.0 mL was discarded and the remaining volume was collected in an LC sample vial. Each sample solution was injected in triplicate.

# CHAPTER 6

# CONCLUDING REMARKS

## 6.1. Conclusion

*S. frutescens* is a "hot" medicinal plant and has been widely used as a folk medicine for the treatment of cancer, AIDS, diabetes, and infectious diseases in southern Africa. A number of biological /pharmacological activities including antiproliferative, antidiabetic, anti-inflammatory, anti-infective, and antistress effects have been demonstrated in the crude extracts of this plant as described in Chapter 1. The limited information on the chemistry and the correlation of chemistry and pharmacology for this plant prompted us to conduct this study with the primary goal to isolate major compounds and develop an analytical method for the appropriate appraisal of the plant's value.

Our studies led to the isolation of eight new cycloartane-type triterpene glycosides sutherlandiosides A–D (**1–4**) and E–H (**9–12**), and four new flavonol glycosides sutherlandins A–D (**5–8**). The structures of these compounds were established by spectroscopic methods and X-ray crystallography. The structures of the cycloartane-type triterpene glycosides are particularly novel. Sutherlandiosides A (**1**) represents the first *seco*-cycloartane skeleton possessing a 7,10-oxygen bridge. Sutherlandiosides B–D (**2–4**), G (**11**), and H (**12**) are the first examples of naturally occurring cycloartanols with C-1 carbonyl functionality. Sutherlandiosides E (**9**) and F (**10**) are a pair of epimers with an A-ring contracted and B-ring expanded *seco*-cycloartane skeleton forming

an unusual 5/7/6/5 tetracyclic ring system.

The structure elucidation of the flavonol glycosides sutherlandins C (**7**) and D (**8**) involved the determination of the absolute configuration of monosaccharides based on an HPLC method. We thus developed a UPLC-UV/MS based method with high sensitivity and better identification, which is the first method that combined UPLC and MS techniques to discriminate multiple aldose enantiomers. The method permitted us to distinguish 16 monosaccharides in a single run. This method was validated using naturally occurring glycosides containing complex sugar moieties.

Using the eight major compounds as chemical markers, we developed an HPLC-UV/ELSD method for the analysis of *S. frutescens*. Sutherlandioside B was found to be the major compound with a content of 2.75% in the dried leaves. This method was successfully applied for the analysis of several dietary supplements claimed to contain the plant material of *S. frutescens*.

The isolated compounds were tested for in vitro antiviral, antibacterial, antiprotozoal, and anticancer activities. It is of significance that the major compound sutherlandioside B showed some antiviral activities against EBV and Tacaribe virus. While we cannot correlate this finding with the medicinal use of this plant for viral infections, the result indicated the presence of biologically active compounds in this plant. However, a bioassay-guided approach should be taken if active compounds responsible for specific biological or pharmacological activities need to be isolated. In this regard, it is important to point out that appropriate bioassays should be developed, and this is also one of the directions for continued studies of this plant in the future.

## 6.2. Future studies

151

A multitude of medicinal uses of *S. frutescens* is related to synergistic effects of a number of chemical components (Tai, Cheung *et al.*, 2004; Prevoo, Swart *et al.*, 2008; MacKenzie, Koekemoer *et al.*, 2012; Vorster, Stander *et al.*, 2012). Understanding the chemical profiles of the plant is important for the explanation of multiple biological activities of *S. frutescens* and the mechanisms of the synergistic effects.

Thus, future work of this project will involve continued isolation and identification of more compounds from *S. frutescens*, including compounds with less polarity. On the other hand, the plant was said to contain a high level of unidentified polysaccharides (Van Wyk and Albrecht, 2008). Since polysaccharides are highly polar molecules that are responsible for a variety of activities, including anticancer and immunomodulatory effects (Wong, Leung *et al.*, 1994), the identification of the polysaccharides in *S. frutescens* should be pursued. Such work may lead to the discovery of interesting compounds that would contribute to the reported pharmacological activities.

The biological activity tests of the new compounds revealed several bioactivity potentials, but the activities of these components were relatively weak as our original goal was not isolating biologically active compounds. Considering the multiple biological activities of the plant extracts, future investigations will involve identification of compounds with potent biological activities, and the study of synergistic effects.

Improved analytical methods with better accuracy and efficiency for the characterization of the marker compounds of *S. frutescens* may be developed. With the growing application of UPLC, the new method based on this technology would bring about improved performance for authentication of plant material and products of *S. frutescens*.

**BIBLIOGRAPHY**

# BIBLIOGRAPHY

Ali, Z. and Khan, I. A.: Alkaloids and saponins from blue cohosh. *Phytochemistry* **2008**, *69*, 1037-1042.

Ali, Z., Khan, S. I., Fronczek, F. R. and Khan, I. A.: 9,10-*Seco*-9,19-cyclolanostane arabinosides from the roots of *Actaea podocarpa*. *Phytochemistry* **2007**, *68*, 373-382.

Ali, Z., Khan, S. I., Pawar, R. S., Ferreira, D. and Khan, I. A.: 9,19-Cyclolanostane derivatives from the roots of *Actaea pachypoda*. *J Nat Prod* **2007**, *70*, 107-110.

APEX II: In *Analytical X-ray Systems*; Bruker AXS, Inc.: Madison, WI, **2005**.

Avula, B., Wang, Y. H., Smillie, T. J., Fu, X., Li, X. C., Mabusela, W., Syce, J., Johnson, Q., Folk, W. and Khan, I. A.: Quantitative determination of flavonoids and cycloartanol glycosides from aerial parts of *Sutherlandia frutescens* (L.) R. BR. by using LC-UV/ELSD methods and confirmation by using LC-MS method. *J Pharm Biomed Anal* **2010**, *52*, 173-180.

Babich, H. and Borenfreund, E.: Cytotoxicity of T-2 toxin and its metabolites determined with the neutral red cell viability assay. *Appl Environ Microbiol* **1991**, *57*, 2101-2103.

Bates, S. H., Jones, R. B. and Bailey, C. J.: Insulin-like effect of pinitol. *Br J Pharmacol* **2000**, *130*, 1944-1948.

Bedir, E. C., Ihsan; Dunbar, Chuck; Sharan, Rudraksh; Buolamwini, John K.; Khan, Ikhlas A.: Two novel cycloartane-type triterpene glycosides from the roots of *Astragalus prusianus*. *Tetrahedron* **2001**, *57*, 5961-5966.

Bence, A. K. and Crooks, P. A.: The mechanism of L-canavanine cytotoxicity: arginyl tRNA synthetase as a novel target for anticancer drug discovery. *J Enzyme Inhib Med Chem* **2003**, *18*, 383-394.

Bence, A. K., Worthen, D. R., Adams, V. R. and Crooks, P. A.: The antiproliferative and immunotoxic effects of L-canavanine and L-canaline. *Anticancer Drugs* **2002**, *13*, 313-320.

Bergot, B. J., Baker, F. C., Lee, E. and Schooley, D. A.: Absolute configuration of homomevalonate and 3-hydroxy-3-ethylglutaryl- and 3-hydroxy-3-methylglutaryl CoA, produced by cell-free extracts of insect corpora allata; cautionary note on prediction of absolute stereochemistry based on liquid chromatographic elution order of diastereomeric derivatives. . *J Am Chem Soc* **1979**, *101*, 7432-7434.

Borenfreund, E., Babich, H. and Martin-Alguacil, N.: Rapid chemosensitivity assay with human normal and tumor cells in vitro. *In Vitro Cell Dev Biol* **1990**, *26*, 1030-1034.

Calis, I., Zor, M., Saracoglu, I., Isimer, A. and Ruegger, H.: Four novel cycloartane glycosides from *Astragalus oleifolius*. *J Nat Prod* **1996**, *59*, 1019-1023.

Cann, S. A., van Netten, J. P. and Ross, A. S.: Correspondence re: D. S. Swaffar *et al.*, Inhibition of the growth of human pancreatic cancer cells by the arginine antimetabolite L-canavanine. Cancer Res., 54: 6045-6048, 1994. *Cancer Res* **1995**, *55*, 4486-4487.

Carratu, B., Boniglia, C., Giammarioli, S., Mosca, M. and Sanzini, E.: Free amino acids in botanicals and botanical preparations. *J Food Sci* **2008**, *73*, C323-328.

Chadwick, W. A., Roux, S., van de Venter, M., Louw, J. and Oelofsen, W.: Anti-diabetic effects of *Sutherlandia frutescens* in Wistar rats fed a diabetogenic diet. *J Ethnopharmacol* **2007**, *109*, 121-127.

Chinkwo, K. A.: *Sutherlandia frutescens* extracts can induce apoptosis in cultured carcinoma cells. *J Ethnopharmacol* **2005**, *98*, 163-170.

Dasgupta, S., Bhattacharya, S., Maitra, S., Pal, D., Majumdar, S. S. and Datta, A.: Mechanism of lipid induced insulin resistance: activated PKC epsilon is a key regulator. *Biochim Biophys Acta* **2011**, *1812*, 495-506.

Dewick, P. M.: *Medicinal Natural Products: a biosynthetic approach*; John Wiley & Sons, Ltd., **2002**.

Fernandes, A. C., Cromarty, A. D., Albrecht, C. and van Rensburg, C. E.: The antioxidant potential of *Sutherlandia frutescens*. *J Ethnopharmacol* **2004**, *95*, 1-5.

Flack, H. D.: On enantiomorph-polarity estimation. *Foundations of Crystallography* **1983**, *39*, 876-881.

Flack, H. D. and Bernardinelli, G.: Reporting and evaluating absolute-structure and absolute-configuration determinations. *J Appl Crystallogr* **2000**, *33*, 1143-1148.

Franzblau, S. G., Witzig, R. S., McLaughlin, J. C., Torres, P., Madico, G., Hernandez, A., Degnan, M. T., Cook, M. B., Quenzer, V. K., Ferguson, R. M. and Gilman, R. H.: Rapid, low-technology MIC determination with clinical *Mycobacterium tuberculosis* isolates by using the microplate Alamar Blue assay. *J Clin Microbiol* **1998**, *36*, 362-366.

Fu, X., Li, X. C., Smillie, T. J., Carvalho, P., Mabusela, W., Syce, J., Johnson, Q., Folk, W., Avery, M. A. and Khan, I. A.: Cycloartane glycosides from *Sutherlandia frutescens*. *J Nat Prod* **2008**, *71*, 1749-1753.

Fu, X., Li, X. C., Wang, Y. H., Avula, B., Smillie, T. J., Mabusela, W., Syce, J., Johnson, Q., Folk, W. and Khan, I. A.: Flavonol glycosides from the South African medicinal plant *Sutherlandia frutescens*. *Planta Med* **2010**, *76*, 178-181.

Fujimoto, H., Nakamura, E., Kim, Y. P., Okuyama, E., Ishibashi, M. and Sassa, T.: Immunomodulatory constituents from an Ascomycete, *Eupenicillium crustaceum*, and revised absolute structure of macrophorin D. *J Nat Prod* **2001**, *64*, 1234-1237.

Hara, S., Okabe, H. and Mihashi, K.: Gas-liquid chromatographic separation of aldose enantiomers as trimethylsilyl ethers of methyl 2-(polyhydroxyalkyl)-thiazolidine-4(R)-carboxylates. *Chem Pharm Bull* **1987**, *35*, 501-506.

Harnett, S. M., Oosthuizen, V. and van de Venter, M.: Anti-HIV activities of organic and aqueous extracts of *Sutherlandia frutescens* and *Lobostemon trigonus*. *J Ethnopharmacol* **2005**, *96*, 113-119.

Henschel, O., Gipson, K. E. and Bordey, A.: GABA$_A$ receptors, anesthetics and anticonvulsants in brain development. *CNS Neurol Disord Drug Targets* **2008**, *7*, 211-224.

Hongda, S., Taga, A., Kotani, M. and Grover, E. R.: Separation of aldoseenantiomers by capillaryelectrophoresis in the presence of optically active *N*-dodecoxycarbonylvalines. *J Chromatogr A* **1997**, *792*, 385-391.

Hubner, G., Wray, V. and Nahrstedt, A.: Flavonol oligosaccharides from the seeds of *Aesculus hippocastanum*. *Planta Med* **1999**, *65*, 636-642.

Ilisz, I., Berkecz, R. and Peter, A.: Retention mechanism of high-performance liquid chromatographic enantioseparation on macrocyclic glycopeptide-based chiral stationary phases. *J Chromatogr A* **2009**, *1216*, 1845-1860.

Imrie, H., Abbas, A. and Kearney, M.: Insulin resistance, lipotoxicity and endothelial dysfunction. *Biochim Biophys Acta* **2010**, *1801*, 320-326.

Isaev, I. M. I., D.A.; Isaev, M.I.;: Triterpene glycosides and their genins from *Astragalus lxxxiv*. secomacrogenin B, a new 9,10-*seco*-cycloartane. *Chem Nat Comp* **2010**, *46*, 36-38.

Ito, M., Yamano, Y., Tode, C. and Wada, A.: Carotenoid synthesis: retrospect and recent progress. *Arch Biochem Biophys* **2009**, *483*, 224-228.

Jadhav, A. N., Pawar, R. S., Avula, B. and Khan, I. A.: Ecdysteroid glycosides from *Sida rhombifolia* L. *Chem Biodivers* **2007**, *4*, 2225-2230.

Janzen, D. H.: Seed predation by animals. *Annu Rev Ecol Syst* **1971**, *2*, 465-492.

Johnson, Q., Syce, J., Nell, H., Rudeen, K. and Folk, W. R.: A randomized, double-blind,

placebo-controlled trial of *Lessertia frutescens* in healthy adults. *PLoS Clin Trials* **2007**, *2*, e16.

Kamo, T., Hirai, N., Matsumoto, C., Ohigashi, H. and Hirota, M.: Revised chirality of the acyl group of 8'-*O*-(3-hydroxy-3-methylglutaryl)-8'-hydroxyabscisic acid. *Phytochemistry* **2004**, *65*, 2517-2520.

Katerere, D. R. and Eloff, J. N.: Antibacterial and antioxidant activity of *Sutherlandia frutescens* (Fabaceae), a reputed anti-HIV/AIDS phytomedicine. *Phytother Res* **2005**, *19*, 779-781.

Kazuma, K., Noda, N. and Suzuki, M.: Malonylated flavonol glycosides from the petals of *Clitoria ternatea*. *Phytochemistry* **2003**, *62*, 229-237.

Kinjo, J., Araki, K., Fukui, K., Higuchi, H., Ikeda, T., Nohara, T., Ida, Y., Takemoto, N., Miyakoshi, M. and Shoji, J.: Six new triterpenoidal glycosides including two new sapogenols from *Albizziae Cortex*. V. *Chem Pharm Bull* **1992**, *40*, 3269-3273.

Kitagawa, I., Hori, K., Sakagami, M., Hashiuchi, F., Yoshikawa, M. and Ren, J.: Saponin and sapogenol. XLIX. On the constituents of the roots of *Glycyrrhiza inflata* Batalin from Xinjiang, China. Characterization of two sweet oleanane-type triterpene oligoglycosides, apioglycyrrhizin and araboglycyrrhizin. *Chem Pharm Bull* **1993**, *41*, 1350-1357.

Kitagawa, M.: A new amino-compound in the jack bean and a corresponding new ferment. *J Biochem* **1930**, *11*, 265-271.

Kundu, J. K., Mossanda, K. S., Na, H. K. and Surh, Y. J.: Inhibitory effects of the extracts of *Sutherlandia frutescens* (L.) R. Br. and *Harpagophytum procumbens* DC. on phorbol ester-induced COX-2 expression in mouse skin: AP-1 and CREB as potential upstream targets. *Cancer Lett* **2005**, *218*, 21-31.

Lee, V. S., Chen, C. R., Liao, Y. W., Tzen, J. T. and Chang, C. I.: Structural determination and DPPH radical-scavenging activity of two acylated flavonoid tetraglycosides in oolong tea (*Camellia sinensis*). *Chem Pharm Bull* **2008**, *56*, 851-853.

Li, X. C., Jacob, M. R., Ding, Y., Agarwal, A. K., Smillie, T. J., Khan, S. I., Nagle, D. G., Ferreira, D. and Clark, A. M.: Capisterones A and B, which enhance fluconazole activity in *Saccharomyces cerevisiae*, from the marine green alga *Penicillus capitatus*. *J Nat Prod* **2006**, *69*, 542-546.

Lopes, J. F. and Gaspar, E. M.: Simultaneous chromatographic separation of enantiomers, anomers and structural isomers of some biologically relevant monosaccharides. *J Chromatogr A* **2008**, *1188*, 34-42.

Ma, G., Khan, S. I., Jacob, M. R., Tekwani, B. L., Li, Z., Pasco, D. S., Walker, L. A. and Khan, I. A.: Antimicrobial and antileishmanial activities of hypocrellins A and B. *Antimicrob Agents Chemother* **2004**, *48*, 4450-4452.

Ma, Z. J., Wang, N., Fujii, I., Ebizuka, Y. and Li, X.: Two new 9,10-*seco*-cycloartanes from the seeds of *Sphaerophysa salsula*. *J Asian Nat Prod Res* **2006**, *8*, 657-661.

Mabry, T. J., Markham, K. R. and Thomas, M. B.: *The systematic identification of flavonoids*.; Springer: Berlin, **1970**.

MacKenzie, J., Koekemoer, T., van de Venter, M., Dealtry, G. and Roux, S.: *Sutherlandia frutescens* limits the development of insulin resistance by decreasing plasma free fatty acid levels. *Phytother Res* **2009**, *23*, 1609-1614.

MacKenzie, J., Koekemoer, T. C., Roux, S., van de Venter, M. and Dealtry, G. B.: Effect of *Sutherlandia frutescens* on the lipid metabolism in an insulin resistant rat model and 3T3-L1 adipocytes. *Phytother Res* **2012**.

Makler, M. T. and Hinrichs, D. J.: Measurement of the lactate dehydrogenase activity of *Plasmodium falciparum* as an assessment of parasitemia. *Am J Trop Med Hyg* **1993**, *48*, 205-210.

Makler, M. T., Ries, J. M., Williams, J. A., Bancroft, J. E., Piper, R. C., Gibbins, B. L. and Hinrichs, D. J.: Parasite lactate dehydrogenase as an assay for *Plasmodium falciparum* drug sensitivity. *Am J Trop Med Hyg* **1993**, *48*, 739-741.

Menter, D. G., Schilsky, R. L. and DuBois, R. N.: Cyclooxygenase-2 and cancer treatment: understanding the risk should be worth the reward. *Clin Cancer Res* **2010**, *16*, 1384-1390.

Mikus, J. and Steverding, D.: A simple colorimetric method to screen drug cytotoxicity against Leishmania using the dye Alamar Blue. *Parasitol Int* **2000**, *48*, 265-269.

Mills, E., Cooper, C., Seely, D. and Kanfer, I.: African herbal medicines in the treatment of HIV: *Hypoxis* and *Sutherlandia*. An overview of evidence and pharmacology. *Nutr J* **2005**, *4*, 19.

Mills, E., Singh, S., Wilson, K., Peters, E., Onia, R. and Kanfer, I.: The challenges of involving traditional healers in HIV/AIDS care. *Int J STD AIDS* **2006**, *17*, 360-363.

Minocha, M., Mandava, N. K., Kwatra, D., Pal, D., Folk, W. R., Earla, R. and Mitra, A. K.: Effect of short term and chronic administration of *Sutherlandia frutescens* on pharmacokinetics of nevirapine in rats. *Int J Pharm* **2011**, *413*, 44-50.

Morris, S. M., Jr.: Regulation of enzymes of the urea cycle and arginine metabolism. *Annu Rev Nutr* **2002**, *22*, 87-105.

Moshe, D. v. d. B., H; van der Bank, M; Van Wyk, BE: Lack of genetic differentiation between 19 populations from seven taxa of *Sutherlandia* Tribe: Galegeae, Fabaceae. *Biochem Syst Ecol* **1998**, *26*, 595-609.

Muller, A. C., Patnala, S., Kis, O., Bendayan, R. and Kanfer, I.: Interactions between phytochemical components of *Sutherlandia frutescens* and the antiretroviral, atazanavir in vitro: implications for absorption and metabolism. *J Pharm Pharm Sci* **2012**, *15*, 221-233.

Mustafa, J., Khan, S. I., Ma, G., Walker, L. A. and Khan, I. A.: Synthesis and anticancer activities of fatty acid analogs of podophyllotoxin. *Lipids* **2004**, *39*, 167-172.

Na, H. K., Mossanda, K. S., Lee, J. Y. and Surh, Y. J.: Inhibition of phorbol ester-induced COX-2 expression by some edible African plants. *Biofactors* **2004**, *21*, 149-153.

NCCLS: Reference method for broth dilution antifungal susceptibility testing of filamentous fungi. In *Approved Standard, M38-A*; National Committee on Clinical Laboratory Standards, **2002**; Vol. *22*.

NCCLS: Reference method for broth dilution antifungal susceptibility testing of yeasts. In *Approved Standard M27-A2*; National Committee on Clinical Laboratory Standards, **2002**; Vol. *22*.

NCCLS: Susceptibility testing of Mycobacteria, Nocardia, and other aerobic Actinomycetes. In *Approved Standard, M24-A*; National Committee on Clinical Laboratory Standards, **2003**; Vol. *23*.

NCCLS: Methods for dilution antimicrobial susceptibility tests for bacteria that grow aerobically. In *Approved Standard M7-A7*; 7 ed.; National Committee on Clinical Laboratory Standards, **2006**; Vol. *26*.

Ojewole, J. A.: Analgesic, antiinflammatory and hypoglycemic effects of *Sutherlandia frutescens* R. BR. (variety Incana E. MEY.) [Fabaceae] shoot aqueous extract. *Methods Find Exp Clin Pharmacol* **2004**, *26*, 409-416.

Ojewole, J. A.: Anticonvulsant property of *Sutherlandia frutescens* R. BR. (variety Incana E. MEY.) [Fabaceae] shoot aqueous extract. *Brain Res Bull* **2008**, *75*, 126-132.

Olivier, D. A., CF; Van Wyk BE; van Heerden, FR: SU3, an oxocycloartane diglucoside from *Sutherlandia humilis*. *Phytochem Lett* **2009**, *2*, 123-125.

Pointinger, S., Promdang, S., Vajrodaya, S., Pannell, C. M., Hofer, O., Mereiter, K. and Greger, H.: Silvaglins and related 2,3-secodammarane derivatives - unusual types of triterpenes from *Aglaia silvestris*. *Phytochemistry* **2008**, *69*, 2696-2703.

Prevoo, D., Smith, C., Swart, P. and Swart, A. C.: The effect of *Sutherlandia frutescens* on steroidogenesis: confirming indigenous wisdom. *Endocr Res* **2004**, *30*, 745-751.

Prevoo, D., Swart, P. and Swart, A. C.: The influence of *Sutherlandia frutescens* on adrenal steroidogenic cytochrome P450 enzymes. *J Ethnopharmacol* **2008**, *118*, 118-126.

Raja Rao, K. R. L. R., Prakasa: An A-ring contracted triterpenoid from *Hyptis suaveolens*. *Phytochemistry* **1990**, *29*, 1326-1329.

Reid, K. A., Maes, J., Maes, A., van Staden, J., De Kimpe, N., Mulholland, D. A. and Verschaeve, L.: Evaluation of the mutagenic and antimutagenic effects of South African plants. *J Ethnopharmacol* **2006**, *106*, 44-50.

Rosenthal, G. A.: Investigations of canavanine biochemistry in the jack bean plant, *Canavalia ensiformia* (L.) DC: I. canavanine utilization in the developing plant. *Plant Physiol* **1970**, *46*, 273-276.

Rosenthal, G. A.: The biological effects and mode of action of L-canavanine, a structural analogue of L-arginine. *Q Rev Biol* **1977**, *52*, 155-178.

SAINT: Version 6.45A. In *Analytical X-ray Systems*; Bruker AXS, Inc.: Madison, WI, **2003**.

Samuel, V. T., Petersen, K. F. and Shulman, G. I.: Lipid-induced insulin resistance: unravelling the mechanism. *Lancet* **2010**, *375*, 2267-2277.

Semmar, N., Fenet, B., Gluchoff-Fiasson, K., Hasan, A. and Jay, M.: Four new flavonol glycosides from the leaves of *Astragalus caprinus*. *J Nat Prod* **2002**, *65*, 576-579.

Sethi, G., Ahn, K. S., Sung, B. and Aggarwal, B. B.: Pinitol targets nuclear factor-kappaB activation pathway leading to inhibition of gene products associated with proliferation, apoptosis, invasion, and angiogenesis. *Mol Cancer Ther* **2008**, *7*, 1604-1614.

Shaik, S., Singh, N. and Nicholas, A.: Comparison of the selected secondary metabolite content present in the cancer-bush *Lessertia* (*Sutherlandia*) *frutescens* L. extracts. *Afr J Tradit Complement Altern Med* **2011**, *8*, 429-434.

Shaik, S., Singh, N. and Nicholas, A.: HPLC and GC analyses of in vitro-grown leaves of the cancer bush *Lessertia* (*Sutherlandia*) *frutescens* L. reveal higher yields of bioactive compounds *Plant Cell Tissue Organ Cult* **2011**, *105*, 431-438.

SHELXTL: V6.12. In *Analytical X-ray Systems*; Bruker AXS, Inc.: Madison, WI, **2002**.

Sia, C.: Spotlight on ethnomedicine: usability of *Sutherlandia frutescens* in the treatment of diabetes. *Rev Diabet Stud* **2004**, *1*, 145-149.

Silverstein, R. M., Webster, F. X. and Kiemle, D. J.: *Spectrometric identification of organic compounds*; 7th ed.; John Wiley & Sons, Inc: Hoboken, **2005**.

Singh, R. K., Pandey, B. L., Tripathi, M. and Pandey, V. B.: Anti-inflammatory effect of (+)-pinitol. *Fitoterapia* **2001**, *72*, 168-170.

Sivakumar, S., Palsamy, P. and Subramanian, S. P.: Impact of D-pinitol on the attenuation of proinflammatory cytokines, hyperglycemia-mediated oxidative stress and protection of kidney tissue ultrastructure in streptozotocin-induced diabetic rats. *Chem Biol Interact* **2010**, *188*, 237-245.

Skerman, N. B., Joubert, A. M. and Cronje, M. J.: The apoptosis inducing effects of *Sutherlandia spp*. extracts on an oesophageal cancer cell line. *J Ethnopharmacol* **2011**, *137*, 1250-1260.

Soumyanath, A.: Traditional medicines for modern times. In *Antidiabetic plants*; Talor & Francis Group: Boca Raton, **2006**; pp 212.

Stander, A., Marais, S., Stivaktas, V., Vorster, C., Albrecht, C., Lottering, M. L. and Joubert, A. M.: In vitro effects of *Sutherlandia frutescens* water extracts on cell numbers, morphology, cell cycle progression and cell death in a tumorigenic and a non-tumorigenic epithelial breast cell line. *J Ethnopharmacol* **2009**, *124*, 45-60.

Stander, B. A., Marais, S., Steynberg, T. J., Theron, D., Joubert, F., Albrecht, C. and Joubert, A. M.: Influence of *Sutherlandia frutescens* extracts on cell numbers, morphology and gene expression in MCF-7 cells. *J Ethnopharmacol* **2007**, *112*, 312-318.

Tai, J., Cheung, S., Chan, E. and Hasman, D.: In vitro culture studies of *Sutherlandia frutescens* on human tumor cell lines. *J Ethnopharmacol* **2004**, *93*, 9-19.

Tanaka, T., Nakashima, T., Ueda, T., Tomii, K. and Kouno, I.: Facile discrimination of aldose enantiomers by reversed-phase HPLC. *Chem Pharm Bull* **2007**, *55*, 899-901.

Tiganis, T.: Reactive oxygen species and insulin resistance: the good, the bad and the ugly. *Trends Pharmacol Sci* **2011**, *32*, 82-89.

Torre, D.: Nitric oxide and endothelial dysfunction in HIV type 1 infection. *Clin Infect Dis* **2006**, *43*, 1086-1087.

Van Wyk, B. E.: A broad review of commercially important Southern African medicinal plants. *J Ethnopharmacol* **2008**, *119*, 342-355.

Van Wyk, B. E. and Albrecht, C.: A review of the taxonomy, ethnobotany, chemistry and pharmacology of *Sutherlandia frutescens* (Fabaceae). *J Ethnopharmacol* **2008**, *119*, 620-629.

Vijayaraghavan, K.: Treatment of dyslipidemia in patients with type 2 diabetes. *Lipids Health Dis* **2010**, *9*, 144.

Volcani, B. E. and Snell, E. E.: The effects of canavanine, arginine, and related compounds on the growth of bacteria. *J Biol Chem* **1948**, *174*, 893-902.

Vorster, C., Stander, A. and Joubert, A.: Differential signaling involved in *Sutherlandia*

*frutescens*-induced cell death in MCF-7 and MCF-12A cells. *J Ethnopharmacol* **2012**, *140*, 123-130.

Vynnytska, B. O., Mayevska, O. M., Kurlishchuk, Y. V., Bobak, Y. P. and Stasyk, O. V.: Canavanine augments proapoptotic effects of arginine deprivation in cultured human cancer cells. *Anticancer Drugs* **2011**, *22*, 148-157.

Wang, F., Li, X. M. and Liu, J. K.: New terpenoids from *Isodon sculponeata*. *Chem Pharm Bull* **2009**, *57*, 525-527.

Wong, C. K., Leung, K. N., Fung, K. P. and Choy, Y. M.: Immunomodulatory and anti-tumour polysaccharides from medicinal plants. *J Int Med Res* **1994**, *22*, 299-312.

Yang, C. R., Zhang, Y., Jacob, M. R., Khan, S. I., Zhang, Y. J. and Li, X. C.: Antifungal activity of C-27 steroidal saponins. *Antimicrob Agents Chemother* **2006**, *50*, 1710-1714.

**APPENDIX**

# VITA

Xiang Fu was born and raised in Kunming, Yunnan province, China. He received his Bachelor of Science degree in Pharmacology at China Pharmaceutical University, Nanjing, China, in 2000. He attended the Graduate School of Chinese Academy of Sciences in Beijing, China for his graduate courses study in the same year. When completing the course study, he joined Dr. Ning-Hua Tan's research group at Kunming Institute of Botany, Chinese Academy of Sciences as a research assistant in her Drug Discovery Lab, which collaborates with Bayer Pharma Research in Wuppertal, Germany. This lab aims at drug discovery from natural occurring small molecules, with the major focus on the discovery of lead compounds with anticancer, anti-osteoporosis, and antifungal potential in plants. He obtained his Master of Science degree in 2003, majoring in Phytochemistry. He was an instructor of Toxicology at Kunming Medical College in Kunming, China before he came to the US. In August 2006, he joined the Department of Pharmacognosy, the University of Mississippi to pursue his doctoral degree, and worked as a research assistant at the National Center for Natural Products Research (NCNPR) under the supervision of Dr. Ikhlas A. Khan.